MICROENCAPSULATION FOR BIOMEDICAL APPLICATIONS

EDITED BY: Raffaele Vecchione, Filippo Causa, Aurelio Salerno and Concepcion Domingo

PUBLISHED IN: Frontiers in Bioengineering and Biotechnology

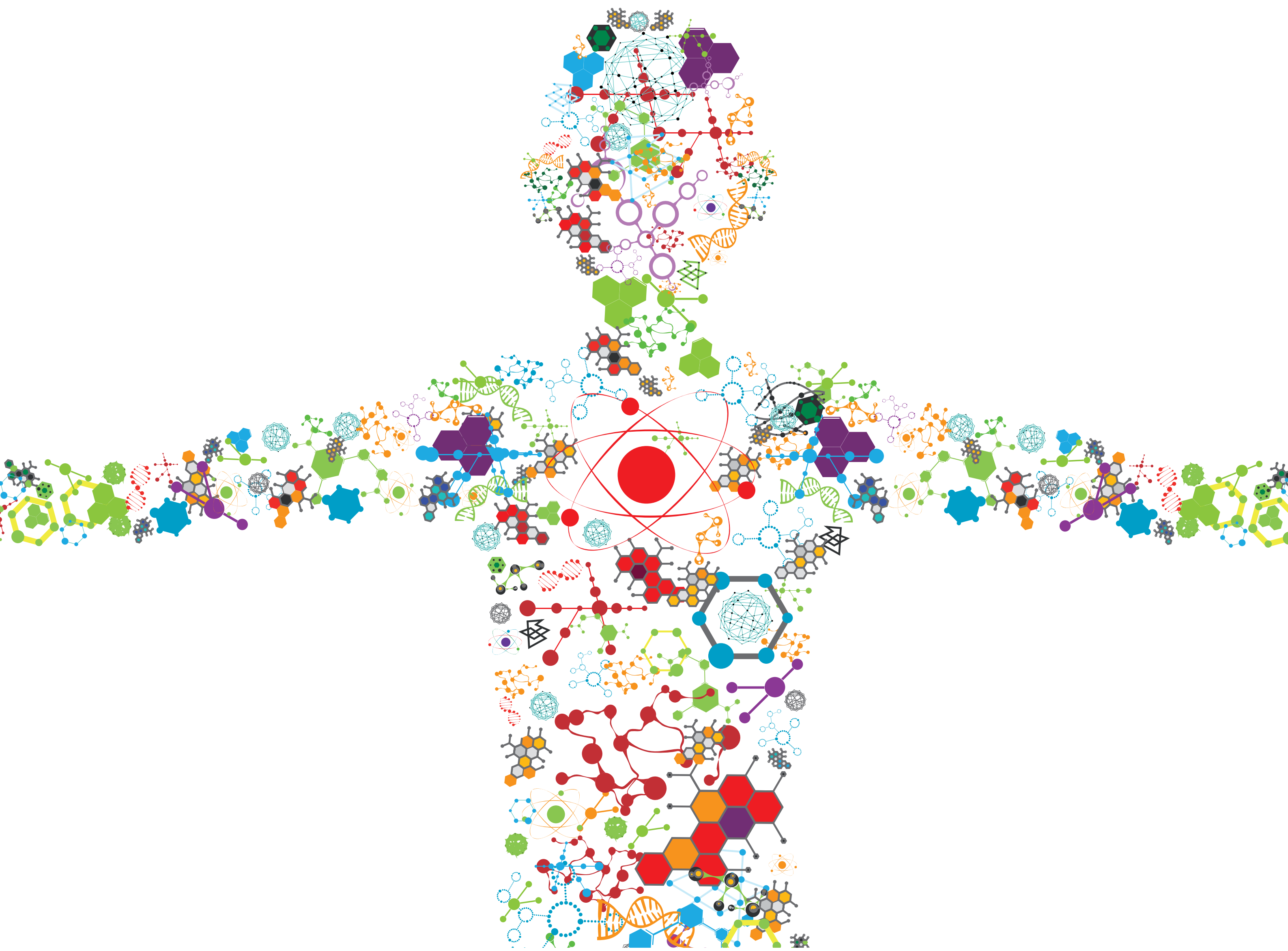

frontiers Research Topics

ISSN 1664-8714
ISBN 978-2-88974-940-9
DOI 10.3389/978-2-88974-940-9

About Frontiers

Frontiers is more than just an open-access publisher of scholarly articles: it is a pioneering approach to the world of academia, radically improving the way scholarly research is managed. The grand vision of Frontiers is a world where all people have an equal opportunity to seek, share and generate knowledge. Frontiers provides immediate and permanent online open access to all its publications, but this alone is not enough to realize our grand goals.

Frontiers Journal Series

The Frontiers Journal Series is a multi-tier and interdisciplinary set of open-access, online journals, promising a paradigm shift from the current review, selection and dissemination processes in academic publishing. All Frontiers journals are driven by researchers for researchers; therefore, they constitute a service to the scholarly community. At the same time, the Frontiers Journal Series operates on a revolutionary invention, the tiered publishing system, initially addressing specific communities of scholars, and gradually climbing up to broader public understanding, thus serving the interests of the lay society, too.

Dedication to Quality

Each Frontiers article is a landmark of the highest quality, thanks to genuinely collaborative interactions between authors and review editors, who include some of the world's best academicians. Research must be certified by peers before entering a stream of knowledge that may eventually reach the public - and shape society; therefore, Frontiers only applies the most rigorous and unbiased reviews.
Frontiers revolutionizes research publishing by freely delivering the most outstanding research, evaluated with no bias from both the academic and social point of view.
By applying the most advanced information technologies, Frontiers is catapulting scholarly publishing into a new generation.

What are Frontiers Research Topics?

Frontiers Research Topics are very popular trademarks of the Frontiers Journals Series: they are collections of at least ten articles, all centered on a particular subject. With their unique mix of varied contributions from Original Research to Review Articles, Frontiers Research Topics unify the most influential researchers, the latest key findings and historical advances in a hot research area! Find out more on how to host your own Frontiers Research Topic or contribute to one as an author by contacting the Frontiers Editorial Office: frontiersin.org/about/contact

MICROENCAPSULATION FOR BIOMEDICAL APPLICATIONS

Topic Editors:
Raffaele Vecchione, Italian Institute of Technology (IIT), Italy
Filippo Causa, University of Naples Federico II, Italy
Aurelio Salerno, Independent Researcher, Spain
Concepcion Domingo, Institute of Marine Sciences, Spanish National Research Council (CSIC), Spain

Citation: Vecchione, R., Causa, F., Salerno, A., Domingo, C., eds. (2022). Microencapsulation for Biomedical Applications. Lausanne: Frontiers Media SA. doi: 10.3389/978-2-88974-940-9

Table of Contents

04 ***Editorial: Microencapsulation for Biomedical Applications***
Aurelio Salerno, Filippo Causa, Concetta Di Natale, Concepción Domingo and Raffaele Vecchione

07 ***Encapsulation of Andrographolide in poly(lactide-co-glycolide) Nanoparticles: Formulation Optimization and* in vitro *Efficacy Studies***
Bukola A. Oseni, Chukwuemeka P. Azubuike, Omotunde O. Okubanjo, Cecilia I. Igwilo and Jayanth Panyam

21 ***Encapsulation of Fullerenes: A Versatile Approach for the Confinement and Release of Materials Within Open-Ended Multiwalled Carbon Nanotubes***
Stefania Sandoval and Gerard Tobias

33 ***A Pathway From Porous Particle Technology Toward Tailoring Aerogels for Pulmonary Drug Administration***
Thoa Duong, Clara López-Iglesias, Piotr K. Szewczyk, Urszula Stachewicz, Joana Barros, Carmen Alvarez-Lorenzo, Mohammad Alnaief and Carlos A. García-González

49 ***Morphological and Rheological Guided Design for the Microencapsulation Process of* Lactobacillus paracasei CBA L74 *in Calcium Alginate Microspheres***
Concetta Di Natale, Elena Lagreca, Valeria Panzetta, Marianna Gallo, Francesca Passannanti, Michele Vitale, Sabato Fusco, Raffaele Vecchione, Roberto Nigro and Paolo Netti

58 ***Review on Computer-Aided Design and Manufacturing of Drug Delivery Scaffolds for Cell Guidance and Tissue Regeneration***
Aurelio Salerno and Paolo A. Netti

77 ***Oregano Essential Oil Micro- and Nanoencapsulation With Bioactive Properties for Biotechnological and Biomedical Applications***
Gloria María Pontes-Quero, Susana Esteban-Rubio, Juan Pérez Cano, María Rosa Aguilar and Blanca Vázquez-Lasa

86 ***Polysaccharide-Based Hydrogels for Microencapsulation of Stem Cells in Regenerative Medicine***
Si-Yuen Lee, Jingyi Ma, Tze Sean Khoo, Norfadhilatuladha Abdullah, Nik Nur Farisha Nik Md Noordin Kahar, Zuratul Ain Abdul Hamid and Muzaimi Mustapha

105 ***One-Step Generation and Purification of Cell-Encapsulated Hydrogel Microsphere With an Easily Assembled Microfluidic Device***
Tao Zhang, Hong Zhang, Wuping Zhou, Keming Jiang, Cong Liu, Ru Wang, Yuanshuai Zhou, Zhiqiang Zhang, Qian Mei, Wen-Fei Dong, Minxuan Sun and Haiwen Li

114 ***Engineered Bacterial Cellulose Nanostructured Matrix for Incubation and Release of Drug-Loaded Oil in Water Nanoemulsion***
Concetta Di Natale, Vincenza De Gregorio, Elena Lagreca, Francesca Mauro, Brunella Corrado, Raffaele Vecchione and Paolo Antonio Netti

frontiers in Bioengineering and Biotechnology

EDITORIAL
published: 25 March 2022
doi: 10.3389/fbioe.2022.891981

Editorial: Microencapsulation for Biomedical Applications

Aurelio Salerno[1]*, *Filippo Causa*[2,3]*, *Concetta Di Natale*[2], *Concepción Domingo*[4]* and *Raffaele Vecchione*[5]*

[1]Independent Researcher, Barcelona, Spain, [2]Interdisciplinary Research Centre on Biomaterials (CRIB), Università degli Studi di Napoli "Federico II", Naples, Italy, [3]Dipartimento di Ingegneria Chimica dei Materiali e della Produzione Industriale (DICMAPI), University "Federico II", Naples, Italy, [4]Institut de Ciència de Materials de Barcelona (ICMAB-CSIC), Barcelona, Spain, [5]Center for Advanced Biomaterials for Health Care (iit@CRIB), Istituto Italiano di Tecnologia, Naples, Italy

Keywords: drug delievery systems, microencapculation, tissue engineering, emulsion, scaffold, nanoparticles, nanotubes, cell encapsulation

Editorial on the Research Topic

Microencapsulation for Biomedical Applications

OPEN ACCESS

Edited and reviewed by:
Hasan Uludag,
University of Alberta, Canada

***Correspondence:**
Aurelio Salerno
asalerno@unina.it
Filippo Causa
causa@unina.it
Concepción Domingo
conchi@icmab.es
Raffaele Vecchione
Raffaele.Vecchione@iit.it

Specialty section:
This article was submitted to Biomaterials, a section of the journal Frontiers in Bioengineering and Biotechnology

Received: *08 March 2022*
Accepted: *11 March 2022*
Published: *25 March 2022*

Citation:
Salerno A, Causa F, Di Natale C, Domingo C and Vecchione R (2022) Editorial: Microencapsulation for Biomedical Applications. Front. Bioeng. Biotechnol. 10:891981. doi: 10.3389/fbioe.2022.891981

The systemic administration of drugs, such as chemotherapeutics, probiotics and anti-inflammatories, is known to be frequently associated to biomolecules short half-life, poor stability and side effects potentially harmful to functional tissues and organs. Advanced drug therapies require patient customization and targeting of drug formulation and dosage to warrant treatment efficacy and reduce possible undesired secondary effects. Nano- and microencapsulation strategies are generally defined as a set of technologies that allow to entrap active ingredients, namely small solid particles, liquid droplets or a gas, using a surrounding material (Silva and Meireles, 2014). These strategies may allow overcoming previous limitations as the encapsulating material protects the drugs, while their delivery can be tailored depending on the specific application by the careful modulation of carrier composition, size and architectural features. A variety of methods, including microfluidic emulsion, coacervation, antisolvent precipitation and soft lithography, have been used to produce drug delivery systems for precision medicine (Wang et al., 2006; Canelas et al., 2009; Liu et al., 2017). Overall, these methods offer control over basic parameters such as material-to-drug composition, carrier size, porosity and shape (**Figure 1**). In this vast and complex panorama, the aim of this Research Topic is to highlight and illustrate important knowledge in the field of micro- and nanoencapsulation and drug delivery systems as shared by experts in these research fields. Most notably, the nine articles collected in this issue, composed of five research articles and four reviews by different countries' teams, are of interest to researchers looking for current drug delivery advances in biomedicine and biotechnology, as described following.

Two articles of this collection are specifically focused on the application of hydrogels on cell microencapsulation for tissue engineering (TE) purposes. TE offers great potential for restoring individual tissues or organs using patient's stem cells incorporated within porous scaffolds or hydrogels (Khademhosseini et al., 2009). However, low new tissue survival, poor engraftment and a lack of site-specificity are major drawbacks. Natural polymers have gained much interest in the construction of extracellular matrix (ECM) analogues for stem cells. Cell-laden hydrogel microspheres with uniform size show great potential for tissue repair and drug screening applications. The article by Lee et al. reviewed the application of polysaccharide-based hydrogels for stem cells microencapsulation in TE. In particular, the work showed an updated vision of microencapsulation techniques, which include emulsion, lithography, microfluidics and bioprinting. Furthermore, current progress in clinical translation of stem-cell encapsulated polysaccharide hydrogels for cell delivery and disease modelling (drug testing and discovery) were discussed with special emphasis on musculoskeletal, nervous, cardiac and cancerous tissues applications. In the

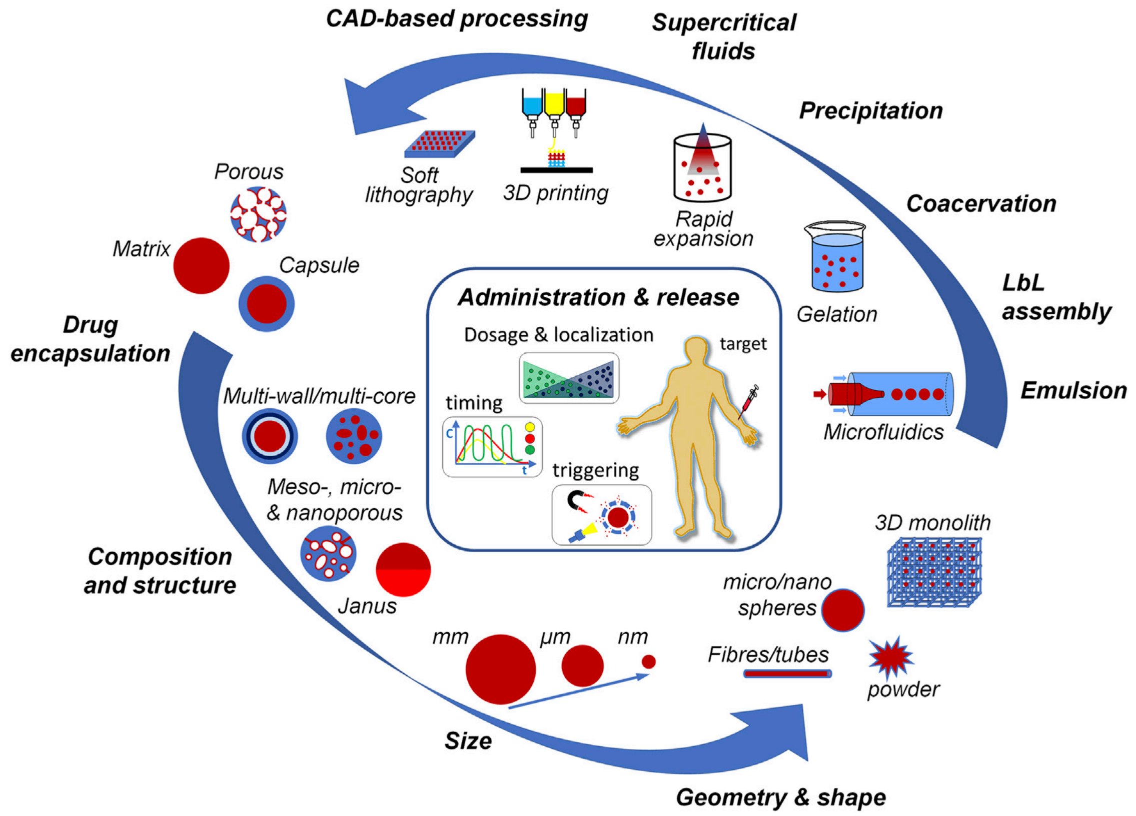

FIGURE 1 | Picture highlighting the main properties of drug delivery carriers and some of the most advanced processing techniques for carriers manufacturing. The drug can be encapsulated within the polymeric matrix (particles), loaded in the core (single and multi-core capsules) or adsorbed onto the inner pore surfaces. The control of drug release is achievable by tuning carriers' composition, structure, size and shape and by the optimization of the fabrication technique and processing conditions.

article by Zhang et al., a simple one-step approach for producing and purifying hydrogel microspheres with an easily assembled microfluidic device was described. Droplets were generated and solidified within a fluidic device and then demulsification and purification from oil was obtained by the simple evaporation of the oil at 37°C. This step allowed gelled microspheres to be released directly into the cell culture media, ready to be tested for cell culture experiments. HCT116 and U87 tumour cells were successfully encapsulated within monodisperse gelatin methacryloyl microspheres ensuring proper cell viability. The U87-encapsulated microspheres were also used to growth tumour spheroids up to 14 days, finally suggesting the possible translational technology of the developed approach. As previously explained, drug delivery scaffolds are essential elements of TE strategies for the repair and regeneration of damaged tissues and organs. Indeed, scaffolds must endow with arrays of biological signals, with adequate dose and timescale, to regulate cellular adhesion, migration and ECM biosynthesis in three dimensions (Salerno et al., 2019). Therefore, scaffolds fabrication requires the concomitant processing of biomaterials, cells and biomolecules to reproduce the cell and ECM composition and architecture of native tissues. The use of computer-aided design (CAD) and manufacturing of drug delivery scaffolds was reviewed by the work of Salerno and Netti. The article highlights some of the most recent advancement of CAD-based strategies to engineering passive and stimuli-responsive drug delivery scaffolds for TE and cancer precision medicine. Furthermore, authors' perspective about the possible integration of CAD techniques with microfluidics and soft lithography was reported for enhancing scaffold bioactivation features.

A valuable application of microencapsulation techniques is to protect probiotics from harmful gastrointestinal tract (GI) environmental factors, such as high acidity and low pH levels, bile salts, and oxidation conditions. This issue was addressed by the work of Di Natale et al., that encapsulated the *L. paracasei CBA L74* bacteria in sodium alginate microspheres by the water-in-oil emulsion technique to protect it in GI and to enhance its viability and beneficial effects. The optimal microencapsulation conditions were obtained by using a micro-rheological analysis as it allowed to understand the relationship between emulsion conditions and microsphere's inner microstructure, which in turn can affect probiotic viability and release.

Nanocarriers are highly versatile and valuable systems for drugs delivery as they provide high specific surface together with small size, typically between 1 and 100 nm. Due to these features, nanocarriers may provide a long-term circulation period with the sustained release of drug, overcoming limitations related to the endosomal/lysosomal membrane transport (Chamundeeswari et al., 2019). Among the different forms of nanocarriers, nanofibers, nanoparticles and nanotubes, are the most investigated as they effectively found application in the biomedical field. In the article by Oseni et al., the chemotherapeutic andrographolide was encapsulated within polylactic-co-glycolic (PLGA) nanoparticles *via* emulsion solvent evaporation technique. The effect of polymer composition, polymer molecular weight, polymer-to-drug ratio, surfactant concentration and the organic solvent used on particles size and encapsulation efficiency was investigated. Nanoparticles formulated using 85:15 PLGA and ethyl acetate as the organic solvent provided the best particle size, drug loading and release towards the inhibition of proliferation of metastatic breast cancer cells. In another study, Sandoval and Tobias used fullerenes to "cork" the open tips of multiwalled carbon nanotubes (MWCNTs), and as promoting species for the on-demand release of the inorganic material filled within the nanotubes' cavities. In particular, fullerenes avoided the release of the encapsulated payloads during samples washing as well as may enable to trigger the release of guest structures from the MWCNTs cavities once dissolved in appropriate solvents. Most notably, the authors demonstrated that MWCNTs can be loaded with chosen bioactive compound before thermal treatment, therefore allowing the loading of heat labile biomolecules within MWCNTs porosity. The application of micro- and nanoencapsulation to the antioxidant, antimicrobial, and therapeutic oregano essential oil (OEO) has been reviewed by the work of Pontes-Quaero et al. In fact, encapsulation is necessary to increase OEO stability and bioactivity and to decrease its volatility. Hence, different drug delivery systems, mainly lipids and cyclodextrins, were discussed respect to scientific literature, in order to find the best candidates for OEO encapsulation. Among different natural polymers, bacterial cellulose (BC) is a highly pure form of cellulose produced by bacteria that can be chemical-physically modulated and optimized to encapsulate and deliver several drugs. The work by Di Natale et al. described the preparation of antioxidant and anti-inflammatory nanofibrous patches by loading CoenzymeQ10 (Co-Q10) nanoemulsions within the porous structure of BC. To this purpose, BC layers were incubated at different time points with a positively-charged oil/water nanoemulsion, previously loaded with Co-Q10, and the efficacy of release was studied at different time points.

The last article presented in this Research Topic Editorial (Duong et al.) rely on the use of porous aerogel particles for pulmonary drug delivery. Aerogels, the lightest processed solid materials on Earth, have enormous composition versatility, modularity, and feasibility of industrial scale manufacturing, facts which are behind the fast emergence of aerogels in the drug delivery field. Particularly, the physical properties of the aerogels appear to be very advantageous for mucosal administration routes, such as pulmonary, nasal, or transdermal. This article in fact gives important insights regarding the use of low-density aerogels for pulmonary administration, both for local treatment of lung diseases and for the systemic delivery (transpulmonary) of labile biopharmaceuticals, including those for gene therapy and vaccination.

In conclusion, all of the articles collected in this Research Topic are proof of the increasing knowledge and importance of micro- and nanoencapsulation for drugs and bioactive molecules delivery. Thanks to the advancement on drug discovery and micro- and nanomaterials processing, it is now possible to design and engineering multifunctional tailor-made drug delivery systems for TE, biotechnology and health care.

AUTHOR CONTRIBUTIONS

All authors listed have made a substantial, direct, and intellectual contribution to the work and approved it for publication.

REFERENCES

Canelas, D. A., Herlihy, K. P., and DeSimone, J. M. (2009). Top-down Particle Fabrication: Control of Size and Shape for Diagnostic Imaging and Drug Delivery. *WIREs Nanomed. Nanobiotechnol.* 1, 391–404. doi:10.1002/wnan.40

Chamundeeswari, M., Jeslin, J., and Verma, M. L. (2019). Nanocarriers for Drug Delivery Applications. *Environ. Chem. Lett.* 17, 849–865. doi:10.1007/s10311-018-00841-1

Khademhosseini, A., Vacanti, J. P., and Langer, R. (2009). Progress in Tissue Engineering. *Sci. Am.* 300, 64–71. doi:10.1038/scientificamerican0509-64

Liu, D., Zhang, H., Fontana, F., Hirvonen, J. T., and Santos, H. A. (2017). Microfluidic-assisted Fabrication of Carriers for Controlled Drug Delivery. *Lab. Chip* 17, 1856–1883. doi:10.1039/c7lc00242d

Salerno, A., Cesarelli, G., Pedram, P., and Netti, P. A. (2019). Modular Strategies to Build Cell-free and Cell-Laden Scaffolds towards Bioengineered Tissues and Organs. *J. Clin. Med.* 8, 1816. doi:10.3390/jcm8111816

Silva, E. K., and Meireles, M. A. A. (2014). Encapsulation of Food Compounds Using Supercritical Technologies: Applications of Supercritical Carbon Dioxide as an Antisolvent. *FPH* 4, 247–258. doi:10.5923/j.fph.20140405.06

Wang, Y., Wang, Y., Yang, J., Pfeffer, R., Dave, R., and Michniak, B. (2006). The Application of a Supercritical Antisolvent Process for Sustained Drug Delivery. *Powder Techn.* 164, 94–102. doi:10.1016/j.powtec.2006.03.004

Conflict of Interest: The authors declare that the research was conducted in the absence of any commercial or financial relationships that could be construed as a potential conflict of interest.

Publisher's Note: All claims expressed in this article are solely those of the authors and do not necessarily represent those of their affiliated organizations, or those of the publisher, the editors and the reviewers. Any product that may be evaluated in this article, or claim that may be made by its manufacturer, is not guaranteed or endorsed by the publisher.

frontiers in Bioengineering and Biotechnology

ORIGINAL RESEARCH
published: 18 February 2021
doi: 10.3389/fbioe.2021.639409

Encapsulation of Andrographolide in poly(lactide-co-glycolide) Nanoparticles: Formulation Optimization and *in vitro* Efficacy Studies

Bukola A. Oseni[1,2], Chukwuemeka P. Azubuike[1], Omotunde O. Okubanjo[1], Cecilia I. Igwilo[1] and Jayanth Panyam[2,3]*

[1] Department of Pharmaceutics and Pharmaceutical Technology, University of Lagos, Lagos, Nigeria, [2] Department of Pharmaceutics, University of Minnesota, Minneapolis, MN, United States, [3] School of Pharmacy, Temple University, Philadelphia, PA, United States

OPEN ACCESS

Edited by:
Aurelio Salerno, Independent Researcher, Barcelona, Spain

Reviewed by:
Vincenzo Quagliariello, Istituto Nazionale Tumori Fondazione G. Pascale (IRCCS), Italy
Javier Saurina, University of Barcelona, Spain

****Correspondence:***
Jayanth Panyam
jayanth.panyam@temple.edu

Specialty section:
This article was submitted to Biomaterials, a section of the journal Frontiers in Bioengineering and Biotechnology

Received: *08 December 2020*
Accepted: *19 January 2021*
Published: *18 February 2021*

Citation:
Oseni BA, Azubuike CP, Okubanjo OO, Igwilo CI and Panyam J (2021) Encapsulation of Andrographolide in poly(lactide-co-glycolide) Nanoparticles: Formulation Optimization and in vitro Efficacy Studies. Front. Bioeng. Biotechnol. 9:639409. doi: 10.3389/fbioe.2021.639409

Andrographolide is a potential chemopreventive and chemotherapeutic agent that suffers from poor aqueous solubility. Encapsulation in poly(lactide-co-glycolide) (PLGA) nanoparticles can overcome solubility issues and enable sustained release of the drug, resulting in improved therapeutic efficacy. In this study, andrographolide was encapsulated in PLGA nanoparticles via emulsion solvent evaporation technique. Effect of various formulation parameters including polymer composition, polymer molecular weight, polymer to drug ratio, surfactant concentration and the organic solvent used on nanoparticle properties were investigated. A selected formulation was used to determine the effect of encapsulation in nanoparticles on andrographolide's *in vitro* anticancer efficacy. Nanoparticles formulated using a polymer with 85:15 lactide to glycolide ratio and ethyl acetate as the organic solvent were found to be optimal based on average hydrodynamic particle size (135 ± 4 nm) and drug loading (2.6 ± 0.6%w/w). This formulation demonstrated sustained release of andrographolide over 48 h and demonstrated significantly greater *in vitro* anticancer efficacy compared to free drug in a metastatic breast cancer cell line. These results suggest that additional, more in-depth efficacy studies are warranted for the nanoparticle formulation of andrographolide.

Keywords: andrographolide, poly(lactide-co-glycolide), nanoparticles, formulation optimization, breast cancer

INTRODUCTION

According to GLOBOCAN—a cancer database created by the International Agency for Research on Cancer (IARC), there is an increase in the global incidence and deaths due to cancer. In 2012, approximately 14.1 million new cases and deaths were recorded (Ferlay et al., 2015) rising to about 18.1 million new incidence and 9.6 million deaths in 2018 (Bray et al., 2018; Ferlay et al., 2019).

Breast cancer remains the most common cancer type globally as well as the cause of most deaths associated with cancer in women. In 2018, breast cancer accounted for 24.2% incidence and 15.0% cancer-related deaths in women (Bray et al., 2018; Ferlay et al., 2019).

Chemotherapy is a mainstay treatment modality employed in the management of cancer. Chemotherapeutic agents such as doxorubicin, cisplatin, and paclitaxel have been utilized in the treatment of breast cancer (Takimoto and Calvo, 2005); however, the major drawback includes the development of resistance and life-threatening side effects (due to non-specificity of the chemical agents to cancerous cells) such as cardiac toxicity, hair loss, bone marrow suppression, and gastrointestinal tract lesions, amongst others (Igarashi, 2008; Monsuez et al., 2010; Nussbaumer et al., 2011). An ideal chemotherapeutic agent will exhibit minimal or no side effects while having intrinsic ability to prevent the development of resistance. No such drug currently exists. Research into new therapeutic agents with the aim of overcoming the above limitations therefore continues to be highly relevant. Natural products of plant origin present a source of potential drug molecules (Hosseini and Ghorbani, 2015); many phytochemicals have been shown experimentally to possess cytotoxic activity against various cancer types (Hadjzadeh et al., 2006; Shu et al., 2010; Tan et al., 2011; Wilken et al., 2011; Lè Ne Teiten et al., 2013).

Andrographolide is a labdane diterpenoid derived from the *Andrographis paniculata* plant (Niranjan et al., 2010; Jayakumar et al., 2013). It is the major bioactive compound in the plant and has been found to possess antimicrobial, hepatoprotective, anticancer, anti-inflammatory, and immunostimulatory activities (Jarukamjorn and Nemoto, 2008; Levita et al., 2010; Lim et al., 2012). The cytotoxic activity of this molecule against various cancer types including ovarian, lung, hepatoma, breast, prostate, and colon cancer has been attributed to its ability to act on several cell signaling pathways. Andrographolide exerts direct chemotherapeutic activity via cell cycle arrest at the G0/G1 or G2/M phase. In addition, the drug has also been shown to induce increased production of interleukin 2 (IL-2) and interferon gamma (IFN-γ), which activate cytotoxic T lymphocytes as well as TNF related apoptosis inducing ligand (TRAIL) and death receptors, which eventually leads to apoptosis (Ajaya Kumar et al., 2004; Sheeja and Kuttan, 2007; Mishra, 2016). In addition, the drug inhibits the generation of pro-inflammatory mediators such as tumor necrosis factor alpha (TNF alpha) and angiogenesis mediators such as vascular endothelial growth factor (VEGF) and nitric oxide (NO). In order to combat cancer resistance, it has been suggested that drug molecule(s) activating different death pathways should be utilized. Therefore, a drug molecule such as andrographolide having multiple mechanisms of anticancer activity will be a suitable candidate. Andrographolide, however, has low aqueous solubility, poor bioavailability, and short half-life, resulting in reduced therapeutic activity (Roy et al., 2012; Ghosh et al., 2016). These barriers can be mitigated by the use of a suitable delivery system. In our previous study, andrographolide was formulated into an emulsion, with the particle size in the micrometer range (Oseni et al., 2020). However, microparticles have relatively low cell uptake and poor tissue penetration. Particles in the nanometer size range (nanoparticles) are more advantageous because of their ability to passively accumulate in tumors via the "enhanced permeability and retention effect" (Bharathala and Sharma, 2019).

Nanoparticles are typically fabricated using natural or synthetic polymers such as chitosan, gelatin, albumin, poly(lactide-co-glycolide) (PLGA), polylactide (PLA), and hyaluronan, amongst others (Pal et al., 2011; Bhatia, 2016). They have been used as carriers for the delivery of small molecules, biologic macromolecules, diagnostic agents, and vaccines (Petros and DeSimone, 2010; Bahrami et al., 2017). Encapsulation in nanoparticles can overcome poor aqueous solubility issues because appropriately formulated nanoparticles exhibit excellent suspension stability in biologic fluids (Jacob et al., 2020). PLGA is an FDA-approved synthetic polymer widely used to formulate drug carriers because the polymer is biocompatible and biodegradable, and nanoparticles formulated using PLGA allow for sustained release of various types of payload and can be surface functionalized for targeted delivery applications (Kumari et al., 2010; Danhier et al., 2012; Gentile et al., 2014; Rizvi and Saleh, 2018).

In this study, the encapsulation of andrographolide in PLGA nanoparticles was explored, and the effect of various formulation parameters such as organic solvent, molecular weight of polymer, and lactide:glycolide ratio on key nanoparticle properties such as size, drug loading (DL), and drug release rate were characterized. The formulation of choice with desired physical properties, optimum DL, and *in vitro* release profile was subjected to *in vitro* cytotoxicity studies using LM2 breast cancer cells (a metastatic variant of the MDA-MB-231 triple negative breast cancer parent cells). Our study shows that the optimized nanoparticulate formulation of andrographolide demonstrates greater and more sustained cytotoxic effect vis à vis the free drug.

MATERIALS AND METHODS

Materials

Poly(lactide-co-glycolide) polymer of various lactide:glycolide ratios (50:50, 65:35, 75:25, 85:15, 100:0) as well as of different molecular weights (0.26–0.54, 0.55–0.75, 0.76–0.94, and 0.95–1.20 dL/g inherent viscosity; all of them were 50:50 lactide to glycolide ratio) was purchased from LACTEL (Birmingham AL). Polyvinyl alcohol (87–90% hydrolyzed, MW 30,000–70,000 Da; PVA), flow buffer, RNase, propidium iodide, dimethylsulfoxide (DMSO), phenazine methosulfate (PMS), and andrographolide were purchased from Sigma Aldrich (St. Louis, MO, United States); tween 20 and all organic solvents (HPLC grade) were purchased from Fischer Scientific (Rockford, IL, United States); phosphate buffered saline (PBS), minimum essential medium (MEM), fetal bovine serum (FBS), penicillin, and streptomycin were procured from Gibco; MTS [3-(4,5-dimethylthiazol-2-yl)-5-(3-carboxymethoxyphenyl)-2-(4-sulfophenyl)-2H-tetrazolium] reagent was obtained from Promega; and 0.5%w/v uranyl acetate was procured from VWR (Radnor PA).

Cell Line

The LM2 breast cancer cell line was cultured in MEM supplemented with 10% FBS, 100 UI/mL of penicillin, and 100 μg/mL streptomycin (referred to as complete media).

Methods

Preparation of Andrographolide Nanoparticles

The andrographolide-loaded PLGA nanoparticles were prepared using the emulsion solvent evaporation method (Toti et al., 2011; Kim et al., 2018a). Briefly, PVA was dispersed in DI water to obtain the aqueous phase; andrographolide and PLGA were dissolved in 1 mL of chloroform and 200 μL methanol. The organic phase was added into 8 mL of the PVA solution. The mixture was sonicated at 18–20 W for 5 min over ice bath using a probe sonicator (Sonicator XL, Misonix, Melville, NY). The resulting emulsion was placed on the magnetic stirrer (Super-Nuova, Swedesboro, NJ) for 17 h to remove the organic solvent. The nanoparticle suspension formed was then placed under vacuum for 1 h to remove residual organic solvent. The nanoparticles were recovered via centrifugation (Optima XPN-80 Ultracentrifuge, Beckman Coulter Inc., Fullerton, CA) at 35,000 rpm for 35 min and washed three times with DI water and recovered by ultracentrifugation between each washing step. After the final wash step, nanoparticles were resuspended in DI water, lyophilized (Labconco FreeZone 4.5, Kansas City, MO), and stored at −20°C till further analysis.

The effect of formulation variables (lactide:glycolide ratio, inherent viscosity of polymer, organic solvent, surfactant concentration, and drug to polymer ratio) was evaluated for optimization of the formulation (**Table 1**). Some minor modifications were made in the formulation fabricated using ethyl acetate as the organic solvent because of the lower solubility of the polymer in the solvent. Briefly, andrographolide and PLGA were dissolved in 1.7 mL of ethyl acetate and 330 μL of methanol. The organic phase was added to 8 mL of the aqueous phase. The mixture was sonicated at 18–20 W for 5 min using a probe sonicator, and the emulsion was placed on a magnetic stirrer for 17 h in ambient conditions and further under vacuum for 1 h. Nanoparticles were recovered via centrifugation at 45,000 rpm for 1 h and washed three times with DI water. The nanoparticles

TABLE 1 | Constituents of the formulation showing the parameters investigated to obtain the optimized formulation.

Formulation code	Lactide to glycolide ratio	Inherent viscosity (dL/g)	Organic solvent	Drug to polymer ratio	PVA surfactant concentration
Lactide:glycolide					
A1[a]	50:50	0.55–0.75	Chloroform	1:6	2.5
A2	65:35	0.75	Chloroform	1:6	2.5
A3	75:25	0.55–0.75	Chloroform	1:6	2.5
A4	85:15	0.64	Chloroform	1:6	2.5
A5	100:0	0.55–0.75	Chloroform	1:6	2.5
Organic solvent					
B1[a]	50:50	0.55–0.75	Chloroform	1:6	2.5
B2	50:50	0.55–0.75	Dichloromethane	1:6	2.5
B3[b]	50:50	0.55–0.75	Ethyl acetate	1:6	2.5
B4	50:50	0.55–0.75	Acetone	1:6	2.5
Inherent viscosity					
C1	50:50	0.26–0.54	Ethyl acetate	1:6	2.5
C2[b]	50:50	0.55–0.75	Ethyl acetate	1:6	2.5
C3	50:50	0.76–0.94	Ethyl acetate	1:6	2.5
C4	50:50	0.95–1.20	Ethyl acetate	1:6	2.5
Drug:Polymer					
D1	50:50	0.55–0.75	Ethyl acetate	1:20	2.5
D2	50:50	0.55–0.75	Ethyl acetate	1: 12	2.5
D3[c]	50:50	0.55–0.75	Ethyl acetate	1:8.5	2.5
D4[b]	50:50	0.55–0.75	Ethyl acetate	1:6	2.5
D5	50:50	0.55–0.75	Ethyl acetate	1:4	2.5
Surfactant concentration					
E1	50:50	0.55–0.75	Ethyl acetate	1:8.5	1
E2	50:50	0.55–0.75	Ethyl acetate	1:8.5	2
E3[c]	50:50	0.55–0.75	Ethyl acetate	1:8.5	2.5
E4	50:50	0.55–0.75	Ethyl acetate	1:8.5	3
E5	50:50	0.55–0.75	Ethyl acetate	1:8.5	4
F*	85:15	0.64	Ethyl acetate	1:8.5	2

a, b, and c, same formulation variables; F, optimized formulation.*

were resuspended in DI water, lyophilized, and stored at −20°C for further analysis.

Characterization of Andrographolide PLGA Nanoparticles

Particle size, polydispersity index, and zeta potential

The hydrodynamic diameter and polydispersity index (PI) of nanoparticles were determined via dynamic light scattering (DLS) technique (Delsa^{TM} Nano C, Beckman Coulter, Inc.) (Kim et al., 2018a,b). The zeta potential was determined by measuring the electrophoretic mobility of the particles using Delsa^{TM} Nano C. Nanoparticle suspension in DI water was sonicated for 30 s prior to analyses.

Surface morphology

Morphology of nanoparticles was determined using transmission electron microscopy (TEM) (FEI Tecnai G2 F30) (Grabowski et al., 2015). Nanoparticle suspension (1 mg/mL) in DI water was deposited on a copper grid. A 0.5% w/v uranyl acetate solution was added as negative stain, excess suspension was blotted out using a filter paper, and the grid was air dried and thereafter observed under the electron microscope.

Drug loading and encapsulation efficiency

Standard concentrations of 5–30 μg/mL in methanol of andrographolide reference standard were prepared and placed in a quartz cuvette; the absorbance of the various andrographolide solution prepared was obtained using an ultraviolet (UV) spectrophotometer (Beckman Coulter, Inc.) at 224 nm wavelength. A graph of absorbance against concentration of andrographolide was plotted. The UV method was validated in line with the International Conference on Harmonization guideline (International Conference on Harmonization, 2005).

Andrographolide was extracted from nanoparticles using methanol (1 mg/mL, 1 mL); the methanol was added to the nanoparticles and placed on a rotating shaker for 18 h (Toti et al., 2011). The dispersion was centrifuged at 13,000 rpm for 20 min, dilution of the supernatant was carried out, and the absorbance of the resulting solution was obtained at 224 nm wavelength. The procedure was repeated for nanoparticles devoid of the drug, and its absorbance was subtracted from the absorbance of nanoparticles with drug. This normalized absorbance value was used in calculating the amount of drug in nanoparticles. Drug loading (DL) and encapsulation efficiency (EE) were calculated using equations 1 and 2, respectively.

$$\text{DL}\ (\%\text{w/w}) = \text{weight of andrographolide}\ (\text{mg})\ \text{encapsulated in 1 mg of nanoparticle} \times 100 \quad (1)$$

$$\text{EE}(\%)\frac{\text{Experimental amount of drug per mg nanoparticle}}{\text{Theoretical amount of drug per mg nanoparticle}} \times 100 \quad (2)$$

In vitro Release Study

Drug release from nanoparticles was determined in (PBS, pH 7.4) with 0.2% tween 20 release buffer using a previously reported method (Toti et al., 2011). Nanoparticle suspensions (0.5 mg/mL, 2 mL) in release buffer were transferred into several tubes; the tubes were placed in a water bath shaker at 100 rpm, 37°C. At predetermined intervals (1, 2, 6, 24, 48, and 72 h), three tubes were centrifuged at 13,000 rpm for 10 min. The supernatant was analyzed for drug content via UV spectroscopy at 224 nm.

In vitro Anticancer Efficacy Studies

In vitro acute viability

LM2 breast cancer cells were cultured in complete MEM in an incubator at 37°C and 5% CO_2 until they were 80% confluent. The cells were seeded in a 96-well plate (1×10^4 cells in 100 μL MEM) and allowed to attach overnight. Cells were incubated with various concentrations of andrographolide solution in DMSO or equivalent concentration of nanoparticles (6.25–50 μM) for 48 h. Medium only and medium containing 50 μM of DMSO or PLGA blank nanoparticles were used as controls. At the end of the incubation period, treatments were removed, cells were washed with PBS, and 100 μL of MTS reagent (containing MTS:PMS:MEM) was added and placed in the incubator at 37°C, 5% CO_2 for 1.5 h. Absorbance was determined at 490 nm using a microplate reader (BioTek Instruments, Inc., VT, United States). Percentage cell viability was calculated as a percentage of number of viable cells in each treatment group relative to that in the untreated control, and IC_{50} (concentration required to cause 50% reduction in the number of viable cells) was determined (Yallapu et al., 2010).

To determine the potential effects of DMSO and blank PLGA nanoparticles, the MTS assay was repeated with 20 μM of free drug, drug-loaded nanoformulation (equivalent concentration as free drug treatment), DMSO (equivalent to concentration present in the free drug), blank PLGA nanoparticles (same concentration of particles present in the nanoformulation), and medium (untreated cells). Percent cell viability was obtained for each treatment group to determine the cytotoxic effect of the DMSO solvent and blank nanoparticles on LM2 cells.

In vitro sustained efficacy study

The antiproliferative activity of the formulation and free drug was studied as described by Panyam et al. (Panyam and Labhasetwar, 2004). Briefly, LM2 cells were seeded in a 96-well plate (1×10^4 cells) and allowed to attach overnight. Cell viability via MTS Assay was carried out as described in section "*In vitro* Acute Viability"—this represents Day 0 with no drug treatment. Cells were treated with andrographolide nanoformulation or free drug at 20 μM concentration and medium (control) for 48 h, treatments were removed and replaced with fresh medium. The medium was changed every other day thereafter, and cell viability as a function of time (representing cell proliferation) was determined via MTS Assay.

Cell cycle analysis

The percent cell number in different phases of cell cycle was determined using flow cytometry as described by Rajagopal et al. (2003), with slight modifications. Briefly, LM2 cells were seeded in a 6-well plate (3×10^5 cells in 3 mL complete MEM) and allowed to attach overnight. The media was removed and replaced with FBS free MEM for 24 h to synchronize the cells to the same phase of the cell cycle. The cells were then incubated with free drug, andrographolide nanoformulation (equivalent to 20 μM andrographolide), or complete medium (untreated control) for 48 h. Cells were harvested by trypsinization and recovered via centrifugation at 1,000 rpm for 5 min. Cells were washed with PBS, resuspended in ice cold 70% ethanol, and incubated at 4°C for 30 min to permeabilize the cells. Cells were washed twice with flow buffer and treated with RNase (10 mg/mL) at 37°C for 15 min. The cells were then stained with propidium iodide (0.5 mg/mL) at room temperature for 2 min; cells were washed and resuspended in flow buffer. DNA content was measured using BD LSR II H4760 flow cytometer (BD Biosciences, San Jose, CA, United States), and data were analyzed using the FlowJo software.

Statistical Analysis

Results were reported as mean ± standard deviation (SD) or mean ± standard error of mean (SEM). Statistical differences between groups were determined using one-way analysis of variance (ANOVA) followed by Tukey's *post hoc* test (if applicable) using the Graphpad® 5 Prism software (GraphPad Software, La Jolla, CA, United States). A p-value <0.05 was considered significant.

RESULTS AND DISCUSSION

Andrographolide is a potential therapeutic agent shown to possess several beneficial pharmacological properties such as suppression of proinflammatory molecules—TNFα, inducible nitric oxide synthase (iNOS), and cyclo oxygenase 2 (COX 2); enhanced induction of immune modulator—IL-2 and induction of cell cycle arrest; and apoptosis, thereby eliciting anti-inflammatory, immunomodulatory, and anticancer activities (Pandey and Rao, 2018). The multiple anticancer mechanisms exerted by andrographolide might be useful in preventing resistance associated with conventional chemotherapeutic agents. However, its low aqueous, poor bioavailability, and short half-life results in decreased activity, hence limiting its clinical translation. To overcome these issues, andrographolide nanoformulation was developed using PLGA polymer.

Andrographolide Nanoparticle Preparation and Characterization

The particle size of a formulation determines its *in vivo* disposition, extent of uptake by cells, and consequently its therapeutic efficacy. It is generally accepted that for *in vivo* applications, smaller particle size is preferred. Particles in the 1–3 nm are prone to clearance by renal filtration, while large particles are rapidly cleared by the reticuloendothelial system, thereby reducing their circulation time (Yin Win and Feng, 2005; Sadat et al., 2016). Furthermore, particles greater than 200 nm when administered intravascularly may cause embolization (Hickey et al., 2015). Nanoparticles in the 50–200 nm size have demonstrated the highest percentage of cellular uptake (Yin Win and Feng, 2005). However, nanoparticles that are less than 50 nm suffer from poor payload capacity (Jain and Thareja, 2019). Therefore, our desired particle size was 50 to 200 nm.

Polydispersity Index is a measure of size distribution within a given sample (Danaei et al., 2018); it ranges from 0.0 (a perfect homogenously dispersed size population) to 1.0 (a heterogeneously dispersed system with multiple size populations). Formulations with wide range of particle distribution result in variations in DL, which will in turn lead to variability in drug release, bioavailability, and eventually efficacy (Betala et al., 2018). Formulations with PI ≤ 0.20 are generally acceptable for a polymer-based nanoformulation (Clarke, 2013; Danaei et al., 2018).

Zeta potential predicts the stability of a nano dispersion; higher absolute values (that is, either positive or negative) of zeta potential result in better suspension stability due to the presence of strong repulsive forces that prevent aggregation of particles (Sawant and Dodiya, 2008; Kedar et al., 2010). However, high surface charge on particles has been shown to result in increased macrophage uptake, resulting in increased clearance, reduced bioavailability and therapeutic efficacy (Honary and Zahir, 2013; Sadat et al., 2016). A formulation with decreased absolute value of surface charge and near zero value may have higher circulation time and higher accumulation in the tumor. For example, a previous study suggested that a formulation with particle size of about 150 nm and a slightly negative surface charge tend to accumulate more within tumor (Honary and Zahir, 2013; Sadat et al., 2016).

High DL and EE enables a reduction in the total amount of the formulation (and by extension, the formulation excipients) that needs to be administered for a given dose of the drug, thus preventing excipient-associated toxicity.

In the current study, we investigated the effect of various formulation parameters with the objective of optimizing the key nanoparticle properties discussed above.

Effect of PLGA Lactide:Glycolide Ratio

The effect of varying the lactide to glycolide ratio on various nanoparticle properties is shown in **Table 2**. In general, no correlation was observed between lactide to glycolide ratio and any of the physical properties. The average particle size varied from 194 to 209 nm, while the PI varied from 0.08 to 0.20 and the zeta potential from −13.5 to −23.5 mV. The DL of the formulations was in the 1.0–1.5%w/w range, with EE of 7.5 –11.5%. The 50:50 PLGA was chosen for further studies because that polymer consistently resulted in high DL compared to other polymers.

Effect of Organic Solvents

The effect of organic solvent used on nanoparticle properties is described in **Table 3**. Andrographolide nanoparticles made with 50:50 PLGA polymer and different organic solvents produced formulations having mean particle size in the range of 112 to 240 nm, PI in the range of 0.10 to 0.20, zeta potential of −10.6 to −23.5 mV, DL of 1.5 to 2.3%w/w, and EE of 11.5 to 18.2%.

The chloroform (B1) and acetone (B4) formulations had similar particle size while the dichloromethane (B2) and ethyl acetate (B3) formulations had the largest and smallest particle

TABLE 2 | Physicochemical properties and drug loading of andrographolide formulation with different lactide to glycolide ratio.

Formulation code	Particle size (nm)	Polydispersity index (PI)	Zeta potential (mV)	Drug loading (%)	Encapsulation efficiency (%)
A1	209 ± 3	0.20 ± 0.01	−23.5 ± 3.8	1.5 ± 0.4	11.5 ± 2.9
A2	197 ± 7	0.14 ± 0.03*	−14.4 ± 0.1*	1.0 ± 0.2	7.5 ± 1.5
A3	200 ± 3	0.09 ± 0.01***	−13.5 ± 2.5*	1.1 ± 0.3	9.1 ± 2.8
A4	194 ± 2*	0.10 ± 0.01***	−17.2 ± 5.6	1.3 ± 0.2	9.8 ± 1.7
A5	202 ± 6	0.08 ± 0.02***	−16.2 ± 1.8	1.2 ± 0.1	8.7 ± 1.0

Results are expressed as mean ± SD (n = 3).
**signifies p < 0.05, ***signifies p < 0.001 significant differences with respect to A1. A1, 50:50 PLGA; A2, 65:35 PLGA; A3, 75:25 PLGA; A4, 85:15 PLGA; A5, 100 PLA.*

TABLE 3 | Physicochemical properties and drug loading of andrographolide nanoformulation with different solvent.

Formulation code	Particle size (nm)	Polydispersity index (PI)	Zeta potential (mV)	Drug loading (%)	Encapsulation efficiency (%)
B1	209 ± 3	0.20 ± 0.01	−23.5 ± 3.8	1.5 ± 0.4	11.5 ± 2.9
B2	240 ± 7***	0.13 ± 0.07	−17.3 ± 3.5	1.7 ± 0.3	12.8 ± 2.0
B3	112 ± 6***	0.20 ± 0.02	−11.4 ± 0.9*	2.3 ± 0.3	18.2 ± 2.1
B4	219 ± 8	0.10 ± 0.01*	−10.6 ± 4.7*	2.3 ± 0.8	17.8 ± 6.2

Results are expressed as mean ± SD (n = 3).
**signifies p < 0.05, ***signifies p < 0.001 significant differences with respect to B1 formulation. B1, chloroform; B2, dichloromethane; B3, ethyl acetate; B4, acetone.*

size, respectively. A similar observation of reduced particle size with ethyl acetate organic solvent was demonstrated by Vineeth et al. (Vineeth et al., 2014); this is attributed to the low interfacial tension of ethyl acetate, which allows for the formation of a stable primary emulsion and consequently formation of smaller nanoparticles (Vineeth et al., 2014). All of these formulations except the one that utilized acetone had similar heterogeneity in size distribution; the acetone formulation had a lesser variation in size uniformity than the other three formulations. The chloroform and dichloromethane formulations (having similar values) had higher absolute charge but lower DL and EE than the ethyl acetate and acetone formulations (possessing similar charge, DL, and EE). The differences in the DL for the various formulations could have resulted in the differences in their zeta potential. The higher DL and EE observed in ethyl acetate and acetone formulations could be attributed to the properties of the solvents. Ethyl acetate and acetone have higher aqueous solubility than chloroform and dichloromethane; this could keep the drug soluble in the emulsion during the encapsulation process, allowing more of the drug to be entrapped in the polymer (Pauli et al., 2019). The ethyl acetate and acetone formulations therefore represent the preferred formulations with respect to surface charge, DL, and EE. The ethyl acetate formulation was chosen for further evaluation because of the lower particle size, higher DL, and EE.

Effect of PLGA Molecular Weight

Andrographolide nanoformulations prepared using ethyl acetate organic solvent and 50:50 PLGA polymer of different molecular weights (as measured through polymer inherent viscosities) had a mean particle size in the range of 107–143 nm, PI of 0.10–0.20, zeta potential of −8.1 to −11.4 mV, DL of 1.1–2.3%w/w, and EE of 8.4–18.2% as shown in **Table 4**.

The 6.7–31.3 kDa (C1) and 31.3–57.6 kDa (C2) formulations had similar smaller size than those of 57.6–91.6 kDa (C3) and 91.6–111.5 kDa (C4) formulations. This suggests that higher molecular weight of the polymer results in larger particle size. The increase in size associated with increased molecular weight can be attributed to the formation of a more viscous solution, which provides resistance to particle size breakdown, and thus more energy is required to achieve smaller particle size. All the formulations had similar size distribution and charge except for the 57.6–91.6 kDa formulation, which demonstrated lesser size variation and lower absolute surface charge value. However, this formulation had the lowest DL. The highest DL and EE was observed in the 31.3–57.6 kDa polymer formulation. This polymer was chosen for further studies because of its small particle size, comparable size heterogeneity, and surface charge to the other formulations, highest DL, and EE.

Effect of Drug–Polymer Ratio

Andrographolide formulations with ethyl acetate organic solvent, 50:50 PLGA polymer (molecular weight 31.3–57.6 kDa) and having different drug–polymer ratios had a mean particle size in the range of 112 to 148 nm, PI of 0.18 to 0.21, zeta potential of −8.1 to −11.4 mV, DL of <1.0 to 2.3%w/w, and EE of <9.8 to 23.2% as shown in **Table 5**.

The 1:20 (D1) and 1:12 (D2) drug–polymer ratio formulations were characterized by larger particle size than the 1:8.5 (D3) and 1:4 (D5) formulations, while the 1:6 (D4) formulation had the least particle size. All the formulations comprised particles with similar size distribution and surface charge. The DL of the 1:20 formulation could not be determined because the drug–polymer ratio was so low that the amount of drug encapsulated could not be detected or quantified accurately. Increase in drug-polymer ratio led to an increase in the amount of drug encapsulated until the 1:6 drug–polymer ratio; a further increase did not yield an increase in DL as observed in the 1:4 formulation. An initial increase in EE was observed with higher drug-polymer ratio, however, a further increase to 1:6 drug-polymer ratio led to a

TABLE 4 | Physicochemical properties and drug loading of andrographolide formulation of different PLGA molecular weights.

Formulation code	Particle size (nm)	Polydispersity index–PI	Zeta potential (mV)	Drug loading (%)	Encapsulation efficiency (%)
C1	107 ± 3	0.20 ± 0.03	−10.4 ± 0.9	1.2 ± 0.1***	9.0 ± 0.6***
C2	112 ± 6	0.20 ± 0.02	−11.4 ± 0.9	2.3 ± 0.3	18.2 ± 2.1
C3	139 ± 4***	0.10 ± 0.05*	−8.1 ± 0.8*	1.1 ± 0.2***	8.4 ± 1.4***
C4	143 ± 6***	0.12 ± 0.04	−10.3 ± 0.1	1.5 ± 0.1**	11.6 ± 0.9**

Results are expressed as mean ± SD (n = 3).
**signifies $p < 0.05$, **signifies $p < 0.01$, ***signifies $p < 0.001$ significant differences with respect to C2 formulation. C1, 6.7–31.3 kDa; C2, 31.3–57.6 kDa; C3, 57.6–91.6 kDa; C4, 91.6–111.5 kDa.*

TABLE 5 | Physicochemical properties and drug loading of andrographolide nanoformulation with different drug-polymer ratio.

Formulation code	Particle size (nm)	Polydispersity index–PI	Zeta potential (mV)	Drug loading (%)	Encapsulation efficiency (%)
D1	144 ± 4***	0.18 ± 0.03	−11.3 ± 1.2	Unquantifiable	Unquantifiable
D2	148 ± 5***	0.20 ± 0.02	−8.2 ± 1.2	1.0 ± 0.0***	13.9 ± 0.4
D3	133 ± 2**	0.20 ± 0.03	−10.1 ± 2.0	2.2 ± 0.3	23.2 ± 3.7
D4	112 ± 6	0.20 ± 0.02	−11.4 ± 10	2.3 ± 0.3	18.2 ± 2.1
D5	130 ± 9*	0.21 ± 0.04	−8.1 ± 2.3	1.8 ± 0.3	9.8 ± 1.8**

Results are expressed as mean ± SD (n = 3).
**signifies $p < 0.05$, **signifies $p < 0.01$, ***signifies $p < 0.001$ significant differences with respect to D4 formulation. D1, 1:20; D2, 1:12; D3, 1:8.5; D4, 1:6; D5, 1:4.*

TABLE 6 | Physicochemical properties and drug loading of andrographolide nanoformulation with different PVA concentration.

Formulation code	Particle size (nm)	Polydispersity index–PI	Zeta potential (mV)	Drug loading (%)	Encapsulation efficiency (%)
E1	163 ± 1***	0.17 ± 0.02	−14.1 ± 1.1	2.5 ± 0.2	24.3 ± 1.7
E2	114 ± 4***	0.17 ± 0.04	−11.6 ± 1.3	2.8 ± 0.4*	27.3 ± 3.6
E3	133 ± 2	0.20 ± 0.03	−10.1 ± 2.0	2.2 ± 0.3	23.2 ± 3.7
E4	137 ± 1	0.20 ± 0.03	−12.6 ± 0.3	1.2 ± 0.1**	12.6 ± 0.5**
E5	129 ± 1	0.16 ± 0.07	−13.5 ± 3.5	1.3 ± 0.1**	13.4 ± 0.9**

*Results are expressed as mean ± S.D (n = 3). *signifies $p < 0.05$, **signifies $p < 0.01$, ***signifies $p < 0.001$ significant differences with respect to E3 formulation. E1, PVA 1% w/v, E2, PVA 2% w/v, E3, PVA 2.5% w/v, E4, PVA 3% w/v, E5, PVA 4% w/v.*

decrease in the EE even though the amount of drug encapsulated is comparable to that of 1:8.5 formulation. This implies that an increase in the quantity of drug utilized in the formulation beyond the 1:8.5 ratio will be a waste of the drug material given that there seems to be no appreciable improvement in DL. The 1:8.5 ratio was therefore chosen for further studies due to its high DL and EE, size distribution and surface charge comparable to other formulations, and relatively small particle size (even though the size was greater than the 1:6 formulation—133 nm vs 112 nm, respectively, it was still within the desired 50–200 nm range).

Effect of Surfactant Concentration

Andrographolide formulations with ethyl acetate organic solvent, 50:50 PLGA polymer (molecular weight 31.3–57.6 kDa), 1:8.5 drug–polymer ratio, and different PVA surfactant concentrations had a mean particle size in the range of 114–163 nm, PI of 0.16–0.20, zeta potential of −10.1 to −14.1 mV, DL of 1.2–2.8%w/w, and EE of 12.6–27.3% as shown in **Table 6**.

The 1% (E1) and 2% w/v (E2) PVA formulations had the largest and smallest mean particle size, respectively, and there was no relationship between the size and surfactant concentration. The PVA concentration did not affect the size distribution and surface charge of the particles as similar PI and zeta potential were obtained in all the formulations. An increase in the surfactant concentration resulted in an increase in the amount of drug encapsulated up to the 2% concentration; a further increase caused a reduction in DL and EE as observed for the 2.5% (E3), 3% (E4), and 4% w/v (E5) PVA concentrations. This can be attributed to the ability of the surfactant to improve the solubility of poorly water-soluble substances in aqueous medium (Vinarov et al., 2018); an increase in surfactant concentration will lead to more andrographolide present in the aqueous phase of the emulsion being lost during washing, resulting in lower DL and EE.

The 2% w/v PVA formulation was found to be the most suitable because it had the smallest particle size but with size distribution and surface charge comparable to other formulations and highest drug content and EE.

In vitro Release Studies of Andrographolide Nanoformulation

The release profiles of andrographolide from formulations having different lactide to glycolide ratios, organic solvent, and PLGA molecular weights are represented in **Figures 1A–C**.

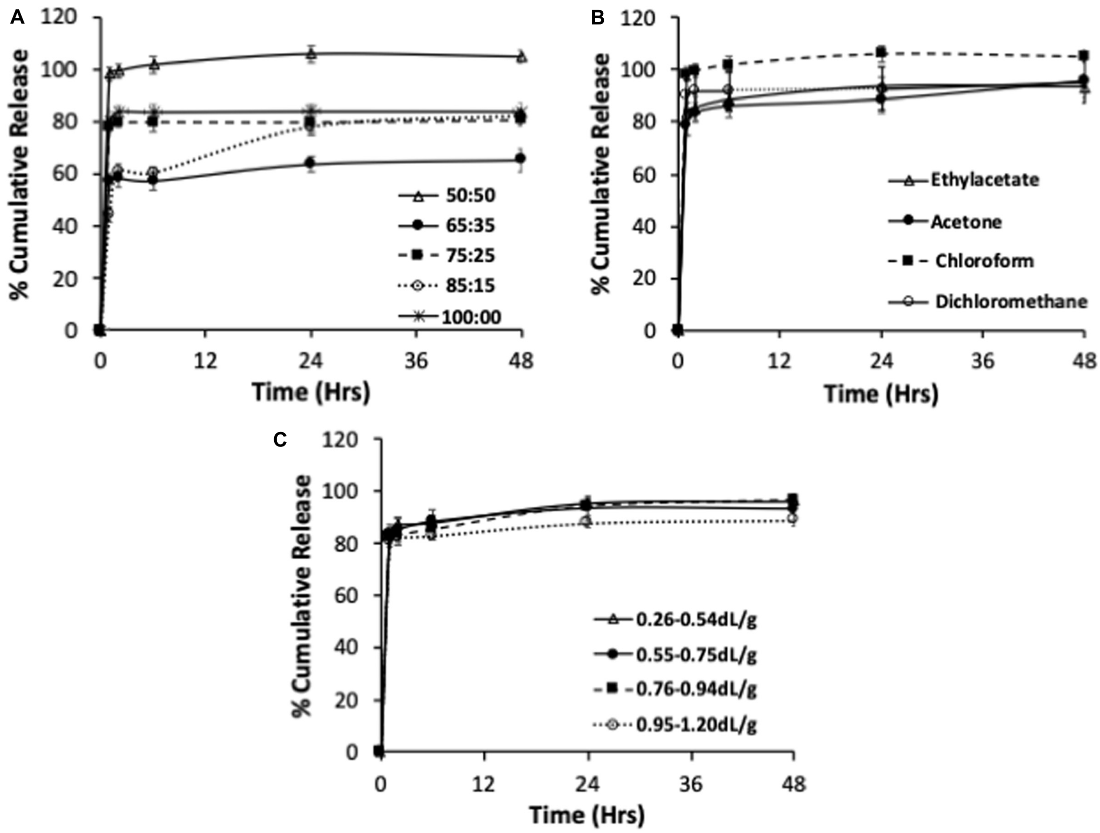

FIGURE 1 | *In vitro* release of andrographolide nanoformulations prepared using different lactide to glycolide ratios **(A)**, organic solvent **(B)**, and PLGA molecular weights **(C)**. Data expressed as mean ± S.D (*n* = 3).

TABLE 7 | Physicochemical properties and drug loading of optimized andrographolide nanoformulation.

Formulation code	Particle size (nm)	Polydispersity index–PI	Zeta potential (mV)	Drug loading (%)	Encapsulation efficiency (%)
Ethyl acetate	135 ± 4***	0.22 ± 0.00***	−11.7 ± 2.4	2.6 ± 0.6*	19.1 ± 4.1***
Chloroform	194 ± 2	0.10 ± 0.01	−17.2 ± 5.6	1.3 ± 0.2	9.7 ± 1.7

Results are expressed as mean ± SD (n = 3).
**signifies $p < 0.05$, ***signifies $p < 0.001$ significant differences with respect to 85:15 chloroform formulation.*

Drug release from polymeric dispersions can occur through several mechanisms including via polymer degradation, desorption from the particle surface followed by diffusion from the bulk, or a combination of these mechanisms (Alhakamy and Md, 2019). PLGA is known to undergo bulk erosion and release of hydrophobic drugs from PLGA matrices occurs through a combination of drug diffusion (dominant during the early phases) and polymer degradation (more dominant during terminal phase) (Makadia and Siegel, 2011). The formulations prepared using polymers of varying lactide to glycolide ratios released their total andrographolide content in 2–48 h (**Figure 1A**). The 75:25, 85:15 PLGA and 100:0 PLA resulted in similar amount of andrographolide release, and this was lower than the 50:50 formulation. The slowest drug release was observed for the 65:35 PLGA formulation. The mechanism(s) underlying this observation is unclear. One possibility is that reduction in the total drug release in the 65:35, 75:25, 85:15, and 100% PLA when compared to the 50:50 formulation might be due to the increase in the hydrophobic content of the polymer conferred by higher lactide content. This might have led to increased affinity of the drug to the polymer, resulting in slower drug release (Park, 1995; Lee et al., 2002). However, both 75:25 PLGA and 100 PLA formulations released their total drug content within 2 h. In contrast, the 65:35 and 85:15 formulations demonstrated a gradual release over 24 and 48 h, with an initial burst release of 57 and 60%, respectively, in 2 h. Thus, the release profile did not directly correlate with the lactide content or the hydrophobicity of the polymer. Differences in particle size and DL for the different formulations could have also contributed to the differences in the observed drug release profiles.

All the formulations prepared using different organic solvents released their andrographolide content between 24 and 48 h (**Figure 1B**). The chloroform and ethyl acetate nanoformulations

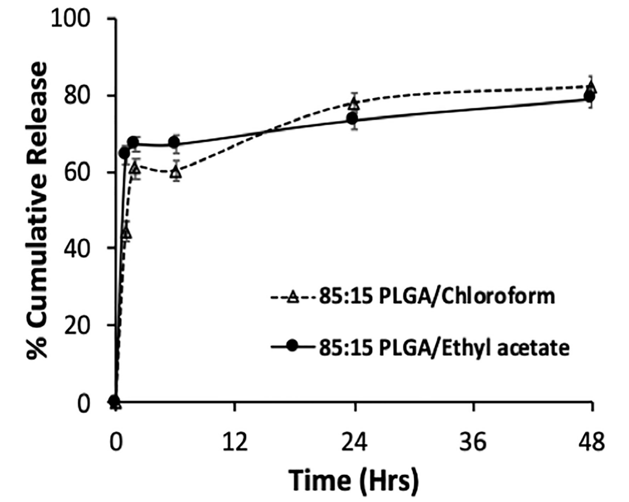

FIGURE 2 | *In vitro* release of andrographolide nanodispersion prepared using 85:15 PLGA polymer and chloroform or ethyl acetate as the organic solvent. Data expressed as mean ± SD (n = 3).

released their drug content in 24 h while the dichloromethane and acetone formulations release their drug over 48 h. All the formulations resulted in a rapid initial burst release of at least 84% within 2 h. The initial rapid release was slightly lower in ethyl acetate and acetone formulations than for dichloromethane and chloroform formulations. The 50:50 PLGA polymer appeared to result in rapid release of the drug content irrespective of the solvent used in the fabrication of the formulation.

The andrographolide nanoformulations obtained from 50:50 PLGA polymer of different molecular weights released their drug content in 24 h (6.7–31.3, 31.3–57.6, and 91.6–111.5 kDa polymeric formulation) to 48 h (57.6–91.6 kDa polymeric formulation) (**Figure 1C**). The andrographolide formulation prepared with a high molecular weight polymer, 91.6–111.5 kDa, demonstrated a slight reduction in the total andrographolide release (88%) when compared with the 6.7–31.3, 31.3–57.6, and 57.6–91,6 kDa formulations that resulted in similar drug release (96, 93, and 97% andrographolide release, respectively). All the 50:50 PLGA inherent viscosity formulations showed a rapid initial release of at least 82% of its drug content within 2 h.

The burst release observed in the formulations can be attributed to both the presence of surface-associated drug and the large surface area of PLGA nanoparticles, which allows for rapid drug diffusion. These physicochemical properties are influenced by factors such as molecular weight of the polymer, polymer concentration and hydrophilicity of the polymer (Mohammadi-Samani and Taghipour, 2015). Therefore, further optimization of the polymer properties may result in a formulation with less burst effect.

Considering that most of the drug was released in few hours in most formulations, the 85:15 PLGA polymer was chosen for the preparation of nanoparticle and subsequent evaluation of its antiproliferative activity on breast cancer cells because it exhibited sustained release potential and high total drug content release (~80% release over 48 h). The andrographolide

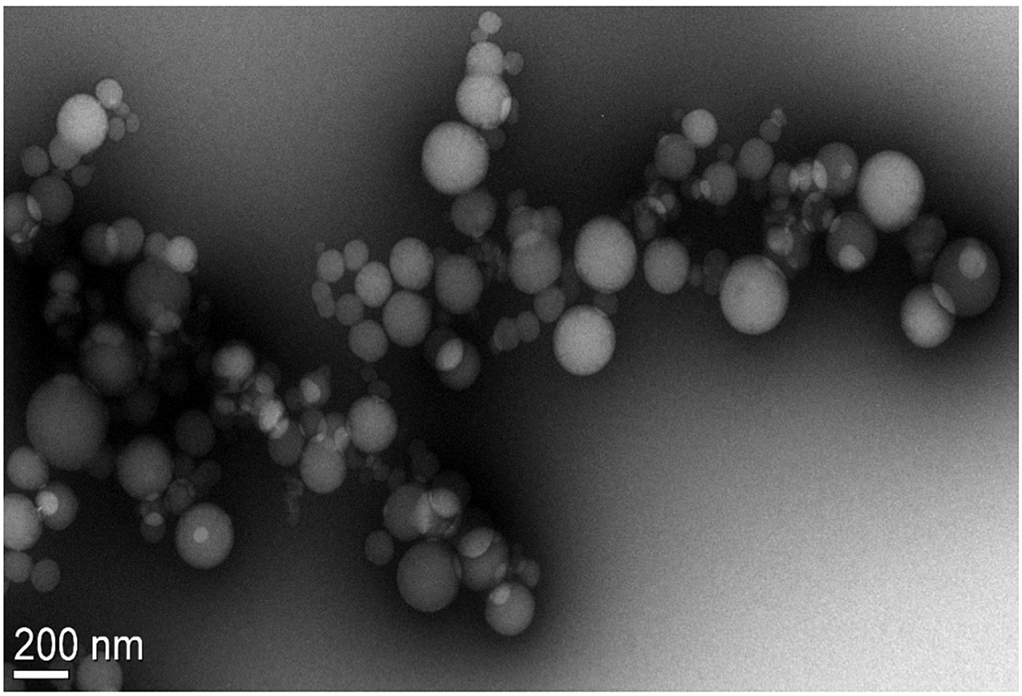

FIGURE 3 | TEM image of Andro 85:15 EA formulation showing discrete spherical particles ranging from 63 to 206 nm in diameter measured using the Gatan® Digital Micrograph software (Pleasanton, CA, United States).

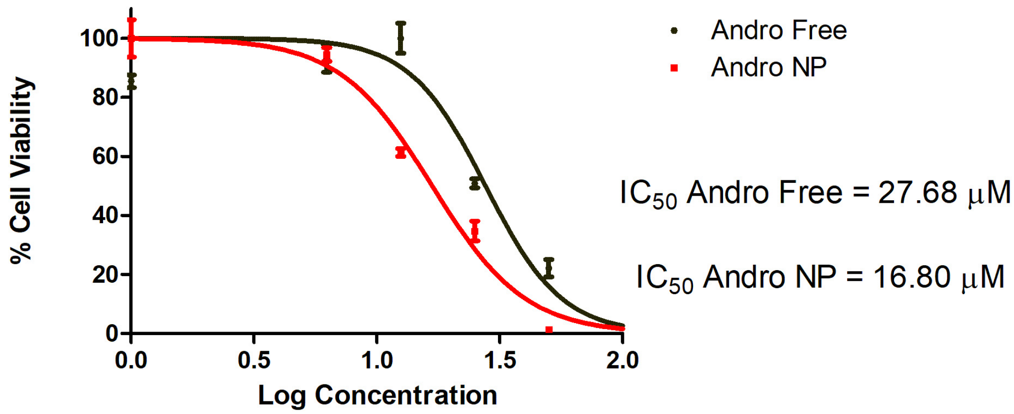

FIGURE 4 | Dose-response curve of andrographolide free drug and nanoformulation on LM2 cells following 48 h treatment. Andro Free, andrographolide free drug, Andro NP, andrographolide nanoformulation.

nanoformulation was made with ethyl acetate as the organic solvent (since it resulted in formulations with reduced particle size and increased DL), 85:15 PLGA polymer, drug-polymer ratio of 1:8.5 and 2% PVA; physicochemical properties, DL, EE, and release of this formulation are shown in **Table 7** and **Figure 2**.

The 85:15 ethyl acetate andrographolide formulation had smaller particle size, increased DL, higher EE, comparable zeta potential, and a more heterogenous particle size distribution when compared with the chloroform formulation. The formulations fabricated using ethyl acetate and chloroform released a total of 79 and 82%, respectively, within 48 h. Both formulations exhibited a similar release pattern, however, more andrographolide was released from the ethyl acetate formulation initially (64 vs 44% at 1 h; 67 vs 60% at 2–6 h for ethyl acetate and chloroform, respectively). This can be attributed to the size of the formulation—the smaller the size, the larger the surface area and the faster the rate of drug release (Rizvi and Saleh, 2018). Based on these desirable properties of smaller size, increased DL, and more sustained *in vitro* release profile, the formulation prepared using the 85:15 PLGA polymer and ethyl acetate as the organic solvent was chosen as the optimized formulation for cell culture studies.

Surface Morphology of Optimized Andrographolide Formulation

A TEM image of the 85:15 PLGA ethyl acetate formulation showed discrete, spherical particles with sizes ranging from 63 to 206 nm (**Figure 3**). This appeared to correlate well with the particle size and size distribution determined using DLS (**Table 7**).

In vitro Anticancer Efficacy Studies With the Optimized Andrographolide Formulation

In vitro Acute Viability

Initial studies evaluated the acute effect of the andrographolide free drug and the nanoformulation on cell viability over 48 h. This study showed that the nanoformulation was better than the free drug (IC_{50} of 27.68 μM for free drug vs 16.80 μM for nanoformulation) as shown in **Figure 4**.

To determine the effect of blank particles and solvent (DMSO), the LM2 cells were treated with the same concentration of DMSO and blank PLGA nanoparticles present in the free drug and nanoformulation treated group. After 48 h, the DMSO and blank PLGA nanoparticle treated cells showed similar viability (99.5% and 100.8%, respectively) as the untreated (100%) group (**Figure 5**). This demonstrates that the DMSO solvent or the PLGA polymer did not have cytotoxic effects on the LM2 cells at the concentration utilized. As in the previous study, nanoformulation was more cytotoxic than the equivalent concentration of the free drug. Untreated cells were used as controls in further experiments since DMSO and blank PLGA nanoformulation demonstrated no cytotoxic activity.

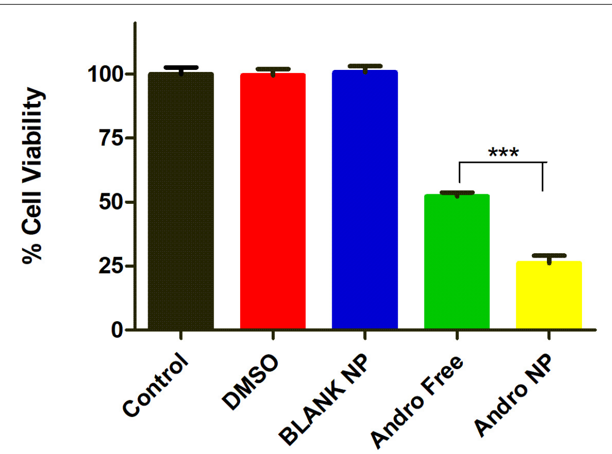

FIGURE 5 | Cell viability of DMSO, blank NP, andrographolide free, and nanoformulation treated LM2 cells showing no cytotoxic effect for DMSO and PLGA nanoparticle at 20 μM after 48 h treatment. Blank NP, blank PLGA nanoformulation, Andro Free, andrographolide free drug, Andro NP, andrographolide nanoformulation.

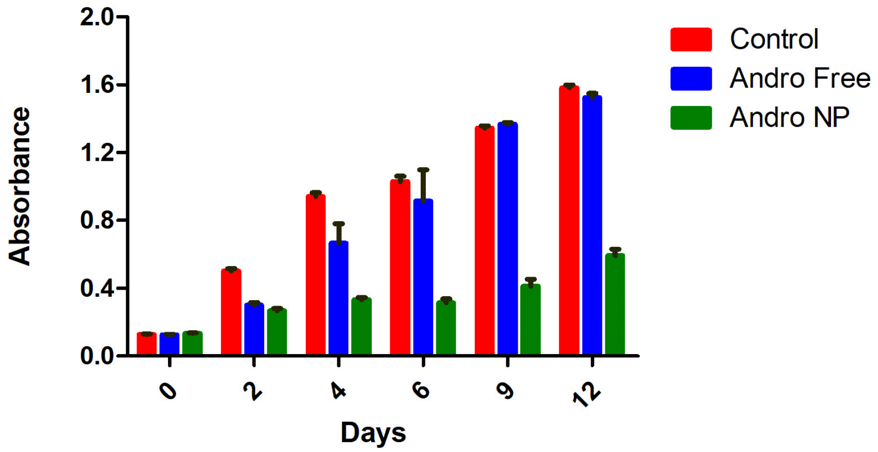

FIGURE 6 | Cell viability of untreated LM2 cells, andrographolide free and nanoformulation post treatment removal showing prolonged cytotoxic effect of andrographolide nanoformulation. Andro Free, andrographolide free drug, Andro NP, andrographolide nanoformulation.

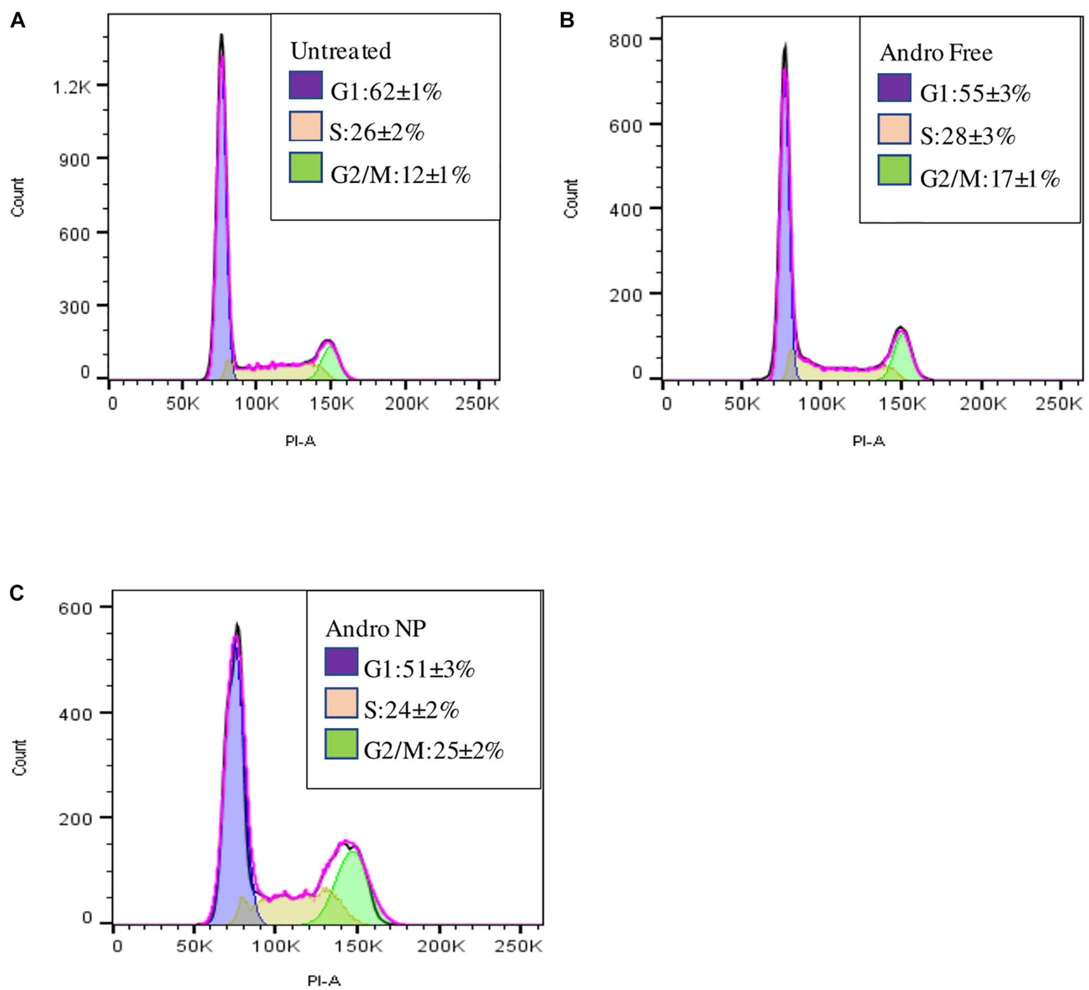

FIGURE 7 | Cell cycle of LM2 cells showing the proportion of cells in the cell cycle phases for untreated cells **(A)**, free andrographolide treated cells **(B)**, and nanoformulation treated cells **(C)**.

In vitro Sustained Efficacy

We then evaluated the effect of nanoformulation on cell viability over 12 days. The cell viability of andrographolide free drug, andrographolide nanoformulation and untreated cells (control) at various time points following treatment removal is shown in **Figure 6**.

Prior to treatment (day 0), the cells seeded showed similar absorbance, indicating similar number of cells present in the different groups. Upon treatment removal, the free drug treatment group showed a transient cytotoxic effect for up to 6 days post treatment. This effect was lost after 6 days, as demonstrated by the presence of similar number of viable cells as in the untreated group. In contrast, the cells treated with andrographolide nanoformulation maintained lower cell numbers upon treatment removal until the 12th day of the study. Thus, the nanoformulation demonstrated a sustained cytotoxic effect. This is in line with the findings of Panyam and Labhasetwar (2004). The sustained inhibition of cell proliferation observed in PLGA nanoformulation in that study was attributed to the sustained intracellular drug levels as opposed to that with the free drug in which intracellular drug levels decreased drastically upon removal of the treatment (Panyam et al., 2002; Panyam and Labhasetwar, 2004).

Cell Cycle Analysis

Cell cycle analysis demonstrated accumulation of cells in the G2/M phase in both andrographolide free drug and nanoformulation compared to that with untreated cells as shown in **Figures 7A–C**.

The andrographolide free drug and nanoformulation treatments resulted in a decrease in the number of cells in the G1 phase with an increase in the G2/M phase when compared to that with the untreated cells. This is in line with a study carried out by Banerjee et al., in which andrographolide elicited cell cycle arrest in the G2/M phase in MDA-MB-231 cells—the parent cell line of LM2 cells used in this study (Banerjee et al., 2016). A higher number of cells were in the G2/M phase for the nanoformulation treated group than in the group treated with the free drug, demonstrating improved therapeutic effect with the nanoformulation.

CONCLUSION

A polymeric nanoformulation of andrographolide was developed, and the effect of different formulation parameters on physicochemical properties and release profile was determined to obtain a formulation with desirable properties. Encapsulation of andrographolide in nanoparticles of approximately 100–150 nm size was achieved using ethyl acetate as the organic solvent. Nanoparticles formulated using 85:15 lactide to glycolide ratio PLGA polymer, drug–polymer ratio of 1:8.5, 2% PVA, and ethyl acetate as the organic solvent were identified as the optimized formulation for andrographolide. This formulation demonstrated enhanced and sustained inhibition of proliferation of triple negative LM2 breast cancer cells when compared to the free drug. This formulation can serve as a template for further development of andrographolide as a potential anticancer agent for clinical use.

DATA AVAILABILITY STATEMENT

The raw data supporting the conclusions of this article will be made available by the authors, without undue reservation.

AUTHOR CONTRIBUTIONS

BO, CA, OO, and JP conceptualized the study. BO and JP developed the methods for the study. BO carried out the experiments, analyzed the data obtained, and wrote the manuscript draft in collaboration with JP. CA, OO, CI, and JP supervised the research and reviewed the manuscript. JP acquired the funds for the study. All authors have read and agreed to the published version of the manuscript.

FUNDING

This research was funded by internal funds from the University of Minnesota.

ACKNOWLEDGMENTS

We thank the United States Department of State for the award of the Fulbright Foreign Student Program fellowship to BO. We also thank Drishti Sehgal and Vidhi Khanna, Department of Pharmaceutics, Panyam Laboratory, University of Minnesota for the cell culture, and flow cytometry training and assistance. The TEM imaging was performed with the assistance of Han Seung Lee and Wei Zhang in the Characterization Facility (University of Minnesota), which receives partial support from NSF through the MRSEC program.

REFERENCES

Ajaya Kumar, R., Sridevi, K., Vijaya Kumar, N., Nanduri, S., and Rajagopal, S. (2004). Anticancer and immunostimulatory compounds from Andrographis paniculata. *J. Ethnopharmacol.* 92, 291–295. doi: 10.1016/j.jep.2004.03.004

Alhakamy, N. A., and Md, S. (2019). Repurposing Itraconazole Loaded PLGA Nanoparticles for Improved Antitumor Efficacy in Non-Small Cell Lung Cancers. *Pharmaceutics* 11, 685–700. doi: 10.3390/pharmaceutics11120685

Bahrami, B., Hojjat-Farsangi, M., Mohammadi, H., Anvari, E., Ghalamfarsa, G., Yousefi, M., et al. (2017). Nanoparticles and targeted drug delivery in cancer therapy. *Immunol. Lett.* 190, 64–83. doi: 10.1016/j.imlet.2017.07.015

Banerjee, M., Chattopadhyay, S., Choudhuri, T., Bera, R., Kumar, S., Chakraborty, B., et al. (2016). Cytotoxicity and cell cycle arrest induced by andrographolide lead to programmed cell death of MDA-MB-231 breast cancer cell line. *J. Biomed. Sci.* 23, 40–55. doi: 10.1186/s12929-016-0257-0

Betala, S., Mohan Varma, M., and Abbulu, K. (2018). Formulation and evaluation of polymeric nanoparticles of an antihypetensive drug for gastroretention. *J. Drug Deliv. Ther.* 8, 82–86. doi: 10.22270/jddt.v8i6.2018

Bharathala, S., and Sharma, P. (2019). ""Biomedical applications of nanoparticles,"," in *Nanotechnology in Modern Animal Biotechnology: Concepts and Applications*, eds S. Maurya and P. K. Singh (Amsterdam: Elsevier), 113–132.

Bhatia, S. (2016). *Nanoparticles Types, Classification, Characterization, Fabrication Methods and Drug Delivery Applications in Natural Polymer Drug Delivery Systems: Nanoparticles, Plants, and Algae*. Switzerland: Springer International, 33–93.

Bray, F., Ferlay, J., Soerjomataram, I., Siegel, R. L., Torre, L. A., and Jemal, A. (2018). Global cancer statistics 2018: GLOBOCAN estimates of incidence and mortality worldwide for 36 cancers in 185 countries. *CA. Cancer J. Clin.* 68, 394–424. doi: 10.3322/caac.21492

Clarke, S. P. (2013). *Development of Hierarchical Magnetic Nanocomposite Materials for Biomedical Applications*. Dissertation/Ph.D, Dublin: Dublin City University.

Danaei, M., Dehghankhold, M., Ataei, S., Hasanzadeh Davarani, F., Javanmard, R., Dokhani, A., et al. (2018). Impact of particle size and polydispersity index on the clinical applications of lipidic nanocarrier systems. *Pharmaceutics* 10, 1–17. doi: 10.3390/pharmaceutics10020057

Danhier, F., Ansorena, E., Silva, J. M., Coco, R., Le Breton, A., and Préat, V. (2012). PLGA-based nanoparticles: An overview of biomedical applications. *J. Control. Release* 161, 505–522. doi: 10.1016/J.JCONREL.2012.01.043

Ferlay, J., Colombet, M., Soerjomataram, I., Mathers, C., Parkin, D. M., Piñeros, M., et al. (2019). Estimating the global cancer incidence and mortality in 2018: GLOBOCAN sources and methods. *Int. J. Cancer* 144, 1941–1953. doi: 10.1002/ijc.31937

Ferlay, J., Soerjomataram, I., Dikshit, R., Eser, S., Mathers, C., Rebelo, M., et al. (2015). Cancer incidence and mortality worldwide: sources, methods and major patterns in GLOBOCAN 2012. *Int. J. cancer* 136, E359–E386. doi: 10.1002/ijc.29210

Gentile, P., Chiono, V., Carmagnola, I., and Hatton, P. V. (2014). An Overview of Poly(lactic-co-glycolic) Acid (PLGA)-Based Biomaterials for Bone Tissue Engineering. *Int. J. Mol. Sci.* 15, 3640–3659. doi: 10.3390/IJMS15033640

Ghosh, P., Mondal, S., and Bera, T. (2016). Preparation and characterization of andrographolide nanoparticles for visceral leishmaniasis chemotherapy: *In vitro* and *in vivo* evaluations. *Int. J. Pharm. Pharm. Sci.* 8, 102–107. doi: 10.22159/ijpps.2016v8i12.14773

Grabowski, N., Hillaireau, H., Vergnaud, J., Tsapis, N., Pallardy, M., Kerdine-Römer, S., et al. (2015). Surface coating mediates the toxicity of polymeric nanoparticles towards human-like macrophages. *Int. J. Pharm.* 482, 75–83. doi: 10.1016/j.ijpharm.2014.11.042

Hadjzadeh, M. A., Tavakol, A. J., Ghorbani, A., and Shakeri, M. (2006). The effects of aqueous extract of Garlic (*Allium sativum* L.) on laryngeal cancer cells (Hep-2) and L929 cells *in vitro*. *J. Med. Plants* 2, 41–48.

Hickey, J. W., Santos, J. L., Williford, J. M., and Mao, H. Q. (2015). Control of polymeric nanoparticle size to improve therapeutic delivery. *J. Control. Release* 219, 536–547. doi: 10.1016/j.jconrel.2015.10.006

Honary, S., and Zahir, F. (2013). Effect of zeta potential on the properties of nano-drug delivery systems - A review (Part 2). *Trop. J. Pharm. Res.* 12, 265–273. doi: 10.4314/tjpr.v12i2.20

Hosseini, A., and Ghorbani, A. (2015). Cancer therapy with phytochemicals: evidence from clinical studies. *Avicenna J. phytomedicine* 5, 84–97. doi: 10.22038/ajp.2015.3872

Igarashi, E. (2008). Factors affecting toxicity and efficacy of polymeric nanomedicines. *Toxicol. Appl. Pharmacol.* 229, 121–134. doi: 10.1016/j.taap.2008.02.007

International Conference on Harmonization (2005). *ICH Topic Q 2 (R1) Validation of Analytical Procedures: Text and Methodology Step 5 Note for Guidance on Validation of Analytical Procedures: Text and Methodology (CPMP/ICH/381/95) Approval by CPMP November 1994 Date for coming into operation*. Available online at: http://www.emea.eu.int [Accessed October 30, 2020]

Jacob, S., Nair, A. B., and Shah, J. (2020). Emerging role of nanosuspensions in drug delivery systems. *Biomater. Res.* 24, 1–16. doi: 10.1186/s40824-020-0184-8

Jain, A. K., and Thareja, S. (2019). *In vitro* and *in vivo* characterization of pharmaceutical nanocarriers used for drug delivery. *Artif. Cells Nanomed. Biotechnol.* 47, 524–539. doi: 10.1080/21691401.2018.1561457

Jarukamjorn, K., and Nemoto, N. (2008). Pharmacological aspects of Andrographis paniculata on health and its major diterpenoid constituent andrographolide. *J. Heal. Sci.* 54, 370–381. doi: 10.1248/jhs.54.370

Jayakumar, T., Hsieh, C.-Y., Lee, J.-J., and Sheu, J.-R. (2013). Experimental and Clinical Pharmacology of Andrographis paniculata and Its Major Bioactive Phytoconstituent Andrographolide. *Evid. Based. Complement. Alternat. Med.* 2013, 846740–846755. doi: 10.1155/2013/846740

Kedar, U., Phutane, P., Shidhaye, S., and Kadam, V. (2010). Advances in polymeric micelles for drug delivery and tumor targeting. *Nanomed. Nanotechnol. Biol. Med.* 6, 714–729. doi: 10.1016/j.nano.2010.05.005

Kim, H., Niu, L., Larson, P., Kucaba, T. A., Murphy, K. A., James, B. R., et al. (2018a). Polymeric nanoparticles encapsulating novel TLR7/8 agonists as immunostimulatory adjuvants for enhanced cancer immunotherapy. *Biomaterials* 164, 38–53. doi: 10.1016/j.biomaterials.2018.02.034

Kim, H., Sehgal, D., Kucaba, T. A., Ferguson, D. M., Griffith, T. S., and Panyam, J. (2018b). Acidic pH-responsive polymer nanoparticles as a TLR7/8 agonist delivery platform for cancer immunotherapy. *Nanoscale* 10, 20851–20862. doi: 10.1039/c8nr07201a

Kumari, A., Yadav, S. K., and Yadav, S. C. (2010). Biodegradable polymeric nanoparticles based drug delivery systems. *Colloids Surf. B. Biointerfaces* 75, 1–18. doi: 10.1016/j.colsurfb.2009.09.001

Lè Ne Teiten, M.-H., Gaascht, F., Dicato, M., and Diederich, M. (2013). Anticancer bioactivity of compounds from medicinal plants used in European medieval traditions. *Biochem. Pharmacol.* 86, 1239–1247. doi: 10.1016/j.bcp.2013.08.007

Lee, W., Park, J., Yang, E. H., Suh, H., Kim, S. H., Chung, D. S., et al. (2002). Investigation of the factors influencing the release rates of cyclosporin A-loaded micro- and nanoparticles prepared by high-pressure homogenizer. *J. Control. Release* 84, 115–123. doi: 10.1016/s0168-3659(02)00239-0

Levita, J., Nawawi, A., Mutalib, A., and Ibrahim, S. (2010). Andrographolide: A Review of its Anti-inflammatory Activity via Inhibition of NF-kappaB Activation from Computational Chemistry Aspects. *Int. J. Pharmacol.* 6, 569–576. doi: 10.3923/ijp.2010.569.576

Lim, J. C. W., Chan, T. K., Ng, D. S., Sagineedu, S. R., Stanslas, J., and Wong, W. F. (2012). Andrographolide and its analogues: versatile bioactive molecules for combating inflammation and cancer. *Clin. Exp. Pharmacol. Physiol.* 39, 300–310. doi: 10.1111/j.1440-1681.2011.05633.x

Makadia, K., and Siegel, S. J. (2011). Poly Lactic-co-Glycolic Acid (PLGA) as biodegradable controlled drug delivery carrier. *Polymers* 3, 1377–1397. doi: 10.3390/polym3031377

Mishra, S. K. (2016). Andrographolide and analogues in cancer prevention. *Front. Biosci.* 7:292–304. doi: 10.2741/e732

Mohammadi-Samani, S., and Taghipour, B. (2015). PLGA micro and nanoparticles in delivery of peptides and proteins; problems and approaches. *Pharm. Dev. Technol.* 20, 385–393. doi: 10.3109/10837450.2014.882940

Monsuez, J. J., Charniot, J. C., Vignat, N., and Artigou, J. Y. (2010). Cardiac side-effects of cancer chemotherapy. *Int. J. Cardiol.* 144, 3–15. doi: 10.1016/j.ijcard.2010.03.003

Niranjan, A., Tewari, S. K., and Lehri, A. (2010). Biological activities of Kalmegh (*Andrographis paniculata* Nees) and its active principles-A review. *Indian J. Nat. Prod. Resour.* 1, 125–135.

Nussbaumer, S., Bonnabry, P., Veuthey, J.-L., and Fleury-Souverain, S. (2011). Analysis of anticancer drugs: A review. *Talanta* 85, 2265–2289. doi: 10.1016/j.talanta.2011.08.034

Oseni, B. A., Azubuike, C. P., Okubanjo, O. O., and Igwilo, C. I. (2020). *In Vitro* Cytotoxic Effect of Andrographolide On MDA-MB-231-LM2 Breast Cancer Cells and Its Formulation and Characterization As An Emulsion. *Trop J. Nat. Prod. Res.* 4, 1–7. doi: 10.26538/tjnpr/v4i1.1

Pal, S. L., Jana, U., Manna, P. K., Mohanta, G. P., and Manavalan, R. (2011). Nanoparticle: An overview of preparation and characterization. *J. Appl. Pharm. Sci.* 1, 228–234.

Pandey, G., and Rao, C. H. (2018). Andrographolide: its pharmacology, natural bioavailability and current approaches to increase its content in *Andrographis paniculata*. *Int. J. Complement Alt. Med.* 11, 355–360. doi: 10.15406/ijcam.2018.11.00425

Panyam, J., and Labhasetwar, V. (2004). Sustained Cytoplasmic Delivery of Drugs with Intracellular Receptors Using Biodegradable Nanoparticles. *Mol. Pharm.* 1, 77–84. doi: 10.1021/mp034002c

Panyam, J., Zhou, W. Z., Prabha, S., Sahoo, S. K., and Labhasetwar, V. (2002). Rapid endo-lysosomal escape of poly(DL-lactide-co-glycolide) nanoparticles: Implications for drug and gene delivery. *FASEB J.* 16, 1217–1226. doi: 10.1096/fj.02-0088com

Park, T. G. (1995). Degradation of poly(lactic-co-glycolic acid) microspheres: effect of copolymer composition. *Biomaterials* 16, 1123–1130. doi: 10.1016/0142-9612(95)93575-x

Pauli, G., Tang, W.-L., and Li, S.-D. (2019). Development and Characterization of the Solvent-Assisted Active Loading Technology (SALT) for Liposomal Loading of Poorly Water-Soluble Compounds. *Pharmaceutics* 11, 465–476. doi: 10.3390/pharmaceutics11090465

Petros, R. A., and DeSimone, J. M. (2010). Strategies in the design of nanoparticles for therapeutic applications. *Nat. Rev. Drug Discov.* 9, 615–627. doi: 10.1038/nrd2591

Rajagopal, S., Kumar, R. A., Deevi, D. S., Satyanarayana, C., and Rajagopalan, R. (2003). Andrographolide, a potential cancer therapeutic agent isolated from Andrographis paniculata. *J. Exp. Ther. Oncol.* 3, 147–158. doi: 10.1046/j.1359-4117.2003.01090.x

Rizvi, S. A. A., and Saleh, A. M. (2018). Applications of nanoparticle systems in drug delivery technology. *Saudi Pharm. J.* 26, 64–70. doi: 10.1016/j.jsps.2017.10.012

Roy, P., Das, S., Mondal, A., Chatterji, U., and Mukherjee, A. (2012). Nanoparticle Engineering Enhances Anticancer Efficacy of Andrographolide in MCF-7 Cells and Mice Bearing EAC. *Curr. Pharm. Biotechnol.* 13, 2669–2681. doi: 10.2174/138920112804724855

Sadat, S. M. A., Jahan, S. T., and Haddadi, A. (2016). Effects of Size and Surface Charge of Polymeric Nanoparticles on *in Vitro* and *in Vivo* Applications. *J. Biomater. Nanobiotechnol.* 07, 91–108. doi: 10.4236/jbnb.2016.72011

Sawant, K., and Dodiya, S. (2008). Recent Advances and Patents on Solid Lipid Nanoparticles. *Recent Pat. Drug Deliv. Formul.* 2, 120–135. doi: 10.2174/187221108784534081

Sheeja, K., and Kuttan, G. (2007). Activation of Cytotoxic T Lymphocyte Responses and Attenuation of Tumor Growth *in vivo* by *Andrographis paniculata* Extract and Andrographolide. *Immunopharmacol. Immunotoxicol.* 29, 81–93. doi: 10.1080/08923970701282726

Shu, L., Cheung, K. L., Khor, T. O., Chen, C., and Kong, A. N. (2010). Phytochemicals: cancer chemoprevention and suppression of tumor onset and metastasis. *Cancer Metastasis. Rev.* 29, 483–502. doi: 10.1007/s10555-010-9239-y

Takimoto, C. H., and Calvo, E. (2005). "Principles of oncologic pharmacotherapy," in *Cancer Management: A Multidisciplinary Approach*, eds R. Pazdur, L. D. Wagman, and K. Camphausen (London: Cmp United Business Media), 19.

Tan, W., Lu, J., Huang, M., Li, Y., Chen, M., Wu, G., et al. (2011). Anti-cancer natural products isolated from chinese medicinal herbs. *Chin. Med.* 6, 27–41. doi: 10.1186/1749-8546-6-27

Toti, U. S., Guru, B. R., Hali, M., Mcpharlin, C., Wykes, S. M., Panyam, J., et al. (2011). Targeted Delivery of Antibiotics to Intracellular Chlamydial Infections using PLGA Nanoparticles. *Biomaterials* 32, 6606–6613. doi: 10.1016/j.biomaterials.2011.05.038

Vinarov, Z., Katev, V., Radeva, D., Tcholakova, S., and Denkov, N. D. (2018). Micellar solubilization of poorly water-soluble drugs: effect of surfactant and solubilizate molecular structure. *Drug Dev. Ind. Pharm.* 44, 677–686. doi: 10.1080/03639045.2017.1408642

Vineeth, P., Rao Vadaparthi, P. R., Kumar, K., Babu, B. D. J., Veerabhadra Rao, A., and Suresh Babu, K. (2014). Influence of organic solvents on nanoparticle formation and surfactants on release behaviour in-vitro using costunolide as model anticancer agent. *Int. J. Pharm. Pharm. Sci.* 6, 638–645.

Wilken, R., Veena, M. S., Wang, M. B., and Srivatsan, E. S. (2011). Curcumin: A review of anti-cancer properties and therapeutic activity in head and neck squamous cell carcinoma. *Mole. Cancer* 10, 1–19. doi: 10.1186/1476-4598-10-12

Yallapu, M. M., Gupta, B. K., Jaggi, M., and Chauhan, S. C. (2010). Fabrication of curcumin encapsulated PLGA nanoparticles for improved therapeutic effects in metastatic cancer cells. *J. Colloid Interface Sci.* 351, 19–29. doi: 10.1016/j.jcis.2010.05.022

Yin Win, K., and Feng, S. S. (2005). Effects of particle size and surface coating on cellular uptake of polymeric nanoparticles for oral delivery of anticancer drugs. *Biomaterials* 26, 2713–2722. doi: 10.1016/j.biomaterials.2004.07.050

Conflict of Interest: The authors declare that the research was conducted in the absence of any commercial or financial relationships that could be construed as a potential conflict of interest.

frontiers in Bioengineering and Biotechnology

ORIGINAL RESEARCH
published: 10 March 2021
doi: 10.3389/fbioe.2021.644793

Check for updates

Encapsulation of Fullerenes: A Versatile Approach for the Confinement and Release of Materials Within Open-Ended Multiwalled Carbon Nanotubes

Stefania Sandoval* and Gerard Tobias*

Institut de Ciència de Materials de Barcelona (ICMAB-CSIC), Campus UAB, Barcelona, Spain

OPEN ACCESS

Edited by:
Aurelio Salerno,
Independent Researcher, Barcelona, Spain

Reviewed by:
Martina Salzano De Luna,
University of Naples Federico II, Italy
Silvana Fiorito,
Institute of Traslational Pharmacology, Italian National Research Council, Italy

****Correspondence:***
Stefania Sandoval
ssandoval@icmab.es
Gerard Tobias
gerard.tobias@icmab.es

Specialty section:
This article was submitted to Biomaterials, a section of the journal Frontiers in Bioengineering and Biotechnology

Received: *21 December 2020*
Accepted: *17 February 2021*
Published: *10 March 2021*

Citation:
Sandoval S and Tobias G (2021) Encapsulation of Fullerenes: A Versatile Approach for the Confinement and Release of Materials Within Open-Ended Multiwalled Carbon Nanotubes. Front. Bioeng. Biotechnol. 9:644793. doi: 10.3389/fbioe.2021.644793

We have employed fullerenes as versatile agents to "cork" the open tips of multiwalled carbon nanotubes (MWCNTs), and as promoting species for the release of the inorganic material filled within the nanotubes' cavities. High Z element compounds, namely, PbI_2, ZnI_2, and CeI_3, were chosen to easily determine the presence of the filler inside the hosting nanotubes by transmission electron microscopy (TEM). Fullerenes can isolate inorganic nanostructures confined within the hollow cavities of MWCNTs, which allows the removal of the external material remnant after the filling. Otherwise, taking advantage of the affinity of fullerenes with selected solvents, we have confirmed the ability of the C_{60} molecules to promote the displacement of the inorganic guest from the host. We propose two different strategies to trigger the release, employing vapor and liquid phase treatments. The first protocol involves annealing filled MWCNTs in presence of fullerenes (to obtain $C_{60}PbI_2$@MWCNTs) and the subsequent washing of the sample in ethanol under mild conditions. On the other hand, the simultaneous introduction of the C_{60} molecules and the liberation of the guest are produced by a single step wet procedure; the latter being potentially useful when materials that are not stable at high temperatures are employed for filling.

Keywords: carbon nanotubes, fullerenes, filling, corking, release

INTRODUCTION

The wide range of diameters of both single walled (SWCNTs) and multiwalled carbon nanotubes (MWCNTs) make their cavities susceptible of filling with diverse foreign species. The presence and nature of the guest material into the hollow cavities can alter the properties of the hosting template, improving its optical and electrical behavior (del Carmen Giménez-López et al., 2011). Moreover, the confinement into a small area might notably alter the morphology, chemical and structural characteristics of the guest, leading to the formation of new crystalline structures (Marega and Bonifazi, 2014; Sandoval et al., 2019). The hollow cavities of CNTs are useful not only as nanoscale templates for the synthesis of nanocomposites or nanostructures, but also provide an alternative toward isolating functional molecules from external environments, preventing any undesirable interaction with outer species that can modify the properties of the inner material or even produce the degradation of its structure.

Different approaches are employed to fill materials within CNTs, the strategy of synthesis depending on the physicochemical properties and stability of the filler (Ajayan and Iijima, 1993; Ujjal et al., 2010; Kharlamova et al., 2012; Sauer et al., 2012). One dimensional nanowires of a wide number of inorganic compounds (Meyer et al., 2000; Sloan et al., 2002; Philp et al., 2003; Kitaura et al., 2009), metallic nanoparticles (Zhang et al., 2013) and organic species, such as β-carotene (Yanagi et al., 2006), small proteins and biomolecules (Guo et al., 1998), as well as graphene derivatives (Chuvilin et al., 2011) and fullerenes (Yudasaka et al., 2003) can be confined within the inner surface of CNTs. In this way, hybrid materials with diverse characteristics are obtained. These can be used in a myriad of applications, namely, molecular magnets (del Carmen Giménez-López et al., 2011), optoelectronics and photovoltaics (Zhou et al., 2015), battery electrodes (Prem Kumar et al., 2004), catalysis (Pan and Bao, 2008), or biomedicine (Klingeler et al., 2008; Martincic and Tobias, 2015).

However, a key factor for achieving a high filling yield is having CNTs with opened ends (Babaa et al., 2003). Regardless of the method used for the encapsulation of materials inside CNTs, an excess of the filling agent is typically employed (Dujardin et al., 1998; Sloan et al., 2002). Thus, an important amount of material remains outside the nanotubes after the filling step. The filling process is usually reproducible; nevertheless, the presence of external material hinders the quantification of the filling yield (Ballesteros et al., 2009). Furthermore, the removal of the non-encapsulated compounds is necessary to both allow a proper characterization of the sample and to determine how the inner material modifies the properties of the resulting nanocomposite. Otherwise, the properties of the sample cannot be exclusively attributed to the confined species but also to the presence of material external to the CNTs (Brown et al., 2003). An area in which filled carbon nanotubes have been extensively studied is in the biomedicine field (Martincic and Tobias, 2015). However, applications for *in vivo* imaging, drug delivery or tumor targeting require the absence of species remnant from the filling process, usually attached to the outer surface of the CNTs (Ge et al., 2017; Wang et al., 2020).

The easiest procedure to clean external material from the sample involves the use of solvents that, in general, are also capable to dissolve the filling agent. Therefore, unless the encapsulated material has a strong interaction with the CNTs, this approach not only removes the external compounds but also washes out the confined nanostructure, since the ends of the CNTs are opened (Shao et al., 2006). In the case of single walled carbon nanotubes (SWCNTs), it has been reported that the ends can be closed by high temperature treatments (ca. 900°C) (Geng et al., 2004); thus, allowing the removal of the external material whilst preserving the encapsulated compounds (Shao et al., 2006). In case of MWCNTs, closing their ends by high temperature annealing is much more difficult and requires the formation of C-C bonds generating high curvature strain (Mazzoni et al., 1999). Moreover, due to the presence of a larger cavity, a much higher energy and hence, much higher annealing temperatures than SWCNTs are necessary to induce the closing (Martincic et al., 2019). Despite the later protocol demonstrated to be highly efficient for the formation of hermetically closed nanocapsules, a wide range of substances can be decomposed at high temperature and an alternative strategy for sealing up the ends of the nanotubes is required. Capobianchi et al. proposed the impregnation of the open ended filled MWCNTs with a solvent unable to solubilize the filling agent when entering into the hollow cavity by capillarity. Afterward, a washing solvent could be added to the mixture without affecting the inner material (provided both liquids present a low miscibility) (Capobianchi et al., 2007). However, the resulting filling yield is low and the elimination of the protecting solvent could be problematic.

Fullerenes, also called buckyballs, are composed entirely of carbon arranged in hexagonal and pentagonal rings (resembling the classic soccer balls), forming of a hollow sphere (Nessim, 2010). Taking advantage of the strong affinity of fullerenes to enter into the inner cavities of SWCNTs, these molecules have also been employed as corking agents for the containment of materials previously confined within their cavities (Shao et al., 2008; Ren and Pastorin, 2008). Sloan et al. (2000) showed that the presence of fullerenes within the hollow cavity of SWCNTs prevents the introduction of other foreign materials and a pH triggered release of materials from SWCNTs has been achieved using functionalized fullerenes as corks (Luksirikul et al., 2010).

The preparation of C_{60}@SWCNTs; usually called nanopeapods (NPPs) has been widely studied. The interaction mechanisms between the nanotubes and fullerenes involved in the filling process, as well as the behavior of the C_{60} upon encapsulation, have attracted much interest due to the particular structures that can be formed (Warner et al., 2008). Theoretical studies have shown that, under the appropriate energetic conditions, fullerenes could be initially adsorbed onto the external walls prior to encapsulation (Berber et al., 2002), and coalesce after confinement (Tang et al., 1999; Hernández et al., 2003). Besides, SWCNTs with the appropriate diameter are able to perfectly accommodate a single molecule of C_{60} within their two walls (Nikolaev et al., 1997). Thus, their proximity to the inner surface of the nanotubes allows a strong interaction between the buckyball and the nanotube. In case of fullerenes' encapsulation into MWCNTs, both theoretical and experimental studies involve considerations that are more complex and have been barely described. The successful encapsulation and stability of the resulting NPPs might be strongly affected by the diameter of the host, being closely linked not only to the surface interaction of fullerenes and the inner walls of the nanotubes, but also to the configuration adopted by the particles inside the tubes and the mutual interaction between them. It has been reported that wider inner diameters allow the introduction of a larger amount of fullerenes, with accommodations within the MWCNTs cavities ranging from zig-zag chains to irregular arrangements (Fröhlich et al., 2004), tending to agglomerate and cluster (Maggini et al., 2014).

Another important issue usually considered for some of the potential applications of filled nanotubes is the controlled release of the encapsulated material. This process requires breaking energy barriers that can be present due to attractive interactions established between the inner structures and the hosting CNTs after filling (Gao et al., 2003). Releasing and transport mechanisms of liquid (Longhurst and Quirke, 2007) or gaseous substances (Wang, 2009), as well as the assisted removal of the filled materials have been explored (Král and Tománek, 1999; Insepov et al., 2006; Longhurst and Quirke, 2007; Panczyk et al., 2013). Considering the high affinity and strong intermolecular forces that can exist between fullerenes and CNTs, theoretical studies on the capability of fullerenes for displacing different species from the cavities of SWCNTs have been carried out (Xue et al., 2012; Saikia et al., 2013).

Previous studies have demonstrated the enormous potential of MWCNTs as isolating agents and carriers of materials with high interest in the field of biomedicine. Considering the limitations still present when preparing clean and hermetically closed MWCNTs-based nanocapsules, the aim of this study was to evaluate the capability of fullerenes to act not only as corking agents to preserve the integrity of the guest molecules confined within MWCNTs, but also their potential as release agents to promote the controlled liberation of the guest molecules. Two different approaches, involving annealing and wet treatments at room temperature, were tested in order to provide an alternative for obtaining nanocapsules. These approaches are compatible with materials unstable at high temperatures.

MATERIALS AND METHODS

MWCNTs Purification

Chemical vapor deposition MWCNTs (Thomas Swan & Co., Ltd.) were steam treated during 5 h at 900°C, in order to remove amorphous carbon and graphitic nanoparticles and to open their ends (Cabana et al., 2015). Subsequently, the sample was treated with a 6 M HCl solution to remove the metal nanoparticles exposed after the annealing treatment (Ballesteros et al., 2008). The obtained dispersion was filtered, rinsed with distilled water until neutral pH and dried overnight at 60°C.

Filling of MWCNTs by Molten Phase Procedure

PbI_2@MWCNTs were prepared employing 6 mg of purified MWCNTs and 140 mg of PbI_2 (Strem Chemicals Inc.). In an argon-filled glove box both, PbI_2 and MWCNTs were ground together with an agate mortar and pestle until the mixture presented a uniform color. Afterward, the powder was transferred into a silica ampoule, evacuated and sealed under vacuum. The ampoule was placed into a furnace, where it dwelled at 500°C (temperature above the melting point of the salt) during 12 h. Finally, the sample was cooled at room temperature and then it was opened under inert atmosphere. ZnI_2@MWCNTs and CeI_3@MWCNTs were prepared following the same protocol; the temperature of treatment being selected taking into account the melting point of the selected materials. The ZnI_2/MWCNTs mixture (300 mg/10 mg) was annealed at 475°C, while the CeI_3@MWCNTs resulted from annealing 10 mg of MWCNTs in presence of 200 mg of CeI_3 at 900°C. Both ZnI_2 (99.99%) and CeI_3 (99.99%) were purchased from Sigma-Aldrich.

C_{60} Corking Into the Opened-Ended Metal Halide Filled MWCNTs (MX@MWCNTs)

C_{60} close-ended filled MWCNTs were prepared by grinding both, fullerenes (C_{60}, 99.5%, SES Research) and MWCNTs previously filled with PbI_2, ZnI_2 or CeI_3. Different ratios of filled CNTs and fullerenes were employed. The corking was carried out by annealing the mixture at 400°C, during 48 h, under vacuum (inside a silica ampoule) (Hirahara et al., 2000).

Washing of the External Material

The material deposited on the external surface of the MWCNTs was removed by sonicating the samples (5 mg) in 30 mL of distilled water for 15 min and refluxing during 24 h at 100°C. Finally, the sample was recovered by filtration employing a 0.2 μm polycarbonate membrane, rinsed with distilled water and the procedure was repeated. The recovered powder was dried at 60°C overnight.

PbI_2 Release Assisted by Ethanol/C_{60}

Protocol 1

Five-mg of the $C_{60}PbI_2$@MWCNTs sample were suspended in absolute ethanol (Panreac, max 0.02% water) and dispersed by sonication during 15 min. Afterward, the mixture was refluxed (80°C) during 16 h, cooled down and filtered using a 0.2 μm polycarbonate membrane. After drying overnight at 60°C, the material was characterized using TEM.

Protocol 2

Five-mg of fullerenes were suspended in pure ethanol and dispersed by sonication during 30 min. Afterward, 5 mg of the PbI_2@MWCNTs were added to the dispersion and sonicated for 15 min. The mixture was refluxed (80°C) during 16 h, cooled down and filtered using a 0.2 μm polycarbonate membrane. After drying overnight at 60°C, the material was characterized using TEM.

Characterization

The filling of the samples was evaluated by means of transmission electron microscopy (TEM) and scanning electron microscopy SEM, while their composition was determined by energy dispersive X-ray (EDX) analysis. TEM images were acquired using a JEOL Jem 1210 electron microscope operating at 120 kV and a FEI Tecnai G2 F20 microscope (High resolution microscope-HRTEM) operating at 200 kV. SEM images and EDX analyses were performed using a QUANTA FEI 200 FEG-ESEM microscope operating at 20.0 kV. Samples were prepared by sonication of a small amount of the powder in anhydrous hexane (95%, Sigma-Aldrich). Afterward, the solution was placed, dropwise, onto a lacey carbon support grid and let to dry. Diffraction patterns were obtained in a Siemens D5000 diffractometer (Kα Cu). 2θ values were acquired at 0.02° intervals between 5° and 60°. Raman spectra were recorded using a Horiba

Jobin Yvon operating at 532 nm and using 50 × objective. Acquisition time was set to 10–30 s and laser power to 0.5 mW. Spectra were recorded in the 100–3,000 cm^{-1} range, from different spots of the powdered samples.

RESULTS

Microscopic Analysis of PbI_2 Filled MWCNTs and C_{60} Corked PbI_2@MWCNTs

The inorganic material present inside the cavities of MWCNTs is easily distinguishable from CNTs when these are observed by TEM, which was employed to verify the encapsulation of PbI_2 within the MWCNTs cavities. **Figure 1A** shows a low magnification image of PbI_2@MWCNTs. A magnification of an open-ended PbI_2@MWCNTs is observed in the inset. A SEM image of the PbI_2@MWCNTs is included in **Figure 1B**, where the characteristic tubular morphology of the hosting nanostructure along with external PbI_2 can be observed. The corresponding EDX spectrum is shown in **Figure 1C**. A *ca.* 3.5 Å lattice spacing was calculated from intensity profile analysis in selected regions of PbI_2 filled MWCNTs [(**Figure 1D**), HRTEM micrographs].

400°C treatment of an open ended PbI_2@MWCNTs/fullerenes mixture lead to the formation of $C_{60}PbI_2$@MWCNTs (**Figures 2A,B**). The presence of the inner nanorods within the hosting nanotubes has not been affected by the interaction of fullerenes with the sample, despite their affinity with the CNTs. TEM micrographs show that fullerenes are located in the inner surface of the nanotubes, blocking the open ends. Besides, a large number of C_{60} molecules are observed along the external walls of the hosts.

Washing and Release Strategies

After multiple washings of open-ended PbI_2 filled MWCNTs with hot water, the inorganic salt was removed from the inner surface of the hosting nanotubes (**Supplementary Figure 1**). Otherwise, fullerenes present in the tips avoid releasing the PbI_2 when $C_{60}PbI_2$@MWCNTs are subjected to the same protocol of washing (**Figure 3**). The proposed corking approach demonstrated to be versatile since allows the successful confinement of other inorganic salts, namely, ZnI_2 and CeI_3, after washing the external material from the outer surface of the nanotubes (**Supplementary Figure 2**).

When ethanol, a solvent with affinity to the fullerenes was employed for washing (16 h under reflux), the C_{60} molecules located in the tips of the MWCNTs act as adjuvants of the displacement of the inorganic salt filled into the nanotubes ($C_{60}PbI_2$@MWCNTs sample). In absence of fullerenes (PbI_2@MWCNTs) the release of PbI_2 from the hosting nanotubes in presence of ethanol was not observed (**Figures 4A,B**). Removal of PbI_2 from PbI_2@MWCNTs was also triggered using a liquid phase approach under mild conditions of reaction. By suspending the sample in a C_{60} ethanol dispersion and refluxing, the inorganic salt was removed from the inner surface of the nanotubes and replaced by the fullerenes present in the medium (**Figures 6A,B**).

XRD and Raman Spectroscopy of Filled Samples

XRD analysis of $C_{60}ZnI_2$@MWCNTs (**Supplementary Figure 3**) shows the characteristic diffraction pattern of C_{60}, which signal induces the attenuation of the broad diffraction peak of MWCNTs (002, 2θ∼26°). Raman spectra (**Supplementary Figure 4**) of samples resulting of wet treatment using EtOH/C_{60} mixtures of both empty and PbI_2 filled MWCNT confirm the presence of fullerenes in the material.

DISCUSSION

End Corking of MWCNTs With Fullerenes

PbI_2 is an interesting compound because is a large bandgap 2D layered material that has potential for semiconductor applications (Sinha et al., 2020) and, bearing heavy elements, could also be employed as contrast agent (Hernández-Rivera et al., 2017). PbI_2 along with the other metal halides (ZnI_2,

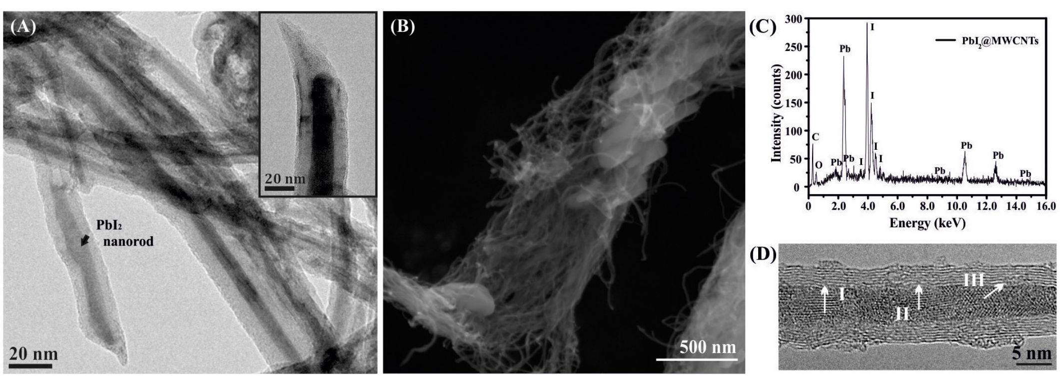

FIGURE 1 | (A) TEM of PbI_2 filled MWCNTs after molten phase capillary wetting synthesis; the inset shows a detail of an open ended PbI_2@MWCNT. **(B)** SEM showing the morphology of the sample and **(C)** the corresponding EDX spectrum, confirming the presence of both Pb and I in the sample. **(D)** HRTEM of a MWCNT filled with polycrystalline PbI_2; d-spacings of PbI_2 determined *via* intensity profiles along the indicated white lines correspond to I = 3.5 Å, II = 3.3 Å, and III = 3.5 Å.

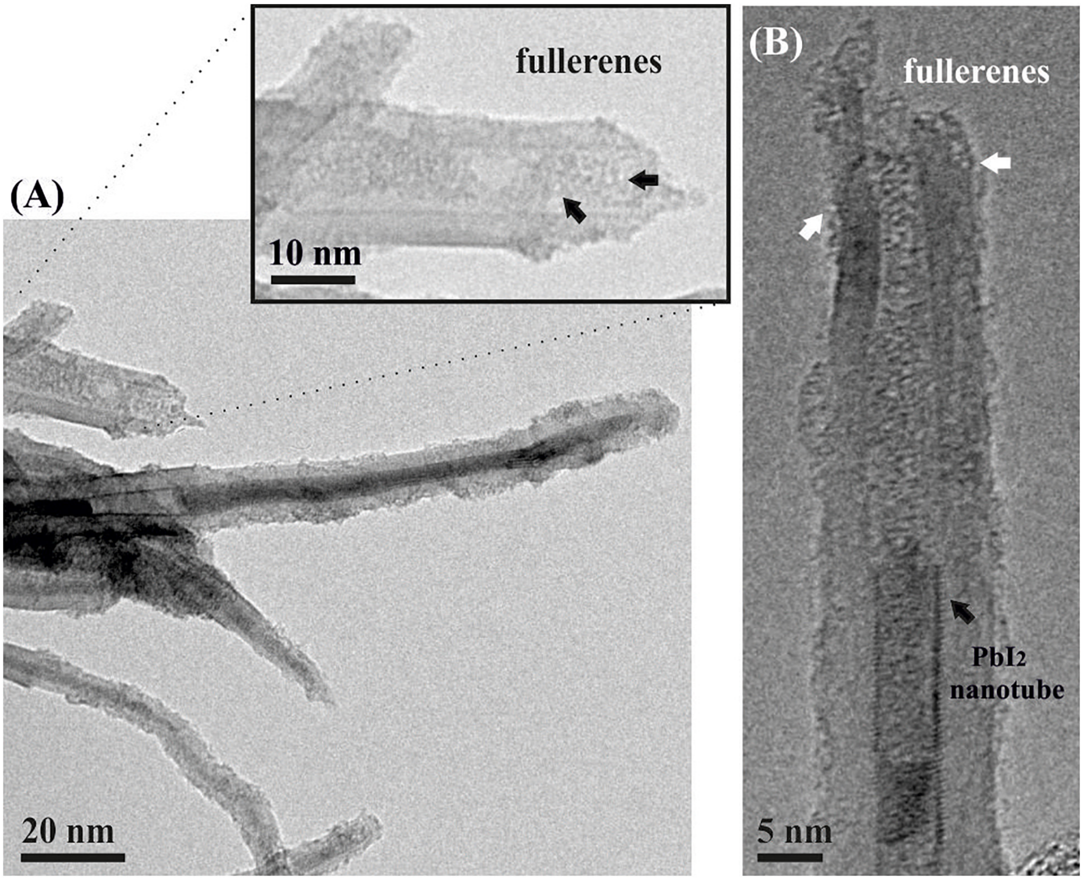

FIGURE 2 | (A) $C_{60}PbI_2$@MWCNTs sample. A magnified area of an open ended CNT containing fullerenes is presented. **(B)** PbI_2 filled nanotube with fullerenes corking and isolating the inorganic nanostructure; fullerenes can be also seen on the external walls of CNTs (pointed by white arrows).

CeI_3) employed in this study are layered structures, which can lead to the formation of tubular van der Waals heterostructures when confined within the cavities of MWCNTs (Cabana et al., 2014; Sandoval et al., 2017; Sandoval et al., 2018). Besides, since the contrast in TEM imaging is highly dependent on the atomic/molecular weight of the material, PbI_2 was chosen as a model compound (both elements, Pb and I, present a high atomic number) for filling MWCNTs. Thus, the inner grown nanorods composed by the relatively heavy atoms are easily distinguished from the CNTs when characterized by TEM (**Figure 1A**). SEM confirms that the morphology of MWCNTs remains unaltered after the filling experiment and also reveals the presence of PbI_2 crystals external to the CNTs (**Figure 1B**). As expected, EDX analysis (**Figure 1C**) indicates the presence of Pb and I in the sample. Different d-spacings of the PbI_2 crystallites present inside the MWCNTs cavities have been measured from the HRTEM images (**Figure 1D**). A spacing of *ca.* 3.5 Å is observed, in agreement with crystallographic data of bulk PbI_2 [(002) reflection plane].

PbI_2 filled MWCNTs were employed to evaluate the capability of fullerenes of blocking the open ends of CNTs. For this purpose, $C_{60}PbI_2$@MWCNTs were prepared from PbI_2@MWCNTs by a vapor-phase method at 400°C, during 48 h (Tang et al., 1999). Temperatures between 300 and 450°C are considered to provide the energy necessary for the formation of NPPs (Ajayan and lijima, 1993) and *in situ* studies have detected mobility of fullerenes along the CNTs walls at ca. 325°C, followed by the entrance of fullerenes within the SWCNTs at 350°C (Hernández et al., 2003). Furthermore, the sublimation of C_{60} molecules, which is necessary for the vapor-phase encapsulation (Nikolaev et al., 1997), has been reported to start at relatively low temperatures (ca. 375°C), being favored under low pressure conditions (Sloan et al., 2000). Taking into account that the probability of C_{60} entering into the nanotubes decreases with the temperature, higher temperatures of treatment were not considered for this study. **Figure 2A** shows a low magnification TEM image of a $C_{60}PbI_2$@MWCNTs sample. As shown, the employed protocol allows the introduction of C_{60} molecules in the cavities of the MWCNTs that remained empty after the filling of the tubes with PbI_2. The inset shows a magnification where the presence of fullerenes contained in an open-ended MWCNT is appreciated. Additionally, a HRTEM image of a MWCNT containing both, a PbI_2 nanotube and fullerenes blocking the opened tips is presented in **Figure 2B**. The presence of fullerenes on the external walls of the nanotubes (pointed by white arrow) is in agreement with theoretical calculations

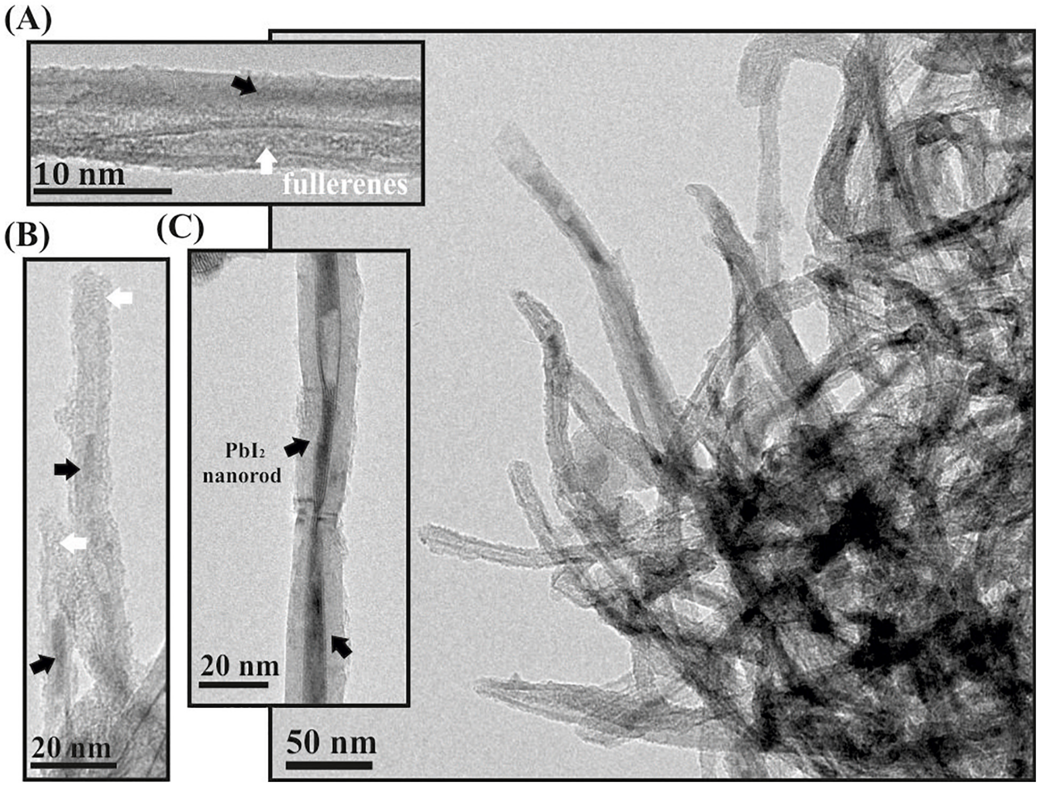

FIGURE 3 | (A–C) show individual nanotubes containing both fullerenes (white arrows) and PbI_2 nanostructures (black arrows) that have not been removed after washing. A low magnification image (right) shows that most of the corked nanotubes maintained their filling after washing.

that suggest an "optimum" trajectory of the C_{60} molecules when approaching to the CNTs. According to the studies of Berber et al. (2002), fullerenes may be initially physisorbed on the outer wall of the nanotube and subsequently diffuse along the CNT surface. In this way, the corking process involves an initial non-covalent functionalization of the CNTs walls with the C_{60} molecules before the filling. Afterward, fullerenes can displace either through the defects of the CNTs walls or *via* the opened tips, establishing strong electrostatic interactions with the inner surface of the nanotubes.

The most common methodology for the elimination of the excess of material present on the external surface of the hosting nanotubes consists in carrying out consecutive washings with a specific solvent, capable of solubilizing the guest specimens (Kierkowicz et al., 2017). PbI_2 is relatively soluble in hot water, which can be employed to remove the external material present after the synthesis of PbI_2@MWCNTs. Nevertheless, since the ends of the CNTs are opened, the process also washes out the material contained inside the nanotubes, and only empty MWCNTs can be seen in the sample (**Supplementary Figure 1**). The strong electrostatic interactions existing between the CNTs walls and the C_{60} molecules, combined with the poor solubility of fullerenes in water (Heymann, 1996), produce the corking of the opened tips of the hosting carbon nanotubes. Thus, C_{60} molecules avoid the removal of the inner nanostructures, while the external material is eliminated. For this reason, when the same protocol of washing (using hot water) is employed for the $C_{60}PbI_2$@MWCNTs, an important amount of PbI_2 remained in the hosting cavity of the nanotubes (**Figure 3**). Images of individual CNTs containing PbI_2 nanorods (pointed by black arrows) as well as fullerenes (white arrows) are also included (**Figures 3A–C**). The presence of PbI_2 inside the MWCNTs confirms that fullerenes not only are useful for the isolation of inorganic material inside SWCNTs (Tobias et al., 2010), but also can be employed for the confinement of compounds within tubular carbon nanostructures with larger diameters (MWCNTs).

The optimum amount of fullerenes necessary to cork the CNTs was explored. Since an important amount of filling agent remains outside the nanotubes, the quantification of the CNTs/C_{60} ratio is not possible. However, the amount of fullerenes was selected in function of the mass of CNTs that was initially mixed with the inorganic salt. Thus, the totality of the sample after the endohedral functionalization with PbI_2 (PbI_2@MWCNTs) was mixed in 1:1, 1:2, 1:3, and 1:10 CNTs/C_{60} ratios. After treatment with the lowest amount of fullerenes (1:1 ratio), an important fraction of C_{60} was observed along the CNTs walls and tips. However, the amount of filled nanotubes decreased considerably after washing with water. Meanwhile, when the samples were treated with two and three parts of fullerenes, and subsequently washed, a higher frequency of filled nanotubes was observed. Finally, the treatment with the highest amount of fullerenes (1:10 CNTs/C_{60}) did not show a significant variation

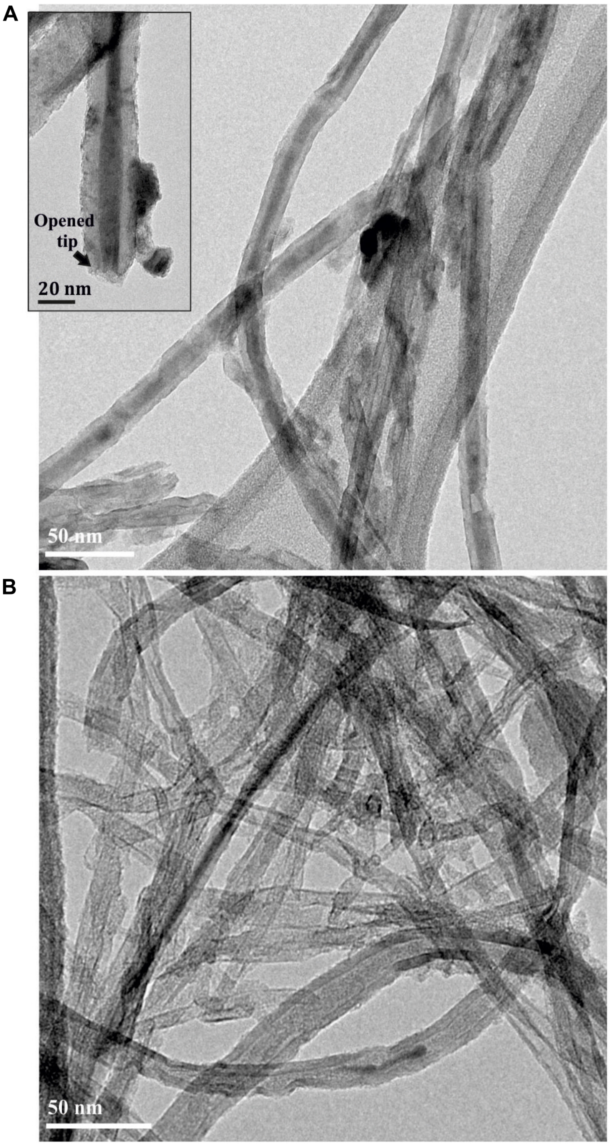

FIGURE 4 | (A) PbI_2@MWCNTs and **(B)** $C_{60}PbI_2$@MWCNTs after washing with anhydrous ethanol at 80°C during 16 h.

in the frequency of PbI_2@MWCNTs, in comparison with the sample annealed in presence of three parts of fullerenes. Since the use of the highest amount of C_{60} did not result in an increase of PbI_2 filled nanotubes after washing, a 1:3 ratio (filled sample: fullerenes) appears to be the highest suitable ratio to be employed for corking.

In order to confirm that the introduction of C_{60} molecules within the filled CNTs is independent on the filling agent, MWCNTs filled with ZnI_2 and CeI_3 were also treated with fullerenes. The solubility of ZnI_2 and CeI_3 in water in normal conditions is considerably high (Lyde et al., 2003-2004), and the external material is thus easily removable by simple washings with aqueous solutions. After washing, the presence of both ZnI_2 and CeI_3 nanorods encapsulated within the MWCNTs is observed (**Supplementary Figure 2**). After XRD analysis of the washed $C_{60}ZnI_2$@MWCNTs (**Supplementary Figure 3**, continuous red line) the 002 diffraction peak (d-space 3.4 Å at ca. 26°), characteristic from MWCNTs is strongly attenuated by the presence of C_{60}, which diffraction pattern can be attributed to the Fm3m fcc lattice (Zhou et al., 2004; Ginzburg et al., 2005). In this way, the use of fullerenes is presented as a useful protocol to isolate inorganic halides grown within MWCNTs, which allows the removal of impurities remnant after the filling process.

Release of Crystalline Structures From MWCNTs Assisted by Fullerenes

The use of fullerenes to assist on the displacement of inorganic encapsulated nanostructures, employing ethanol as promoting solvent, was additionally explored. If the physicochemical properties of fullerenes are considered, employing a solvent with certain affinity with the C_{60} molecules may facilitate their mobility inside the CNTs. These species could act as appropriate replacing agents favoring the displacement of the inorganic nanomaterial and triggering its release from the host. For this purpose, the $C_{60}PbI_2$@MWCNTs were dispersed and refluxed in ethanol during 16 h. PbI_2 is not soluble in ethanol (Lyde et al., 2003-2004) and under normal conditions (in absence of fullerenes), the inorganic PbI_2 confined within the hosting cavity should be retained in the MWCNTs. Thus, PbI_2@MWCNTs was additionally washed with ethanol as control. The obtained samples were characterized employing TEM imaging. **Figure 4A** shows a low magnification TEM image of the PbI_2@MWCNTs after washing with ethanol. As expected, the solvent was unable to remove PbI_2 from the interior of the MWCNTs despite being exposed to the solvent through the opened tips (inset), due to the low solubility of the PbI_2 in ethanol. In contrast, when the sample was previously annealed in presence of fullerenes and subsequently washed using the same conditions, the majority of the inorganic guests were washed out from the MWCNTs (**Figure 4B**), indicating that in this case fullerenes foster the release of the encapsulated compounds.

The entrance of the C_{60} molecules into the nanotubes requires specific energies (Berber et al., 2002), which can be provided either by high temperature treatments (Smith et al., 1998), or by the assistance of a solvent with certain characteristics (Yudasaka et al., 2003). Yudasaka et al. (2003) proposed a successful methodology, which they called "nano-extraction," consisting in the incorporation of fullerenes within SWCNTs, promoted by the suspension of a mixture of both materials in ethanol. This liquid phase technique, leads to the formation of NPPs and takes advantage of the solubility of the C_{60} molecules in the solvent, which although poor, is strong enough to promote the interaction between the fullerenes and the CNTs, provoking the incorporation of the C_{60} molecules into the nanotubes.

One could think that the strong non-covalent interactions (Okada et al., 2001) formed between the C_{60} molecules and the CNTs walls should constitute a highly energetic barrier to be overcome in order to produce the mobility of the fullerenes along the inner cavity of the nanotube. Additionally, electrostatic interactions, such as van der Waal forces, existing between the inorganic nanostructure and the CNTs may be an additional difficulty toward the displacement of the guests outside the nanotubes. Theoretical studies have described the energetic stability of C_{60} encapsulated within a SWCNT (nanopeapod, NPP), including the high binding energies present between the fullerenes and the nanotube (Dubay and Kresse, 2004). The strength and stability of these interactions depends on the symmetry and dimensions of the nanotube. Meanwhile, the release process requires the use of a solvent in which fullerenes are highly soluble (Simon et al., 2007). Fan et al. (2007) studied the effect of the diameter in both the incorporation of fullerenes into SWCNTs and their release assisted by toluene, finding that small diameters of the host favor the encapsulation, while the removal of the encapsulated C_{60} molecules presents the opposite trend. For a system formed by MWCNTs and fullerenes, a theoretical approach would be more complex. In fact, the

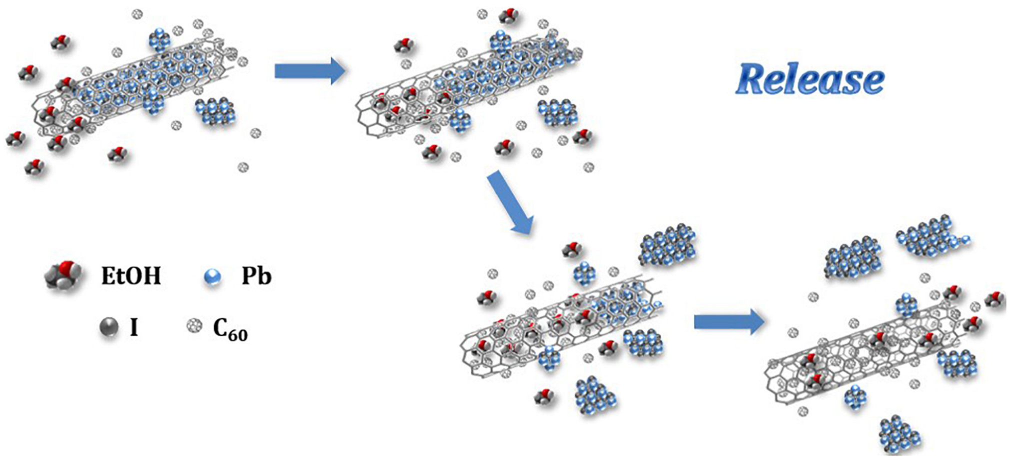

FIGURE 5 | Schematic representation of the fullerene assisted release of PbI_2 from MWCNTs employing ethanol as promoting solvent.

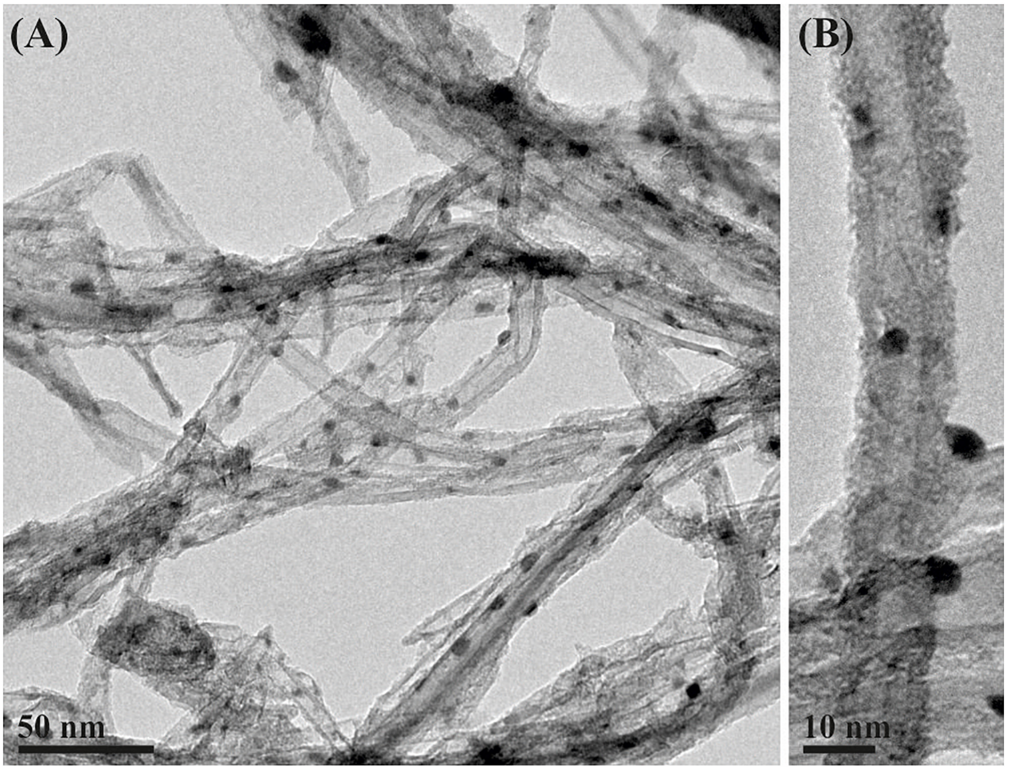

FIGURE 6 | (A) PbI_2@MWCNTs after washing at 80°C during 16 h with a dispersion of fullerenes in absolute ethanol. **(B)** Detail of a PbI_2@MWCNT after washing with an EtOH/C_{60} mixture.

incorporation of fullerenes within MWCNTs has been barely reported (Kondo et al., 2003).

Considering that the diameter and the contact surface between the nanotubes and the C_{60} molecules may play a role in the release of the inorganic material, fullerenes incorporated within the cavities of MWCNTs should possess weaker affinity with the inner walls if compares to SWCNTs. Nevertheless, the established interactions appear to still be strong and the trafficking of the fullerenes along the cavities of the nanotubes may also require a driving force. According to our observations, the attraction forces between the C_{60} molecules and the inner walls are significantly altered when fullerenes are confined within MWCNTs. This is in agreement with theoretical studies on SWCNTs of different dimensions filled with drug molecules, where an increase in the release of the inner material is observed for nanotubes with higher diameters (Saikia et al., 2013).

A graphical representation of the process of release of the inorganic salt from the MWCNTs cavities is presented in **Figure 5**. A competitive replacement of the inorganic salt fraction (bluish crystals) contained within the tube is produced. The high diffusivity of the liquid solvent (EtOH) contributes toward the mobility of the fullerenes within the MWCNT, expelling out the inorganic salt. Additionally, the increase in the contact area between the fullerenes and the CNT wall might enhance the stability of the system by the creation of van der Waal forces between the hosting nanotubes and the C_{60} molecules (Xue et al., 2012).

Considering that many materials susceptible of being filled within the cavities of CNTs are not stable at high temperatures, and those other approaches, different from the molten phase capillary wetting or vapor-phase reactions are necessary for their incorporation inside the nanotubes and the subsequent C_{60} corking; we applied an alternative strategy for the release process. Employing the nano-extraction technique (Yudasaka et al., 2003) to the removal of the inner structure assisted by fullerenes, the process not only was reduced to a single step, but also allowed the insertion of fullerenes at mild conditions, having potential applications to the release of non-thermally stable guest nanostructures. By suspending PbI_2@MWCNTs in a dispersion of fullerenes in pure ethanol and subsequently refluxing the mixture, we have been able to remove the inorganic halide from the inner cavities of the MWCNTs. A low magnification image of the PbI_2 filled MWCNTs after washing with the ethanolic dispersion of fullerenes is presented in **Figure 6A**. Microscopy analyses confirm the replacement of the encapsulated PbI_2 by the C_{60} molecules. The small nanoparticles observed on the outer surface of the nanotubes correspond to the PbI_2 displaced from the cavities of CNTs. The latest protocol results in a higher amount of fullerenes present along the nanotubes. C_{60} molecules were homogeneously distributed through both the external walls of the nanotubes and inside their cavities (**Figure 6B**). Raman spectra of both PbI_2@MWCNTs before and after washing with ethanol are presented in **Supplementary Figure 4**. C_{60} alone and MWCNTs before and after introducing fullerenes within their cavities (by dispersing them in a C_{60}/ethanol mixture) are included for comparison. In all cases (except for C_{60}) the characteristic D (1,341 cm^{-1}, out of plane vibration) and G (1,585 cm^{-1}, stretching of sp^2 bonds from the graphitic

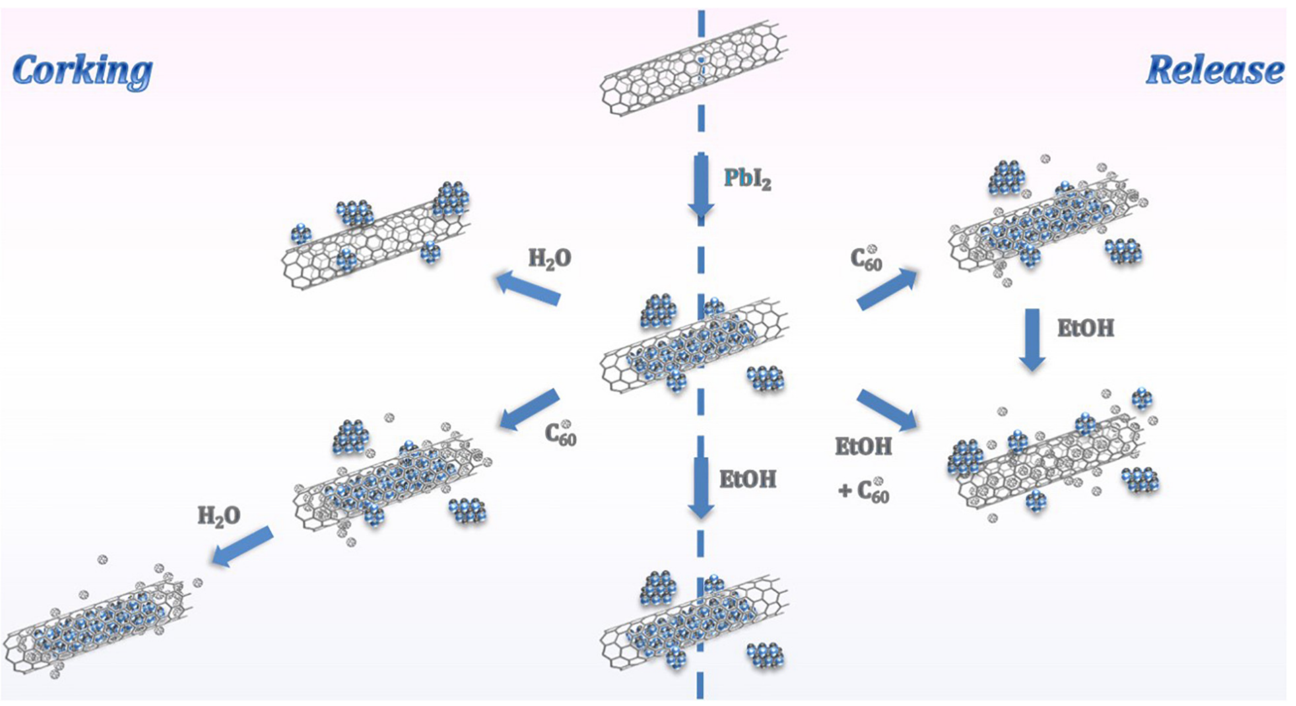

FIGURE 7 | Schematic representation of the mechanisms of corking of MWCNTs and release of the guest material from the hosting nanotubes promoted by fullerenes.

structure) bands of graphitic-based materials are observed. After treatment of both empty and PbI_2 filled MWCNTs in presence of C_{60}, the signal arising from MWCNTs is attenuated and the most prominent peak, corresponding to the pentagonal pinch mode Ag(2) of fullerenes (1,461.7 cm^{-1}) appears, confirming their presence in the analyzed powder.

Figure 7 summarizes the proposed complementary approaches: corking of MWCNTs and release of inner material confined within their cavities. On the one hand, fullerenes can be employed as efficient corking agents of open-ended MWCNTs, which facilitates the removal of external material resulting from the filling process (left). This protocol is useful as long as the cleaning of the filled nanotubes is carried out employing solvents which affinity with the C_{60} molecules is extremely low. On the other hand a versatile protocol for the removal of inorganic material from the inner cavities of MWCNTs is proposed (right). The encapsulation of fullerenes, followed by the ethanol assisted migration of the C_{60} molecules, arises as a potential strategy to trigger the liberation of materials. Otherwise, a liquid phase methodology, involving a single step procedure and mild conditions is suggested for the simultaneous incorporation of fullerenes and release of compounds from the hosting CNTs.

CONCLUSION

We have studied the use of fullerenes, either to isolate inorganic materials present in the cavities of MWCNTs, or to promote the release of the guest structures. Fullerenes act as corking agents, as long as the cleaning of the filled nanotubes is carried out with solvents which affinity with the C_{60} molecules is very low. The presence of fullerenes avoids the release of the encapsulated payloads during the removal of the external non-filled inorganic material remnant after the filling procedure. Otherwise, fullerenes are useful to trigger the liberation of guest structures from the MWCNTs cavities when solvents with considerable affinity to the C_{60} molecules are employed to promote the release. In the present study, ethanol was employed as promoting solvent to favor the mobility of the C_{60} molecules within MWCNTs, assisting the removal of inorganic nanostructures previously grown within the hosting nanotubes. A versatile protocol, involving high temperature treatments and liquid phase techniques has been proposed to induce the liberation of guest structures from the cavities of MWCNTs. We believe that this approach can be employed for a large variety of both organic and inorganic compounds, opening up new possibilities for their containment and controlled release from carbon nanotubes.

DATA AVAILABILITY STATEMENT

The raw data supporting the conclusions of this article will be made available by the authors, without undue reservation.

AUTHOR CONTRIBUTIONS

SS and GT designed the experiments, analyzed the data, and wrote the manuscript. SS performed the experiments. Both authors have given approval to the final version of the manuscript.

FUNDING

The research leading to these results has received funding from the Spanish Ministry of Economy and Competitiveness (MINECO, Spain) through the grant MAT2014-53500-R. ICMAB acknowledges financial support from the Spanish Ministry of Economy and Competitiveness, through the "Severo Ochoa" Programme for Centres of Excellence in R&D (CEX2019-000917-S).

ACKNOWLEDGMENTS

Raman spectroscopy data were acquired in the Centres Científics i Tecnològics- Universitat de Barcelona, Spain.

SUPPLEMENTARY MATERIAL

The Supplementary Material for this article can be found online at: https://www.frontiersin.org/articles/10.3389/fbioe.2021.644793/full#supplementary-material

REFERENCES

Ajayan, P. M., and Iijima, S. (1993). Capillarity-induced filling of carbon nanotubes. *Nature* 361, 333–334. doi: 10.1038/361333a0

Babaa, M. R., Stepanek, I., Masenelli-Varlot, K., Dupont-Pavlovsky, N., McRae, E., and Bernier, P. (2003). Opening of single-walled carbon nanotubes: evidence given by krypton and xenon adsorption. *Surface Sci.* 531, 86–92. doi: 10.1016/s0039-6028(03)00442-4

Ballesteros, B., Tobias, G., Shao, L., Pellicer, E., Nogués, J., Mendoza, E., et al. (2008). Steam Purification for the Removal of Graphitic Shells Coating Catalytic Particles and the Shortening of Single-Walled Carbon Nanotubes. *Small* 4, 1501–1506. doi: 10.1002/smll.200701283

Ballesteros, B., Tobias, G., Ward, M. A. H., and Green, M. L. H. (2009). Quantitative Assessment of the Amount of Material Encapsulated in Filled Carbon Nanotubes. *J. Phys. Chem. C* 113, 2653–2656. doi: 10.1021/jp810717b

Berber, S., Kwon, Y.-K., and Tománek, D. (2002). Microscopic Formation Mechanism of Nanotube Peapods. *Phys. Rev. Lett.* 88:185502.

Brown, G., Bailey, S. R., Novotny, M., Carter, R., Flahaut, E., Coleman, K. S., et al. (2003). High yield incorporation and washing properties of halides incorporated into single walled carbon nanotubes. *Appl. Phys. A* 76, 457–462. doi: 10.1007/s00339-002-2040-1

Cabana, L., Ballesteros, B., Batista, E., Magén, C., Arenal, R., Oró-Solé, J., et al. (2014). Synthesis of PbI_2 Single-Layered Inorganic Nanotubes Encapsulated Within Carbon Nanotubes. *Adv. Mater.* 26, 2016–2021. doi: 10.1002/adma.201305169

Cabana, L., Ke, X., Kepić, D., Oro-Solé, J., Tobías-Rossell, E., Van Tendeloo, G., et al. (2015). The role of steam treatment on the structure, purity and length distribution of multi-walled carbon nanotubes. *Carbon* 93, 1059–1067. doi: 10.1016/j.carbon.2015.06.027

Capobianchi, A., Foglia, S., Imperatori, P., Notargiacomo, A., Giammatteo, M., Buono, T. D., et al. (2007). Controlled filling and external cleaning of multi-wall carbon nanotubes using a wet chemical method. *Carbon* 45, 2205–2208. doi: 10.1016/j.carbon.2007.06.050

Chuvilin, A., Bichoutskaia, E., Gimenez-Lopez, M. C., Chamberlain, T. W., Rance, G. A., Kuganathan, N., et al. (2011). Self-assembly of a sulphur-terminated graphene nanoribbon within a single-walled carbon nanotube. *Nat. Mater.* 10, 687–692. doi: 10.1038/nmat3082

del Carmen Giménez-López, M., Moro, F., La Torre, A., Gómez-García, C. J., Brown, P. D., et al. (2011). Encapsulation of single-molecule magnets in carbon nanotubes. *Nat. Commun.* 2:407.

Dubay, O., and Kresse, G. (2004). Density functional calculations for C_{60} peapods. *Phys. Rev. B* 70:165424.

Dujardin, E., Ebbesen, T. W., Krishnan, A., and Treacy, M. M. J. (1998). Wetting of Single Shell Carbon Nanotubes. *Adv. Mater.* 10, 1472–1475. doi: 10.1002/(sici)1521-4095(199812)10:17<1472::aid-adma1472>3.0.co;2-r

Fan, J., Yudasaka, M., Yuge, R., Futaba, D. N., Hata, K., and Iijima, S. (2007). Efficiency of C_{60} incorporation in and release from single-wall carbon nanotubes depending on their diameters. *Carbon* 45, 722–726. doi: 10.1016/j.carbon.2006.11.034

Fröhlich, T., Scharff, P., Schliefke, W., Romanus, H., Gupta, V., Siegmund, C., et al. (2004). Insertion of C_{60} into multi-wall carbon nanotubes—-a synthesis of C_{60}@MWCNT. *Carbon* 42, 2759–2762. doi: 10.1016/j.carbon.2004.05.025

Gao, H., Kong, Y., Cui, D., and Ozkan, C. S. (2003). Spontaneous Insertion of DNA Oligonucleotides into Carbon Nanotubes. *Nano Lett.* 3, 471–473. doi: 10.1021/nl025967a

Ge, H., Riss, P. J., Mirabello, V., Calatayud, D. G., Flower, S. E., Arrowsmith, R. L., et al. (2017). Behavior of Supramolecular Assemblies of Radiometal-Filled and Fluorescent Carbon Nanocapsules In Vitro and In Vivo. *Chem* 3, 437–460. doi: 10.1016/j.chempr.2017.06.013

Geng, H. Z., Zhang, X. B., Mao, S. H., Kleinhammes, A., Shimoda, H., Wu, Y., et al. (2004). Opening and closing of single-wall carbon nanotubes. *Chem. Phys. Lett.* 399, 109–113. doi: 10.1016/j.cplett.2004.09.150

Ginzburg, B. M., Tuichiev, S., Tabarov, S. K., Shepelevskii, A. A., and Shibaev, L. A. (2005). X-ray diffraction analysis of C_{60} fullerene powder and fullerene soot. *Technical Phys.* 50, 1458–1461. doi: 10.1134/1.2131953

Guo, Z., Sadler, P. J., and Tsang, S. C. (1998). Immobilization and Visualization of DNA and Proteins on Carbon Nanotubes. *Adv. Mater.* 10, 701–703. doi: 10.1002/(sici)1521-4095(199806)10:9<701::aid-adma701>3.0.co;2-4

Hernández, E., Meunier, V., Smith, B. W., Rurali, R., Terrones, H., Buongiorno Nardelli, M., et al. (2003). Fullerene Coalescence in Nanopeapods: A Path to Novel Tubular Carbon. *Nano Lett.* 3, 1037–1042. doi: 10.1021/nl034283f

Hernández-Rivera, M., Kumar, I., Cho, S. Y., Cheong, B. Y., Pulikkathara, M. X., Moghaddam, S. E., et al. (2017). High-Performance Hybrid Bismuth–Carbon Nanotube Based Contrast Agent for X-ray CT Imaging. *ACS Appl. Mater. Interf.* 9, 5709–5716. doi: 10.1021/acsami.6b12768

Heymann, D. (1996). Solubility of Fullerenes C_{60} and C_{70} in Water. *Lunar Planet. Sci.* 27:543.

Hirahara, K., Suenaga, K., Bandow, S., Kato, H., Okazaki, T., Shinohara, H., et al. (2000). One-Dimensional Metallofullerene Crystal Generated Inside Single-Walled Carbon Nanotubes. *Phys. Rev. Lett.* 85, 5384–5387. doi: 10.1103/physrevlett.85.5384

Insepov, Z., Wolf, D., and Hassanein, A. (2006). Nanopumping Using Carbon Nanotubes. *Nano Lett.* 6, 1893–1895. doi: 10.1021/nl060932m

Kharlamova, M. V., Yashina, L. V., Eliseev, A. A., Volykhov, A. A., Neudachina, V. S., Brzhezinskaya, M. M., et al. (2012). Single-walled carbon nanotubes filled with nickel halogenides: Atomic structure and doping effect. *Phys. Status Solidi B* 249, 2328–2332. doi: 10.1002/pssb.201200060

Kierkowicz, M., González-Domínguez, J. M., Pach, E., Sandoval, S., Ballesteros, B., Da Ros, T., et al. (2017). Filling Single-Walled Carbon Nanotubes with Lutetium Chloride: A Sustainable Production of Nanocapsules Free of Nonencapsulated Material. *ACS Sustain. Chem. Engine.* 5, 2501–2508. doi: 10.1021/acssuschemeng.6b02850

Kitaura, R., Nakanishi, R., Saito, T., Yoshikawa, H., Awaga, K., and Shinohara, H. (2009). High-Yield Synthesis of Ultrathin Metal Nanowires in Carbon Nanotubes. *Angewandte Chemie Int. Edit.* 48, 8298–8302. doi: 10.1002/anie.200902615

Klingeler, R., Hampel, S., and Büchner, B. (2008). Carbon nanotube based biomedical agents for heating, temperature sensoring and drug delivery. *Int. J. Hyperther.* 24, 496–505. doi: 10.1080/02656730802154786

Kondo, D., Kawabata, A., Horibe, M., Nihei, M., and Awano, Y. (2003). Vertically aligned peapod formation of position-controlled multi-walled carbon nanotubes (MWNTs). *Superlatt. Microstruct.* 34, 389–394. doi: 10.1016/j.spmi.2004.03.034

Král, P., and Tománek, D. (1999). Laser-Driven Atomic Pump. *Phys. Rev. Lett.* 82, 5373–5376. doi: 10.1103/physrevlett.82.5373

Longhurst, M. J., and Quirke, N. (2007). Temperature-Driven Pumping of Fluid through Single-Walled Carbon Nanotubes. *Nano Lett.* 7, 3324–3328. doi: 10.1021/nl071537e

Luksirikul, P., Ballesteros, B., Tobias, G., Moloney, M. G., and Green, M. L. H. (2010). pH-triggered release of materials from single-walled carbon nanotubes using dimethylamino-functionalized fullerenes as removable "corks". *Carbon* 48, 1912–1917. doi: 10.1016/j.carbon.2010.01.053

Lyde, D. R., Berger, L. I, Covington, A. K., and Fox, R. B. (2003-2004). *Handbook of Chemistry and Physics*. Florida: CRC Press.

Maggini, L., Füstös, M.-E., Chamberlain, T. W., Cebrián, C., Natali, M., Pietraszkiewicz, M., et al. (2014). Fullerene-driven encapsulation of a luminescent Eu(III) complex in carbon nanotubes. *Nanoscale* 6, 2887–2894. doi: 10.1039/C3NR05876J

Marega, R., and Bonifazi, D. (2014). Filling carbon nanotubes for nanobiotechnological applications. *N. J. Chem.* 38, 22–27. doi: 10.1039/c3nj01008b

Martincic, M., and Tobias, G. (2015). Filled carbon nanotubes in biomedical imaging and drug delivery. *Expert Opin. Drug Delivery* 12, 563–581. doi: 10.1517/17425247.2015.971751

Martincic, M., Vranic, S., Pach, E., Sandoval, S., Ballesteros, B., Kostarelos, K., et al. (2019). Non-cytotoxic carbon nanocapsules synthesized via one-pot filling and end-closing of multi-walled carbon nanotubes. *Carbon* 141, 782–793. doi: 10.1016/j.carbon.2018.10.006

Mazzoni, M. S. C., Chacham, H., Ordejón, P., Sánchez-Portal, D., Soler, J. M., and Artacho, E. (1999). Energetics of the oxidation and opening of a carbon nanotube. *Phys. Rev. B* 60, R2208–R2211.

Meyer, R. R., Sloan, J., Dunin-Borkowski, R. E., Kirkland, A. I., Novotny, M. C., Bailey, S. R., et al. (2000). Discrete Atom Imaging of One-Dimensional Crystals Formed Within Single-Walled Carbon Nanotubes. *Science* 289, 1324–1326. doi: 10.1126/science.289.5483.1324

Nessim, G. D. (2010). Properties, synthesis, and growth mechanisms of carbon nanotubes with special focus on thermal chemical vapor deposition. *Nanoscale* 2, 1306–1323. doi: 10.1039/b9nr00427k

Nikolaev, P., Thess, A., Rinzler, A. G., Colbert, D. T., and Smalley, R. E. (1997). Diameter doubling of single-wall nanotubes. *Chem. Phys. Lett.* 266, 422–426. doi: 10.1016/S0009-2614(97)00053-5

Okada, S., Saito, S., and Oshiyama, A. (2001). Energetics and Electronic Structures of Encapsulated C_{60} in a Carbon Nanotube. *Phys. Rev. Lett.* 86, 3835–3838. doi: 10.1103/physrevlett.86.3835

Pan, X., and Bao, X. (2008). Reactions over catalysts confined in carbon nanotubes. *Chem. Commun.* 47, 6271–6281. doi: 10.1039/b810994j

Panczyk, T., Jagusiak, A., Pastorin, G., Ang, W. H., and Narkiewicz-Michalek, J. (2013). Molecular Dynamics Study of Cisplatin Release from Carbon Nanotubes Capped by Magnetic Nanoparticles. *J. Phys. Chem. C* 117, 17327–17336. doi: 10.1021/jp405593u

Philp, E., Sloan, J., Kirkland, A. I., Meyer, R. R., Friedrichs, S., Hutchison, J. L., et al. (2003). An encapsulated helical one-dimensional cobalt iodide nanostructure. *Nat. Mater.* 2, 788–791. doi: 10.1038/nmat1020

Prem Kumar, T., Ramesh, R., Lin, Y. Y., and Fey, G. T.-K. (2004). Tin-filled carbon nanotubes as insertion anode materials for lithium-ion batteries. *Electrochem. Commun.* 6, 520–525. doi: 10.1016/j.elecom.2004.03.009

Ren, Y., and Pastorin, G. (2008). Incorporation of Hexamethylmelamine inside Capped Carbon Nanotubes. *Adv. Mater.* 20, 2031–2036. doi: 10.1002/adma.200702292

Saikia, N., Jha, A. N., and Deka, R. C. (2013). Dynamics of Fullerene-Mediated Heat-Driven Release of Drug Molecules from Carbon Nanotubes. *J. Phys. Chem. Lett.* 4, 4126–4132. doi: 10.1021/jz402231p

Sandoval, S., Kepić, D., Pérez del Pino, Á, György, E., Gómez, A., Pfannmoeller, M., et al. (2018). Selective Laser-Assisted Synthesis of Tubular van der Waals Heterostructures of Single-Layered PbI_2 within Carbon Nanotubes Exhibiting Carrier Photogeneration. *ACS Nano* 12, 6648–6656. doi: 10.1021/acsnano.8b01638

Sandoval, S., Pach, E., Ballesteros, B., and Tobias, G. (2017). Encapsulation of two-dimensional materials inside carbon nanotubes: Towards an enhanced synthesis of single-layered metal halides. *Carbon* 123, 129–134. doi: 10.1016/j.carbon.2017.07.031

Sandoval, S., Tobias, G., and Flahaut, E. (2019). Structure of inorganic nanocrystals confined within carbon nanotubes. *Inorganica Chim. Acta* 492, 66–75. doi: 10.1016/j.ica.2019.04.004

Sauer, M., Shiozawa, H., Ayala, P., Ruiz-Soria, G., Kataura, H., Yanagi, K., et al. (2012). In situ filling of metallic single-walled carbon nanotubes with ferrocene molecules. *Phys. Status Solidi B* 249, 2408–2411. doi: 10.1002/pssb.201200127

Shao, L., Lin, T.-W., Tobias, G., and Green, M. L. H. (2008). A simple method for the containment and purification of filled open-ended single wall carbon nanotubes using C_{60} molecules. *Chem. Commun.* 2008, 2164–2166. doi: 10.1039/b800881g

Shao, L., Tobias, G., Huh, Y., and Green, M. L. H. (2006). Reversible filling of single walled carbon nanotubes opened by alkali hydroxides. *Carbon* 44, 2855–2858. doi: 10.1016/j.carbon.2006.06.010

Simon, F., Peterlik, H., Pfeiffer, R., Bernardi, J., and Kuzmany, H. (2007). Fullerene release from the inside of carbon nanotubes: A possible route toward drug delivery. *Chem. Phys. Lett.* 445, 288–292. doi: 10.1016/j.cplett.2007.08.014

Sinha, S., Zhu, T., France-Lanord, A., Sheng, Y., Grossman, J. C., Porfyrakis, K., et al. (2020). Atomic structure and defect dynamics of monolayer lead iodide nanodisks with epitaxial alignment on graphene. *Nat. Commun.* 11:823. doi: 10.1038/s41467-020-14481-z

Sloan, J., Dunin-Borkowski, R. E., Hutchison, J. L., Coleman, K. S., Clifford Williams, V., Claridge, J. B., et al. (2000). The size distribution, imaging and obstructing properties of C_{60} and higher fullerenes formed within arc-grown single walled carbon nanotubes. *Chem. Phys. Lett.* 316, 191–198. doi: 10.1016/S0009-2614(99)01250-6

Sloan, J., Kirkland, A. I., Hutchison, J. L., and Green, M. L. H. (2002). Integral atomic layer architectures of 1D crystals inserted into single walled carbon nanotubes. *Chem. Commun.* 1319–1332. doi: 10.1039/b200537a

Smith, B. W., Monthioux, M., and Luzzi, D. E. (1998). Encapsulated C_{60} in carbon nanotubes. *Nature* 396, 323–324. doi: 10.1038/24521

Tang, Z.-C., Cai, X.-W., Gao, J.-S., Mao, B.-W., Tian, Z.-Q., Huang, R.-B., et al. (1999). In-situ characterization of C_{60} coalescence reaction. *Chem. Phys. Lett.* 306, 345–351. doi: 10.1016/S0009-2614(99)00485-6

Tobias, G., Ballesteros, B., and Green, M. L. H. (2010). Carbon nanocapsules: blocking materials inside carbon nanotubes. *Phys. Status Solidi C* 7, 2739–2742. doi: 10.1002/pssc.200983823

Ujjal, K. G., Pedro, M. F. J. C., Yoshio, B., Xiaosheng, F., Liang, L., Masataka, I., et al. (2010). Recent developments in inorganically filled carbon nanotubes: successes and challenges. *Sci. Technol. Adv. Mater.* 11:054501. doi: 10.1088/1468-6996/11/5/054501

Wang, J. T. W., Klippstein, R., Martincic, M., Pach, E., Feldman, R., Šefl, M., et al. (2020). Neutron Activated 153Sm Sealed in Carbon Nanocapsules for in Vivo Imaging and Tumor Radiotherapy. *ACS Nano* 14, 129–141. doi: 10.1021/acsnano.9b04898

Wang, Q. (2009). Atomic Transportation via Carbon Nanotubes. *Nano Lett.* 9, 245–249. doi: 10.1021/nl802829z

Warner, J. H., Ito, Y., Zaka, M., Ge, L., Akachi, T., Okimoto, H., et al. (2008). Rotating Fullerene Chains in Carbon Nanopeapods. *Nano Lett.* 8, 2328–2335. doi: 10.1021/nl801149z

Xue, Q., Jing, N., Chu, L., Ling, C., and Zhang, H. (2012). Release of encapsulated molecules from carbon nanotubes using a displacing method: a MD simulation study. *RSC Adv.* 2, 6913–6920. doi: 10.1039/c2ra20446k

Yanagi, K., Miyata, Y., and Kataura, H. (2006). Highly Stabilized β-Carotene in Carbon Nanotubes. *Adv. Mater.* 18, 437–441. doi: 10.1002/adma.200501839

Yudasaka, M., Ajima, K., Suenaga, K., Ichihashi, T., Hashimoto, A., and Iijima, S. (2003). Nano-extraction and nano-condensation for C_{60} incorporation into single-wall carbon nanotubes in liquid phases. *Chem. Phys. Lett.* 380, 42–46. doi: 10.1016/j.cplett.2003.08.095

Zhang, J., Guo, S., Wei, J., Xu, Q., Yan, W., Fu, J., et al. (2013). High-Efficiency Encapsulation of Pt Nanoparticles into the Channel of Carbon Nanotubes as an Enhanced Electrocatalyst for Methanol Oxidation. *Chem. A Eur. J.* 19, 16087–16092. doi: 10.1002/chem.201302416

Zhou, M., Duan, W., Chen, Y., and Du, A. (2015). Single layer lead iodide: computational exploration of structural, electronic and optical properties, strain induced band modulation and the role of spin-orbital-coupling. *Nanoscale* 7, 15168–15174. doi: 10.1039/C5NR04431F

Zhou, W., Winey, K. I., Fischer, J. E., Sreekumar, T. V., Kumar, S., and Kataura, H. (2004). Out-of-plane mosaic of single-wall carbon nanotube films. *Appl. Phys. Lett.* 84, 2172–2174. doi: 10.1063/1.1689405

Conflict of Interest: The authors declare that the research was conducted in the absence of any commercial or financial relationships that could be construed as a potential conflict of interest.

frontiers in Bioengineering and Biotechnology

REVIEW
published: 04 May 2021
doi: 10.3389/fbioe.2021.671381

A Pathway From Porous Particle Technology Toward Tailoring Aerogels for Pulmonary Drug Administration

*Thoa Duong[1], Clara López-Iglesias[1], Piotr K. Szewczyk[2], Urszula Stachewicz[2], Joana Barros[3], Carmen Alvarez-Lorenzo[1], Mohammad Alnaief[4] and Carlos A. García-González[1]**

[1] Department of Pharmacology, Pharmacy and Pharmaceutical Technology, I+D Farma group (GI-1645), Faculty of Pharmacy, and Health Research Institute of Santiago de Compostela (IDIS), Universidade de Santiago de Compostela, Santiago de Compostela, Spain, [2] Faculty of Metals Engineering and Industrial Computer Science, AGH University of Science and Technology, Krakow, Poland, [3] i3S – Instituto de Investigação e Inovação em Saúde da Universidade do Porto – Associação, INEB – Instituto de Engenharia Biomédica, FEUP – Faculdade de Engenharia, Universidade do Porto, Porto, Portugal, [4] Department of Pharmaceutical and Chemical Engineering, Faculty of Applied Medical Sciences, German Jordanian University, Amman, Jordan

OPEN ACCESS

Edited by:
Concepcion Domingo,
Instituto de Ciencias del Mar, Consejo Superior de Investigaciones Científicas (CSIC), Spain

Reviewed by:
Pascale Subra Paternault,
Centre National de la Recherche Scientifique (CNRS), France
Nenad Filipovic,
University of Kragujevac, Serbia
Irina Smirnova,
Hamburg University of Technology, Germany

Correspondence:
Carlos A. García-González
carlos.garcia@usc.es

Specialty section:
This article was submitted to Biomaterials, a section of the journal Frontiers in Bioengineering and Biotechnology

Received: *23 February 2021*
Accepted: *06 April 2021*
Published: *04 May 2021*

Citation:
Duong T, López-Iglesias C, Szewczyk PK, Stachewicz U, Barros J, Alvarez-Lorenzo C, Alnaief M and García-González CA (2021) A Pathway From Porous Particle Technology Toward Tailoring Aerogels for Pulmonary Drug Administration. Front. Bioeng. Biotechnol. 9:671381. doi: 10.3389/fbioe.2021.671381

Pulmonary drug delivery has recognized benefits for both local and systemic treatments. Dry powder inhalers (DPIs) are convenient, portable and environmentally friendly devices, becoming an optimal choice for patients. The tailoring of novel formulations for DPIs, namely in the form of porous particles, is stimulating in the pharmaceutical research area to improve delivery efficiency. Suitable powder technological approaches are being sought to design such formulations. Namely, aerogel powders are nanostructured porous particles with particularly attractive properties (large surface area, excellent aerodynamic properties and high fluid uptake capacity) for these purposes. In this review, the most recent development on powder technologies used for the processing of particulate porous carriers are described via updated examples and critically discussed. A special focus will be devoted to the most recent advances and uses of aerogel technology to obtain porous particles with advanced performance in pulmonary delivery.

Keywords: porous particles, dry powder inhalers (DPIs), powder technology, pulmonary delivery, aerogels

PULMONARY DRUG DELIVERY: CURRENT STATUS AND RELEVANCE OF POROUS PARTICLES IN DPIs

Pulmonary route is explored for the systemic delivery of drugs as well as for the treatment of respiratory disorders. This administration route can enhance the absorption of drugs for systemic treatments due to the special character of alveoli region, like high surface area (*ca.* 100 m^2), thin epithelium layer and high vascularization (Borghardt et al., 2018; Hadiwinoto et al., 2018; Deshkar and Vas, 2019; Kadota et al., 2020). The inhalation therapy can also provide local treatments with higher efficacy and reduce side effects compared to systemic administration, by targeting directly the desired region and by increasing the drug concentration in the lungs (Borghardt et al., 2018). The current annual rate of the global respiratory drugs markets is estimated at 4–6% with prospects of increase in the short-mid term (Movia and Prina-Mello, 2020). The increasing interest

GRAPHICAL ABSTRACT | Aerogel powders are advantageous porous particles in dry powder inhalers for the pulmonary drug delivery in local and systemic treatments.

in pulmonary drug delivery can be evaluated by the evolution of the number of publications on this topic, particularly in the recent years (**Figure 1**). The pulmonary drug delivery systems and their relevance in the treatment of respiratory diseases is also gaining a lot of interest due to the current COVID-19 pandemics (Ivanoska-Dacikj and Stachewicz, 2020; Zuo et al., 2020), where patients seeks new therapies (Gil et al., 2020; Jarai et al., 2020; Kipshidze et al., 2020).

Current challenges in the development of orally inhaled drugs are targeted to face the high overall attrition rate (70%) (Movia and Prina-Mello, 2020). The complexity of lungs renders lung deposition as a critical factor in pulmonary administration determining the drug efficiency, which is generally associated with the volume of lungs, clinical status and breath patterns of patients, physicochemical properties of inhaled particles and design of inhalation devices (Borghardt et al., 2018; Lavorini et al., 2019). Namely, incorrect handling skills of patients indicates more exacerbations and the negative impact of daily activity and lung function (Gregoriano et al., 2018).

Patients' needs for inhaler products to favor medication adherence are summarized in the 6E's principle: "Effective, Efficient, Engaging, Error-tolerant, Easy-to-teach, Easy-to-switch to" (Levy et al., 2019). Moreover, several criteria have been set to guide the medical doctors on the suitable (START [Screening Tool to Alert doctors to Right Treatment]) and potentially unsuitable (STOPP [Screening Tool of Older Person's Prescriptions]) treatments for patients to avoid adverse drug events and to reduce sociosanitary costs (O'Mahony et al., 2014; Lavan et al., 2017; Fahrni et al., 2019). These criteria label as "potentially inappropriate" the systemic administration of corticosteroids for the prolonged treatment of moderate-to-severe chronic obstructive pulmonary disease (COPD) and recommend the replacement to a local delivery by oral inhalation. Applying these criteria, the oral inhalation route is suggested for the prescription of anticholinergic drugs in case of asthma or mild-to-moderate COPD. Dry powder inhalers (DPIs) are the recommended inhaler devices in clinical practices and become the optimal choice for patients with lung diseases (Kadota et al., 2020).

DPIs are inhaler devices gaining special interest and market share for pulmonary delivery as they are portable, environmentally-friendly and convenient to achieve a high degree of patient compliance (Hadiwinoto et al., 2018; Levy et al., 2019; Kadota et al., 2020). Moreover, the solid form of the formulation in DPIs favors the stability of drugs. DPIs disperse dry powder formulations without the need of a liquefied propellant (Hadiwinoto et al., 2018). DPIs are mainly classified as active or passive DPIs category depending on the mechanism (Moon et al., 2019). Active DPI devices include the internal energy to aerosolize the particles inside. Passive DPIs use the patient'inspiratory flow to disperse the inhaled particle into the pulmonary tract (de Boer et al., 2017; Moon et al., 2019). DPIs are easy to self-administer by the majority of patients since there is no requirement of coordination between actuation and inhalation (Shakshuki and Agu, 2017; Lavorini et al., 2019). Currently, the aerosol therapy should be delivered with precaution especially for the patients with COVID-19 (Ari, 2020).

Lung deposition is a determinant factor to reach the desired therapeutic outcomes in pulmonary drug delivery (Borghardt et al., 2018; Kadota et al., 2020). Mathematical models to study particle deposition in different areas of the lungs or in the whole respiratory tract have been developed since the 1930s (Fernández Tena and Casan Clarà, 2012). While the first models only considered a few number of respiratory conditions and divided the respiratory tract in a low number of regions, the most used one (Weibel model) considers several ways of bifurcation and 23 regions from the trachea to the alveolar duct. Later studies are based on computational fluid dynamics, which simulate fluid

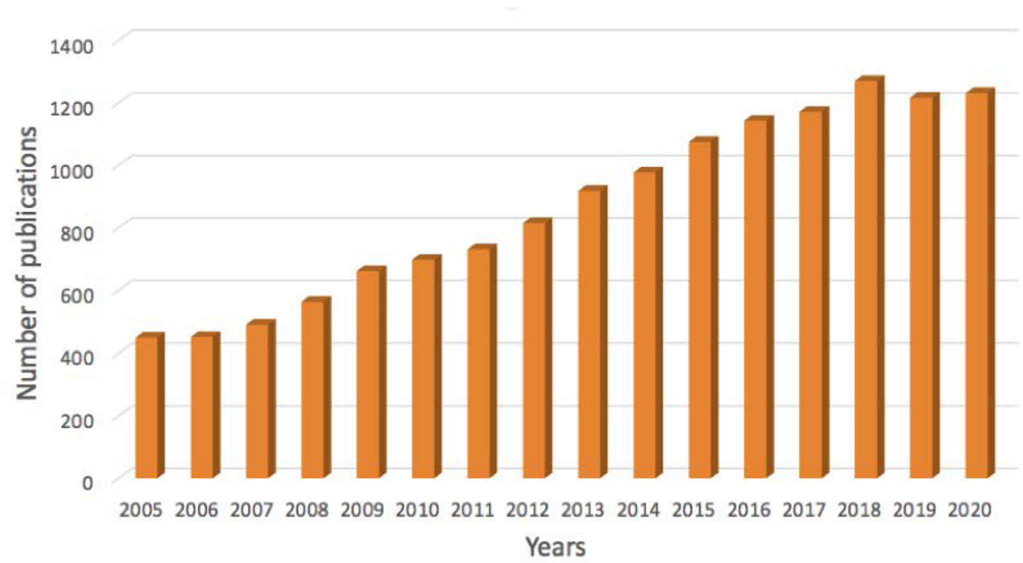

FIGURE 1 | Number of publications in PubMed database for the search criteria "Pulmonary drug delivery" (search date: February 15, 2021).

movement and stablish mathematical equations to describe the particle path. Experimental models usually correlate well with mathematical models and are very useful to calculate the total deposition of aerosols in the tract.

There are three main mechanisms of particle deposition in the respiratory system: inertial impaction, sedimentation and Brownian diffusion. These mechanisms are mainly governed by the aerodynamic diameter of the inhaled particles (d_a) (Hadiwinoto et al., 2018; Kadota et al., 2020). The microparticles with d_a higher than 5 μm are normally trapped in the oropharynx by inertial impaction, while particles with d_a smaller than 0.5 μm could be exhaled through Brownian motion. Particles with d_a in the 1–5 μm range are generally deposited deeply into the lungs by sedimentation. Meanwhile, there is a clearance mechanism by mucocilliary clearance in the conducting airway and alveolar macrophages following the deposition of particles of small geometric diameter (d_g, 1–2 μm diameter range) in the alveolar region (Hadiwinoto et al., 2018; Deshkar and Vas, 2019; Moon et al., 2019; Shetty et al., 2020). The tailoring of inhaled particles with higher geometric diameters or decreasing to nanoparticle size are strategic approaches to prevent clearance mechanisms in the pulmonary tract (Gharse and Fiegel, 2016).

The relationship between the aerodynamic size and the particle size, morphology, shape and density of inhaled particles can be expressed by the simplified Stokes law (Hickey and Edwards, 2018):

$$d_a = d_g . \sqrt{\frac{\rho_b}{\chi}} \tag{1}$$

where ρ_b is the bulk density, and χ is the dynamic shape factor, defined as the deviation from the sphericity related to the shape, surface roughness and surface area of inhaled particles.

According to Eq. 1, particles with acceptable aerodynamic diameters and high geometric diameters could be achieved by reducing the bulk density or by enhancing the dynamic shape factor (Hadiwinoto et al., 2018; Moon et al., 2019; Kadota et al., 2020). The dynamic shape factor is conditioned by the shape of the particles. For example, spherical particles present a dynamic size factor of 1, whereas pollen, cube-shaped and plate-shaped particles have higher dynamic shapes as $\chi = 1.2$, 1.3, and 1.5, respectively (Hassan and Lau, 2009). Higher values are found in needle-shaped particles ($\chi = 1.7$), however, the manufacturing of inhaled particles with needle-shaped particles poses a challenge on the industrial scale (Moon et al., 2019). Despite that, fine particle fraction (FPF) obtained from plate-and needle-shaped particles are lower than those with spherical, pollen and cube-shaped particles (Chaurasiya and Zhao, 2020).

Micronized particles (d_a = 1–5 μm) could create strong intermolecular forces causing the aggregation and reducing the flowability of the inhaled powder (de Boer et al., 2017; Weers and Clark, 2017; Hadiwinoto et al., 2018; Shetty et al., 2020). Coarse lactose powder is normally used as carrier to reduce the cohesive forces and enhance the dispersion performance of DPIs (Weers and Clark, 2017; Moon et al., 2019; Lechanteur and Evrard, 2020). Despite that, 50% of APIs could not be released from particle formulations due to intense carrier-API adhesive forces (de Boer et al., 2017). Airflow turbulence created by the inspiratory flow rate and the resistance of inhaled devices contribute to the detachment of APIs from the carriers (Levy et al., 2019). The inspiratory flow rate of the patient depends on the muscle strength, effort, clinical status, age and gender and can impact significantly the drug particle depositions (Weers and Clark, 2017; Moon et al., 2019). A reduction in the inspiratory flow rate from 60 to 30 L/min could decrease by 50% the total lung deposition (% nominal dose).

Porous particles are alternative powder formulations to tackle the existing challenges of DPIs. Based on Eq. 1, porous particles have a low bulk density that can achieve appropriate aerodynamic diameters with larger geometric diameters than solid non-porous particles. The tendency for aggregation of these porous particles is much lower than that of their non-porous counterparts due to their reduced interparticulate contact (Weers and Clark, 2017). Moreover, the performance of porous particles does not depend on the patient's respiratory flow rate exhibiting a low flow rate dependence (6.4 ± 6.6%). In contrast, spheronized solid particles and lactose blends showed high (60.8 ± 12.2%) and medium (33.3 ± 19.3%) flow rate dependence, respectively. Hence, the development of porous formulations requires novel powder technologies, since conventional powder technologies like jet milling and wet milling mainly focus on micronized inhaled non-porous particles (Hadiwinoto et al., 2018; Kadota et al., 2020). The aerodynamic properties of porous and non-porous particles were compared at a low inspiratory flow rate (30 L/min) (Chvatal et al., 2019). The FPF and emitted fraction (EF) of the porous formulation were significantly higher than the non-porous counterparts. These results were explained by the cohesive forces between particles resulting in agglomeration and low flowability performance of denser nonporous formulations. In contrast, inhaled particles with bulk density lower than 0.4 g/cm^3 can favor the aerosol penetration into the deep lung (Chaurasiya and Zhao, 2020). In this favorable context of porous formulations for DPIs, aerogel particles are novel porous materials that consist in solid, lightweight and open porous networks of bonded particles or nanoscale fibers obtained from the removal of the fluid of a gel without significant structural modifications, so they maintain large surface areas and extremely low densities (García-González et al., 2019). In this review article, current technologies for the design of porous particle formulations for pulmonary drug delivery will be described with updated examples of the most recent advances (Section "Production Strategies of Porous Particles Using Powder Technology"). Then, Section "Current Developments on Highly Porous Aerogel-Based Materials in Pulmonary Drug Delivery" will analyze the current developments in the production of novel ultra-light porous particles in the form of aerogels for inhalation formulations.

The evaluation of aerogel particles from a morphological, flow behavior and biological performance will be discussed with results from the literature and unpublished experimental data from the authors. Finally, current challenges in aerogel engineering for DPIs and future trends are discussed in Section "Future Trends of Bioaerogel Carriers for pulmonary Drug Delivery."

TABLE 1 | Updated research on powder technology applied in the preparation of porous particles in pulmonary drug delivery.

Method of production	Drugs	Excipients	Outcomes	References
Spray drying	Meloxicam	L-leucin, ammonium bicarbonate, sodium hyaluronate	LPP and non-porous particles containing meloxicam for carrier-free formulations were compared at low inspiratory flow rate (30 L/min). While mass median aerodynamic diameter (MMAD) of both formulations was the same (2.55 μm), fine particle fraction (FPF) and emitted fraction (EF) of LPP formulation were significantly higher than the non-porous counterparts.	Chvatal et al., 2019
Spray drying	Dexamethasone palmitate (Pro-drug of dexamethasone)	1,2-Dipalmitoyl-sn-Glycero-3-Phosphocholine (DPPC) and Hyaluronic Acid (HA)	LPP containing dexamethasone palmitate shows a sustained release pattern up to 24 h. Systemic exposure is considerably smaller compared to local effect. Aerodynamic performance varies depending on the concentration of dexamethasone palmitate, which affects to powder cohesion	N'Guessan et al., 2018
SCF (Supercritical fluid antisolvent process, SAS)	Beclomethasone dipropionate (BDP)	Poly-ethylene glycol 4000 (PEG 4000). Subcritical water (SBCW) and cold water were employed during the process	The dissolution rate of obtained BDP nanoparticles increases significantly. The process is "green" without using organic solvents.	Pu et al., 2017
SCF (Precipitation of compressed CO_2 antisolvent, PCA)	Insulin	Poly-L-lactic (PLLA PMs), ammonium bicarbonate	Desired aerodynamic deposition and particle size distribution, and low inflammatory responses due to solvent-free residues. The sustained release pattern provided a similar *in vivo* hypoglycemic performance to that produced after subcutaneous injection.	Lin et al., 2019
SFD	Voriconazole	Mannitol	Optimal fine particle fraction (FPF) obtained using high concentration of voriconazole and tert-butyl alcohol. The dissolution rate of voriconazole was increased.	Liao et al., 2019
SFD	SiRNA	Mannitol	The integrity of the structure of SiRNA is protected after SFD. The emitted fraction reaches significantly high values (92.4%), but fine particle fraction FPF is unsatisfied (≈ 20%).	Liang et al., 2018

PRODUCTION STRATEGIES OF POROUS PARTICLES USING POWDER TECHNOLOGY

Powder technologies to produce dry porous particles can be mainly categorized as "non-freezing induced" (e.g., spray drying, supercritical fluid technologies) and "freezing induced" (e.g., spray freeze drying) (Overhoff et al., 2009). Selected research updates on the preparation of porous particles for pulmonary drug delivery with these techniques are summarized in **Table 1**.

Spray Drying Technology

Spray drying is a well-established technique in the pharmaceutical industry (Hadiwinoto et al., 2018; Weers et al., 2019; Kadota et al., 2020). Briefly, this technique consists on the atomization of a drug solution into liquid droplets in contact with a drying gas stream. The evaporation of the solvent in the liquid droplets in the spray drying chamber results in the formation of dry solid particles. The main fraction of the dried product is collected from a cyclonic powder collection, while filter bags or additional cyclones are used to separate residual amounts of remaining fine powder from the outlet gas stream (Hadiwinoto et al., 2018). Processing parameters of spray drying include temperature, feed pressure, drug solution feed rate, air flow rate, and nozzle type (Hadiwinoto et al., 2018; Kadota et al., 2020). The tuning of these parameters can flexibly modify the physicochemical properties of the resulting particles, like surface properties, shape and size.

Modified versions of the spray drying technology are used to produce porous particles with high porosity and low tapped density, such as the PulmoSphere^{TM} formulations and large porous particles (LPP) used in commercial drug products (Healy et al., 2014).

PulmoSphere^{TM} formulations are phospholipid-based small porous particles with low tapped density and geometric sizes in the 1–5 μm range (Weers and Tarara, 2014; Weers et al., 2019). PulmoSphere^{TM} formulations are produced from perfluorooctyl bromide (PFOB)-in-water emulsions as liquid feed containing also calcium chloride and distearoylphosphatidylcholine (DSPC), a primary component of endogenous pulmonary surfactant (**Figure 2A**). The discontinuous phase of these emulsions consists on submicron droplets. The PFOB is quickly evaporated from the emulsion by the heat energy via spray drying producing pores in the structure of particles. Three different PulmoSphere^{TM} types can be used to incorporate APIs into the porous particles depending on the nature of the drug and the desired solid state (Weers et al., 2019):

(1) Solution-based PulmoSphere^{TM}: the continuous phase of the emulsion is responsible to dissolve API and then this emulsion is spray dried producing porous formulations containing amorphous drugs. Commercial product TOBI® Podhaler^{TM} (tobramycin) is produced using solution-based PulmoSphere^{TM} (**Figure 2B**).

(2) Suspension-based PulmoSphere^{TM}: API is added into the emulsion feed in form of fine particles. The obtained suspension is spray-dried producing the final product with the amorphous or crystalline drug covered by a porous surface (**Figure 2C**).

(3) Carrier-based PulmoSphere^{TM}: the liquid feed contains fluorinated medium to suspend micronized API and prepare particles as small porous carriers. Agglomeration of API and porous PulmoSphere^{TM} carriers occurs when liquid feed is evaporated via spray drying (**Figure 2D**).

Large porous particles (LPP) are characterized by geometric sizes in the 5–30 μm range (Ni et al., 2017; Chvatal et al., 2019). Compared to non-porous particles, LPP formulations have a highly efficient penetration into the deep lung and have the ability to avoid the clearance mechanism by alveolar macrophages (Liang et al., 2015; Ni et al., 2017; Shiehzadeh et al., 2019). A suitable porogen (normally ammonium bicarbonate) is commonly required to produce the porous LPP matrix (Liang et al., 2015). Due to the immediate release of ammonia and carbon dioxide from ammonium bicarbonate, a porous structure is formed (**Figure 3**). Cyclodextrin is another common porogen that could apply as an osmogene, which produces different osmotic pressure between inner and outer aqueous phases. Thus, water influx into the organic phase leads to the creation of pores in the porous matrix. Recently, spray dried INBRIJA^{TM} (levodopa) LPP-powder received EMA and FDA commercialization authorizations functioning as quick response doubled with increasing rapidly the concentration of levodopa in plasma for the treatment of Parkinson (Patel and Jimenez-Shahed, 2018).

Supercritical Fluid-Assisted Anti-solvent Technology

Supercritical fluids (SCF) are used in green powder technologies receiving attention for the formulation of DPIs as cost-effective, non-toxic approach able to modify the solid-state form of the dry powder (Kankala et al., 2017; Hadiwinoto et al., 2018; Chakravarty et al., 2019). SCF technology typically overcomes the problems of conventional techniques by minimizing the consumption of organic solvents, effectively modifying solid-state, and achieving the target particle size and narrow size distribution of DPIs. Supercritical CO_2 ($scCO_2$) is the most common fluid in SCF technology and an approved solvent by the FDA, due to its harmless and non-combustible nature. Moreover, it has a recycled source and is economic. The low viscosity, high diffusivity and null surface tension of $scCO_2$ allow its easy penetration to porous matrices under mild conditions (Kankala et al., 2017; Hadiwinoto et al., 2018; Chakravarty et al., 2019; Lin et al., 2019). The affinity and high solvation power of $scCO_2$ to several organic solvents (acetone, ethanol, dichloromethane, among others) are exploited in particle technology through anti-solvent strategies. Namely, the so-called precipitation of compressed CO_2 antisolvent (PCA) and supercritical fluid anti-solvent process (SAS) techniques offer a great advantage for inhaled particles with desired size (Chen et al., 2013; Lin et al., 2019).

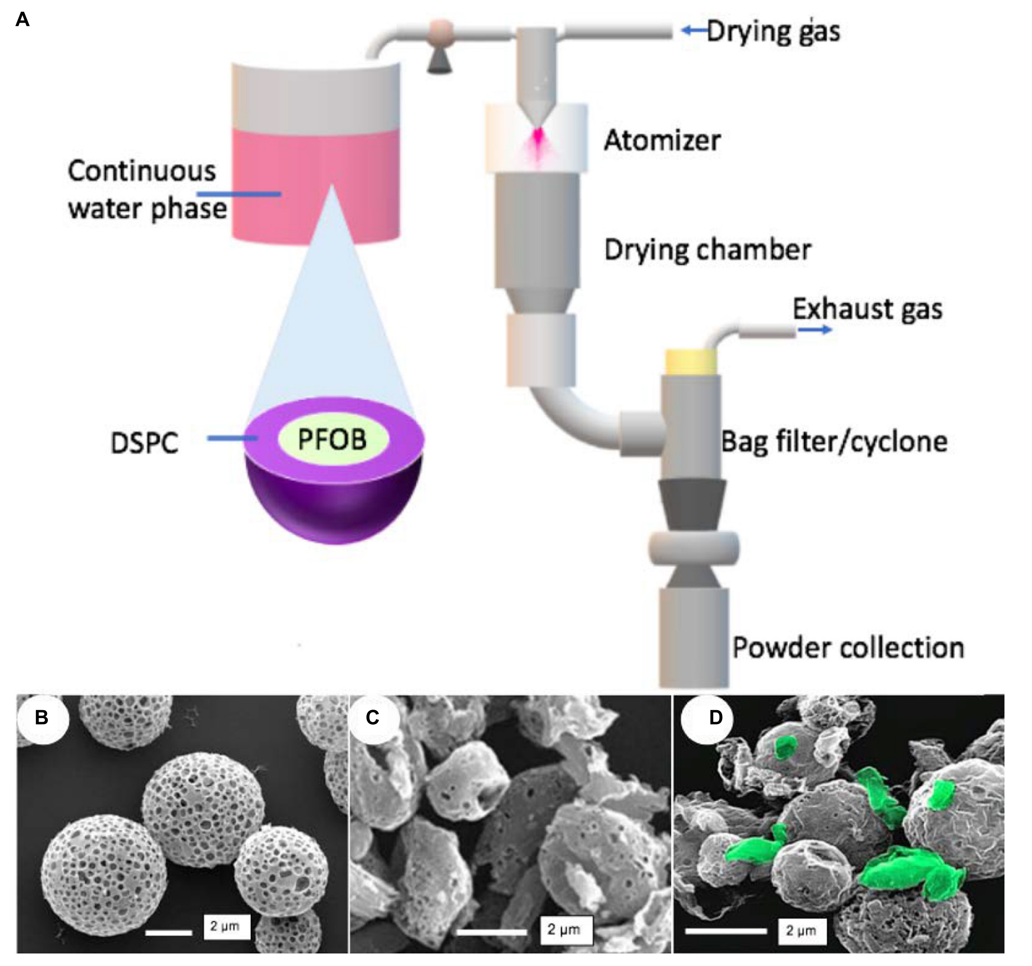

FIGURE 2 | PulmoSphere™ formulations for DPIs: **(A)** Scheme of manufacturing method and mechanism to generate porous, micron-sized particles. **(B)** Tobramycin produced from Solution-based PulmoSphere™, **(C)** Ciprofloxacin produced from Suspension-based PulmoSphere™ and **(D)** Carrier-based PulmoSphere™ (drug crystals in green). Picture **(B)** reprinted from Lam et al. (2013) with permission from SAGE Publishing. Picture **(C)** reprinted from McShane et al. (2018) with permission from Elsevier. Picture **(D)** reprinted from Weers et al. (2019) with permission from Springer Nature.

Insulin-loaded poly-L-lactide porous microspheres were prepared using PCA technique and ammonium bicarbonate as porogen (Lin et al., 2019; **Figure 4A**). Briefly, the water phase consisting on an aqueous solution with insulin and ammonium bicarbonate was contacted with an oil phase consisting of Pluronic F-127 with poly−L−lactide in dichloromethane. The obtained water-in-oil emulsion was processed by PCA technique using compressed CO_2. Then, ammonium bicarbonate porogen was removed by vacuum drying. High insulin encapsulation efficiency (97%) and the desired aerodynamic deposition (4.46 ± 0.06 μm) were reported in the obtained porous particles (**Figure 4B**). Low inflammatory responses were confirmed due to solvent-free residues. The sustained release pattern of insulin from the porous particles provided a similar *in vivo* hypoglycemic performance to that produced after subcutaneous injection.

Spray Freeze Drying

Spray freeze drying (SFD) is an advanced technology for the production of LPP in pulmonary drug delivery with high production yields and being especially suitable for thermally sensitive materials (Hadiwinoto et al., 2018; Liao et al., 2019). Three subprocesses are involved: (i) Atomization; the prepared drug solution is atomized quickly into a refrigerant media assisted by an atomization gas. (ii) Freezing; this step takes place in a chamber using a refrigerant medium (normally containing liquid nitrogen) to provide a fast cooling to obtain frozen granules. (iii) Lyophilization; porous particles are obtained by the sublimation of solvent under high vacuum venting (**Figure 5**).

The porous structure of the particles obtained by SFD not only can satisfy aerodynamic deposition demands, but also can improve the apparent solubility of the formulations (Hastedt et al., 2016; Liao et al., 2019). Voriconazole-loaded LPP were successfully prepared using SFD for the treatment of pulmonary aspergillosis (Liao et al., 2019). Voriconazole in the LPP-based formulation was immediately released in the medium of the dissolution test, whereas raw voriconazole required 2 h to completely dissolve. Besides that SFD is a suitable technology to keep the integrity of biologicals intact (Shetty et al., 2020).

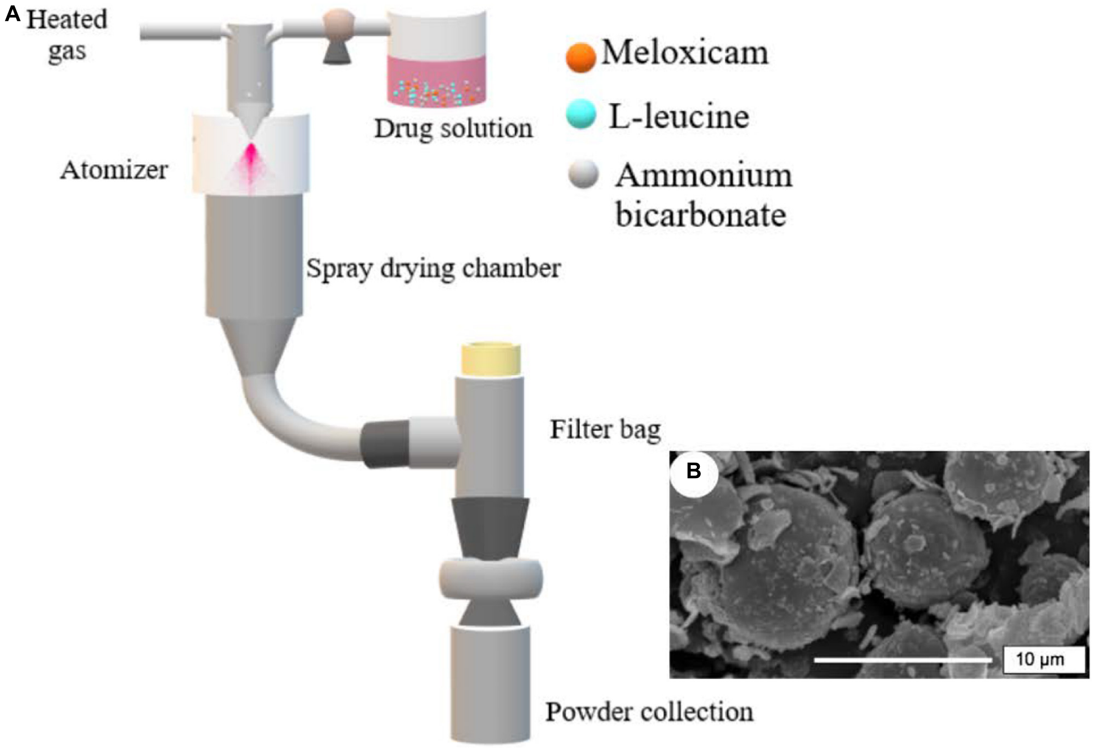

FIGURE 3 | Use of spray drying for the production of LPP: **(A)** Scheme of the spray drying approach to obtain LPP formulations, and **(B)** image of LPP particles containing meloxicam. SEM figure adapted from Chvatal et al. (2019) with permissions.

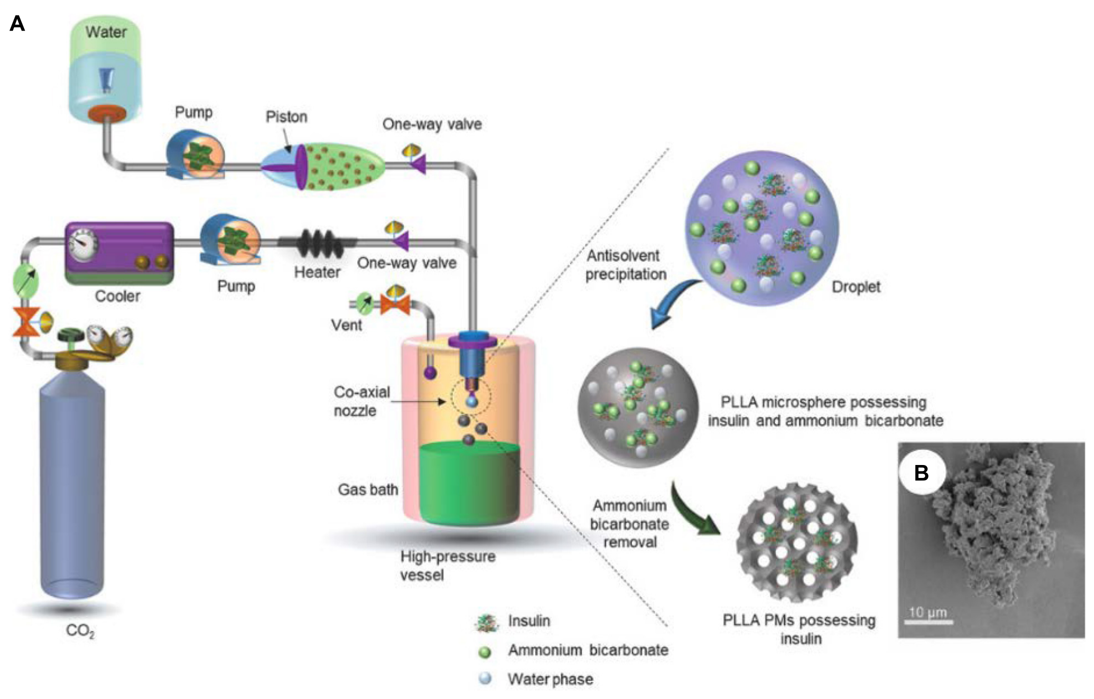

FIGURE 4 | Use of supercritical fluid-assisted anti-solvent technologies for the production of DPI formulations: **(A)** Scheme of the production method, and **(B)** image of insulin-loaded porous microspheres using PCA technique. Figures adapted from Lin et al. (2019) with permisssions.

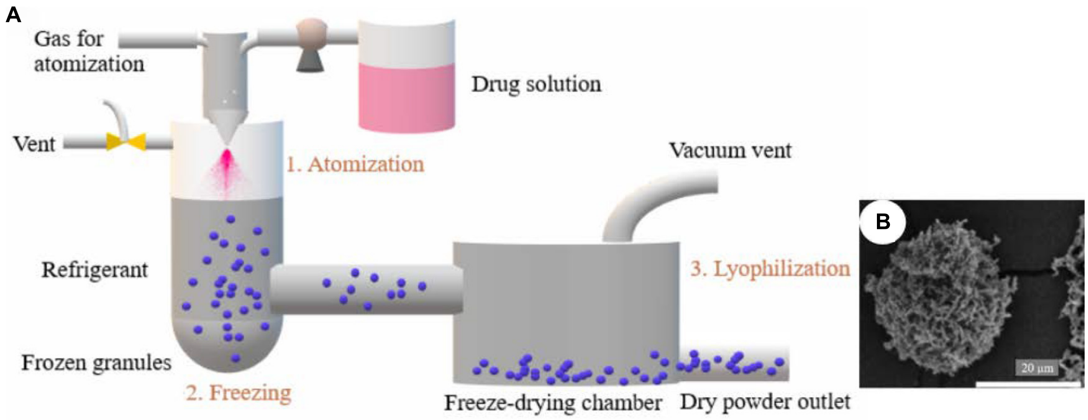

FIGURE 5 | Use of spray freeze drying technology for the production of porous particles: **(A)** Scheme of the production method, and **(B)** image of inhaled voriconazole formulation prepared by this technology **(B)**. SEM picture adapted from Liao et al. (2019) with permission.

However, LPP prepared by SFD can have lower porosities than spray dried powders, since SFD produces more hygroscopic powder absorbing more moisture (Shetty et al., 2020).

CURRENT DEVELOPMENTS ON HIGHLY POROUS AEROGEL-BASED MATERIALS IN PULMONARY DRUG DELIVERY

Aerogels for Drug Delivery System

Aerogels are ultra-light porous materials with a potential scarcely explored for biomedical applications so far (García-González et al., 2019). Aerogel-based materials may find application in bone tissue engineering, wound healing, bioimaging and carriers for drug delivery systems (García-González et al., 2018, 2021; López-Iglesias et al., 2020; Zheng et al., 2020). The vast surface area and accessible pores along with good aerodynamic properties and physicochemical stability of the aerogels are promising to achieve satisfactory drug loadings in various administration routes, especially for therapeutic proteins, cytotoxic drugs or poorly bioavailable drugs (Gonçalves et al., 2016; García-González et al., 2019; López-Iglesias et al., 2019a; Muñoz-Ruíz et al., 2019; Wang et al., 2019).

Aerogels were firstly prepared in 1931 by Samuel Kistler who replaced liquid inside gels without causing the collapse of the structure (Kistler, 1931). However, the interest of aerogels for drug delivery has only started at the beginning of the 21st century (Smirnova et al., 2004) with a fast growth in the publication rate on the topic in the last decade (García-González et al., 2021). Aerogels are attracting attention by their diversity of textural properties and overall porosity, which depend on the synthetic conditions (Lee et al., 2019). Inorganic and organic aerogels are applicable in the engineering of carriers for water-insoluble drugs (Chakravarty et al., 2019; García-González et al., 2019). Inorganic aerogels, such as silica aerogels, usually have higher surface areas than organic aerogels, which enhances the drug loading efficiency (Chakravarty et al., 2019). However, due to the biodegradability and biocompatibility, biopolymer or polysaccharide aerogels (gelatine, agar, cellulose, alginate, chitin and pectin) are preferred in biomedical applications (Chakravarty et al., 2019; García-González et al., 2019). Aerogels can be obtained in several shapes, such as in the form of microspheres, cylinders, films and three-dimensional scaffolds.

Loading of drugs into aerogels can be mainly achieved by four approaches that can determine the mechanisms of drug release (García-González et al., 2021). Drugs can be incorporated (i) before gelling, (ii) during solvent exchange, (iii) during drying or (iv) with prepared aerogels using supercritical fluid impregnation. In general, the choice of the loading strategy depends on the physicochemical properties of the drugs, namely the solubility of drugs in organic solvents and supercritical fluid; hydrophilic and lipophilic properties, and the stability of drugs in the selected solvent. For example, incorporation via solvent exchange can be used if drugs are soluble in the organic solvents and poorly soluble in supercritical fluids. In contrast, supercritical fluid impregnation is becoming an optimal choice if drugs are soluble in supercritical fluids but not in the organic solvents.

Regarding the drug release from the aerogel carriers, it mainly depends on the hydration properties of both drugs and carriers (erosion and swelling), the intermolecular forces between drugs and carriers (hydrogen bond, ionic bonding) and the mass transfer (García-González et al., 2021). Hydration properties of drugs are determinant factors deciding the dissolution rate of drug compounds in the dissolution medium. For instance, hydrophilic drugs in the hydrophilic aerogel matrix normally lead to a fast dissolution rate. In this context, the mass transfer of drug to the body fluids has an important role in the release profile of bioactive compounds. On the contrary, the release profiles of hydrophobic compounds in the aerogel matrix are normally delayed. The hydration properties of aerogel carriers is strongly conditioned by the hydrophilic or hydrophobic character of the aerogels. In the specific context of pulmonary inhalation, the hydration in respiratory fluid can determine the release rate of the drug, erosion and/or swelling of the aerogel structure.

Aerogel carriers can be formulated containing amorphous APIs with enhanced stability. The adsorptive deposition of bioactive compounds from $scCO_2$ solutions into the pores of aerogels usually takes place in a non-crystalline form as reflected by XRD analysis of drug-loaded aerogels, which greatly enhances the dissolution rate and bioavailability of these ingredients (Gurikov and Smirnova, 2018; Veres et al., 2018). Polysaccharide-based aerogels (starch, pectin and alginate) were produced as carriers for poorly water-soluble drugs (ketoprofen and benzoic acid) for oral drug delivery (García-González et al., 2015). The XRD analysis showed no peaks of the drugs in the obtained aerogels. In other study, alginate aerogels loaded with ketoprofen, nimesulide and loratadine as model drugs showed a stable amorphous form under storage conditions at room temperature for 6 months (Lovskaya and Menshutina, 2020). Compared to the raw materials, the dissolution rate was significantly improved as confirmed by the decrease of the half-life time.

An Overview of Aerogel Production

Aerogels are normally prepared via the following sequential steps: sol-gel, solvent exchange, and solvent removal from the wet gel by drying.

Aerogels produced in the shape of particles are practical in terms of production costs and manufacturing times, as the solvent exchange step and drying of the wet gel are simplified (Ganesan et al., 2018). Biopolymer-based aerogel particles are mainly produced by two different techniques: the dripping method (external gelation) and the emulsification method (internal gelation) (Ganesan et al., 2018; Valente et al., 2019; **Figure 6**).

The conventional dripping methods make use of dripping devices available in the lab-scale, such as syringes, vibrating nozzles, electrovalves or pipettes. Gravity causes the droplet of polymer solution to fall into the gelation bath, leading to aerogel beads with large droplet sizes of few millimeters (Ganesan et al., 2018) that do not meet the requirements in inhaled formulations. A modified dripping method using the thermal inkjet printing method has been recently proposed to obtain aerogel microspheres of 10–20 μm for DPI formulations (López-Iglesias et al., 2019b).

The solvent-emulsification technique uses internal gelation to fabricate gel microparticles (Ganesan et al., 2018). Under constant agitation, the polymer solution (aqueous phase) is dispersed in the oil phase forming an emulsion. An emulsifier with a hydrophilic-lipophilic balance (HLB) in the range of 3–6 is normally employed to stabilize the two immiscible liquids. The water-to-oil ratio is generally applied from 1:2 to 1:10 on a small scale, while the viscosities ratio of water-to-oil phase should be less than 1 to create an emulsion.

The drying step of the gel precursor is an essential step to produce aerogel particles. Ambient pressure drying, freeze-drying and supercritical fluid-assisted drying are common methods to dry wet gels, being the latter technique the most reliable approach to obtain aerogels (Şahin et al., 2017; García-González et al., 2019; Rodríguez-Dorado et al., 2019; Soorbaghi et al., 2019). Xerogels and cryogels are dried gels produced by oven/ambient drying and freeze-drying, respectively. Drying of gels with ambient pressure results in xerogels, which does not preserve the fragile porous structure of the wet gels due to the high capillary pressure taking place during solvent evaporation

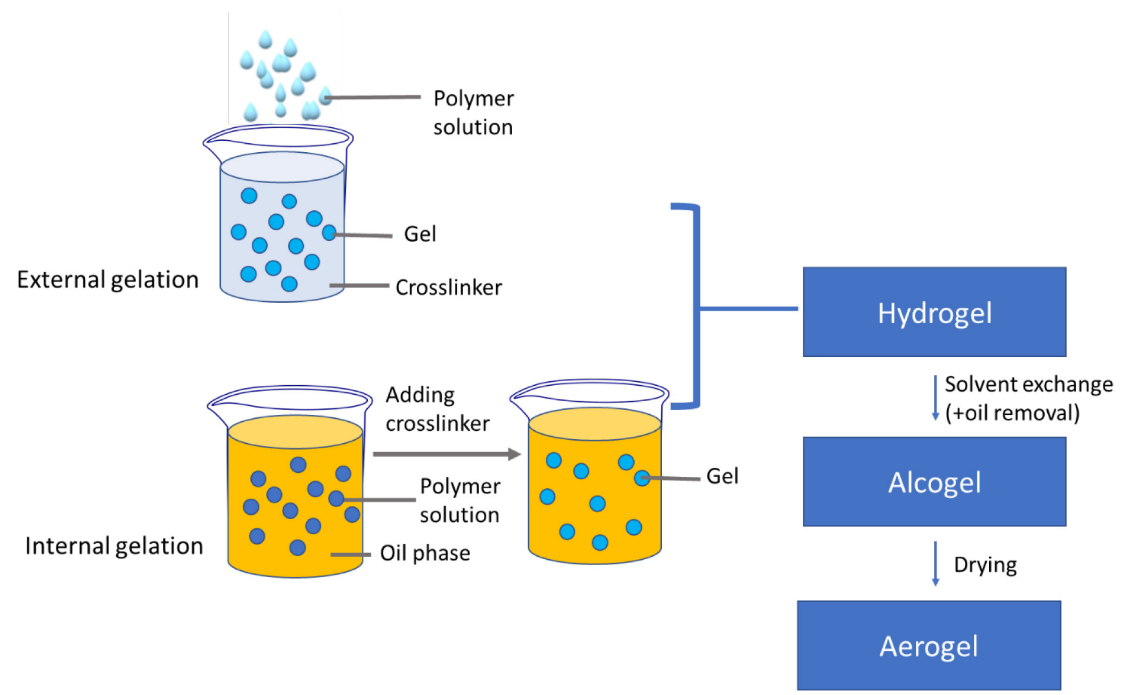

FIGURE 6 | Multi-step aerogel particles production for pulmonary delivery by external gelation and internal gelation.

(Şahin et al., 2017; Rodríguez-Dorado et al., 2019). Freeze-drying is another method that uses solvent sublimation to form porous solid structures called cryogels. During the freezing step, the formation of crystals inside the pores causes a stress that can damage the polymeric structure of the gels (Şahin et al., 2017; Rodríguez-Dorado et al., 2019). Supercritical fluid drying is the preferred technique to prevent pore collapse and maintain the physicochemical properties of the aerogels due to the low surface tension and high diffusivity of CO_2 (Ulker and Erkey, 2014, 2017; Şahin et al., 2017; Chakravarty et al., 2019; García-González et al., 2019; Rodríguez-Dorado et al., 2019). The physical structure of alginate aerogels, xerogels and cryogels was studied. Compared with aerogels, xerogels did not show significant porosity under nitrogen adsorption-desorption analysis, while in cryogels porosity was dramatically reduced due to partial collapse of the network (Rodríguez-Dorado et al., 2019).

Recent Research Using Aerogel Carriers for Pulmonary Drug Delivery

The high porosity of aerogel microparticles is not only an important key to fit the requirement of the aerodynamic size in pulmonary drug delivery, but also improves the flow dispersibility of particles (García-González et al., 2019). Besides, the high porosity of aerogel carriers will result in formulations with a low flow rate dependence on the respiratory capacity of the patient when used in DPIs.

The dissolution rate-limiting process in pulmonary absorption of poorly water-soluble substances could reduce the therapeutic outcomes or cause acute toxicity to the lungs by drug accumulation (Kumar et al., 2017; Franek et al., 2018; Eriksson et al., 2019). Two main classes of drugs with limited dissolution rates in pulmonary drug delivery are distinguished: (i) "potent inhaled corticosteroids with a nominal dose less than 1 mg," and (ii) "high-dose antiinfectives with a nominal dose >1 mg" (Hastedt et al., 2016). In these cases, the dissolution rate plays an important role in inhalation therapy when drug solubility is lower than 1 or 100 μg/mL, respectively (Hastedt et al., 2016).

Aerogels are nanostructured carriers with very high surface areas that, in accordance to Noyes-Whitney equation, can improve the drug dissolution rate. This porous structure of the aerogels also permit to load drugs on the surface or to impregnate them into the accessible pores of the aerogels (Chakravarty et al., 2019; Rodríguez-Dorado et al., 2019). Additionally, the solid state of drugs is another factor that largely influences the dissolution rate of drug in pulmonary administration. Compared to the crystalline state, the amorphous form is often advantageous for solubility and dissolution rate resulting by higher free energy than other forms. Accordingly, the potential of aerogel-based carriers, particularly from polysaccharides like alginate, chitosan or hybrids, is receiving attention for pulmonary drug delivery and are presented here forth.

Porous chitosan aerogel carriers loaded with salbutamol as a sustained drug delivery system were prepared for inhalation applications (Obaidat et al., 2015). Chitosans of different molecular weight (8, 16, and 250 kDa) were firstly mixed with different concentrations of sodium tripolyphosphate (TPP), which acted as crosslinker. Then, the chitosan gel was soaked in ethanol before salbutamol sulfate loading in ethanolic solution and supercritical fluid drying or freeze drying. The drying method was considered as a critical factor to obtain inhaled particles with suitable characteristics. Salbutamol-loaded chitosan aerogel particles produced by supercritical drying preserved better the morphology of the wet gel, and showed smaller particle sizes (7–12 μm), and lower tapped densities (0.10–0.14 g/mL) compared with freeze drying (60–68 μm and 0.22–0.25 g/mL, respectively). Additionally, the processing time of supercritical drying (2 h) was much faster than that of freeze drying (48 h). The release profile of salbutamol depended on the concentration of TPP and the molecular weight of chitosan. The concentration of TPP can modulate the swelling behavior of the aerogels, and therefore can modify the drug release profiles.

The ionic interactions between alginate, an anionic polysaccharide, and chitosan, a cationic polysaccharide, were exploited to obtain hybrid aerogel-based carriers for pulmonary drug delivery (Alnaief et al., 2020). These aerogels were produced by the emulsion-gelation method. The order of addition of the two polymers influenced end aerogel properties. Higher specific surface areas and lower particle sizes were obtained when chitosan was added to the alginate solution. The choice of surfactant (Span 80 -HLB = 4.3-, or Span 85 -HLB = 1.8-) had a great influence on the zeta potential value and final properties of the prepared aerogels. Higher zeta potential values and aerodynamic sizes and better performances were obtained for the aerogels produced with Span 85, while particles prepared using Span 80 or a mixture of the two surfactants presented low zeta potential values, and with higher tendency for agglomeration of the particles. In addition to the abovementioned parameters, the best operating conditions were 4% of surfactant concentration, 4,000 rpm as mixing rate for the emulsification step, and extraction time of 2 h. Temperature of emulsion preparation did not show a significant effect on the resulting gel particle sizes. Further optimization of the process resulted in fine particles with specific surface areas of 500 ± 45 m^2/g.

Chitosan-alginate aerogel carriers were tested for inhaled chemotherapy against lung cancer (Alsmadi et al., 2020). A new generation of inhalers is tailored for inhaled chemotherapy as they can be directly applied in the lung tumor to improve the safety of the treatment (Rosière et al., 2019). Most of the chemotherapeutic agents are water-insoluble compounds, causing limited efficiency of clinical treatment and unacceptable side effects due to accumulation. Therefore, solving the problem of poor water solubility to target cell lung cancer at a sufficient concentration and protecting healthy cells is the main challenge in novel inhaled chemotherapy. Chitosan is known to facilitate the incorporation of both water-soluble and poorly water-soluble drugs into its structure, which may enhance the drug encapsulation efficiency of both types of components. As an example, cisplatin was incorporated into hybrid chitosan-alginate nanoporous carriers by SCF impregnation resulting in drug loadings higher than 76% (Alsmadi et al., 2020). The safety of the chitosan-alginate aerogel formulation loaded with cisplatin was studied *in vivo* in a rat model after intratracheal administration. Though hepatic toxicity and dose-dependent renal toxicity were confirmed, the benefits of using the cisplatin formulation outweighed the side effects as confirmed by the reduction of lung toxicity and mortality rate in the rat model.

Alginate and hybrid alginate/hyaluronic acid aerogel microspheres were prepared using the emulsion-gelation technique followed by supercritical drying (Athamneh et al., 2019; **Figure 7**). The use of hyaluronic acid (HA) improves the mucoadhesive properties of the aerogels thus increasing the pulmonary retention time (Athamneh et al., 2019). The gelation mechanism was explained by various interactions between the alginate, the hyaluronic acid, and divalent cations. In general, the ionic gelation between G units of alginate and Ca^{2+} divalent cations creating an "egg-box" structure was reported as the main gelation mechanism, although hydrogen bonding between alginate and HA and interaction between HA and Ca^{2+} also occurred. Energy input and viscosity of the aqueous phase were considered as sol-gel parameters that influenced the end properties of the aerogels. Mean aerogel particle diameter and aerodynamic size was controlled by varying the stirring rate and the polymers ratio, respectively. High textural properties were obtained for all the prepared aerogels and did not depend on these parameters. In general, the emulsion-gelation method is useful to easily prepare large quantities of aerogel-based materials in a very short period of time and opens up the possibility to scale-up the process.

In an innovative approach, drug-loaded aerogel microspheres were produced by thermal inkjet printing (López-Iglesias et al., 2019b). This approach allows to produce microspheres without the use of emulsifiers. This "drop-on-demand" technique is applied to inks contained in thermal printheads as follows: an electric voltage heats a resistor in contact with the ink, so the temperature of the ink increases locally (4–10°C) and causes vaporization and nucleation of a bubble that expels a droplet through the printhead nozzles (Basit and Gaisford, 2018; Azizi Machekposhti et al., 2019). The cost-effectiveness, high productivity and efficiency of inkjet printing are compatible with various biomedical applications such as drug discovery (Azizi Machekposhti et al., 2019; Lamichhane et al., 2019), drug delivery (injectables, inhalation, oral or buccal) (Lamichhane et al., 2019; López-Iglesias et al., 2019b), tissue engineering (Nguyen and Pentoney, 2017; Santos-Rosales et al., 2020), modeling of human diseases, and toxicology (Nguyen and Pentoney, 2017). Namely, the field of drug development may apply inkjet printing to formulate drugs as well as to control the drug release profile (Azizi Machekposhti et al., 2019).

Alginate-based aerogels loaded with salbutamol sulfate for a sustained pulmonary drug delivery were obtained by thermal inkjet printing combined with supercritical drying (López-Iglesias et al., 2019b). The ink consisted on an alginate solution. A computer was connected with the inkjet printer to control the horizontal movement of the cartridges (**Figure 8A**). The ink cartridge contained several small chambers, each chamber involving a nozzle and a micro-thermal element. Vapor bubbles were created in the chamber, propelled the alginate-based ink as pico-droplets via the nozzle to the gelation bath containing calcium chloride (crosslinker) and salbutamol sulfate (drug). Concentration of the alginate solution was a critical parameter for ink printability. High concentrations of the alginate solution increased the viscosity of the solution, leading to the blockage of the micro-nozzle, while low concentrations reduced the stability of the alginate-based gel structure, leading to particles with decreased porosity and sphericity. The optimal alginate concentration was 0.35% (w/v) to balance the printability of the ink and the stability of the gel network. The obtained alginate-based aerogels presented a high BET specific surface area (180–397 m^2/g), high porosity (97.7%) and nanometric pore sizes (**Figures 8B–F**). Additionally, the narrow particle size distribution and spherical shape of alginate aerogels were confirmed by SEM microscopy.

The internal porous structure of the alginate aerogel particles was analyzed by focused ion beam-scanning electron microscopy (FIB-SEM) combined with image analysis (**Figures 8F,G**). FIB-SEM technique is unique to unveil the inner morphology of many beam sensitive materials such as polymers and aerogels structure without damaging the delicate structure of these nanostructured materials (Stachewicz et al., 2015, 2019). Using this technique, the

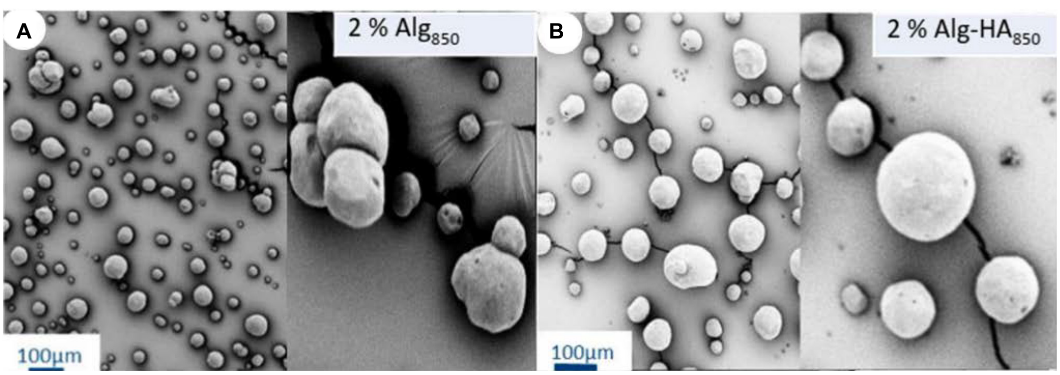

FIGURE 7 | SEM images of **(A)** alginate and **(B)** hybrid alginate/hyaluronic acid aerogel microspheres prepared by the emulsion-gelation technique. Figure adapted from Athamneh et al. (2019) with permission.

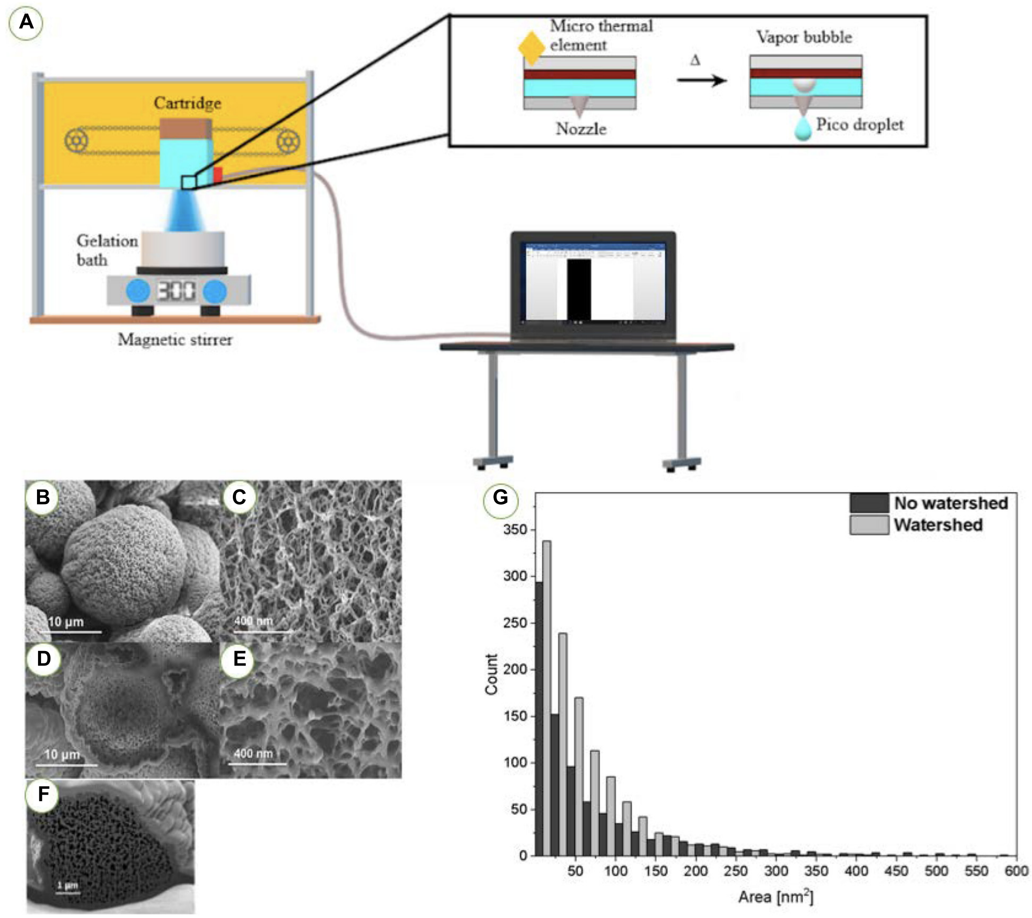

FIGURE 8 | Application of thermal inkjet printing for inhaled alginate aerogel-based formulations. **(A)** Schematic representation of thermal inkjet printing of gels. SEM images of **(B)** external morphology and **(C)** external nanostructure of alginate aerogel microspheres. **(D–F)** Images by FIB-SEM microscopy of internal cross section and nanostructure of alginate aerogel microspheres. **(G)** Pore size distribution of alginate aerogels obtained from image analysis with ImageJ software, with and without watershed segmentation. Figures adapted from López-Iglesias et al. (2019b).

narrow pore size distribution of alginate aerogel microspheres was confirmed by the pores size analysis from the SEM micrographs of cross-sections of the particles. In **Figure 8G**, the histogram showing the pore size distribution in microspheres is presented. The pore size was calculated using ImageJ software (1.51v, NIH, United States). Prior to measurements all images were binarized using percentile option in ImageJ. Additionally, watershed was used to reduce curtain effect influence on the obtained values. Statistical measurements of average pore size with standard deviations were calculated using OriginPro (2019b, OriginLab, United States). The mean values of pores in alginate aerogel microspheres reached 53.9 ± 1.75 nm^2 from FIB-SEM analysis with a standard deviation of 59.5 nm^2.

Alginate aerogel particles had suitable aerodynamic sizes (d_a = 2.4 µm) (López-Iglesias et al., 2019b). The *in vitro* aerodynamic drug deposition behavior revealed higher emitted dose (ED) and higher fine particle fraction (FPF) than some commercial formulations. The aerogels also sustained the release of salbutamol sulfate for 10 h. Finally, recent (unpublished) works confirmed that these salbutamol-loaded aerogels processed by inkjet printing resulted in formulations which are cytocompatible with human lung epithelial cell lines. Thus, alginate aerogels produced by thermal inkjet printing followed by supercritical drying proved to be suitable and safe carriers for pulmonary drug delivery.

FUTURE TRENDS OF BIOAEROGEL CARRIERS FOR PULMONARY DRUG DELIVERY

Aerogels are advanced materials with high potential for novel inhaled formulations (**Figure 9**). The combination of aerogels and SCF technology can lead to a new generation of bio-carriers for pulmonary drug delivery. The remarkable features of bioaerogels produced by supercritical drying opens the pathway to novel DPIs with enhanced effectiveness, affordability, and environmental friendliness.

From a therapeutic impact perspective, the primary goal of innovative inhaled compounds using aerogels carriers is to tackle

FIGURE 9 | Potential benefits of aerogel-based carriers for pulmonary drug delivery.

the current needs in local treatment of respiratory diseases. The large surface area of the aerogels allows enhancing the dissolution rate of poorly water-soluble drugs, which can be especially valuable for novel inhaled chemotherapy. Additionally, aerogels have a high porosity and vast surface area that also make them well-qualified candidates for inhaled systemic delivery or vaccination. Namely, inhaled vaccination is known as "one-off administration," which requires high performance of aerodynamic deposition in the target site (de Boer et al., 2017). Research on aerogels for these purposes is still incipient and needs further effort to exploit their potential in this administration route. Importantly, in the current COVID-19 state the aerogel technologies show a great promise for addressing the challenges in pulmonary drug delivery.

From a technological point of view, bioaerogels present high porosity and can deliver drugs to the bronchi minimizing systemic exposure, besides the possibility of reducing the total drug dose with less frequency of inhaled administration in a controlled-release system. Since patients with respiratory diseases normally find difficulty to supply sufficient flow rate in using DPIs, aerogel-based novel inhaled formulations can have a better performance as they depend less on the respiratory flow rate of patients. The validation of mathematical models or the development of new ones to predict aerogel particle deposition in the lungs might be advantageous for the aerogel design. Moreover, a higher knowledge on the drug-aerogel interaction at the molecular level would also favor the prediction of drug loading capacities and drug release behavior in respiratory fluid medium. The chemical, physical and biopharmaceutical stability of aerogels under controlled storage conditions also needs to be evaluated as this will influence the feasibility of the formulation of the drug product as well as the packaging and shelf conditions required. The safety of aerogels regarding the cytocompatibility with lung cells and the absence of inflammatory responses should be evaluated for each specific drug-aerogel combination. Current aerogel formulations tested for pulmonary delivery correspond to bench-scale production. The evaluation of the possibility of the aerogel production at a large (industrial) scale and under GMP guideline practices is still required.

Finally, from an environmental point of view, bioaerogels also open the possibility to reduce the burden of sociosanitary costs by using available and renewable materials. The valorisation of CO_2 with SCF technology also contributes in tailoring green inhalers that could contribute to reduce the greenhouse effect. In other words, "green inhalers" containing bioaerogels could make a joint effort creating a "zero-carbon" healthcare system fit for the 21st century.

AUTHOR CONTRIBUTIONS

All authors listed have made a substantial, direct and intellectual contribution to the work, and approved it for publication.

FUNDING

Work carried out in the framework of COST Action CA18125 "Advanced Engineering and Research of aeroGels for Environment and Life Sciences" (AERoGELS), funded by the European Commission. This work was also supported by Xunta de Galicia [ED431C 2020/17], MCIUN [RTI2018-094131-A-I00], Agencia Estatal de Investigación [AEI], and FEDER funds. CG-G acknowledges to MINECO for a Ramón y Cajal Fellowship [RYC2014-15239].

REFERENCES

Alnaief, M., Obaidat, R. M., and Alsmadi, M. M. (2020). Preparation of hybrid alginate-chitosan aerogel as potential carriers for pulmonary drug delivery. *Polymers* 12:2223. doi: 10.3390/polym12102223

Alsmadi, M. M., Obaidat, R. M., Alnaief, M., Albiss, B. A., and Hailat, N. (2020). Development, in vitro characterization, and in vivo toxicity evaluation of chitosan-alginate nanoporous carriers loaded with cisplatin for lung cancer treatment. *AAPS PharmSciTech.* 21:191. doi: 10.1208/s12249-020-01735-8

Ari, A. (2020). Practical strategies for a safe and effective delivery of aerosolized medications to patients with COVID-19. *Respir. Med.* 167:105987. doi: 10.1016/j.rmed.2020.105987

Athamneh, T., Amin, A., Benke, E., Ambrus, R., Leopold, C. S., Gurikov, P., et al. (2019). Alginate and hybrid alginate-hyaluronic acid aerogel microspheres as potential carrier for pulmonary drug delivery. *J. Supercrit. Fluids* 150, 49–55. doi: 10.1016/j.supflu.2019.04.013

Azizi Machekposhti, S., Mohaved, S., and Narayan, R. J. (2019). Inkjet dispensing technologies: recent advances for novel drug discovery. *Expert Opin. Drug Discov.* 14, 101–113. doi: 10.1080/17460441.2019.1567489

Basit, A. W., and Gaisford, S. (2018). *3D Printing of Pharmaceuticals*. New York, NY: Springer.

Borghardt, J. M., Kloft, C., and Sharma, A. (2018). Inhaled therapy in respiratory disease: the complex interplay of pulmonary kinetic processes. *Can. Respir. J.* 2018:2732017. doi: 10.1155/2018/2732017

Chakravarty, P., Famili, A., Nagapudi, K., and Al-Sayah, M. A. (2019). Using supercritical fluid technology as a green alternative during the preparation of drug delivery systems. *Pharmaceutics* 11:629. doi: 10.3390/pharmaceutics11120629

Chaurasiya, B., and Zhao, Y.-Y. (2020). Dry powder for pulmonary delivery: a comprehensive review. *Pharmaceutics* 13:31. doi: 10.3390/pharmaceutics13010031

Chen, A.-Z., Zhao, C., Wang, S.-B., Liu, Y.-G., and Lin, D.-L. (2013). Generation of porous poly-l-lactide microspheres by emulsion-combined precipitation with a compressed CO2 antisolvent process. *J. Mater. Chem. B* 1:2967. doi: 10.1039/c3tb20468e

Chvatal, A., Ambrus, R., Party, P., Katona, G., ójárt-Laczkovich, O. J., Szabó-Révész, P., et al. (2019). Formulation and comparison of spray dried non-porous and large porous particles containing meloxicam for pulmonary drug delivery. *Int. J. Pharm.* 559, 68–75. doi: 10.1016/j.ijpharm.2019.01.034

de Boer, A. H., Hagedoorn, P., Hoppentocht, M., Buttini, F., Grasmeijer, F., and Frijlink, H. W. (2017). Dry powder inhalation: past, present and future. *Expert Opin. Drug Deliv.* 14, 499–512. doi: 10.1080/17425247.2016.1224846

Eriksson, J., Thörn, H., Sjögren, E., Holmstén, L., Rubin, K., and Lennernäs, H. (2019). Pulmonary dissolution of poorly soluble compounds studied in an Ex Vivo rat lung model. *Mol. Pharm.* 16, 3053–3064. doi: 10.1021/acs.molpharmaceut.9b00289

Fahrni, M. L., Azmy, M. T., Usir, E., Aziz, N. A., and Hassan, Y. (2019). Inappropriate prescribing defined by STOPP and START criteria and its association with adverse drug events among hospitalized older patients: a multicentre, prospective study. Edited by Melissa T. Baysari. *PLoS One* 14:e0219898. doi: 10.1371/journal.pone.0219898

Fernández Tena, A., and Casan Clarà, P. (2012). Depósito pulmonar de partículas inhaladas. *Arch. Bronconeumol.* 48, 240–246. doi: 10.1016/j.arbres.2012.02.003

Franek, F., Fransson, R., Thörn, H., Bäckman, P., Andersson, P. U., and Tehler, U. (2018). Ranking in vitro dissolution of inhaled micronized drug powders including a candidate drug with two different particle sizes. *Mol. Pharm.* 15, 5319–5326. doi: 10.1021/acs.molpharmaceut.8b00796

Ganesan, K., Budtova, T., Ratke, L., Gurikov, P., Baudron, V., Preibisch, I., et al. (2018). Review on the production of polysaccharide aerogel particles. *Materials* 11:2144. doi: 10.3390/ma11112144

García-González, C. A., Budtova, T., Durães, L., Erkey, C., Gaudio, P. D., Gurikov, P., et al. (2019). An opinion paper on aerogels for biomedical and environmental applications. *Molecules* 24:1815. doi: 10.3390/molecules24091815

García-González, C. A., Jin, M., Gerth, J., Alvarez-Lorenzo, C., and Smirnova, I. (2015). Polysaccharide-based aerogel microspheres for oral drug delivery. *Carbohydr. Polym.* 117, 797–806. doi: 10.1016/j.carbpol.2014.10.045

García-González, C. A., López-Iglesias, C., Concheiro, A., and Alvarez-Lorenzo, C. (2018). "Chapter 16. biomedical applications of polysaccharide and protein based aerogels," in *Green Chemistry Series*, eds S. Thomas, L. A. Pothan, and R. Mavelil-Sam (Cambridge: Royal Society of Chemistry), 295–323. doi: 10.1039/9781782629979-00295

García-González, C. A., Sosnik, A., Kalmár, J., De Marco, I., Erkey, C., Concheiro, A., et al. (2021). Aerogels in drug delivery: from design to application. *J. Control. Release* 332, 40–63. doi: 10.1016/j.jconrel.2021.02.012

Gharse, S., and Fiegel, J. (2016). Large porous hollow particles: lightweight champions of pulmonary drug delivery. *Curr. Pharm. Design* 22, 2463–2469. doi: 10.2174/1381612822666160128145356

Gil, C., Ginex, T., Maestro, I., Nozal, V., Barrado-Gil, L., Cuesta-Geijo, M. Á, et al. (2020). COVID-19: drug targets and potential treatments. *J. Med. Chem.* 63, 12359–12386. doi: 10.1021/acs.jmedchem.0c00606

Gonçalves, V. S. S., Gurikov, P., Poejo, J., Matias, A. A., Heinrich, S., Duarte, C. M. M., et al. (2016). Alginate-based hybrid aerogel microparticles for mucosal drug delivery. *Eur. J. Pharm. Biopharm.* 107, 160–170. doi: 10.1016/j.ejpb.2016.07.003

Gregoriano, C., Dieterle, T., Breitenstein, A.-L., Dürr, S., Baum, A., Maier, S., et al. (2018). Use and inhalation technique of inhaled medication in patients with asthma and COPD: data from a randomized controlled trial. *Respir. Res.* 19:237. doi: 10.1186/s12931-018-0936-3

Gurikov, P., and Smirnova, I. (2018). Amorphization of drugs by adsorptive precipitation from supercritical solutions: a review. *J. Supercrit. Fluids* 132, 105–125. doi: 10.1016/j.supflu.2017.03.005

Hadiwinoto, G. D., Lip Kwok, P. C., and Lakerveld, R. (2018). A review on recent technologies for the manufacture of pulmonary drugs. *Ther. Deliv.* 9, 47–70. doi: 10.4155/tde-2017-0083

Hassan, M. S., and Lau, R. W. (2009). Effect of particle shape on dry particle inhalation: study of flowability, aerosolization, and deposition properties. *AAPS PharmSciTech.* 10:1252. doi: 10.1208/s12249-009-9313-3

Hastedt, J. E., Bäckman, P., Clark, A. R., Doub, W., Hickey, A., Hochhaus, G., et al. (2016). Scope and relevance of a pulmonary biopharmaceutical classification system AAPS/FDA/USP workshop March 16-17th, 2015 in Baltimore, MD. *AAPS Open* 2, 1–20. doi: 10.1186/s41120-015-0002-x

Healy, A. M., Amaro, M. I., Paluch, K. J., and Tajber, L. (2014). Dry powders for oral inhalation free of lactose carrier particles. *Adv. Drug Deliv. Rev.* 75, 32–52. doi: 10.1016/j.addr.2014.04.005

Hickey, A. J., and Edwards, D. A. (2018). Density and shape factor terms in Stokes' equation for aerodynamic behavior of aerosols. *J. Pharm. Sci.* 107, 794–796. doi: 10.1016/j.xphs.2017.11.005

Ivanoska-Dacikj, A., and Stachewicz, U. (2020). Smart textiles and wearable technologies–opportunities offered in the fight against pandemics in relation to current COVID-19 state. *Rev. Adv. Mater. Sci.* 59, 487–505. doi: 10.1515/rams-2020-0048

Jarai, B. M., Stillman, Z., Bomb, K., Kloxin, A. M., and Fromen, C. A. (2020). Biomaterials-based opportunities to engineer the pulmonary host immune response in COVID-19. *ACS Biomater. Sci. Eng.* (in press). doi: 10.1021/acsbiomaterials.0c01287

Kadota, K., Sosnowski, T. R., Tobita, S., Tachibana, I., Tse, J. Y., Uchiyama, H., et al. (2020). A particle technology approach toward designing dry-powder inhaler formulations for personalized medicine in respiratory diseases. *Adv. Powder Technol.* 31, 219–226. doi: 10.1016/j.apt.2019.10.013

Kankala, R. K., Zhang, Y. S., Wang, S.-B., Lee, C.-H., and Chen, A.-Z. (2017). Supercritical fluid technology: an emphasis on drug delivery and related biomedical applications. *Adv. Healthc. Mater.* 6:1700433. doi: 10.1002/adhm.201700433

Kipshidze, N., Iversen, P., Porter, T. R., Kipshidze, N., Siddiqui, F., Dangas, G., et al. (2020). Targeted, site-specific, delivery vehicles of therapeutics for COVID-19 patients. brief review. *Clin. Appl. Thromb. Hemost.* 26, 1–4.

Kistler, S. (1931). Coherent expanded aerogels and jellies. *Nature* 127:741. doi: 10.1038/127741a0

Kumar, A., Terakosolphan, W., Hassoun, M., Vandera, K.-K., Novicky, A., Harvey, R., et al. (2017). A biocompatible synthetic lung fluid based on human respiratory tract lining fluid composition. *Pharm. Res.* 34, 2454–2465. doi: 10.1007/s11095-017-2169-4

Lam, J., Vaughan, S., and Parkins, M. D. (2013). Tobramycin Inhalation Powder (TIP): an efficient treatment strategy for the management of chronic *Pseudomonas Aeruginosa* infection in cystic fibrosis. *Clin. Med. Insights Circ. Respir. Pulm. Med.* 7, 61–77. doi: 10.4137/CCRPM.S10592

Lamichhane, S., Bashyal, S., Keum, T., Noh, G., Seo, J. E., Bastola, R., et al. (2019). Complex formulations, simple techniques: can 3D printing technology be the Midas Touch in pharmaceutical industry? *Asian J. Pharm. Sci.* 14, 465–479. doi: 10.1016/j.ajps.2018.11.008

Lavan, A. H., Gallagher, P., Parsons, C., and O'Mahony, D. (2017). STOPPFrail (Screening tool of older persons prescriptions in frail adults with limited life expectancy): consensus validation. *Age Ageing* 46, 600–607. doi: 10.1093/ageing/afx005

Lavorini, F., Janson, C., Braido, F., Stratelis, G., and Løkke, A. (2019). What to consider before prescribing inhaled medications: a pragmatic approach for evaluating the current inhaler landscape. *Ther. Adv. Respir. Dis.* 13:175346661988453. doi: 10.1177/1753466619884532

Lechanteur, A., and Evrard, B. (2020). Influence of composition and spray-drying process parameters on carrier-free DPI properties and behaviors in the lung: a review. *Pharmaceutics* 12:55. doi: 10.3390/pharmaceutics12010055

Lee, D., Kim, J., Kim, S., Kim, G., Roh, J., Lee, S., et al. (2019). Tunable pore size and porosity of spherical polyimide aerogel by introducing swelling method based on spherulitic formation mechanism. *Microporous Mesoporous Mater.* 288:109546. doi: 10.1016/j.micromeso.2019.06.008

Levy, M. L., Carroll, W., Izquierdo Alonso, J. L., Keller, C., Lavorini, F., and Lehtimäki, L. (2019). Understanding dry powder inhalers: key technical and patient preference attributes. *Adv. Ther.* 36, 2547–2557. doi: 10.1007/s12325-019-01066-6

Liang, W., Chan, A. Y. L., Chow, M. Y. T., Lo, F. F. K., Qiu, Y., Kwok, P. C. L., et al. (2018). Spray freeze drying of small nucleic acids as inhaled powder for pulmonary delivery. *Asian J. Pharm. Sci.* 13, 163–172. doi: 10.1016/j.ajps.2017.10.002

Liang, Z., Ni, R., Zhou, J., and Mao, S. (2015). Recent advances in controlled pulmonary drug delivery. *Drug Discov. Today* 20, 380–389. doi: 10.1016/j.drudis.2014.09.020

Liao, Q., Yip, L., Chow, M. Y. T., Chow, S. F., Chan, H.-K., Kwok, P. C. L., et al. (2019). Porous and highly dispersible voriconazole dry powders produced by spray freeze drying for pulmonary delivery with efficient lung deposition. *Int. J. Pharm.* 560, 144–154. doi: 10.1016/j.ijpharm.2019.01.057

Lin, X. -F., Kankala, R. K., Tang, N., Xu, P. -Y., Hao, L. -Z., Yang, D. -Y., et al. (2019). Supercritical fluid-assisted porous microspheres for efficient delivery of insulin and inhalation therapy of diabetes. *Adv. Healthc. Mater.* 8:1800910. doi: 10.1002/adhm.201800910

López-Iglesias, C., Barros, J., Ardao, I., Gurikov, P., Monteiro, F. J., Smirnova, I., et al. (2020). Jet cutting technique for the production of chitosan aerogel microparticles loaded with vancomycin. *Polymers* 12:273. doi: 10.3390/polym12020273

López-Iglesias, C., Barros, J., Ardao, I., Monteiro, F. J., Alvarez-Lorenzo, C., Gómez Amoza, J. L. G., et al. (2019a). Vancomycin-loaded chitosan aerogel particles for chronic wound applications. *Carbohydr. Polym.* 204, 223–231. doi: 10.1016/j.carbpol.2018.10.012

López-Iglesias, C., Casielles, A. M., Altay, A., Bettini, R., Alvarez-Lorenzo, C., and García-González, C. A. (2019b). From the printer to the lungs: inkjet-printed aerogel particles for pulmonary delivery. *Chem. Eng. J.* 357, 559–566. doi: 10.1016/j.cej.2018.09.159

Lovskaya, D., and Menshutina, N. (2020). Alginate-based aerogel particles as drug delivery systems: investigation of the supercritical adsorption and in vitro evaluations. *Materials* 13:329. doi: 10.3390/ma13020329

McShane, P. J., Weers, J. G., Tarara, T. E., Haynes, A., Durbha, P., Miller, D. P., et al. (2018). Ciprofloxacin dry powder for inhalation (Ciprofloxacin DPI): technical design and features of an efficient drug–device combination. *Pulm. Pharmacol. Ther.* 50, 72–79. doi: 10.1016/j.pupt.2018.03.005

Moon, C., Smyth, H. D. C., Watts, A. B., and Williams, R. O. (2019). Delivery technologies for orally inhaled products: an update. *AAPS PharmSciTech.* 20:117. doi: 10.1208/s12249-019-1314-2

Movia, D., and Prina-Mello, A. (2020). Preclinical development of orally inhaled drugs (OIDs)—are animal models predictive or shall we move towards in vitro non-animal models? *Animals* 10:1259. doi: 10.3390/ani10081259

Muñoz-Ruíz, A., Escobar-García, D. M., Quintana, M., Pozos-Guillén, A., and Flores, H. (2019). Synthesis and characterization of a new collagen-alginate aerogel for tissue engineering. *J. Nanomater.* 2019, 1–10. doi: 10.1155/2019/2875375

N'Guessan, A., Fattal, E., Chapron, D., Gueutin, C., Koffi, A., and Tsapis, N. (2018). Dexamethasone palmitate large porous particles: a controlled release formulation for lung delivery of corticosteroids. *Eur. J. Pharm. Sci.* 113, 185–192. doi: 10.1016/j.ejps.2017.09.013

Nguyen, D. G., and Pentoney, S. L. (2017). Bioprinted three dimensional human tissues for toxicology and disease modeling. *Drug Discov. Today Technol.* 23, 37–44. doi: 10.1016/j.ddtec.2017.03.001

Ni, R., Muenster, U., Zhao, J., Zhang, L., Becker-Pelster, E.-M., Rosenbruch, M., et al. (2017). Exploring polyvinylpyrrolidone in the engineering of large porous PLGA microparticles via single emulsion method with tunable sustained release in the lung: in vitro and in vivo characterization. *J. Control. Release* 249, 11–22. doi: 10.1016/j.jconrel.2017.01.023

Obaidat, R. M., Tashtoush, B. M., Bayan, M. F., Al Bustami, R. T., and Alnaief, M. (2015). Drying using supercritical fluid technology as a potential method for preparation of chitosan aerogel microparticles. *AAPS PharmSciTech.* 16, 1235–1244. doi: 10.1208/s12249-015-0312-2

O'Mahony, D., O'Sullivan, D., Byrne, S., O'Connor, M. N., Ryan, C., and Gallagher, P. (2014). STOPP/START criteria for potentially inappropriate prescribing in older people: version 2. *Age Ageing* 44, 213–218. doi: 10.1093/ageing/afu145

Overhoff, K. A., Johnston, K. P., Tam, J., Engstrom, J., and Williams, R. O. (2009). Use of thin film freezing to enable drug delivery: a review. *J. Drug Deliv. Sci. Technol.* 19, 89–98. doi: 10.1016/S1773-2247(09)50016-0

Patel, A., and Jimenez-Shahed, J. (2018). Profile of inhaled levodopa and its potential in the treatment of Parkinson's disease: evidence to date. *Neuropsychiatr. Dis. Treat.* 14, 2955–2964. doi: 10.2147/NDT.S147633

Pu, Y., Li, Y., Wang, D., Foster, N. R., Wang, J.-X., and Chen, J.-F. (2017). A green route to beclomethasone dipropionate nanoparticles via solvent anti-solvent precipitation by using subcritical water as the solvent. *Powder Technol.* 308, 200–205. doi: 10.1016/j.powtec.2016.12.019

Rodríguez-Dorado, R., López-Iglesias, C., García-González, C., Auriemma, G., Aquino, R., and Gaudio, P. D. (2019). Design of aerogels, cryogels and xerogels of alginate: effect of molecular weight, gelation conditions and drying method on particles'. Micromeritics. *Molecules* 24:1049. doi: 10.3390/molecules24061049

Rosière, R., Berghmans, T., De Vuyst, P., Amighi, K., and Wauthoz, N. (2019). The position of inhaled chemotherapy in the care of patients with lung tumors: clinical feasibility and indications according to recent pharmaceutical progresses. *Cancers* 11:329. doi: 10.3390/cancers11030329

Şahin, İ, Özbakır, Y., İnönü, Z., Ulker, Z., and Erkey, C. (2017). Kinetics of supercritical drying of gels. *Gels* 4:3. doi: 10.3390/gels4010003

Deshkar, S. S., and Vas, A. S. (2019). Recent updates on dry powder for inhalation for pulmonary drug delivery systems. *International J. Res. Pharm. Sci.* 10, 2944–2959. doi: 10.26452/ijrps.v10i4.1575

Santos-Rosales, V., Iglesias-Mejuto, A., and García-González, C. A. (2020). Solvent-free approaches for the processing of scaffolds in regenerative medicine. *Polymers* 12:533. doi: 10.3390/polym12030533

Shakshuki, A., and Agu, R. U. (2017). Improving the efficiency of respiratory drug delivery: a review of current treatment trends and future strategies for asthma and chronic obstructive pulmonary disease. *Pulm. Ther.* 3, 267–281. doi: 10.1007/s41030-017-0046-2

Shetty, N., Cipolla, D., Park, H., and Zhou, Q. T. (2020). Physical stability of dry powder inhaler formulations. *Expert Opin. Drug Deliv.* 17, 77–96. doi: 10.1080/17425247.2020.1702643

Shiehzadeh, F., Tafaghodi, M., Laal-Dehghani, M., Mashhoori, F., Fazly Bazzaz, B. S., and Imenshahidi, M. (2019). Preparation and characterization of a dry powder inhaler composed of PLGA large porous particles encapsulating gentamicin sulfate. *Adv. Pharm. Bull.* 9, 255–261. doi: 10.15171/apb.2019.029

Smirnova, I., Suttiruengwong, S., Seiler, M., and Arlt, W. (2004). Dissolution rate enhancement by adsorption of poorly soluble drugs on hydrophilic silica aerogels. *Pharm. Dev. Technol.* 9, 443–452. doi: 10.1081/PDT-200035804

Soorbaghi, F. P., Isanejad, M., Salatin, S., Ghorbani, M., Jafari, S., and Derakhshankhah, H. (2019). Bioaerogels: synthesis approaches, cellular uptake, and the biomedical applications. *Biomed. Pharmacother.* 111, 964–975. doi: 10.1016/j.biopha.2019.01.014

Stachewicz, U., Qiao, T., Rawlinson, S. C. F., Almeida, F. V., Li, W.-Q., Cattell, M., et al. (2015). 3D imaging of cell interactions with electrospun PLGA nanofiber membranes for bone regeneration. *Acta Biomaterilia* 27, 88–100.

Stachewicz, U., Szewczyk, P. K., Kruk, A., Barber, A. H., and Czyrska-Filemonowicz, A. (2019). Pore shape and size dependence on cell growth into electrospun fiber scaffolds for tissue engineering: 2D and 3D analyses using SEM and FIB-SEM tomography. *Mater. Sci. Eng. C* 95, 397–408. doi: 10.1016/j.msec.2017.08.076

Ulker, Z., and Erkey, C. (2014). An emerging platform for drug delivery: aerogel based systems. *J. Control. Release* 177, 51–63. doi: 10.1016/j.jconrel.2013.12.033

Ulker, Z., and Erkey, C. (2017). An advantageous technique to load drugs into aerogels: gas antisolvent crystallization inside the pores. *J. Supercrit. Fluids* 120, 310–319. doi: 10.1016/j.supflu.2016.05.033

Valente, J. F. A., Dias, J. R., Sousa, A., and Alves, N. (2019). Composite Central Face Design—An Approach to Achieve Efficient Alginate Microcarriers. *Polymers* 11:1949. doi: 10.3390/polym11121949

Veres, P., Sebõk, D., Dékány, I., Gurikov, P., Smirnova, I., Fábián, I., et al. (2018). A redox strategy to tailor the release properties of Fe(III)-alginate aerogels for oral drug delivery. *Carbohydr. Polym.* 188, 159–167. doi: 10.1016/j.carbpol.2018.01.098

Wang, X., Wang, J., Feng, S., Zhang, Z., Wu, C., Zhang, X., et al. (2019). Nano-porous silica aerogels as promising biomaterials for oral drug delivery of paclitaxel. *J. Biomed. Nanotechnol.* 15, 1532–1545. doi: 10.1166/jbn.2019.2763

Weers, J., and Clark, A. (2017). The impact of inspiratory flow rate on drug delivery to the lungs with dry powder inhalers. *Pharm. Res.* 34, 507–528. doi: 10.1007/s11095-016-2050-x

Weers, J., and Tarara, T. (2014). The pulmoSphere^{TM} platform for pulmonary drug delivery. *Ther. Deliv.* 5, 277–295. doi: 10.4155/tde.14.3

Weers, J. G., Miller, D. P., and Tarara, T. E. (2019). Spray-dried PulmoSphere^{TM} formulations for inhalation comprising crystalline drug particles. *AAPS PharmSciTech.* 20:103. doi: 10.1208/s12249-018-1280-0

Zheng, L., Zhang, S., Ying, Z., Liu, J., Zhou, Y., and Chen, F. (2020). Engineering of aerogel-based biomaterials for biomedical applications. *Int. J. Nanomed.* Vol. 15, 2363–2378. doi: 10.2147/IJN.S238005

Zuo, Y. Y., Uspal, W. E., and Wei, T. (2020). Airborne transmission of COVID-19: aerosol dispersion, lung deposition, and virus-receptor interactions. *ACS Nano* 14, 16502–16524. doi: 10.1021/acsnano.0c08484

Conflict of Interest: The authors declare that the research was conducted in the absence of any commercial or financial relationships that could be construed as a potential conflict of interest.

frontiers
in Bioengineering and Biotechnology

ORIGINAL RESEARCH
published: 28 May 2021
doi: 10.3389/fbioe.2021.660691

Check for updates

Morphological and Rheological Guided Design for the Microencapsulation Process of *Lactobacillus paracasei CBA L74* in Calcium Alginate Microspheres

Concetta Di Natale[1,2], *Elena Lagreca*[1], *Valeria Panzetta*[1,2,3], *Marianna Gallo*[3,4,5], *Francesca Passannanti*[5], *Michele Vitale*[3], *Sabato Fusco*[2,6], *Raffaele Vecchione*[1]*, *Roberto Nigro*[3]* and *Paolo Netti*[1,2,3]

[1] Istituto Italiano di Tecnologia, IIT@CRIB, Largo Barsanti e Matteucci, Naples, Italy, [2] Centro di Ricerca Interdipartimentale sui Biomateriali CRIB, University of Naples Federico II, Naples, Italy, [3] Department of Chemical, Materials and Production Engineering, University of Naples Federico II, Naples, Italy, [4] Department of Engineering, University of Rome Niccolò Cusano, Rome, Italy, [5] Innovation & Technology Provider (ITP S.r.l.), Naples, Italy, [6] Dipartimento di Medicina e Scienze della Salute "Vincenzo Tiberio", Università del Molise, Campobasso, Italy

OPEN ACCESS

Edited by:
Lalit Pandey,
Indian Institute of Technology Guwahati, India

Reviewed by:
Yashveer Singh,
Indian Institute of Technology Ropar, India
Debabrata Mandal,
National Institute of Pharmaceutical Education and Research, India

***Correspondence:**
Raffaele Vecchione
Raffaele.vecchione@iit.it
Roberto Nigro
Roberto.nigro@unina.it

Specialty section:
This article was submitted to Biomaterials, a section of the journal Frontiers in Bioengineering and Biotechnology

Received: *29 January 2021*
Accepted: *16 April 2021*
Published: *28 May 2021*

Citation:
Di Natale C, Lagreca E, Panzetta V, Gallo M, Passannanti F, Vitale M, Fusco S, Vecchione R, Nigro R and Netti P (2021) Morphological and Rheological Guided Design for the Microencapsulation Process of Lactobacillus paracasei CBA L74 in Calcium Alginate Microspheres. Front. Bioeng. Biotechnol. 9:660691. doi: 10.3389/fbioe.2021.660691

The intestinal microbiota is a real ecosystem composed of several bacterial species and a very huge amount of strains that through their metabolic activities play a crucial role in the development and performance of the immune system and other functions. Microbiota modulation by probiotics establishes a new era into the pharmaceutical and healthcare market. Probiotics play, in fact, an important role in helping and sustaining human health, but in order to produce benefits, their viability must be preserved throughout the production process up to consumption, and in addition, their bioactivity required to be safeguarded while passing through the gastrointestinal tract. In this frame, encouraging results come from encapsulation strategies that have proven to be very promising in protecting bacteria and their viability. However, specific effort has to be dedicated to the design optimization of the encapsulation process and, in particular, to the processing parameters that affect capsules microstructure. Herein, focusing on calcium alginate microspheres, after a preliminary selection of their processing conditions based on size distribution, we implemented a micro-rheological analysis, by using the multiple-particle tracking technique, to correlate the inner microstructure to the selected process conditions and to the viability of the *Lactobacillus paracasei CBA L74*. It was assessed that the explored levels of cross-linking, although changing the microorganism constriction, did not affect its viability. The obtained results confirm how this technology is a promising and a valid strategy to protect the microorganism viability and ensure its stability during the production process.

Keywords: microencapsulation, calcium alginate microsphere, multiple-particle tracking, probiotics, drug delivery

INTRODUCTION

Microbiota plays a key role in the development of the immune system being its interaction with immune cells decisive for human health from early childhood (Yu et al., 2018). Its composition is very specific for every individual and seems to be strongly affected by dynamic changes and different dietary patterns and/or environmental conditions of the intestine (Salonen et al., 2014). Microbiota modulation by using probiotics constitutes a valuable strategy for the development of nutritional or pharmaceutical tools for healthcare (Ianiro et al., 2014; Sehrawat et al., 2020). Probiotics are usually defined as live microbial food ingredients able to provide beneficial effects on humans, including serum cholesterol level control, balance of intestinal microflora, enhancement of immunity defense, decrease in lactose intolerance, or anticariogenic activity (Lin, 2003). Anyway, these advantageous effects are linked to the concentration of probiotics reaching the intestine that should be at least of 10^6 CFU/ml[6]. This implies that microorganisms, being taken orally, must be resistant to the passage through the gastrointestinal (GI) tract, surviving the action of gastric and bile juices (Scheinbach, 1998; Zoghi et al., 2019). In addition to the problem of probiotics' survival in the passage through the GI tract, several studies have also shown low viability of probiotics bacteria in functional foods (Zoghi et al., 2019). These observations indicate the necessity to introduce a protective carrier, which can safely reach the intestine and provide the necessary concentrations for metabolic activities. Up to now, several methods have been performed to enhance probiotic viability, such as selection of strains tolerant to bile and acids or appropriate packaging materials, including protective compounds or oxygen scavengers (Sarkar, 2010). Among them, encapsulation has been reported to be the most useful method to protect probiotics from harmful environmental factors, such as high acidity and low pH levels, bile salts, and oxidation conditions (Scheinbach, 1998). This technology is used to "package" microorganisms cells in miniaturized capsules able to release it at controlled rates (Chávarri et al., 2010). Various polysaccharides as alginate, chitosan, or gellan gum have been employed to encapsulate probiotics (Tripathi and Giri, 2014); in particular, alginate is the most used thanks to its non-toxic nature, bioavailability, biocompatibility, low cost, and easy preparation as ionotropic gelation beads (George et al., 2019; Martău et al., 2019). Specifically, alginate has been widely used as capsules materials to protect probiotic during the GI transit, and the stability of alginate beads has already been tested (Hansen et al., 2002; Ding and Shah, 2007; Cook et al., 2012; Holkem et al., 2016). However, even recently, there have been some efforts to further enhance the degree of protection of bacterial cells in the gastric conditions by microencapsulating them into alginate-dairy bases microcapsules or by using chitosan or poly-L-lysine-coated microspheres (MPs) (Martín et al., 2015; Yeung et al., 2016; Prasanna and Charalampopoulos, 2018).

Very importantly, the role of processing parameters should be thoroughly investigated for comprehensive understanding of how they influence microcapsule formation and microstructure and to overcome some of the limitations observed for alginate or other materials. To this purpose, we propose here the development of sodium alginate MPs with potential probiotic action *via* the water-in-oil emulsion technique and with inner microstructure properties that can be highly controlled by varying cross-linking agent ($CaCl_2$) concentration and/or cross-linking time. In particular, after a preliminary selection of the processing conditions based on the analysis of size distribution, we adopted a micro-rheological analysis for an in-depth understanding on how processing parameters can affect inner microstructure, thus the probiotic viability and potentially release kinetics. To this aim, we implemented the multiple-particle tracking (MPT) technique to study the MPs rheology at different processing conditions. Indeed, MPT evaluates the diffusion of fluorescent probes embedded in a viscoelastic sample by studying their Brownian motion, directly related to the network's mechanical properties, therefore to the cross-linkage degree (Moschakis, 2013). Then, we evaluated the post-production viability of microencapsulated *Lactobacillus paracasei CBA L74* at minimum and maximum cross-linking conditions. This microorganism is not able to withstand an acidic environment; therefore, encapsulation could be a good tool to ensure its protection. Its activity was assessed in both conditions meaning that the levels of constriction, induced by the polymer matrix associated to different cross-linkage levels, were not critical for the probiotics. Consequently, the entire selected cross-linking range is usable to tune alginate material degradation with consequent impact on the gastro-protection properties and on the kinetic release of the encapsulated compound that one may modulate depending on the GI compartment to be reached and treated. Moreover, as compared with classic mineral and paraffinic oils, which possess toxicity characteristics, a greener vegetable oil, namely, soybean oil, has been used as an outer emulsion phase.

MATERIALS AND METHODS

Materials

The following materials were used: alginic acid sodium salt from brown algae (W201502; Sigma-Aldrich), calcium carbonate anhydrous, free-flowing, Redi-Dri^{TM} ($CaCO_3$, 795445, ACS reagent, ≥99%), soybean oil, dietary source of long-chain triglycerides and other lipids (S7381; Sigma-Aldrich), SPAN® 80 (viscosity 1,000–2,000 mPa at 20°C; Sigma-Aldrich), acetic acid glacial (401406, ACS reagent; CARLO ERBA), calcium chloride dihydrate ($CaCl_2$, ACS Reagent, ≥99%; Sigma-Aldrich), 200 nm yellow-green fluorescent (505–515), carboxylate-modified polystyrene nanoparticles (NPs) (Invitrogen Nanoprobes), *L. paracasei CBA L74* (Heinz Italia S.p.A., Latina, Italy), 20 g/L Bacto Yeast Extract (BD Biosciences, Milan, Italy), 0.5 g/L $MgSO_4$ (Sigma-Aldrich, Milan, Italy), 50 g/L glucose (Sigma-Aldrich), and 0.5 g/L citric acid (Sigma-Aldrich).

Methods

Microorganisms and Culture Conditions

Lactobacillus paracasei CBA L74 is a Gram-positive homo-fermentative, facultative anaerobic bacteria for which a potential probiotic activity has been demonstrated by previous studies (Sarno et al., 2014; Gallo et al., 2019; Labruna et al., 2019). The strain was stored at −20°C and revitalized in 10 ml of an animal free broth (20 g/L Bacto Yeast Extract, 0.5 g/L $MgSO_4$, 50 g/L glucose, 0.5 g/L citric acid) by incubation at 37°C. After 24 h, the suspension was centrifuged (1,600 rpm, 10 min), the supernatant discharged, and the pellet re-suspended in 10 ml of 2% w/v alginate.

Alginate MPs Preparation

Microspheres were prepared through the single emulsion water-in-oil technique by using $CaCO_3$ as cross-linking agents. Particularly, the water phase was obtained by homogenization of 10 ml of 2% (w/v) alginate with 0.5 ml of $CaCO_3$ with a concentration of 0.5 M by Ultra-Turrax (IKA T25 Digital) for 2 min at 3,000 rpm. This water phase was added drop by drop to 50 ml of the oil phase (soybean oil) with 500 μl of SPAN® 80 and stirred at 200 rpm (Heidolph RZR 2102-BR 10) for 15 min. Then, a solution of 40 μl of acetic acid glacial and 10 ml of soybean oil was added to the W/O emulsion in order to obtain a pH variation able to promote the $CaCO_3$ dissociation that allowed the first step of Ca^{2+}-mediated cross-linking.

This first cross-linking phase was followed by a second one with the addition of several concentrations of $CaCl_2$ (0.05, 0.1, 0.2 M) at different cross-linking times (5, 10, 15, 30, and 60 min). Based on these parameters, 15 different production formulations have been obtained and characterized (**Table 1**).

To allow MPs collection, these final emulsions were treated with 10% (v/v) TWEEN® 20 to promote the separation between the two phases. The particles were washed with TWEEN® 20 using a centrifuge at 25,000 rpm for 5 min at 4°C (SL16R Centrifuge; Thermo Scientific, United States) to remove soybean oil residues and to avoid aggregation phenomena during particle collection. To obtain the production yields of each formulation, MPs suspensions were filtered and then lyophilized overnight (−50°C, 0.73 hPa, Heto PowerDry PL6000 Freeze Dryer; Thermo Electron Corp., United States). The production yield was obtained by dividing the weight of lyophilized MPs with respect to the initial weight of polymer used for the preparation.

$$\%\text{yield} = \frac{g \text{ lyophilizedMPs}}{g \text{ alginate}}$$

The same preparation procedure was also used for MPs encapsulated *L. paracasei CBA L74* or fluorescent NPs (200 nm; Invitrogen Nanoprobes). In particular, NPs were encapsulated into alginate MPs by adding 33 μl of 1% solution of fluorescent NPs into 10 ml of 2% (w/v) alginate and 0.5 ml of 0.5 M $CaCO_3$ before the homogenization step, whereas CBA L74-loaded-MPs were prepared by dissolving bacterial strain into 2% (w/v) alginate solution previously sterilized. All chemical reactions for MP synthesis are schematically represented in **Figure 1**.

TABLE 1 | Formulation tested in this study.

Formulation	($CaCl_2$) M	Cross-linking time (min)
F1	0.05	5
F2	0.05	10
F3	0.05	15
F4	0.05	30
F5	0.05	60
F6	0.1	5
F7	0.1	10
F8	0.1	15
F9	0.1	30
F10	0.1	60
F11	0.2	5
F12	0.2	10
F13	0.2	15
F14	0.2	30
F15	0.2	60

MP Characterization

Dimensional and Morphological Characterization: Optical Microscopy and Static Light Scattering

Each batch of alginate MPs was morphologically and dimensionally characterized by optical microscopy (OM) using an Inverted Microscope OLYMPUS IX73 magnified 40× by an oil objective (Di Natale et al., 2020, 2021). Moreover, the precise size of MPs was evaluated by static light scattering (LD) (Mastersizer 2000; Malvern Instruments, Malvern, United Kingdom) of 0.4 mg/ml alginate-MP suspension in TWEEN® 20 (Celetti et al., 2016; Di Natale et al., 2018; Battisti et al., 2019; Jamaledin et al., 2020). Together with the average diameter (d50), for each size distribution, the SPAN value has also been evaluated, which is the distribution width calculated as:

$$\text{SPAN} = \left(\frac{\text{d90} - \text{d10}}{\text{d50}}\right)$$

where d90 is the particle diameter at which 90% of the particles is smaller than this value, whereas d10 is the diameter at which 10% of the particles is smaller than this value.

Multiple-Particle Tracking

The role of cross-linking agent concentration [$CaCl_2$ (0.05, 0.1, and 0.2 M)] on the radial distribution of MPs network mesh-size was evaluated through the MPT technique. Videos of fluorescent 200 nm polystyrene-FITC-NPs embedded in alginate MPs (50 MPs for each sample) were acquired in time-lapse for a total time of 10 s at 10 frames per second (fps), using an inverted fluorescence microscope (Olympus IX81; Olympus), equipped with a 60× water immersion objective (high numerical aperture, N. A. 1.3) and a Hamamatsu ORCA-Flash 2.8 CMOS camera (Hamamatsu). The trajectories of fluorescent NPs were obtained by using our self-developed MATLAB 7 code. By this routine, each particle position was determined by intensity measurements of different areas and localized by each area's centroid; afterward, it was compared frame by frame to produce the trajectory of each particle, based on the principle that the two closest positions in successive frames belong to the same particle (proximity principle). Then, mean square displacements (MSDs) curves were

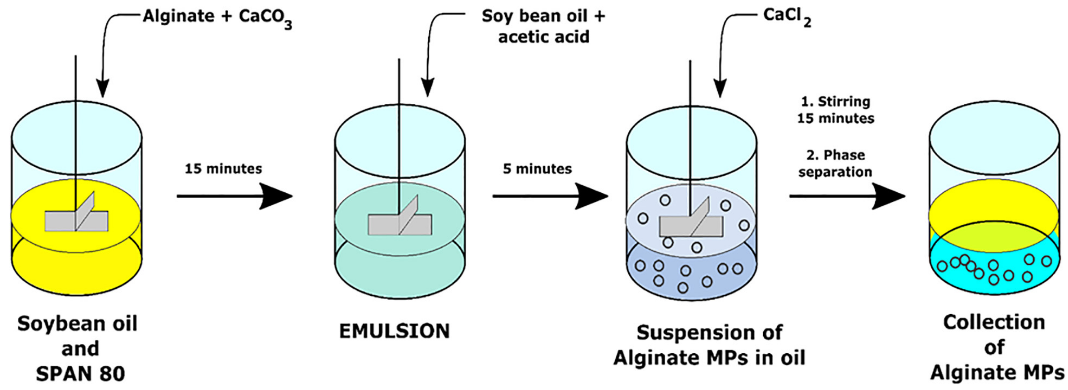

FIGURE 1 | Schematic representation of alginate MS production.

calculated from NPs trajectories using equation (a) and fitted by equation (b):

$$a)\ \mathrm{MSD} = \frac{1}{N}\sum_{t=1}^{N} < [R_i(t) - R_i(0)]^2 >$$

$$b)\ \mathrm{MSD} = 2nDt^{\alpha}$$

where n is the dimension of the system (2 in this case), D is the diffusion coefficient $\left(\mu m^2/_s\right)$, t is the time (s), and α is a non-dimensional parameter, which describes the way of motion (free diffusion α = 1, sub-diffusive α < 1, or super-diffusive α > 1). Curve fitting with a coefficient of determination (R^2) less than 0.5 was discarded from the analysis and considered not reliable from a statistical point of view. The radial diffusion map of investigated MPs was determined by correlating the diffusion coefficient D to the starting position of each tracked particle. In particular, the MP centroid position and radium were calculated by image analysis using the freeware NIH software (ImageJ 1.37c). From NPs trajectories, the distances between the initial position of NPs and alginate MPs centroids were obtained and normalized by MPs radium (r/R). The normalized distance was divided into 10 sections to allow the statistical analysis. For each section, the mean value of D was plotted as a function of normalized distance. All data were compared with a non-polarized alginate solution.

Microbiological Assay

The viability of *L. paracasei CBA L74* after encapsulation was evaluated by MRS Agar assay (Oxoid, United Kingdom). After serial dilutions, substrate was spread on Petri dishes of MRS agar and incubated at 37°C for 72 h at the end of which it is possible to count the colonies formed on each plate. Plate inseminations were carried out pre- and post-microencapsulation. Before the microencapsulation process, an insemination was carried out using an alginate sample in which the bacterial strain was dispersed.

The entrapped probiotics were instead evaluated dissolving the MPs into 1% w/w sodium citrate solution at pH 6.

RESULTS AND DISCUSSION

MP Production and Characterization

Microspheres were produced by the single emulsion method as reported in the Materials and Methods section. By combining two different processing parameters, cross-linking concentration and time of production, 15 different production formulations were obtained and characterized. The objective of these first experiments was to carry out a prior screening of the MPs produced at various cross-linking concentrations and at different times, based on the dimensional parameter calculated with two different techniques, such as Mastersizer and OM. In particular, the target diameter was set at 100 μm since larger particle diameters could alter the quality of the final product (Zuidam and Shimoni, 2010; Lavelli et al., 2014), and the value of the SPAN parameter, which indicates the width of the diameter distribution curve, was calculated as described in the "Materials and Methods" section. These parameters were evaluated for all formulations and reported in **Table 2**. The obtained results showed that the F1 and F2 formulations

TABLE 2 | Values of d50 and SPAN for all the studied formulations, n = 3.

Formulation	($CaCl_2$) M	Cross-linking time (min)	d50 (μ m)	SPAN
F1	0.05	5	297.87 ± 2.72	1.6
F2	0.05	10	191. 95 ± 3.48	1.8
F3	0.05	15	93.10 ± 0.12	0.9
F4	0.05	30	128.08 ± 3.69	1.6
F5	0.05	60	156.88 ± 2.20	1.5
F6	0.1	5	97.71 ± 1.18	1.7
F7	0.1	10	106.25 ± 0.48	1.8
F8	0.1	15	95.10 ± 1.37	0.8
F9	0.1	30	104.27 ± 2.23	0.9
F10	0.1	60	105.73 ± 1.00	1.3
F11	0.2	5	86.74 ± 0.25	1.4
F12	0.2	10	116.51 ± 0.87	3.7
F13	0.2	15	90.72 ± 0.89	1.1
F14	0.2	30	88.54 ± 0.15	1.1
F15	0.2	60	105.84 ± 2.94	4.2

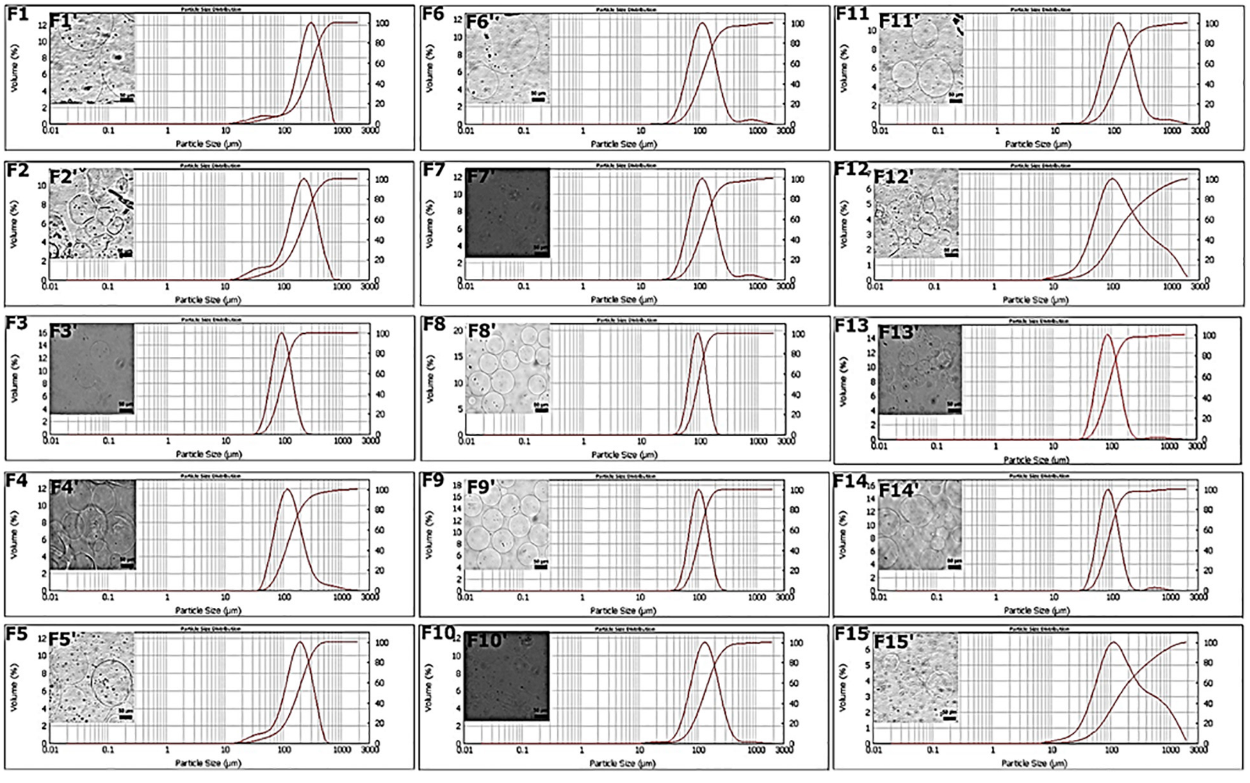

FIGURE 2 | Chemical–physical **(F1–F2)** and morphological characterization **(F1′–F2′)** of microspheres.

displayed non-symmetrical distributions ranging from 10 to 700 μm and high value of SPAN between 1.6 and 1.8 (**Figures 2F1–F2**). This behavior can be explained by the presence of pronounced aggregation phenomena between MPs (**Figures 2F1′–F2′**). Better results were obtained for the F3 formulation, which showed an average diameter of 93.10 ± 0.12 μm and a SPAN value of 0.9 (**Figures 2F3–F3′**). On the contrary, increasing the cross-linking time (F4 and F5) curves with a very wide distribution were obtained together with average diameters larger than 100 μm (**Figures 2F4–F5, F4′–F5′**). The distribution curves obtained with 0.1 M cross-linking agent showed a constant trend; indeed, for all formulations, the mean diameter was near the target value of 100 μm. In particular, F8 and F9 (**Figures 2F8–F9**) revealed high symmetrical distribution with SPAN values less than 1, and their mono-dispersion was also confirmed by OM (**Figures 2F8′–F9′**). As to the formulation F10, even if the distribution was symmetrical, the SPAN value was 1.3 indicating the beginning of aggregation phenomena also confirmed by optical images (**Figures 2F10–F10′**). The widest and least symmetrical distributions were obtained for F6 and F7 (SPAN of 1.7 and 1.8, respectively), corresponding to cross-linking times of 5 and 10 min (**Figures 2F6–F7, F6′–F7′**), maybe not enough to provide sufficient cross-linking. Similar results were obtained for formulations with 0.2 M $CaCl_2$; they showed highly variable distribution curves according to the cross-linking time. Particularly, the curve of formulation F11, relating to the time of 5 min, showed the presence of a peak relative to particles with diameters greater than 1,000 μm and a SPAN value of 1.4 (**Figure 2F11**). These values are due to aggregation phenomena between MPs (**Figure 2F11′**). The same considerations were for the F12, in which the distribution curve is non-uniform with a SPAN value of 3.7 and an average diameter of 116 μm (**Figures 2F12–F12′**). For formulations F13 and F14, relating to the cross-linking times of 15 and 30 min, no differences were observed in terms of peaks of the distributions (**Figures 2F13–F14**). The average diameter settles around the target value of 100 μm, and the SPAN values are slightly greater than 1. However, it is possible to note how, even if these formulations showed the most homogeneous distribution curves (**Figures 2F13–F14**), a second peak related to particles of about 500 μm was found, confirming the occurrence of aggregation phenomena (**Figures 2F13′–F14′**). The last formulation tested, F15, displayed a fewer uniform distribution with a SPAN value of 4.2 despite the average diameter recorded was equal to 105.84 ± 2.94 μm (**Figures 2F15–F15′**).

Therefore, from the analysis of particle diameters, we concluded that time affects the quality of the particle distribution below and above certain values. For times below 15 min especially for the minimum concentration of cross-linking agent equal to 0.05 M, there is aggregation due to low cross-linkage. For all the concentrations, the minimum time to have good quality particles with SPAN close to or below 0.1 is 15 min. Remarkably, in all the cases, the maximum cross-linking time of 60 min always promoted some aggregation, which was particularly evident for the maximum cross-linker concentration of 0.2 M. For the minimum cross-linker concentration (0.05 M), the increase of the SPAN value was registered already at 30 min. SPAN increase at prolonged cross-linking times indicates some aggregation most probably due to a cross reticulation between particles, whereas for short cross-linking times especially for lower cross-linker concentrations, processing conditions are not sufficient to stabilize structurally the particles that can undergo coalescence as well as differentiated *swelling* or *shrinkage* phenomena (Oliveira and Mano, 2011). An analysis on production yields was also performed. As shown in **Supplementary Table 1**, at each cross-linking concentration, the yield was improved by increasing the cross-linking time. A similar trend was obtained by setting the cross-linking time, in this case, the yield enhanced as the concentration increased. This behavior can be justified by the diffusion kinetics of Ca^{2+} cations that become faster when both parameters grow. The best result was obtained using the cross-linking time of 30 min where a yield of 96% was achieved at 0.2 M (**Supplementary Table 1**). The lowest yield (27%) was instead obtained for the formulation with the lowest parameters: 0.05 M and 15 min (**Supplementary Table 1**). In this case, the combination of the two parameters is not sufficient to ensure that the cross-linking phenomenon is homogeneous for all the droplets of alginate dispersed in the oil phase within the emulsion. Moreover, the 0.05 M concentration was able to reach only 39% of the production yield at 30 min, which instead for the concentration of 0.1 M was achieved already at 15 min (**Supplementary Table 1**). One future aim will be to optimize process conditions in order to improve the production yield for the selected cross-linking conditions.

Microencapsulation of *L. paracasei CBA L74*

Based on MPT data in which the condition of minimum cross-linking guarantees greater mobility to the encapsulated component, whereas the condition of maximum cross-linking immobilizes the encapsulated component in a dense polymeric network, we decided to carry out the microencapsulation tests of *L. paracasei CBA L74* in the critical conditions of minimum cross-linkage (F3: 0.05 M $CaCl_2$, 15 min) and maximum cross-linkage (F14: 0.2 M $CaCl_2$, 30 min). These two extreme conditions among the formulations gave us the best results in terms of SPAN. A less dense cross-linking should guarantee greater mobility to the microorganism, whereas a complete cross-linking should immobilize the microorganism in the polymerized alginic acid.

Viability tests confirmed that in both cases, minimum and maximum cross-linking conditions, the encapsulated microorganism remained viable, maintaining the initial bacterial load unaltered. In detail, as shown in **Table 3**, no significant differences were found when the data obtained in the post-encapsulation phase were compared with those of the initial microbial load related to bacterial strain dispersed in alginate solution at time t_0. That means that at least in terms of strain viability, the explored range of processing conditions is viable for further investigation.

TABLE 3 | Evaluation of *Lactobacillus paracasei CBA L74* viability before and after encapsulation processes.

	Strain (CFU ml^{-1})	t_0 (CFU ml^{-1})	Post-encaps (CFU ml^{-1})
F3	1.98×10^8	5.03×10^8	1.57×10^8
F14	1.98×10^8	1.33×10^8	1.54×10^8

The measurement of the number of colonies reported was in CFU ml^{-1} (Colony Forming Units); n = 3.

MPT

After a first screening based on the size of the average diameter, MPs were investigated in terms of microstructure by implementing an innovative technique based on MPT. MPT is a micro-rheological technique able to investigate the rheological properties of a polymeric network by studying the mobility of NPs embedded within the polymer matrix. Such mobility is connected to the MPs cross-linking degree, which determines MP functionality. First of all, the cross-linking degree is linked to mechanical stresses to which the encapsulated components are subjected, which in the case of *L. paracasei CBA L74*, could lead to a possible decrease in the bacterial load. Anyway, at least in the explored range, this circumstance was excluded by the viability test performed at the extremes of such range. Moreover, the cross-linking degree is connected to the degree of protection against the surrounding environment and to the release kinetics of the encapsulated components. First, we checked by MPT if a complete and uniform cross-linking within the MPs was obtained.

In particular, by using 200 nm fluorescent NPs embedded into the alginate MPs, we calculated the diffusivity coefficients along the normalized radius of the MPs (**Figures 3A,B**), as described in the "Materials and Methods" section. **Figure 4A** shows the results obtained by plotting the diffusion coefficient (D) as a function of the normalized distance along the MPs radius. Comparing the samples at 15 min (F3, F8, and F13), the coefficient D was almost constant along the radius of the MPs for both F8 and F13 formulations and lower for the 0.2 M concentration (F13), whereas for the 0.05 M concentration (F3), the diffusion coefficient did not show a constant trend with a peak in correspondence to the normalized radius value equal to 0.45 close to the diffusivity of the alginate solution ($\sim 3.2 \times 10^{-3}$ $\mu m^2/s$). We interpreted this behavior as related to an uncompleted outside-in $CaCl_2$ polymerization process during the MP fabrication. In particular, we supposed that the polymerization process was stopped when the diffusion of the divalent Ca^{2+} cations covered about 40% of the radius (**Figure 4B**). In other words, when a concentration of 0.05 M was used for 15 min of cross-linking time, the polymerization front due to the external gelation mechanism did not advance along the entire MP radius. To complete the polymerization and obtain a uniform cross-linking within the MPs, a cross-linking time of 30 min (F4) was necessary (**Supplementary Figure 1**). Conversely, for the 0.1 and 0.2 M cross-linker concentrations, a time of 15 min was sufficient to guarantee a uniform and complete cross-linking within MPs. Starting from these observations, we compared the three formulations obtained

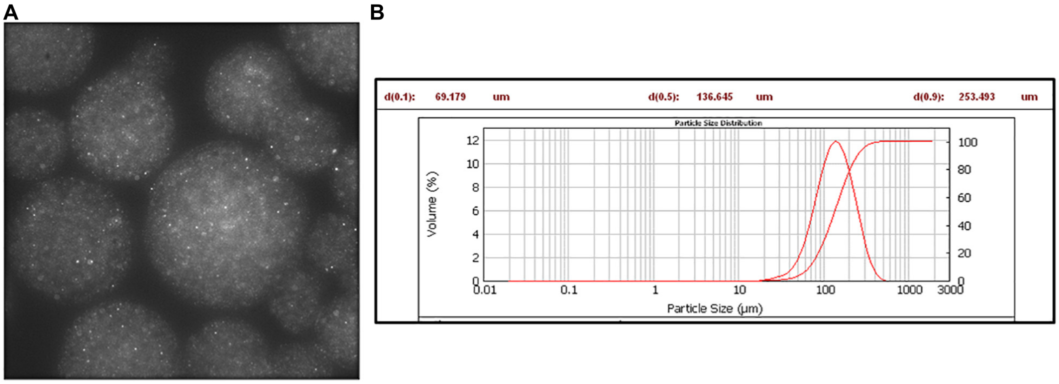

FIGURE 3 | Fluorescent NPs encapsulated in alginate microspheres. **(A)** Fluorescence image: λ_{exc} 488 nm, λ_{emiss} 520–600 nm. **(B)** Mastersizer analysis.

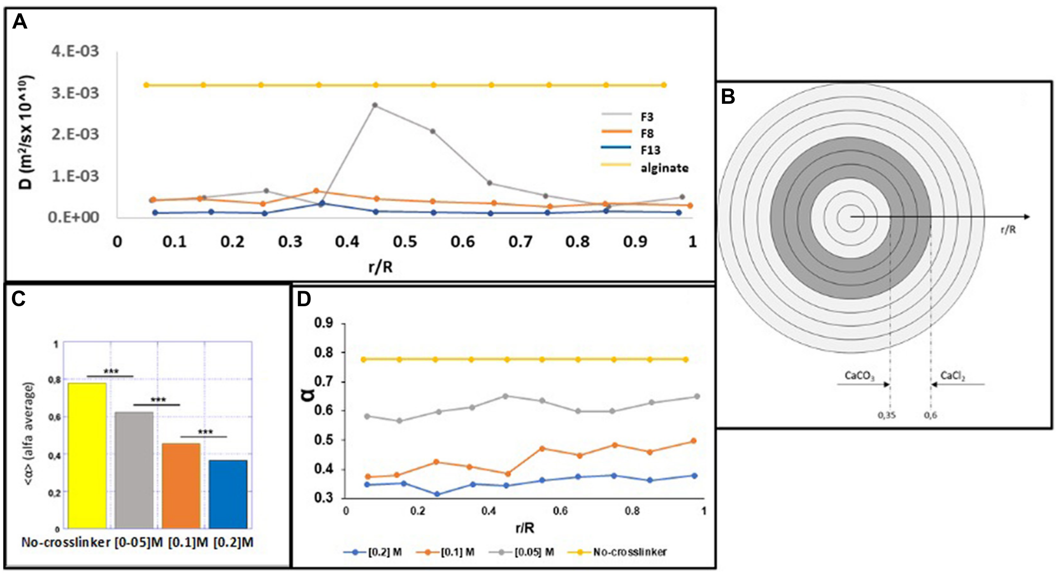

FIGURE 4 | MPT microsphere analysis. **(A)** The *D* coefficient was correlated to the normalized distance along the radius of the microspheres for all formulations. **(B)** Internal and external gelation mechanisms for the concentration of 0.05 M $CaCl_2$ and the non-polymerization area of the bare alginate. **(C)** Average values of α for the bare alginate and F3, F8, and F13 formulations. **(D)** α Values are plotted as a function of the normalized distance along the radius from the center of the microspheres.

at 15 min (F3, F8, and F13) analyzing their motion regime. The parameter (α) was obtained by fitting the MSD of NPs with a power-law equation as described in the "Materials and Methods" section and was used to obtain information on the mode of motion of NPs encapsulated within MPs. In detail, α equal to one identifies a purely diffusive regime, α less than one identifies a sub-diffusive regime, and α greater than one identifies a super-diffusive regime.

In **Figure 4C**, the average values of α for the formulations F3, F8, and F13, compared with the value obtained by analyzing the starting solution of 2% uncured alginate (v/w), are shown. The identified motion regimes were all sub-diffusive, and as expected, α parameter decreases when the cross-linking concentration rises up. This is made evident in **Figure 4D**, where α is plotted as a function of the normalized distance along the radius from the MP center. For each concentration of tested cross-linker, the NPs mobility remains almost unchanged (the percentage variation is $\simeq$1%) from the center to the outer MP section and decreases as the cross-linker concentration increases. **Figures 4A,C** shows that the parameters α and *D* present an inverse correlation with the cross-linker concentration (both decreasing with increasing the cross-linker concentration), suggesting that the mesh-size of the polymer network is lowering, posing a steric hindrance for NPs mobility. Furthermore, the power law dependence of the MSD on the time lag is a signature of mechanical behavior of the polymer network (Fusco et al., 2015; Panzetta et al., 2017); thus, the reduction of *D* can be considered accompanied by a stiffening process of the alginate MPs when the cross-linker concentration increases. Importantly, the possibility to control the mechanical properties of the MPs microstructure can be used to finely tune their degradation and then the kinetic release of the encapsulated compound.

Thanks to the MPT analysis, we can understand the impact of the processing parameters (cross-linker concentration and cross-linking time) toward inner microstructure parameters (D and α), which, upon future *in vitro* digestion tests, can help in the optimal design of the MPs.

CONCLUSION

This study presents a simple method for the encapsulation of the probiotic *L. paracasei CBA L74* in sodium alginate MPs by the water-in-oil emulsion technique. The optimization of the formulation parameters was obtained by varying cross-linking agent concentrations and cross-linking times and by replacing mineral and paraffinic oils with a greener and safer vegetable oil. Then, once shortlisted, the parameters ranges, an MPT based micro-rheological analysis was performed within the MPs in order to understand the relation between processing parameters and inner microstructures, which in turn can affect probiotic viability and its release. Post-production viability of microencapsulated *L. paracasei CBA L74* was assessed at minimum and maximum cross-linking conditions meaning that the entire selected cross-linkage range is viable to tune MP microstructure. Additionally, we could understand the impact of the processing parameter on MP properties (ex. D and α), which can help in the optimal design of the system upon future *in vitro* digestion tests. The latter tests will indeed provide useful feedback on the MP degradation and, therefore, on the gastro-protection and release kinetic properties, which will be correlated to the MPs properties. In this way, a fine tuning of the processing parameters will be theoretically performed and then experimentally assessed. The final aim will be to ensure the viability of the microorganism and, at the same time, its release into the colon and place the bases for application in the industrial field, particularly in the food industry. Subsequent studies will concern the development of a functional food with beneficial properties for the intestinal microbiota.

DATA AVAILABILITY STATEMENT

The original contributions presented in the study are included in the article/**Supplementary Material**, further inquiries can be directed to the corresponding author/s.

AUTHOR CONTRIBUTIONS

CD and RV prepared the draft and the final version of the manuscript. CD, EL, and MV performed the MP synthesis and morphological characterization. VP, MV, and SF achieved the MPT analysis. VP and SF also revised the original draft. MG and FP performed the biological assays and revised the original draft. RV, RN, and PN conceived the research and revised the original draft. All authors contributed to the article and approved the submitted version.

SUPPLEMENTARY MATERIAL

The Supplementary Material for this article can be found online at: https://www.frontiersin.org/articles/10.3389/fbioe.2021.660691/full#supplementary-material

Supplementary Figure 1 | *D* coefficient of F3 and F4 formulations along the radius (0–1r).

REFERENCES

Battisti, M., Vecchione, R., Casale, C., Pennacchio, F. A., Lettera, V., Jamaledin, R., et al. (2019). Non-invasive production of multi-compartmental biodegradable polymer microneedles for controlled intradermal drug release of labile molecules. *Front. Bioeng. Biotechnol.* 7:296. doi: 10.3389/fbioe.2019.00296

Celetti, G., Di Natale, C., Causa, F., Battista, E., and Netti, P. A. (2016). Functionalized poly (ethylene glycol) diacrylate microgels by microfluidics: in situ peptide encapsulation for in serum selective protein detection. *Colloids Surf. B Biointerfaces* 145, 21–29. doi: 10.1016/j.colsurfb.2016.04.036

Chávarri, M., Marañón, I., Ares, R., Ibáñez, F. C., Marzo, F., and del Carmen Villarán, M. (2010). Microencapsulation of a probiotic and prebiotic in alginate-chitosan capsules improves survival in simulated gastro-intestinal conditions. *Int. J. Food Microbiol.* 142, 185–189. doi: 10.1016/j.ijfoodmicro.2010.06.022

Cook, M. T., Tzortzis, G., Charalampopoulos, D., and Khutoryanskiy, V. V. (2012). Microencapsulation of probiotics for gastrointestinal delivery. *J. Control. Release* 162, 56–67. doi: 10.1016/j.jconrel.2012.06.003

Di Natale, C., Celetti, G., Scognamiglio, P. L., Cosenza, C., Battista, E., Causa, F., et al. (2018). Molecularly endowed hydrogel with an in silico-assisted screened peptide for highly sensitive small molecule harvesting. *Chem. Commun.* 54, 10088–10091. doi: 10.1039/c8cc04943b

Di Natale, C., De Rosa, D., Profeta, M., Jamaledin, R., Attanasio, A., Lagreca, E., et al. (2021). Design of biodegradable bi-compartmental microneedles for the stabilization and the controlled release of the labile molecule collagenase for skin healthcare. *J. Mater. Chem. B* 9, 392–403. doi: 10.1039/d0tb02279a

Di Natale, C., Onesto, V., Lagreca, E., Vecchione, R., and Netti, P. A. (2020). Tunable release of curcumin with an in silico-supported approach from mixtures of highly porous PLGA microparticles. *Materials* 13:1807. doi: 10.3390/ma13081807

Ding, W., and Shah, N. (2007). Acid, bile, and heat tolerance of free and microencapsulated probiotic bacteria. *J. Food Sci.* 72, M446–M450.

Fusco, S., Panzetta, V., Embrione, V., and Netti, P. A. (2015). Crosstalk between focal adhesions and material mechanical properties governs cell mechanics and functions. *Acta Biomater.* 23, 63–71. doi: 10.1016/j.actbio.2015.05.008

Gallo, M., Nigro, F., Passannanti, F., Nanayakkara, M., Lania, G., Parisi, F., et al. (2019). Effect of pH control during rice fermentation in preventing a gliadin P31-43 entrance in epithelial cells. *Int. J. Food Sci. Nutrit.* 70, 950–958. doi: 10.1080/09637486.2019.1599827

George, A., Shah, P. A., and Shrivastav, P. S. (2019). Natural biodegradable polymers based nano-formulations for drug delivery: a review. *Int. J. Pharm.* 561, 244–264. doi: 10.1016/j.ijpharm.2019.03.011

Hansen, L. T., Allan-Wojtas, P., Jin, Y.-L., and Paulson, A. (2002). Survival of Ca-alginate microencapsulated *Bifidobacterium* spp. in milk and simulated gastrointestinal conditions. *Food Microbiol.* 19, 35–45. doi: 10.1006/fmic.2001.0452

Holkem, A. T., Raddatz, G. C., Nunes, G. L., Cichoski, A. J., Jacob-Lopes, E., Grosso, C. R. F., et al. (2016). Development and characterization of alginate microcapsules containing Bifidobacterium BB-12 produced by emulsification/internal gelation followed by freeze drying. *LWT Food Sci. Technol.* 71, 302–308. doi: 10.1016/j.lwt.2016.04.012

Ianiro, G., Bibbo, S., Gasbarrini, A., and Cammarota, G. (2014). Therapeutic modulation of gut microbiota: current clinical applications and future perspectives. *Curr. Drug Targets* 15, 762–770. doi: 10.2174/1389450115666140606111402

Jamaledin, R., Sartorius, R., Di Natale, C., Vecchione, R., De Berardinis, P., and Netti, P. A. (2020). Recombinant filamentous bacteriophages encapsulated in biodegradable polymeric microparticles for stimulation of innate and adaptive immune responses. *Microorganisms* 8:650. doi: 10.3390/microorganisms8050650

Labruna, G., Nanayakkara, M., Pagliuca, C., Nunziato, M., Iaffaldano, L., D'Argenio, V., et al. (2019). Celiac disease−associated *Neisseria flavescens* decreases mitochondrial respiration in CaCo−2 epithelial cells: impact of *Lactobacillus paracasei* CBA L74 on bacterial−induced cellular imbalance. *Cell. Microbiol.* 21:e13035.

Lavelli, V., Harsha, P. S., Torri, L., and Zeppa, G. (2014). Use of winemaking by-products as an ingredient for tomato puree: the effect of particle size on product quality. *Food Chem.* 152, 162–168. doi: 10.1016/j.foodchem.2013.11.103

Lin, D. C. (2003). Probiotics as functional foods. *Nutrit. Clin. Pract.* 18, 497–506.

Martău, G. A., Mihai, M., and Vodnar, D. C. (2019). The use of chitosan, alginate, and pectin in the biomedical and food sector—biocompatibility, bioadhesiveness, and biodegradability. *Polymers* 11:1837. doi: 10.3390/polym11111837

Martín, M. J., Lara-Villoslada, F., Ruiz, M. A., and Morales, M. E. (2015). Microencapsulation of bacteria: a review of different technologies and their impact on the probiotic effects. *Innov. Food Sci. Emerg. Technol.* 27, 15–25. doi: 10.1016/j.ifset.2014.09.010

Moschakis, T. (2013). Microrheology and particle tracking in food gels and emulsions. *Curr. Opin. Colloid Interface Sci.* 18, 311–323. doi: 10.1016/j.cocis.2013.04.011

Oliveira, M. B., and Mano, J. F. (2011). Polymer−based microparticles in tissue engineering and regenerative medicine. *Biotechnol. Progr.* 27, 897–912. doi: 10.1002/btpr.618

Panzetta, V., Musella, I., Rapa, I., Volante, M., Netti, P. A., and Fusco, S. (2017). Mechanical phenotyping of cells and extracellular matrix as grade and stage markers of lung tumor tissues. *Acta Biomater.* 57, 334–341. doi: 10.1016/j.actbio.2017.05.002

Prasanna, P., and Charalampopoulos, D. (2018). Encapsulation of *Bifidobacterium longum* in alginate-dairy matrices and survival in simulated gastrointestinal conditions, refrigeration, cow milk and goat milk. *Food Biosci.* 21, 72–79. doi: 10.1016/j.fbio.2017.12.002

Salonen, A., Lahti, L., Salojärvi, J., Holtrop, G., Korpela, K., Duncan, S. H., et al. (2014). Impact of diet and individual variation on intestinal microbiota composition and fermentation products in obese men. *ISME J.* 8, 2218–2230. doi: 10.1038/ismej.2014.63

Sarkar, S. (2010). Approaches for enhancing the viability of probiotics: a review. *Br. Food J.* 112, 329–349. doi: 10.1108/00070701011034376

Sarno, M., Lania, G., Cuomo, M., Nigro, F., Passannanti, F., Budelli, A., et al. (2014). *Lactobacillus paracasei* CBA L74 interferes with gliadin peptides entrance in Caco-2 cells. *Int. J. Food Sci. Nutrit.* 65, 953–959. doi: 10.3109/09637486.2014.940283

Scheinbach, S. (1998). Probiotics: functionality and commercial status. *Biotechnol. Adv.* 16, 581–608. doi: 10.1016/s0734-9750(98)00002-0

Sehrawat, N., Yadav, M., Singh, M., Kumar, V., Sharma, V. R., and Sharma, A. K. (2020). Probiotics in microbiome ecological balance providing a therapeutic window against cancer. *Semin. Cancer Biol.* 70, 24–36. doi: 10.1016/j.semcancer.2020.06.009

Tripathi, M. K., and Giri, S. K. (2014). Probiotic functional foods: survival of probiotics during processing and storage. *J. Funct. Foods* 9, 225–241. doi: 10.1016/j.jff.2014.04.030

Yeung, T. W., Üçok, E. F., Tiani, K. A., McClements, D. J., and Sela, D. A. (2016). Microencapsulation in alginate and chitosan microgels to enhance viability of *Bifidobacterium longum* for oral delivery. *Front. Microbiol.* 7:494. doi: 10.3389/fmicb.2016.00494

Yu, Q., Jia, A., Li, Y., Bi, Y., and Liu, G. (2018). Microbiota regulate the development and function of the immune cells. *Int. Rev. Immunol.* 37, 79–89. doi: 10.1080/08830185.2018.1429428

Zoghi, A., Khosravi-Darani, K., Sohrabvandi, S., Attar, H., and Alavi, S. A. (2019). Survival of probiotics in synbiotic apple juice during refrigeration and subsequent exposure to simulated gastro-intestinal conditions. *Iran. J. Chem. Chem. Eng. (IJCCE)* 38, 159–170.

Zuidam, N. J., and Shimoni, E. (2010). "Overview of microencapsulates for use in food products or processes and methods to make them," in *Encapsulation Technologies for Active Food Ingredients and Food Processing*, eds N. Zuidam and V. Nedovic (New York, NY: Springer), 3–29. doi: 10.1007/978-1-4419-1008-0_2

Conflict of Interest: The authors declare that the research was conducted in the absence of any commercial or financial relationships that could be construed as a potential conflict of interest.

frontiers
in Bioengineering and Biotechnology

REVIEW
published: 24 June 2021
doi: 10.3389/fbioe.2021.682133

Check for updates

Review on Computer-Aided Design and Manufacturing of Drug Delivery Scaffolds for Cell Guidance and Tissue Regeneration

Aurelio Salerno[1] and Paolo A. Netti[2,3,4]*

[1] Independent Researcher, Barcelona, Spain, [2] Center for Advanced Biomaterials for Healthcare, Istituto Italiano di Tecnologia, Naples, Italy, [3] Department of Chemical, Materials and Industrial Production Engineering, University of Naples Federico II, Naples, Italy, [4] Interdisciplinary Research Center on Biomaterials, University of Naples Federico II, Naples, Italy

OPEN ACCESS

Edited by:
Tim B. F. Woodfield,
University of Otago, New Zealand

Reviewed by:
Gustavo A. Abraham,
Consejo Nacional de Investigaciones Científicas y Técnicas (CONICET), Argentina
Xiaojun Yu,
Stevens Institute of Technology, United States

****Correspondence:***
Aurelio Salerno
asalerno@unina.it

Specialty section:
This article was submitted to Biomaterials, a section of the journal Frontiers in Bioengineering and Biotechnology

Received: *17 March 2021*
Accepted: *26 May 2021*
Published: *24 June 2021*

Citation:
Salerno A and Netti PA (2021) Review on Computer-Aided Design and Manufacturing of Drug Delivery Scaffolds for Cell Guidance and Tissue Regeneration. Front. Bioeng. Biotechnol. 9:682133. doi: 10.3389/fbioe.2021.682133

In the last decade, additive manufacturing (AM) processes have updated the fields of biomaterials science and drug delivery as they promise to realize bioengineered multifunctional devices and implantable tissue engineering (TE) scaffolds virtually designed by using computer-aided design (CAD) models. However, the current technological gap between virtual scaffold design and practical AM processes makes it still challenging to realize scaffolds capable of encoding all structural and cell regulatory functions of the native extracellular matrix (ECM) of health and diseased tissues. Indeed, engineering porous scaffolds capable of sequestering and presenting even a complex array of biochemical and biophysical signals in a time- and space-regulated manner, require advanced automated platforms suitable of processing simultaneously biomaterials, cells, and biomolecules at nanometric-size scale. The aim of this work was to review the recent scientific literature about AM fabrication of drug delivery scaffolds for TE. This review focused on bioactive molecule loading into three-dimensional (3D) porous scaffolds, and their release effects on cell fate and tissue growth. We reviewed CAD-based strategies, such as bioprinting, to achieve passive and stimuli-responsive drug delivery scaffolds for TE and cancer precision medicine. Finally, we describe the authors' perspective regarding the next generation of CAD techniques and the advantages of AM, microfluidic, and soft lithography integration for enhancing 3D porous scaffold bioactivation toward functional bioengineered tissues and organs.

Keywords: additive manufacturing, biomimetic scaffolds, computer-aided design (CAD) processes, drug delivery, growth factor

INTRODUCTION TO COMPUTER-AIDED DESIGN AND MANUFACTURING OF DRUG DELIVERY SCAFFOLDS

Advanced drug therapies require customization and targeting of drug formulation and dosage to each specific patient to warrant treatment efficacy and reduce possible undesired secondary effects. To this purpose, engineering strategies for drug delivery system design and fabrication necessitate the combination and manipulation of materials and drugs to obtain even complex bioactive systems. Most specifically, the composition, chemical functions, morphology, and architectural features of new drug delivery systems must be controlled and designed at nanometric-scale resolution.

In the past decade, the combination of computer-aided design (CAD) and additive manufacturing (AM) has revolutionized the fields of personalized medicine and drug delivery systems (Guzzi and Tibbitt, 2020; Mohammed et al., 2020). Indeed, CAD-AM approaches have enabled the manufacturing of biomedical devices with unique features for *in vitro* and *in vivo* applications. Some examples are three dimensional (3D) drug delivery scaffolds for tissue growth and repair as well as 3D models for cancer precision medicine (Moreno Madrid et al., 2019; Shafiee, 2020). As shown in **Figure 1**, this broad category of design and fabrication techniques used medical imaging combined with virtual scaffold models and automated layer-by-layer processing to produce patient-specific devices characterized by highly controlled geometrical features, reliable microstructural properties, and spatial and temporal drug delivery capability. In particular, data acquired from computerized tomography or nuclear magnetic resonance (NMR) tests were used to generate a customized CAD model and define the consequent scaffold geometry and internal features to fit the specific tissue defect site. The scaffold model was subsequently divided into multiple layers for fabrication. AM techniques are modular approaches based on the assembly/sintering of layered structures obtained by continuous or discontinuous processes (Salerno et al., 2019). The advantages of employing AM processes, such as 3D printing, include the capability of precisely controlling the spatial loading of an active molecule within even minute quantities and generate multiple delivery profiles by creating different depots and complex geometries (Caballero-Aguilar et al., 2020; Jacob et al., 2020). These aspects enabled the compounding of personalized dosage form to minimize costs, to improve patient compliance, and to maximize drug efficacy. Besides, 3D printing technology can be successfully used in initial stages of drug development and testing, including preclinical studies and trials of dosage form with excellent dose flexibility (Jacob et al., 2020). The quality of the produced device can be adjusted by altering the fabrication parameters, mainly printing inkjets and speed, substrate of deposition, and extrusion parameters (e.g., temperature and pumping pressure) (Datta et al., 2018; Parak et al., 2019; Wang et al., 2020).

The aim of this work is to review the recent advances of CAD-AM processes focusing on the preparation of even complex drug delivery scaffolds for cell guidance and tissue repair. In particular, emphasis will be devoted to those processes/approaches allowing the fabrication of multifunctional extracellular matrix (ECM)-mimicking scaffolds and stimuli-responsive drug-loaded devices for tissue engineering (TE) and cancer precision medicine. Insight into current drawbacks and future challenges of CAD-AM processes are also provided in the concluding section of this work.

STRATEGIES FOR POROUS SCAFFOLD BIOACTIVATION BY DRUG ENTRAPMENT AND DELIVERY

Tissue engineering aims to repair and restore damaged tissue functions by using ECM-mimicking drug-releasing scaffolds or by incorporating drug delivery devices into TE scaffolds (Salerno et al., 2017; Calori et al., 2020). The ECM is a hierarchical biomolecular environment in which many cell-signaling molecules are continuously synthesized, sequestered, and released aiming to modulate cell adhesion, maintenance and self-renewal, and to guide cell proliferation, migration, and differentiation behaviors (Dutta and Dutta, 2009). For instance, the ECM of soft connective tissues is composed of fiber-forming proteins, such as collagens, elastin, and fibronectin organized into collagenous nanofibrous bundles (Ghosh et al., 2019). Furthermore, a glycosaminoglycan and proteoglycan hydrogel fills the pores of this woven fibrous bundle. These polysaccharides contain numerous instructive signals and soluble factors secreted by the resident cells that are critical for tissue development, homeostasis, and repair, and that influence cell-mediated assembly and degradation of ECM components (Ghosh et al., 2019). Besides, the natural cellular environment is heterogeneous and dynamic as the ECM composition and structure change with tissue site and developmental stage (Peng et al., 2021).

In the TE field, 3D porous scaffolds are central elements for tissue regeneration *in vitro* and/or *in vivo* as they regulate essential cellular events such as adhesion, migration, proliferation, and morphogenesis (Salerno et al., 2013, 2014; Bruggeman et al., 2017). Furthermore, scaffolds must encode arrays of biological signals, with an adequate dose and for a desired period, to cell-surface receptors to recapitulate the spatial and temporal microenvironments presented by the natural ECM. Growth factors (GFs) are biomolecules belonging to a family of intracellular signaling polypeptides able to modulate cellular activities, such as stimulating or inhibiting cellular proliferation, induce stem cell migration and recruitment from adjacent tissues, and direct their differentiation (Bittner et al., 2018). Naturally, GF stimuli are transmitted into the cell via activation of specific, transmembrane receptors that influence important regulatory proteins residing into the cytoplasm. These proteins, in turn, control cellular activities, including changes in gene expression and response to other factors (Cross and Dexter, 1991). The responding cell type, concentration of factor, and presence of other stimuli, often in a complex variable manner, determine GF effect (Wang et al., 2009). In TE strategies, GFs can be supplied directly into the culture medium at regular intervals to guide cell behavior *in vitro*. However, direct administration *in vivo* is difficult, as it requires large delivery quantities to overcome possible GF inactivation and clearance. High GF levels are, in fact, associated with high risk of adverse effects and increasing treatment costs (Wang et al., 2009). GF encapsulation strategies allowed researchers to overcome these limitations as the encapsulating material protects these molecules, while their delivery can be controlled by the modulation of carrier composition, size, and structure (Calori et al., 2020; Hwa Kim et al., 2020). Although GFs are among the most used biomolecules in TE, scaffolds delivering genetic material, including DNA and RNA, may provide a potential alternative to GFs as nucleic acids can induce changes in the gene expression of cells (Biondi et al., 2008; Kelly et al., 2019). For example, transplanted cells can take up the delivered DNA and be transfected to express proteins that

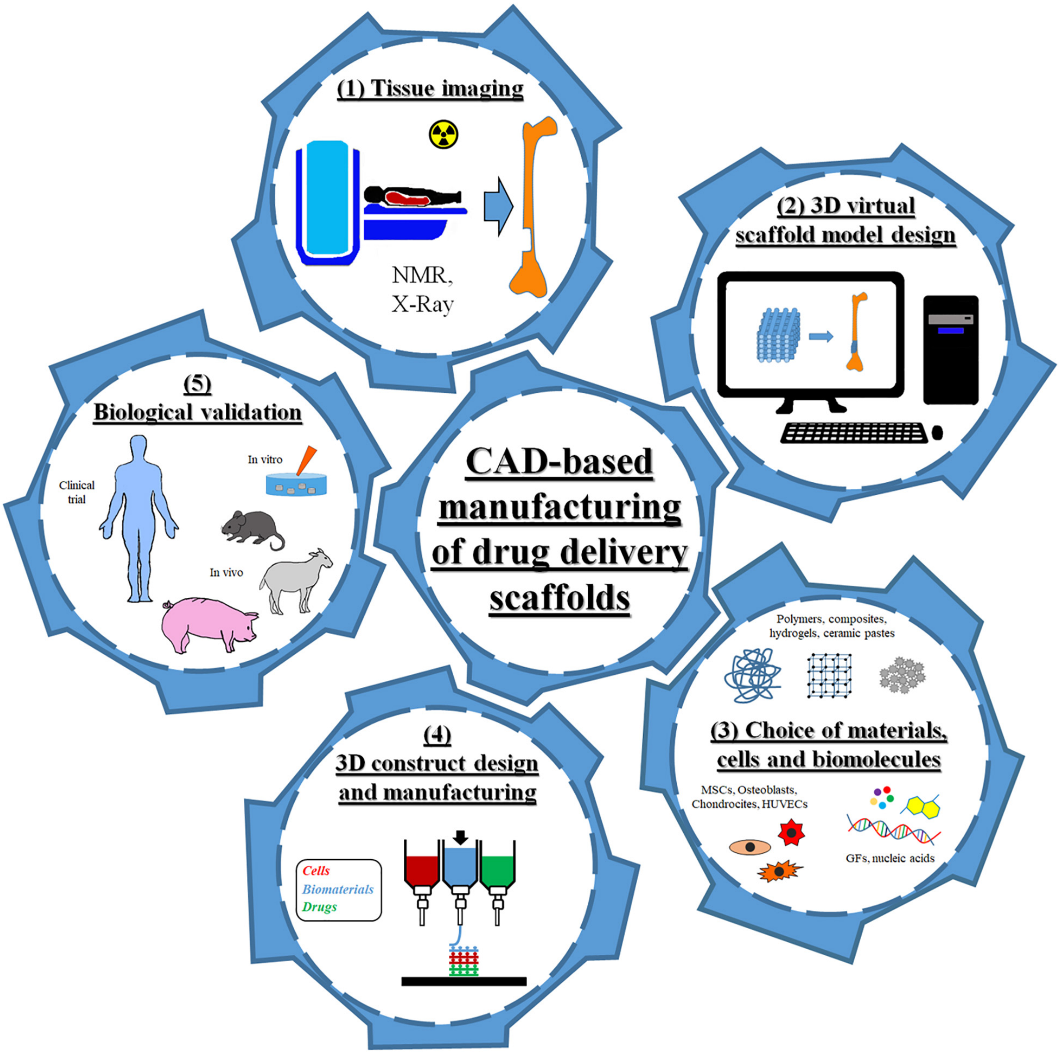

FIGURE 1 | Scheme of the different steps of computer-aided design (CAD)-based approaches for the fabrication of drug delivery scaffolds for tissue engineering.

may aid in healing a defect. As DNA aims to encode for new protein production, it must first enter the cell and then reach the nucleus often by the aid of viral vectors (Kelly et al., 2019). Antibiotic, anti-inflammatory, or differentiation agents are other drugs that can be useful for TE purposes (Wang et al., 2014). Implantation of engineered scaffolds might, in fact, cause local prolonged inflammation owing to the host immune response, which therefore requires the use of anti-inflammatory agents (Li et al., 2018). Glucocorticoids (e.g., dexamethasone) or non-steroids (e.g., ibuprofen) were delivered by the implanted biomaterials to control and modulate the local inflammatory response, avoiding possible side effects associated with systemic administration (Cantón et al., 2010; Li et al., 2018). Similarly, scaffolds delivering antibiotics, such as gentamicin, vancomycin, and antibacterial ions, may prevent infections from occurring after implantation (Yao et al., 2013; Visscher et al., 2018). It is therefore clear that the loading, as well as spatial and temporal delivery of bioactive factors from porous scaffolds is an important issue of scaffold bioactivation, and it will be discussed in the next paragraphs.

Biomolecule Delivery by Passive Release

One of the most used strategies for bioactive factor loading into scaffolds relies on the physical entrapment of signaling molecules within the scaffold matrix. This approach is widely adopted for scaffolds made of hydrogels, as biomolecules can be easily and safely loaded into the polymeric solution mixture before crosslinking or, alternatively, by swelling crosslinked samples into a solution containing the biomolecules. The delivery of the loaded factors is often a balance between free diffusion and hydrolytic degradation of the polymeric material, and can be tuned by choosing the properties of the entangled fiber structure, such as surface area, pore size, and mesh size (Li and Mooney, 2016; He et al., 2020; Shultz and Zhong, 2021). In particular, when the hydrodynamic diameter of the diffusing molecule approaches the hydrogel mesh size, the release is not only dependent on diffusion but also is controlled by polymer degradation, either hydrolytic or enzymatic. As a direct consequence, the delivery rate from hydrogel scaffolds is lowered by increasing crosslink density and polymer concentration (He et al., 2020). Both synthetic and natural polymers have been used for the design of hydrolytically degradable hydrogels in which chemical or physical crosslinking offers the possibility of controlling the diffusion of solubilized hydrophilic drugs. Naturally derived hydrogels, such as collagens, hyaluronic acid, and derivatives, are excellent materials for hydrogel preparation due to their chemical composition and structure resembling the features of the native ECM (Skardal et al., 2017; Mondal et al., 2020). For example, Skardal et al. (2017) optimized a fast photocrosslinkable heparin-conjugated hyaluronic acid hydrogel system capable of sequestering and releasing growth factors secreted from encapsulated cells. Furthermore, the authors varied hydrogel crosslinking to obtain a sustained release of proteins and heparin-binding growth factors (Skardal et al., 2017). The breakdown of polymeric chains, by hydrolysis or enzyme activity, causes the hydrogel structure to rupture and accelerates the release of drugs (Campbell et al., 2018). Hydrogel features that affect water diffusion, such as pore size and crosslink density, can also have a direct role on polymeric chain degradation and, therefore, modulate hydrogel degradation rate. Wang et al. (2018) designed an injectable macroporous hydrogel composed of gelatin/oxidized alginate/adipic acid dihydrazide loaded with human epidermal growth factor for self-healing purposes. The obtained hydrogels had an interconnected macroporous structure with porosity in the 60%–83% range and pore size from 125 to 380 μm. The authors observed that increasing hydrogel pore size and porosity accelerated the degradation and resulted in a faster growth factor release. Similarly, Campbell et al. (2018) designed an injectable alginate hydrogel that becomes porous *in situ* to enhance vascular progenitor cell release. The group of Ehrbar et al. (2007) also demonstrated the importance of hydrogel composition and degradation on biomolecule release and, therefore, tissue regeneration. In their work, biomolecular poly(ethylene glycol)-based hydrogels synthesized and degraded via site-specific enzymatic reactions were developed. These hydrogels evidenced cell-secreted metalloproteinase degradation properties mimicking the cell material crosstalk occurring in the native ECM. By this way, the authors engineered novel scaffolds for the cell-mediated modulation of biomolecule release (Ehrbar et al., 2007).

Vascular endothelial growth factor (VEGF)-delivering hydrogels have been widely used to enhance cell survival and scaffold vascularization in 3D. Indeed, VEGF initiates the sprouting of existing blood vessels by its mitogenic and chemotactic effects, drives the processes of angiogenesis and arteriogenesis, and stimulates the rapid development of a vascular network within 3D scaffolds (Cao and Mooney, 2007). However, VEGF efficacy is dose-dependent as downregulation can be unsuccessful at stimulating blood vessel-forming processes, while upregulation can produce an uncontrollable and detrimental blood vessel growth. VEGF-loaded alginate hydrogels have been deeply tested by Sun et al. (2005) and Cao and Mooney (2007) to validate the efficacy of VEGF release matrixes in the treatment of ischemic tissue. Alginate hydrogels were chosen as delivery scaffolds because VEGF can be easily loaded into the hydrogel at desired concentration and without significant growth factor deactivation during manufacturing. Concomitantly, the hydrogel provided a controlled release into the local cellular microenvironment to yield desirable concentrations over a period of days to months (Cao and Mooney, 2007; Shvartsman et al., 2014). Although VEGF is a well-established initiator of angiogenesis, its presence is often not sufficient for the formation of a complex, mature vascular network, and it was necessary to deliver multiple morphogens acting in distinct aspects of the tissue regeneration process to drive tissue regeneration to completion. Drug delivery hydrogel strategies combined VEGF with insulin-like growth factor-1 to promote functional innervation (Borselli et al., 2010a; Raimondo et al., 2019). Alternatively, VEGF and platelet-derived growth factor (PDGF) were used to stimulate blood vessel maturation and stabilization by muscle cell recruitment (Hao et al., 2007), while VEGF and bone morphogenetic protein-2 (BMP-2) enhanced osteogenic and vasculogenic differentiation of hydrogel-encapsulated cells for bone regeneration (Barati et al., 2016).

Synthetic solid biodegradable materials were also used in TE to prepare drug delivery platforms, especially for load-bearing applications. This is because, different from hydrogels, scaffolds made of these materials have mechanical properties suitable for hard-tissue repair (Lin et al., 2020). However, growth factor encapsulation within solid scaffolds posed serious issues regarding bioactive molecule leaching and degradation during processing. Reducing the use of organic solvents and/or high temperatures during the manufacturing processes and avoiding contact between the protein and aqueous solution are consequently key issues to protect biomolecule functionalities (Borselli et al., 2010b). The most currently used bio-safe technology for the production of drug-loaded devices is supercritical CO_2 ($scCO_2$) technology as it allows for upscaling drug deactivation problems related to the use of organic solvents and/or high temperatures (Salerno et al., 2015). Indeed, CO_2 is ecofriendly and non-flammable, whereas $scCO_2$ is achievable at a rather low critical temperature (Tc = 31.1°C) and moderate critical pressure (Pc = 7.4 MPa) (Salerno et al., 2017, 2018). Several works reported the use of $scCO_2$ as a blowing agent for thermoplastic biocompatible polymer foaming and porous scaffold manufacturing (Champeau et al., 2015; Salerno and Domingo, 2015). For example, porous scaffolds made of VEGF-loaded polylactic-co-glycolic acid (PLGA) were prepared by a high-pressure CO_2 fabrication process (Sun et al., 2005). Briefly, PLGA microspheres were mixed with human VEGF lyophilized with alginate and salt particles, and the mixture was processed with CO_2 at 5.5-MPa pressure and room temperature for 72 h. When the pressure was released, the PLGA particles expanded into the spaces between the salt particles and fused, trapping VEGF and the salt. Subsequently, the salt particles were leached out in water to yield porous scaffolds. The as-prepared porous scaffolds evidenced sustained VEGF delivery for up to 2 months and were able to promote *in vivo* tissue perfusion, greater capillary density, and more mature vasculature if compared with the VEGF-free PLGA scaffold used as control

(Sun et al., 2005). More recently, de Rieux et al. (2011) enhanced VEGF loading efficiency into gas foaming/salt leaching porous scaffolds by growth factor loading into chitosan nanoparticles before scaffold incorporation. In fact, the addition of GF-encapsulating carriers within porous scaffolds is a suitable way to enhance bioactive factor loading and delivery. Using nano- and micro-carrier delivery systems also opens new routes for the engineering of scaffolds releasing multiple GFs. Richardson et al. (2001), to direct the formation of a mature vasculature, tested the dual delivery of VEGF and PDGF from porous PLGA scaffolds. PDGF was pre-encapsulated in PLGA microspheres by double emulsion, while VEGF was incorporated into the PLGA scaffold matrix by CO_2 foaming. The fast VEGF delivery induced the rapid initiation of blood vessels, while the late PDGF delivery from PLGA microspheres promoted the stabilization of the preformed vascular network, finally demonstrating the versatility of this approach to study blood vessel regression and remodeling upon controlled GF release (Richardson et al., 2001). Microsphere-loaded porous scaffolds prepared by gas foaming/salt leaching were also used for bone regeneration. In particular, PLGA microspheres loaded with either VEGF and BMP-2 were incorporated into PLGA porous scaffolds to evaluate the *in vivo* osteogenic response to different GF ratios (Hernández et al., 2012).

Scaffold Bioactivation by Physical–Chemical-Triggered Biomolecule Release

Many applications in medicine require controlled release devices able to provide a pulsed protein and peptide release profile. This is the case, for example, in hormone and vaccine release, for drugs with an extensive first-pass metabolism and that develop biological tolerance when they are constantly present at their target site, and for drugs that require administration during sleeping (Stubbe et al., 2004). Adaptable drug delivery biomaterials represent the cutting edge of biomedical engineering, as drug delivery can be "programmed" by the inner mechanism of the device (e.g., degradation) or "triggered," where the release is governed by changes in the physiologic environment. Temperature-responsive hydrogels, made of lower critical solution temperature (LCST) polymers, are liquid below a critical solution temperature and become a gel above it. Physiological gelation temperatures enable injectable materials, such as poly(*N*-isopropylacrylamide) (PNIPAAm) and chitosan-based solutions, to be administered through a syringe and gel upon injection into the body, where they may serve as a drug or biomolecule reservoir (Pal et al., 2020; Tao et al., 2020). PNIPAAm features hydrophilic amide groups, which are buried during its coil-to-globule transition above the LCST point, and hydrophobic isopropyl groups, which are conversely exposed. On the contrary, chitosan is not inherently thermoresponsive, while the addition of phosphate salts, polyol-phosphates, and polyol molecules yields a thermogelling system with an LCST in the 15–85°C range. Chitosan and PNIPAAm can be also combined to form multiphase wound healing hydrogels where chitosan imparted improved biocompatibility, while PNIPAAm provided a thermally triggered volume change for enhanced control of drug delivery (Hogan and Mikos, 2020). Another approach in developing "smart' multiresponsive hydrogels is via the incorporation of temperature-sensitive additives, such as liposomes or nanoparticles (Lu and Ten Hagen, 2020; Palmese et al., 2020). Recently, Pedersen et al. (2020) developed hydrogel biomaterials with triggered liquefaction in response to internal, localized heating, mediated by near-infrared light as external stimulus. This adaptable behavior was obtained by combining poly(vinyl alcohol) hydrogel with gold nanoparticles or an organic photothermal dye as heat generators. Upon laser light irradiation, composite hydrogel underwent liquefaction within seconds allowing the controlled, on-demand release of the incorporated cargo (Pedersen et al., 2020).

Thermoresponsive polymeric nanocarriers, including micelles, liposomes, dendrimers, and polymersomes are other interesting systems for drug delivery purposes. Liposomes that are characterized by an aqueous core surrounded by one or more concentric lipid bilayer allowed loading of either hydrophilic or hydrophobic drug molecules, while their release behavior was engineered to respond to external stimuli such as heat, light, ultrasound, and pH. Thermosensitive liposomes (TSLs) are among the most studied due to their ability to generate rapid and massive drug release in the heated area, and marginal release of contents in non-heated parts of the body (Lu and Ten Hagen, 2020; Yuba, 2020). This rapid release feature of TSLs occurred at a temperature range at which the liposomal membrane is going through a phase transition, which causes membrane openings and drug release. During the phase transition, manipulating temperatures can alter the density of gaps in the liposomal membrane, thus, also controlling the amount of released biomolecules. Typically, the temperature range for clinical hyperthermia is 40–45°C. Therefore, temperature-responsive liposomes that can show sharp responsiveness at this temperature range are promising in a viewpoint of clinical application. Clinically, liposome-based delivery systems were used for the delivery of bioactives, such as genes, drugs, and other biological molecules, especially for applications such as cancer treatment. Zhang et al. (2014) developed docetaxel-encapsulated thermosensitive liposomes for the targeted delivery of a drug to a tumor. The release rate of DOX was high at 42°C compared with 37°C and enabled higher tumor growth suppression *in vivo* if compared with the free drug-treated group. Growth factor receptor-bound protein-2 liposomes were prepared to inhibit the production of the growth factor receptor-bound protein-2 and, thereby, to reduce the proliferation of tumor cells (Saraf et al., 2020). TSL administration can be done directly in suspension (e.g., intravenous injection) or by loading them into injectable hydrogels to sequential delivery of multiple drugs (Lu and Ten Hagen, 2020; Palmese et al., 2020). In a recent work, Palmese et al. (2020) synthesized an injectable crosslinked poly(ethylene glycol) hydrogel containing both chemically crosslinked TSLs and matrix metalloproteinase-sensitive peptide crosslinks capable of independently responding to matrix metalloproteinase and applied hyperthermia. Doxorubicin, a widely used anticancer drug, was loaded in the TSLs with a high encapsulation efficiency, and the subsequent release was temperature dependent. Experiments characterizing the *in situ* drug delivery and degradation of these materials indicate that the TSL gel responds to both thermal and enzymatic stimuli in a local environment. The timescales of release associated with these two stimuli are distinct, allowing for the potential loading and independent delivery of multiple compounds (Palmese et al., 2020).

Light as an external stimulus for smart drug delivery systems is advantageous for a number of reasons including its non-invasive nature, high spatial resolution and temporal control, and convenience and ease of use. Light-based strategies used to design novel delivery systems can be classified into three main groups (Linsley and Wu, 2017; Ruskowitz and DeForest, 2018): photochemically triggered, where the absorbed light energy is sufficient to break covalent bonds directly or by a photochemical reaction; photoisomerization, where the excess energy causes structural changes; and photothermal, where the absorbed photon energy is dissipated via vibrational motion. Photochemically triggered drug delivery systems are usually made of an ortho-nitrobenzyl photolinker, or coumarin- and pyrene-containing random copolymers with light-responsive pyrene ester bonds that irreversibly cleave upon UV irradiation (Wang et al., 2015). Mesoporous silica nanocontainers loaded with cyclodextrin were combined with photoactivation of "snap-top" stoppers over the pore openings for triggered release (Guardado-Alvarez et al., 2013). The on-command release was stimulated by UV photon activation that is suitable for use in biological systems because it enabled good tissue penetration and precise spatial control. Penetration of UV-responsive systems into the clinic is favored by the fact that light-based therapies are already being used. However, practical and regulatory issues, such as depth of tissue penetration and possible phototoxicity of the light used, are limiting the UV-triggered drug delivery system used today (Barhoumi et al., 2015). In fact, the type of light employed as well as its dosages and power have to be adjusted based on the target organs. Light-actuated drug delivery was also achieved by the reversible conformational change of molecules, such as azobenzenes, induced by irradiation with UV and visible light. These molecules contain two phenyl groups joined by N=N bond that change from *trans* to *cis* conformation once excited by UV light. The *cis* conformation relaxes with the thermodynamically stable *trans* isomer in the dark or under visible light (Dhammika Bandara and Burdette, 2012). For example, Geng et al. (2017) synthesized an azobenzene derivative, 4-cholesterocarbonyl-4′-(*N*,*N*,*N*-triethylamine butyloxyl bromide) azobenzene, and incorporated it into liposomal membranes to serve as an on–off switch of doxorubicin release. In another work, Cao et al. (2014) prepared a photoresponsive hydrogel by free radical copolymerization of xylan-type hemicellulose methacrylate with 4-[(4-acryloyloxyphenyl)azo]benzoic acid. Under UV irradiation, the *trans* conformation of azobenzene in the hydrogel convert into the *cis* conformation and resulted in the hydrophilic/hydrophobic balance variation of the hydrogel that accelerated the release of vitamin B12. Although the majority of light-triggered release platform works focused on cancer treatments, in recent years, these active materials were also designed for the delivery of growth factors for TE purposes. Photoresponsive supramolecular polysaccharide hydrogels were prepared through host–guest interactions between azobenzene and β-cyclodextrin groups conjugated to hyaluronic acid chains (Zhao et al., 2020). The hydrogel showed a decrease in the spatial network crosslink density under the application of UV light stimulus that resulted in the fast release of epidermal growth factor for wound healing. In another work, a library of polymerizable ortho-nitrobenzyl macromers with different functionalities at the benzylic position was synthesized to allow for the direct conjugation of therapeutic agent and its subsequent controlled photorelease from a hydrogel network (Griffin et al., 2013). Utilizing the photodegradable macromer incorporating an activated disulfide, the authors conjugated transforming growth factor-β1 (TGF-β1) into the hydrogel and controlled their release with light to induce chondrogenic differentiation of human mesenchymal stem cells (hMSCs).

Additional methods to trigger the release of biomolecules from biomedical devices and scaffolds aided by external activation involve the use application of electrical and/or magnetic fields as well as by acoustic and/or ultrasound stimulation (Moncion et al., 2017; Gao et al., 2019; Ahmadi et al., 2020; Lu et al., 2020; Oliva and Almquist, 2020; Thébault et al., 2020). Ultrasound-sensitive microbubbles, liposomes, and emulsions have advanced the field of ultrasound-triggered drug delivery systems as they undergo the phenomenon of cavitation and destruction followed by encapsulated drug release. This strategy was applied, among others, for improvement of angiogenesis and osteogenesis in bone defect repair with ultrasound-targeted VEGF-loaded PLGA microbubbles (Gong et al., 2019) or to trigger the release of an avascular agent, combretastatin A4 phosphate, from ultramagnetic liposomes monitored by NMR (Thébault et al., 2020). Ultrasound-triggered drug delivery emulsions were also recently loaded inside a fibrin hydrogel to spatially direct cell migration and angiogenesis in acoustically responsive fibroblast growth factor (bFGF) delivery scaffolds (Moncion et al., 2017; Lu et al., 2020). By applying spatial patterns of ultrasounds to the *in vivo* implanted scaffolds, the authors spatially controlled bFGF release to elicit a spatially directed response from the host (Lu et al., 2020). Magnetically responsive scaffolds are another important class of responsive drug delivery platforms and can be prepared by the incorporation of iron oxide nanoparticles inside a biocompatible matrix to obtain a so-called ferrogel. The basic principle of release control is that the entrapped nanoparticle moves under the effect of magnetic field and deformed the scaffolds accelerating the release of therapeutic loads (Oliva and Almquist, 2020). By using this principle, authors triggered the release of PDGF from methacrylated chondroitin sulfate-based hydrogels without inducing structure degradation. This released PDGF promoted the proliferation of human tendon-derived cells and human adipose-derived stem cells as well as the expression of tendon- and bone-related markers, respectively (Silva et al., 2018). With a similar approach, alginate ferrogels modified with heparin enabled the sustained release of TGF-β1 upon magnetic field stimulation, enhancing chondrogenic differentiation of mouse teratocarcinoma cells (Kim et al., 2016).

The works herein described highlighted some of the most used ways to control, both passively and actively, the delivery of drugs and GFs from nanocarriers and scaffolds for biomedical applications. In the next part of this review, we focus our attention on the most novel and advanced techniques that applied these drug delivery strategies to scaffolds prepared by AM, aiming to tune the spatial and temporal release of biomolecules for recreating complex biomimetic 3D systems for new tissue growth.

SPATIAL AND TEMPORAL CONTROL OF BIOMOLECULE PRESENTATION IN 3D SCAFFOLDS PREPARED BY ADDITIVE MANUFACTURING

Advancement in TE strategies require the design of smart, functional, and high-performance scaffolds with robust and versatile manufacturing processes and capable of replicating the morphological, microstructural, and biochemical features of ECM. AM techniques revolutionized the means by which biomaterials, cells, and drugs are designed, developed, processed, and integrated and, therefore, represent the present and future of 3D drug delivery scaffold design and manufacturing.

Additive manufacturing techniques can be conveniently classified into discontinuous techniques, where layers' fabrication and assembly involve two distinct processing steps, and continuous techniques, where these two steps are mostly automatized and take place at once (Salerno et al., 2019). Both approaches have been used in the past years to load GFs to stimulate cell growth (Bittner et al., 2018; Koons and Mikos, 2019); anti-inflammatories and immunomodulators were used to control *in vivo* body response after scaffold implantation (Zhu et al., 2020); chemotherapist molecules were delivered to kill cancer cells and stop tumor progression (Shi et al., 2020). As summarized in **Figure 2**, loading bioactive molecules in AM scaffolds was achieved during manufacturing or by postprocessing treatments and following four main methods.

Bulk loading (strategy n°1) requires drug/polymer blending before scaffold fabrication and represents the most common and facile strategy for obtaining bioactive polymeric scaffolds. Blends can be prepared by dissolving both compounds into organic solvents or by mixing drugs and polymers in the melt state. Melting is the preferred way to avoid the use of toxic organic solvents and when the use of high temperatures does not affect the bioactivity of the entrapped molecules. The distribution and morphology of the drug in the scaffolds depend upon the physical–chemical interaction between the drug and polymer. A favorable interaction may allow for achieving high levels of drug loading and homogeneous drug distribution. Conversely, a poor interaction resulted in phase segregation with the majority of the drug crystallized onto a scaffold surface and the difficult control over the release kinetic (Calori et al., 2020). Porous scaffolds prepared by bulk loading were developed for the purpose of regenerating complex tissues such as bone and blood vessels (Ahlfeld et al., 2019; Zhang et al., 2019; Tamjid et al., 2020). For instance, 3D printing technology was used to prepare bioresorbable vascular polylactic acid scaffolds loaded with sirolimus, to solve problems such as long-term stent restenosis (Zhang et al., 2019). Sirolimus is a natural macrocyclic lactone, which inhibits smooth muscle cell proliferation and migration to reduce neointima formation and stent stenosis (Jelonek et al., 2018). Mixing the drug with scaffold preparation material in solution ensured reducing burst release and, consequently, avoided possible acute cytotoxicity to the surrounding tissues. The implant enabled a sustained release up to 16 months *in vivo* providing the required therapeutic treatment. Bulk loading combined with a 3D printing process was also applied to fabricate biphasic scaffolds for the spatial–temporal controlled release of VEGF toward bone regeneration (Ahlfeld et al., 2019). The scaffold was obtained by extrusion-based 3D multichannel plotting of a calcium phosphate cement paste and a VEGF-loaded alginate/gellan gum (AlgGG) hydrogel paste. The outer geometry of the biphasic scaffold was designed as a cylinder with a 5-mm diameter base to fit in the femur diaphysis of rats and make tight contact with the osteosynthesis plate. A triangular pore structure with 60° strand orientation was used in the inner architecture design, while the scaffolds had a gradient of VEGF-loaded AlgGG strands, increasing from the outer to the inner scaffold regions. The scaffold revealed good handling and fitting properties as well as bone tissue ingrowth and vascularization in response to locally released VEGF (Ahlfeld et al., 2019). As previously discussed, drug impregnation postprocessing can be classified depending on the drug impregnation medium into wet and supercritical impregnation strategies. The first strategy was applied, for instance, to load VEGF onto laponite–alginate–methylcellulose bone hydrogel scaffolds encapsulating human bone marrow stromal cells (Cidonio et al., 2020). In the treatment of acute and chronic skin loss conditions, such as venous ulcer and diabetes, the development of skin grafts may allow for overcoming possible donor site morbidity and immune-rejection problems often occurring when using autografts and allografts. A 3D-printed gelatin patch coated with sulfonated silk fibroin derivative was developed to serve as a "porous magnet" to sequester and concentrate basic fibroblast growth factor (FGF-2) and to promote the formation of granulation tissue and enhance the repair of full-thickness skin defects (Xiong et al., 2017). Incorporation of FGF-2 within the scaffold was obtain by soaking the scaffold in FGF-2 solution, while its release enhanced cell proliferation rate, tissue morphology, collagen fibril assembly, and blood vessel formation, and demonstrated great potential for major cutaneous defects, such as repairing large-area skin damage and chronic skin wounds due to lower granulation (Xiong et al., 2017). However, wet absorption is often unsuitable for loading bioactive molecules into scaffolds made of thermoplastic polymers due to slow solution diffusion into the bulk. By using $scCO_2$, Ngo et al. (2020) fabricated flurbiprofen-loaded acrylate-based 3D-printed systems and modulated the amount of loaded drug in the range of 12.72–24.08% by varying the operating temperature and pressure. Concomitantly, 3D-printed scaffolds processed with $scCO_2$ enabled the tuning of surface roughness features and macro/microporous porosities for

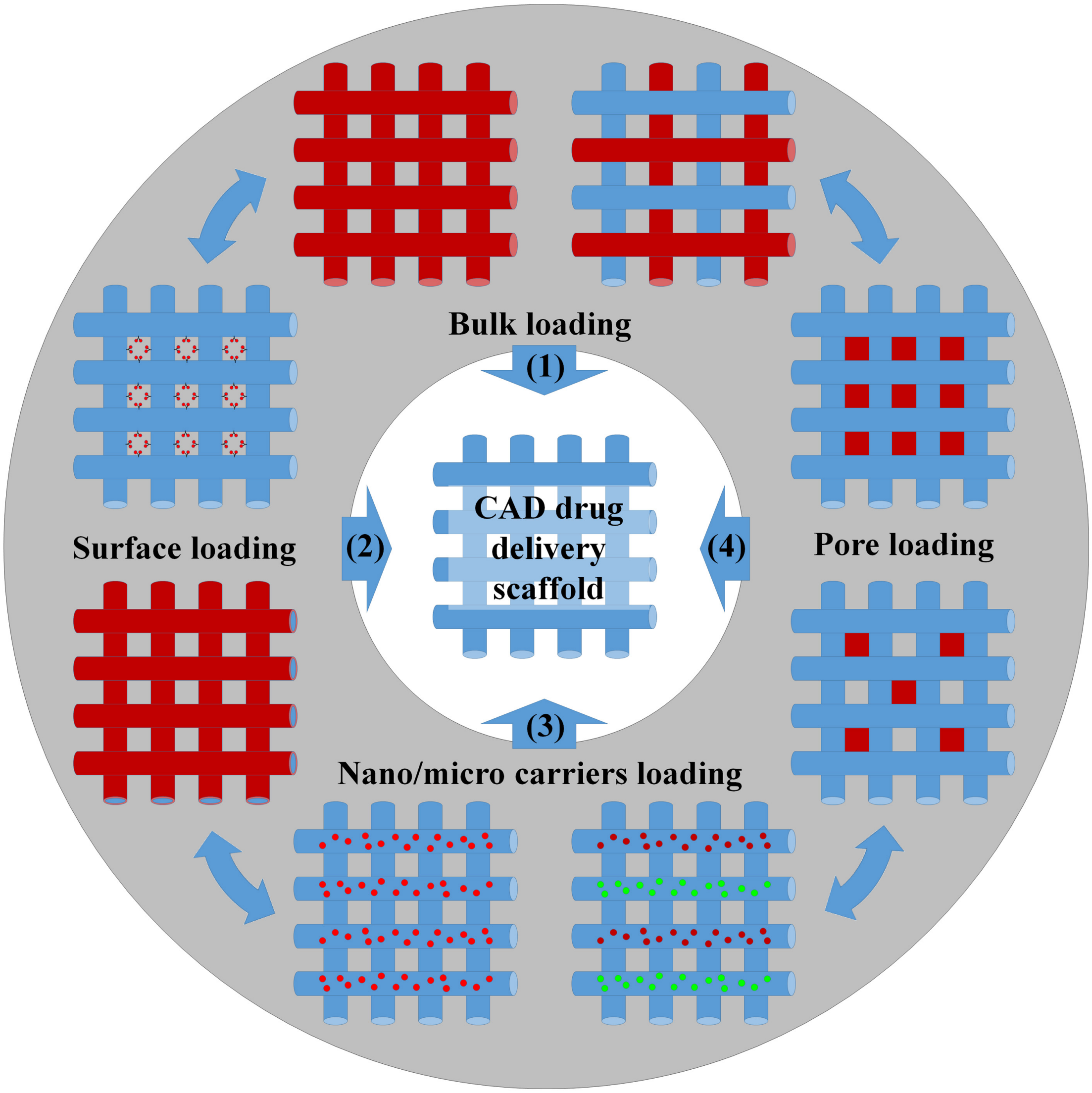

FIGURE 2 | Scheme of the different methods for the preparation of drug-loading scaffolds: (1) Bulk loading involved mixing drugs and biomaterials by melt/solution blending before 3D structure fabrication or, alternatively, by wet/supercritical CO_2 impregnation of the settled scaffold. (2) Surface bioactivation required the adsorption/grafting of the biomolecules to the scaffold surface or the incorporation of the biomolecules inside the coatings. (3) Biomolecules were loaded inside nano/microcarriers, and the carriers were further blended with the scaffold matrix before manufacturing. (4) The biomolecules were loaded into the scaffold pores using a carrier system (e.g., hydrogel).

specific application needs (Zhou et al., 2016; Ngo et al., 2020). Surface loading (strategy n°2) of bioactive molecules requires scaffold postprocessing treatments similar to the wet and vapor treatments described previously. In fact, biomolecule loading depended on their physical or chemical adsorption onto the scaffold pore surface, while biomolecule delivery depended on the interaction between scaffold material and drug, the specific surface, and the diffusion of the release medium into the scaffold core. An example of this approach was the work by Saska et al. (2018) that investigated the postprinting functionalization with osteogenic growth peptide (OGP) and its C-terminal sequence OGP(10–14) of poly(3-hydroxybutyrate) scaffolds. OGP peptide loading was carried out by immersing the scaffolds into a peptide solution for 72 h at 10°C followed by air drying at 37°C. Similarly, Tamjid et al. (2020) loaded tetracycline hydrochloride into PCL composite scaffolds to enhance its antibacterial properties, while Gbureck et al. (2007) bioactivated bioceramic bone implants with spatially localized angiogenic factors. If compared with bulk loading, surface bioactivation has some important advantages. In fact, the bioactivation of porous scaffolds by postprocessing enabled overcoming problems related to possible biomolecule deactivation that may conversely occur during drug–polymer premixing and scaffold manufacturing. Besides, by carrying out scaffold manufacturing and drug loading into two independent steps, it was possible to expand material choice and scaffold formulation possibilities and incorporate hydrophilic compounds into hydrophobic scaffolds. For example, hollow poly(lactic acid) (PLA) scaffolds prepared by fused deposition modeling were coated by solution-casting mixtures of differing molecular weights of PCL and poly(ethylene glycol) (PEG) (Stewart et al., 2020). These implants demonstrated *in vitro* release rates for hydrophilic model compounds (methylene blue and ibuprofen sodium) that were modulated in a facile way by changing the formulation of the polymeric coating. However, if compared with bulk loading, scaffolds prepared by surface bioactivation usually evidenced lower drug loading and limited control of drug release kinetic and spatial distribution. Overcoming the limitations required the increase of the specific surface of the scaffolds, for instance, by creating bimodal macro-microporosity (Visscher et al., 2018; Liu et al., 2020) or by grafting the biomolecules to the polymeric chains. Nevertheless, the difficult control of the contact points between solution/vapor carrying biomolecules and scaffold surfaces hindered the fabrication of scaffolds having spatial gradients of bioactive factors.

In order to achieve spatiotemporal delivery, recent advances in AM of scaffolds have paved the way for incorporating micro or nanoparticles loaded with biomolecules inside scaffolding material (strategy n°3) (Fahimipour et al., 2017; Zhu et al., 2018; Guzzi et al., 2019). Indeed, these carriers not only protect the encapsulated molecules against solvents and temperature during processing but also release the molecule in a sustainable manner. Furthermore, their localization inside the scaffold was controlled during manufacturing, finally resulting in a spatial and temporal controlled release. In order to optimize VEGF release timing at the preferred location within 3D bioprinted scaffolds, Poldervaart et al. (2014) fabricated Matrigel scaffolds containing human endothelial progenitor cells (EPCs) and VEGF-loaded gelatin microparticles. These scaffolds allowed a sustained VEGF release and enhanced vessel formation after implantation in subcutaneous pockets in nude mice. The use of microcarriers was also implemented to achieve sequential release function of chemokine stromal cell-derived factor-1 (SDF-1) and Y27632 factors from polyurethane scaffolds for cartilage TE (Wen et al., 2019). The fast release of SDF-1 attracted MSCs from the surrounding tissues, while the later release of Y27632 factor stimulated MSCs differentiation into chondrocytes. Microprecise spatiotemporal delivery scaffolds were achieved by the proper choice of microspheres and scaffold strut materials. For instance, the formation of multitissue interfaces from bone marrow-derived mesenchymal stem/progenitor cells was achieved by controlling the localization of PLGA microspheres loaded with connective tissue growth factor (CTGF) and transforming growth factor β3 (TGF-β3) inside PCL scaffolds (Tarafder et al., 2016). Given the substantial difference in the melting points between PLGA and PCL and their low heat conductivity, the microsphere structure was not altered during the process, protecting biomolecules from thermal degradation. This microprecise spatial control of multiple GFs was achieved by interchanging dispensing cartridges during a single printing process, and the as-prepared scaffolds significantly prevented arthritic changes on temporomandibular joint condyles (Tarafder et al., 2016).

The last strategy (n°4) to bioactivate porous scaffold is to fill the pores with a carrier material loaded with the biomolecules. Although this approach reduces scaffold porosity for cells and tissue ingrowth, it was suitable to control drug delivery behavior and to impart additional features to porous scaffolds made of thermoplastic materials or bioactive ceramics. For example, beta-tricalcium phosphate scaffolds with CAD designed structure were filled with a collagen–heparin thermogel encapsulating both BMP-2 and MSCs to enhance bone regeneration (Fahimipour et al., 2019). The heparin-functionalized collagen gel retained the bioactivity of growth factors and supported MSC viability and differentiation. Concomitantly, the ceramic fibers ensured the adequate mechanical support and the correct integration with surrounding bone tissue. Tuning hydrogel properties allowed for the development of composite scaffolds providing drug release and on-demand photothermal conversion functions (Jiang et al., 2020). This approach was also used to obtain miniaturized modular LEGO-like cage scaffolds loaded with biologic cargo of different compositions and assembled into highly complex structures to pattern therapeutics within the material in 3D (Hipfinger et al., 2020). It is worth noting that all of the approaches described in **Figure 2** can also be combined to others aiming to increase scaffold design complexity. For example, a collagen type 1 solution containing PLGA microspheres loaded with VEGF, BMP-2, or FGF-2 was incorporated into the pores of polycaprolactone fumarate scaffolds and crosslinked under UV light to stimulate vascular ingrowth and tissue regeneration (Wagner et al., 2018). Growth factor-loaded microspheres were also deposited on the surface of melt electrowriting scaffold pores by an inkjet spray drying technique to prepare three layers of scaffolds for repairing cartilage injury (Han et al., 2020). The scaffold consisted of a surface layer loaded with BMP-7 and TGF-β1, a middle layer loaded with IGF-1 and TGF-β1, and a deep layer loaded with hydroxyapatite (HA) and TGF-β1. This design stimulated the adhesion, proliferation, and differentiation of MSCs recruited from the bone marrow and blood, while contributing to the regional heterogeneity of chondrocytes and secreted proteins to promote functional cartilage regeneration. Novel scaffolds performing multidrug spatiotemporal release were also engineered by filling the pores of bioprinted scaffolds with electrospun nanofibers loaded with biomolecules (Liu et al., 2016). These scaffolds provided a biomimetic nanofibrous pore morphology to support cell growth and enhance cell retention, while ensuring the controlled delivery of growth factors and other drugs for tissue regeneration.

BIOPRINTING OF BIOACTIVE HYBRID SCAFFOLDS FOR MUSCULOSKELETAL TISSUES

Musculoskeletal tissue damage and degeneration as a consequence of traumas and/or diseases are common and debilitating events that cannot be often healed by one's own body tissue regeneration capability due to extensive inflammation and the high degree of damage (Loebel and Burdick, 2018). The high prevalence of musculoskeletal tissue injuries has directed significant investments in the development of TE therapies to enhance healing of damaged musculoskeletal tissues, such as bone, cartilage, and osteochondral tissues. However, the biologically and architecturally complex composition and structure of these tissues are challenging goals for TE. For example, bone is a connective tissue characterized by a multitude of mechanical, chemical, and hematological functions. Furthermore, bone is subjected to continuous remodeling based on time- and spatial-dependent physiological changes (Hutmacher et al., 2007). From a material point of view, bone is a natural composite consisting mainly of a collagen organic phase and a hydroxyapatite inorganic phase. The interaction and balance between these two phases are responsible for the biomechanical properties of bone tissue, characterized by elastic compression moduli in the 18- to 20-GPa range (Bayractar et al., 2004). Bone tissue intraosseous vasculature is highly organized and ensure essential nutrients to closed osteocytes and allow the removal of cellular metabolic wastes (Santos and Reis, 2020). Articular cartilage is a highly organized tissue that provides a low-friction and wear-resistant bearing surface and exhibits regional organization, e.g., structure, cells, and ECM biochemical composition, to match biomechanical requirements (Steele et al., 2014). Indeed, the superficial zone exhibits a collagenous fibrous structure aligned to the surface and rich in chondrocytes to ensure high tensile strength upon wearing and a deeper region richer in proteoglycan concentration while reducing cell concentration to guarantee cartilage compression resistance by producing a high osmotic pressure within the tissue (Steele et al., 2014).

To fabricate biomimetic tissues, with zone-specific heterogeneity like musculoskeletal tissues, multimaterial and multicell-type bioprinting with micrometric scale control of localization is demanding. Bioprinting allows the fabrication of patient-specific, implantable 3D constructs by using in a simultaneous and controlled way cartridge loaded with different matters: biomaterials in form of pastes, polymeric composite melt or solution; free drug or drug-encapsulated carriers; and cells of different origins in suspension or encapsulated within hydrogels. Bioprinting techniques can be broadly classified into three main categories (Murphy et al., 2017): (i) laser-assisted, (ii) inkjet-based, and (iii) extrusion-based printing. To date, extrusion-based 3D bioprinting is the most successful biofabrication process as cells, hydrogels, and other materials are deposited onto a substrate by using one or multiple pressurized syringes. The pressure system consists of either a mechanical piston or a pneumatic pressure source (mostly compressed air) that is computer-controlled. Besides, through bioprinting, it was possible to design and fabricate evenly complex hybrid scaffolding systems to mimic biological tissue hierarchical architecture and composition and suitable to enhance tissue regeneration potential.

Table 1 highlights some of the most recently published work on the engineering of musculoskeletal tissue scaffolds with spatial and temporal controlled release capability by means of bioprinting technique. In a recent study, a multiple-tool biofabrication technique was used to deliver VEGF and BMP-2 with distinct spatiotemporal release profiles from porous composite scaffold made of PCL and alginate to enhance the regeneration of critically sized bone defects (Freeman et al., 2020). The fabrication process started by printing a PCL structural scaffold (4-mm diameter and 5-mm height) having both lateral and horizontal porosity, and a fiber spacing of 1.2 mm. The scaffold was subsequently loaded with two different alginate-based nanocomposite bioinks. The vascular bioink, consisting of 3.5% w/v RGD-alginate, 1.75% w/v methylcellulose, 3.5% w/v nHA, and 500 ng/ml VEGF in alpha minimum essential medium (αMEM), 10% fetal bovine serum (FBS), penicillin (5% v/v), and streptomycin (5% v/v), was loaded in the scaffold center to stimulate blood vessel ingrowth. The osteoinductive bioink, consisting of 3.5% w/v RGD-alginate, 1.75% w/v methylcellulose, 0.5% w/v laponite, and 10 μg/ml of BMP-2 solubilized in the previously described medium, was loaded in the periphery to promote bone growth and implant integration with surrounding tissue. A proof-of-concept study in nude mice validated the benefit of this precise localization of growth factors in both time and space on angiogenesis and new tissue formation (Freeman et al., 2020). In fact, the composite scaffold demonstrated accelerated bone defect healing with higher levels of vessel invasion and less heterotopic bone formation if compared with implants homogeneously loaded with the same total amount of growth factors. Similar hydrogel-PCL composite scaffold strategies were proposed by the group of Sun et al. (2020a,b, 2021) to generate living anisotropic cartilaginous tissues (**Figure 2**). In the case of meniscus, PCL was molten to fabricate the physically supporting structure for the scaffold, choosing needle diameter, layer thickness, and fiber spacing of 200, 200, and 350 μm, respectively. Furthermore, inspired by the heterogeneity of native meniscus structure, a composite hydrogel was made mixing gelatin (45 mg/ml), fibrinogen (30 mg/ml), hyaluronic acid (30 mg/ml), and glycerol (10% v/v) and loaded with MSCs and PLGA microparticles carrying connective tissue growth factor (CTGF) and TGF-β3. These growth factors induced differentiation of MSCs into fibrochondrocytes and were located in different porous regions of the scaffold. In particular, to chemically simulate the anisotropic phenotypes in native meniscus, microcarriers carrying CTGF were positioned in the outer one-third region, while those carrying TGF-β3 were used for the inner two-thirds regions of the meniscus construct. *In vivo* implantation into sheep showed that the ECM composition of the 3D-bioprinted constructs shared many characteristics of native meniscus, including the heterogeneous zonal expression of types I, II collagen and therewith the conferred anisotropic zonal function properties (Sun et al., 2020a). Dual-factor releasing and gradient-structured bioprinted constructs were also used for anisotropic cartilage regeneration (Sun et al., 2020b). As native articular cartilage transitions from the superficial zone to the deep zone, gradient anisotropic cartilage scaffold was constructed by one-step 3D bioprinting gradient polymeric scaffolding structure. The gradient PCL fiber spacing ranged gradually from 150 μm of the superficial zone of the cartilage, providing higher mechanical properties and smaller pores for chondrocyte differentiation, up to 750-μm pores in the construct core to enhance diffusion of nutrients and vessel ingrowth. Furthermore, as in the case of meniscus construct, dual protein-releasing composite hydrogels

TABLE 1 | Examples about the use of the bioprinting technique to fabricate complex drug delivery scaffolding systems for the regeneration of musculoskeletal tissues.

Tissue	Bioactive scaffold			Outcome	References
	Design features		Composition		
Bone	Structural support	Cylindrical construct (d = 4 mm and h = 5 mm) with 1.2-mm fiber spacing	PCL	High vessel invasion and accelerated large bone defect healing with little heterotopic bone formation	Freeman et al. (2020)
	Delivery system	Osteoinductive composite hydrogel printed in the pores of the periphery	RGD-modified alginate, methylcellulose, and laponite		
		Vascular composite hydrogel printed in the pores of the center	RGD-modified alginate, methylcellulose and hydroxyapatite nanoparticles		
	Biological component	No cells	/		
Cartilage	Structural support	Four-layer graded cubic scaffold (l = 4 mm) with fiber spacing varying from 150-μm wide from the superficial zone to 750-μm wide in the deep zone of the cartilage construct	PCL	Whole-layer integrity, lubrication of superficial layers, nutrient supply in deep layers, and cartilage tissue maturation suitable for translation to patients	Sun et al. (2020a)
	Delivery system	Chondrogenic microsphere-laden hydrogel printed in the pores of the first three layers	Composite hydrogel made of gelatin, fibrinogen, hyaluronic acid, and glycerol and incorporating polylactic-co-glycolic acid (PLGA) microspheres encapsulating transforming growth factor-β1 (TGF-β3)		
		Osteoinductive microsphere-laden hydrogel printed in the pores of the deepest layer with a 750-μm PCL fiber spacing	Composite hydrogel made of gelatin, fibrinogen, hyaluronic acid, and glycerol and incorporating PLGA microspheres encapsulating bone morphogenetic protein-2 (BMP-4)		
	Biological component	Cell-laden osteoinductive and chondrogenic bioinks	Bone marrow-derived mesenchymal stem cells (MSCs)		
Meniscus	Structural support	Anatomically shaped meniscus structure with fiber size of 200 μm and fiber spacing of 350 μm	PCL	Goat anisotropic meniscus construct having the heterogeneous zonal expression of types I, II collagen and ready for implantation	Sun et al. (2020b)
	Delivery system	Chondrogenic microsphere-laden hydrogel printed in the pores of the inner 2/3 region of the meniscus construct	Composite hydrogel made of gelatin, fibrinogen, hyaluronic acid, and glycerol and incorporating PLGA microspheres encapsulating TGF-β3		
		Chondrogenic microsphere-laden hydrogel printed in the pores of the outer 1/3 region of the meniscus construct	Composite hydrogel made of gelatin, fibrinogen, hyaluronic acid, and glycerol and incorporating PLGA microspheres encapsulating connective tissue growth factor (CTGF)		
	Biological component	Cell-laden chondrogenic bioinks	Bone marrow-derived MSCs		

(Continued)

TABLE 1 | Continued

Tissue	Bioactive scaffold			Outcome	References
	Design features		Composition		
Intervertebral disk (IVD)	Structural support	Anatomically shaped IVD scaffold consisting of five parts: (1) the upper cartilage endplate; (2) the lower cartilage endplate; (3) the nucleus pulposus; (4) the annulus fibrous, and (5) the annulus fibrous support	PCL	The reconstructed IVD scaffold exhibited a zone-specific matrix phenotype with type II collagen and glycosaminoglycan in the core zone, and type I collagen in the surrounding zone	Sun et al. (2021)
	Delivery system	Nucleus pulposus bioink printed in the pores of the nucleus pulposus	Composite hydrogel made of gelatin, sodium alginate, and hyaluronic acid and loaded with polydopamine nanoparticles encapsulating TGF-β3		
		Annulus fibrous bioink printed in the pores of the annulus fibrous	Composite hydrogel made of gelatin, sodium alginate, and hyaluronic acid and loaded with polydopamine nanoparticles encapsulating CTGF		
	Biological component	Cell-laden nucleus pulpous and fibrous annulus bioinks	Bone marrow-derived MSCs		
Osteochondral	Structural support	Cylindrical construct (d = 6 mm; h = 5 mm) with 160-μm fiber diameter and 250-μm fiber spacing	PCL	Gene-activated bioprinted construct supported the vascularization and mineralization in the osseous region, while sGAG and type II collagen-rich cell clusters formation in the cartilage region	Gonzalez-Fernandez et al. (2019)
	Delivery system	Osteogenic bioink casted in the bottom layer of 4 mm	Alginate-methyl cellulose composite hydrogel containing nanohydroxyapatite particles-pBMP-2 complexes		
		Chondrogenic bioink casted in the top layer of 2 mm	Alginate-methyl cellulose hydrogel containing RALA–pTGF-β3–pBMP2–pSOX9 complexes		
	Biological component	Cell-laden osteogenic and chondrogenic bioinks	Bone marrow-derived MSCs		

encapsulating MSCs and PLGA microspheres loaded with either TGF-β3 and BMP-4 were bioprinted into the pores between PCL fibers (Sun et al., 2020b). Specifically, the BMP-4 hydrogel was located in the deepest layer with a 750-μm PCL fiber spacing, while the TGF-β3 hydrogel was used for the other three layers of the cartilage construct.

The versatility of the bioprinting strategy combining a structural support made of a thermoplastic polymer (PCL) and drug delivery composite hydrogels incorporating GF-loaded carriers was demonstrated by the same group to engineer also an anatomically correct intervertebral disk (IVD) scaffold (Sun et al., 2021). Connective tissue growth factor (CTGF) and TGF-β3 were loaded into polydopamine nanoparticles mixed with MSCs for regenerating and simulating the structure and function of the nucleus pulposus and annular fibrous. A 3D virtual model of the IVD scaffold was designed into five parts: (1) the upper cartilage endplate, (2) the lower cartilage endplate, (3) the nucleus pulposus, (4) the annulus fibrous, and (5) the annulus fibrous support. The CTGF/MSCs ink and TGF-β3/MSCs ink were loaded into the annulus fibrous and nucleus pulposus parts, respectively. *In vivo* experiments confirmed that the reconstructed IVD scaffold exhibited a zone-specific matrix phenotype, as the TGF-β3 promoted the biosynthesis of glycosaminoglycan and collagen II in the nucleus pulposus, while the CTGF stimulated the biosynthesis of glycosaminoglycan and collagen I in the annulus fibrous (Sun et al., 2021).

Engineering cells to synthesize and deliver *in situ* growth factors through gene delivery represents an alternative approach to direct stem cell fate within the tissue construct. Non-viral gene-activated bioprinted scaffolds providing a temporal and spatial control of plasmid gene delivery to stem cells were developed to engineer an osteochondral implantable cell-laden construct consisting of a cartilaginous matrix overlaying a vascularized bone tissue (Gonzalez-Fernandez et al., 2019). The newly developed bioink was obtained by blending sacrificial and stable hydrogels, providing an active platform to temporally modulate transfection of host or transplanted cells *in vivo* by increasing scaffold porosity over time with transient or sustained rates (**Table 1**) (Gonzalez-Fernandez et al., 2019). In particular, the bioinks containing stem cells and plasmids encoding for either osteogenic (BMP-2) or chondrogenic (combination of TGF-β3, BMP-2, and SOX9) genes were printed inside specific porous zones of 3D-printed PCL scaffold, and the composite constructs guided the formation of a vascularized, bony tissue overlaid by a layer of stable cartilage (Gonzalez-Fernandez et al., 2019).

Although all of the previous reported works clearly demonstrated the advancement of bioprinting in musculoskeletal tissue reconstruction, researchers working on tissue bioprinting have to face up to two major limitations in the future (Sigaux et al., 2019). First, there are so many options in bioink composition and patient-specific tissue properties that defining a unique strategy for each tissue is complex. Vascularization of the printed tissues is the other main challenge as cells and tissues cannot survive without adequate blood circulation, and integrating a full vascular network (from large vessels to capillaries) into the printed tissues is still a challenge. Once the vascularization of the *in silico* designed tissues is overcome, the translation of bioprinted tissues to personalized medical treatments and reconstructed surgery will be possible by a two-step management for patients (Sigaux et al., 2019). In a first 1-day appointment, the patient is subjected to specific biopsies to obtain autologous cell sources for tissue printing and maturation *in vitro*. Then, a second step surgery is performed to implant the *in vitro* grew tissue.

RECENT APPLICATIONS OF COMPUTER-AIDED DESIGN DRUG DELIVERY PLATFORMS FOR CANCER TREATMENT

Cancer is one of the major causes of morbidity and mortality worldwide, leading to significantly increased healthcare costs and the great need to better understand cancer to improve therapy (Shrike Zhang et al., 2016). The biochemical (e.g., growth factors and cytokines) and biophysical cues (e.g., ECM mechanics) of tumor microenvironment are highly complex and dynamic and play a significant role in tumor growth and metastasis development (Shrike Zhang et al., 2016). The application of TE scaffold-based strategies toward cancer genesis and treatment are therefore highly desirable as they could help in understanding *in vitro* how cancer cells and the ECM become implicated in tumor growth and migration, and they can be used in the clinic to stimulate tissue repair after tumor resection and reduce tumor cell migration risks (Katt et al., 2016; Mao et al., 2020; Oztan et al., 2020; Shafiee, 2020). Scaffolds for the treatment of human tissue defects after tumor resection required loading and release of chemotherapy molecules for residual tumor cell suppression after surgery. In fact, if compared with high-dose intravenous chemotherapy, drug-loaded implants have the advantages of single-drug administration, minimal systemic toxicity, and increased delivery efficacy. Furthermore, when fabricated starting from 3D reconstruction images of critical size tissue defect, these patient-specific implants served as space holders to prevent undesired tissue invasion from the immediate vicinity into the affected site and simultaneously provided a temporary biomechanical support for the growing tissue and sustain *in vivo* loads. To address these issues for postsurgical bone tumor management, a multifunctional bone graft substitute was designed by incorporating the soy isoflavones genistein, daidzein, and glycitein in a 5:4:1 ratio, onto a 3D-printed tricalcium phosphate (TCP) porous scaffold (Sarkar and Bose, 2020). The TCP scaffold was designed as having an interconnected porosity and biodegradation rate to control isoflavone release kinetics. Most importantly, genistein delivery was designed to reduce osteosarcoma cell viability and proliferation, while daidzein and glycitein promoted osteoblast attachment, viability, and proliferation *in vivo* into a critical-sized bicortical defect in the lateral epicondyle. The efficacy of AM scaffolds for local release of chemotherapist for osteosarcoma treatment was also demonstrated *in vitro* by using composite scaffolds made of silica nanoparticles and PCL incorporating ruthenium-loaded PEGylated liposomes (Ye et al., 2019). The authors found that the scaffolds had a relatively slow sustained chemotherapist release and a good antitumor efficacy over a relatively long period. The use of porous scaffolds as local drug reservoirs to prevent cancer recurrence and stimulate new tissue regeneration was also suitable for soft tissues applications, such as breast cancer therapy (Dang et al., 2020; Yang et al., 2020). AM and salt-leaching techniques were combined to produce bimodal porous PCL scaffolds that were subsequently loaded with doxorubicin by the wet dipping method. The scaffolds displayed a chemotherapeutic effect against breast cancer cells and, if compared with systemic administration, reduced local cancer recurrence and showed lower cardio-cytotoxicity effect (Dang et al., 2020). Similarly, PLGA scaffolds fabricated by 3D printing and loaded with anticancer molecules significantly reduced the required drug dosages and ensured curative drug levels near tumor sites for prolonged periods, while drug exposure to normal tissues was minimized (Yang et al., 2020).

The utilization of CAD-based processes for *in vitro* creation of tumor models is widespread as it enabled testing drug efficacy and studying tumor growth and progression mechanisms. For example, modeling tumor microenvironments through bioprinting had the potential to overcome limitations related to cancer study on 2D systems and/or cell spheroids thanks to its freeform nature, adaptability, customizability, scalability, and diversity (Salerno and Netti, 2014; Oztan et al., 2020). Existing bioprinting methods used in cancer research involved extrusion, stereolithography, and inkjet printing techniques and have significantly improved accuracy and composition of tumor environment design and, therefore, drug testing reliability and scale-up to humans. Bioprinted tumor models were fabricated to mimic *in vitro* the physical and cellular properties of cancer of tissues like the breast, brain, bone, and lung (Kang et al., 2020; Radhakrishnan et al., 2020). For example, a series of 3D bone matrices of variable geometry were printed using stereolithography and used to study breast cancer cell growth (Zhu et al., 2016). It was found that matrix geometry and composition, together with the coculture of breast cancer cells and MSCs, influenced cell proliferation and enhanced cell migration capability (Zhu et al., 2016). Although 3D cancer models contribute to the recapitulation of important features of cancers and may represent suitable alternatives of the animal-based models, their standardization is still far to be possible (Shafiee, 2020). In fact, as discussed in the previous section, both cancer tissue heterogeneity and experimental processing conditions make it difficult to define standardized models, and the analysis of the mechanisms involved in cancer development are often incomplete. Concomitantly, scientific literature about drug-loaded scaffolds for a tumor model is limited, and future advances in this field depend on the efforts that will be done to integrate knowledge from cancer cell biology and drug delivery scaffold biofabrication to engineer patient-specific tumor tissue models for immediate translation to clinical applications.

CONCLUSION AND FUTURE PERSPECTIVES

In this review, we described the state-of-the-art of drug delivery scaffolds prepared by AM processes for TE and cancer precision medicine. Common strategies for porous scaffolds and hydrogel bioactivation were overviewed to elucidate the importance of material selection together with 3D structure design on drug loading and delivery efficacy. To date, there is a plethora of drugs and biomolecules, such as GFs and anti-inflammatories, that can be incorporated inside porous scaffolds to guide cellular processes involved in new tissue regeneration. Among them, VEGF is an excellent biomolecule to enhance the vasculogenic potential of the scaffold, especially when combined with PDGF and BMP. However, it was demonstrated that the efficacy of these molecules depend on their bioactivity, their presentation to cell-surface receptors, and their spatial and temporal controlled release. In view of these important aspects, great attention must be paid to the way these biomolecules are incorporated into the scaffolds, in order to avoid possible deactivation as well as to maximize biomolecule loading and achieve a sustained release over the entire time required for the biological stimulation process. The use of drug-loaded micro and nanocarriers have opened new possibilities for scaffold design as they allow for enhanced control over scaffold release features, together with the possibility of protecting the bioactive molecules during scaffold manufacturing, especially when high temperature and/or aggressive solvents are used. Besides, these carriers allow for loading multiple biomolecules inside porous scaffolds and test the efficacy of synergic biomolecule delivery on scaffold biocompatibility and integration into the host body. The development of advanced biomaterials whose properties can be adjusted by variation of biophysical and biochemical conditions, such as changes in temperature or magnetic field, has also opened new routes to enhance therapeutic efficacy of biomolecule-releasing scaffolds.

It is universally recognized that, among the different AM scaffold fabrication processes, bioprinting represents, nowadays, the most powerful technique addressing patient-specific demand for tissue repair mediated by drug delivery implantable scaffolds. In fact, this technique enabled the manipulation of almost any kind of material, spanning from thermoplastic polymers to hydrogels and ceramic pastes, cells, and biomolecules such as GFs, and create evenly complex 3D structures mimicking the composition, architecture, and functionalities of the native ECM. The importance of the bioprinting technique in biomedicine was demonstrated by recent works applying this technique to design and manufacture ECM-mimicking scaffolds for the regeneration of complex musculoskeletal tissues. Bioprinting is also the first choice in cancer precision medicine when tissue regeneration must be achieved after tumor resection or to study chemotherapist efficacy against tumors in 3D *in vitro* models.

Despite these advancements, the translation of bioactive delivering scaffolds from bench to bedside is still a challenging goal, and further efforts are necessary to design and fabricate scaffolds providing ECM guidance functions that are suitable to successfully regenerate tissue analogs for clinical demand. It is, however, worth noting that technological advancement in the fields of materials science, cellular therapy, and drug discovery can boost AM processes advancement toward the next generation of drug delivery scaffold development. For instance, the integration of nanotechnology (e.g., soft lithography), micro/nanofluid, and bioprinting is a promising approach to enhance the control of scaffold processing/structure/delivery (Davoodi et al., 2020; Richard et al., 2020). Indeed, the formation of multiple emulsions within microfluidic devices may enable the fabrication of microparticles with multiple cores and drug/cell loading and delivery capability (Omidi et al., 2020; Tomeh and Zhao, 2020; Moreira et al., 2021). Similarly, lithography-based processes, such as those using UV-photopolymerization or patterned polydimethyl siloxane molds, offer the possibility for precise structuring drug and cell delivery microcontainers (Salerno et al., 2019; Mirza and Saha, 2020; Saraswat et al., 2020). These microcontainers may be charged with multiple drugs and biomolecules in powder form or by using scCO_2 processing to protect the bioactive ingredient against degradation and deactivation and achieve full loading efficiency (Marizza et al., 2014; Abid et al., 2017). Furthermore, the combination of monodisperse porosity and enhanced diffusion in an even nanometric volume together with the possibility of integrating stimuli-responsive components for triggered drug delivery may allow the precise tuning of biomolecule release profiles (Randall et al., 2007; McHugh et al., 2017). All of these novel-designed carriers can be further incorporated into the bioprinted scaffold structure, inside the filament otherwise located into the pores aided by micromanipulation systems (Mekhileri et al., 2018; Hacohen et al., 2020). The as-engineered scaffolds can achieve, in principle, the nanometric scale control of biomolecule loading, and their programmed/triggered release following cell and tissue demands can finally have a tremendous impact on the production of customized clinical-grade functional tissues.

AUTHOR CONTRIBUTIONS

AS conceptualized and visualized the study, and wrote the manuscript. PN conceptualized the study and wrote the manuscript. Both authors contributed to the article and approved the submitted version.

REFERENCES

Abid, Z., Gundlach, C., Durucan, O., von Halling Laier, C., Hagner Nielsen, L., Boisen, A., et al. (2017). Powder embossing method for selective loading of polymeric microcontainers with drug formulation. *Microelectron. Eng.* 171, 20–24. doi: 10.1016/j.mee.2017.01.018

Ahlfeld, T., Schuster, F. P., Föster, Y., Quade, M., Akkineni, A. R., Rentsch, C., et al. (2019). 3D plotted biphasic bone scaffolds for growth factor delivery: biological characterization in vitro and in vivo. *Adv. Healthc. Mater.* 8:1801512. doi: 10.1002/adhm.201801512

Ahmadi, A., Hosseini-Nami, S., Abed, Z., Beik, J., Aranda-Lara, L., Samadian, H., et al. (2020). Recent advances in ultrasound-triggered drug delivery through lipid-based nanomaterials. *Drug Discov. Today* 25, 2182–2342. doi: 10.1016/j.drudis.2020.09.026

Barati, D., Ramin Pajoum Shariati, S., Moeinzadeh, S., Melero-Martin, J. M., Khademhosseini, A., and Jabbari, E. (2016). Spatiotemporal release of BMP-2 and VEGF enhances osteogenic and vasculogenic differentiation of human mesenchymal stem cells and endothelial colony-forming cells co-encapsulated in a patterned hydrogel. *J. Control. Release* 223, 126–136. doi: 10.1016/j.jconrel.2015.12.031

Barhoumi, A., Liu, Q., and Kohane, D. S. (2015). Ultraviolet light-mediated drug delivery: principles, applications, and challenges. *J. Controlled Release* 219, 31–42. doi: 10.1016/j.jconrel.2015.07.018

Bayractar, H. H., Morgan, E. F., Niebur, G. L., Morris, G. E., Wong, E. K., and Keaveny, T. M. (2004). Comparison of the elastic and yield properties of human femoral trabecular and cortical bone tissue. *J. Biomech.* 37, 27–35. doi: 10.1016/S0021-9290(03)00257-4

Biondi, M., Ungaro, F., Quaglia, F., and Netti, P. A. (2008). Controlled drug delivery in tissue engineering. *Adv. Drug Deliv. Rev.* 60, 229–242. doi: 10.1016/j.addr.2007.08.038

Bittner, S. M., Guo, J. L., and Mikos, A. G. (2018). Spatiotemporal control of growth factors in three-dimensional printed scaffolds. *Bioprinting* 12:e00032. doi: 10.1016/j.bprint.2018.e00032

Borselli, C., Storrie, H., Benesch-Leec, F., Shvartsman, D., Cezar, C., Lichtman, J. W., et al. (2010a). Functional muscle regeneration with combined delivery of angiogenesis and myogenesis factors. *Proc. Natl. Acad. Sci. U.S.A.* 107, 3287–3292. doi: 10.1073/pnas.0903875106

Borselli, C., Ungaro, F., Oliviero, O., d'Angelo, I., Quaglia, F., La Rotonda, M. I., et al. (2010b). Bioactivation of collagen matrices through sustained VEGF release from PLGA microspheres. *J. Biomed. Mater. Res.* 92A:94. doi: 10.1002/jbm.a.32332

Bruggeman, K. F., Wang, Y., Maclean, F. L., Parish, C. L., Williams, R. J., and Nisbed, D. R. (2017). Temporally controlled growth factor delivery from a self-assembling peptide hydrogel and electrospun nanofibre composite scaffold. *Nanoscale* 9, 13661–13669. doi: 10.1039/C7NR05004F

Caballero-Aguilar, L. M., Moraes Silva, S., and Moulton, S. E. (2020). "Three-dimensional printed drugdelivery systems," in *Engineering Drug Delivery Systems*, eds A. Seyfoddin, S. M. Dezfooli, and C. A. Greene (Amsterdam: Woodhead Publishing), 147–162. doi: 10.1016/B978-0-08-102548-2.00006-8

Calori, I. R., Braga, G., da Costa Carvalho de Jesus, P., Bi, H., and Tedesco, A. C. (2020). Polymer scaffolds as drug delivery systems. *Eur. Polym. J.* 129:109621. doi: 10.1016/j.eurpolymj.2020.109621

Campbell, K. T., Stilhano, R. S., and Silva, E. A. (2018). Enzymatically degradable alginate hydrogel systems to deliver endothelial progenitor cells for potential revasculature applications. *Biomaterials* 179, 109–121. doi: 10.1016/j.biomaterials.2018.06.038

Cantón, I., Mckean, R., Charnley, M., Blackwood, K. A., Fiorica, C., Ryan, A. J., et al. (2010). Development of an ibuprofen-releasing biodegradable PLA/PGA Electrospun scaffold for tissue regeneration. *Biotechnol. Bioeng.* 105, 396–408. doi: 10.1002/bit.22530

Cao, L., and Mooney, D. J. (2007). Spatiotemporal control over growth factor signaling for therapeutic neovascularization. *Adv. Drug Deliver. Rev.* 59, 1340–1350. doi: 10.1016/j.addr.2007.08.012

Cao, X., Peng, X., Zhong, L., and Sun, R. (2014). Multiresponsive hydrogels based on xylan-type hemicelluloses and photoisomerized azobenzene copolymer as drug delivery carrier. *J. Agric. Food Chem.* 62, 10000–10007. doi: 10.1021/jf504040s

Champeau, M., Thomassin, J., Tassaing, T., and Jérôme, C. (2015). Drug loading of polymer implants by supercritical CO_2 assisted impregnation: a review. *J. Controlled Release* 209, 248–259. doi: 10.1016/j.jconrel.2015.05.002

Cidonio, G., Glinka, M., Kim, Y., Kanczler, J. M., Lanham, S. A., Ahlfeld, T., et al. (2020). Nanoclay-based 3D printed scaffolds promote vascular ingrowth ex vivo and generate bone mineral tissue in vitro and in vivo. *Biofabrication* 12:035010. doi: 10.1088/1758-5090/ab8753

Cross, M., and Dexter, T. M. (1991). Growth factors in development, transformation, and tumorigenesis. *Cell* 64, 271–280. doi: 10.1016/0092-8674(91)90638-F

Dang, H. P., Shafiee, A., Lahr, C. A., Dargaville, T. R., and Tran, P. A. (2020). Local doxorubicin delivery via 3d-printed porous scaffolds reduces systemic cytotoxicity and breast cancer recurrence in mice. *Adv. Therap.* 3:2000056. doi: 10.1002/adtp.202000056

Datta, P., Barui, A., Wu, Y., Ozbolat, V., Moncal, K. K., and Ozbolat, I. T. (2018). Essential steps in bioprinting: from pre- to post-bioprinting. *Biotechnol. Adv.* 36, 1481–1504. doi: 10.1016/j.biotechadv.2018.06.003

Davoodi, E., Sarikhani, E., Montazerian, H., Ahadian, S., Costantini, M., Swieszkowski, W., et al. (2020). Extrusion and microfluidic-based bioprinting to fabricate biomimetic tissues and organs. *Adv. Mater. Technol.* 5:1901044. doi: 10.1002/admt.201901044

de Rieux, A., Ucakar, B., Kaishusha Mupendwa, B. P., Colau, D., Feron, O., Carmeliet, P., et al. (2011). 3D systems delivering VEGF to promote angiogenesis for tissue engineering. *J. Control. Release* 150, 272–278. doi: 10.1016/j.jconrel.2010.11.028

Dhammika Bandara, H. M., and Burdette, S. C. (2012). Photoisomerization in different classes of azobenzene. *Chem. Soc. Rev.* 41, 1809–1825. doi: 10.1039/c1cs15179g

Dutta, R. C., and Dutta, A. K. (2009). Cell-interactive 3D-scaffold; advances and applications. *Biotechnol. Adv.* 27, 334–339. doi: 10.1016/j.biotechadv.2009.02.002

Ehrbar, M., Rizzi, S. C., Schoenmakers, R. G., San Miguel, B., Hubbell, J. A., Weber, F. E., et al. (2007). Biomolecular hydrogels formed and degraded via site-specific enzymatic reactions. *Biomacromolecules* 8, 3000–3007. doi: 10.1021/bm070228f

Fahimipour, F., Dashtimoghadam, E., Mahdi Hasani-Sadrabadi, M., Vargas, J., Vashaee, D., Lobner, D.C., et al. (2019). Enhancing cell seeding and osteogenesis of MSCs on 3D printed scaffolds through injectable BMP2 immobilized ECM-Mimetic gel. *Dent. Mater.* 35, 990–1006. doi: 10.1016/j.dental.2019.04.004

Fahimipour, F., Rasoulianboroujeni, M., Dashtimoghadam, E., Khoshroo, K., Tahriri, M., Bastami, F., et al. (2017). 3D printed TCP-based scaffold incorporating VEGF-loaded PLGA microspheres for craniofacial tissue engineering. *Dent. Mater.* 33, 1205–1216. doi: 10.1016/j.dental.2017.06.016

Freeman, F. E., Pitacco, P., van Dommelen, L. H. A., Nulty, J., Browe, D. C., Shin, J., et al. (2020). 3D bioprinting spatiotemporally defined patterns of growth factors to tightly control tissue regeneration. *Sci. Adv.* 6:eabb5093. doi: 10.1126/sciadv.abb5093

Gao, S., Tang, G., Hua, D., Xiong, R., Han, J., Jiang, S., et al. (2019). Stimuli-responsive bio-based polymeric systems and their applications. *J. Mater. Chem. B* 7, 709–729. doi: 10.1039/C8TB02491J

Gbureck, U., Hölzel, T., Doillon, C. J., Müller, F. A., and Barralet, J. E. (2007). Direct printing of bioceramic implants with spatially localized angiogenic factors. *Adv. Mater.* 19:795. doi: 10.1002/adma.200601370

Geng, S., Wang, Y., Wang, L., Kouyama, T., Gotoh, T., Wada, S., et al. (2017). A light-responsive self-assembly formed by a cationic azobenzene derivative and sds as a drug delivery system. *Sci. Rep.* 7:39202. doi: 10.1038/srep39202

Ghosh, M., Halperin-Sternfeld, M., and Adler-Abramovich, L. (2019). "Bio Mimicking of Extracellular Matrix," in *Biological and Bio-Inspired Nanomaterials. Advances in Experimental Medicine and Biology*, eds S. Perrett, A. Buell, and T. Knowles (Singapore: Springer), 371–399. doi: 10.1007/978-981-13-9791-2_12

Gong, Y., Li, S., Zeng, W., Yu, J., Chen, Y., and Yu, B. (2019). Controlled in vivo bone formation and vascularization using ultrasound-triggered release of recombinant vascular endothelial growth factor from poly(D,L-lactic-co-glycolicacid) microbubbles. *Front. Pharmacol.* 10:413. doi: 10.3389/fphar.2019.00413

Gonzalez-Fernandez, T., Rathan, S., Hobbs, C., Pitacco, P., Freeman, F. E., Cunniffe, G. M., et al. (2019). Pore-forming bioinks to enable spatio-temporally defined gene delivery in bioprinted tissues. *J. Controlled Release* 301, 13–27. doi: 10.1016/j.jconrel.2019.03.006

Griffin, D. R., Schlosser, J. L., Lam, S. F., Nguyen, T. H., Maynard, H. D., and Kasko, A. M. (2013). Synthesis of photodegradable macromers for conjugation and release of bioactive molecules. *Biomacromolecules* 14, 1199–1207. doi: 10.1021/bm400169d

Guardado-Alvarez, T. M., Sudha Devi, L., Russell, M. M., Schwartz, B. J., and Zink, J. I. (2013). Activation of snap-top capped mesoporous silica nanocontainers using two near-infrared photons. *J. Am. Chem. Soc.* 135:17652. doi: 10.1021/ja410105b

Guzzi, E. A., Bovone, G., and Tibbit, M. W. (2019). Universal Nanocarrier Ink Platform for Biomaterials Additive Manufacturing. *Small* 15:1905421. doi: 10.1002/smll.201905421

Guzzi, E. A., and Tibbitt, M. W. (2020). Additive manufacturing of precision biomaterials. *Adv. Mater.* 32:1901994. doi: 10.1002/adma.201901994

Hacohen, A., Jessel, H. R., Richter-Levin, A., and Shefi, O. (2020). Patterning of particles and live cells at single cell resolution. *Micromachines* 11:505. doi: 10.3390/mi11050505

Han, Y., Lian, M., Sun, B., Jia, B., Wu, Q., Qiao, Z., et al. (2020). Preparation of high precision multilayer scaffolds based on Melt Electro-Writing to repair cartilage injury. *Theranostic* 10:10214. doi: 10.7150/thno.47909

Hao, X., Silva, E. A., Månsson-Broberg, A., Grinnemo, K., Siddiqui, A. J., Dellgren, G., et al. (2007). Angiogenic effects of sequential release of VEGF-A165 and PDGF-BB with alginate hydrogels after myocardial infarction. *Cardiovasc. Res.* 75, 178–185. doi: 10.1016/j.cardiores.2007.03.028

He, W., Reaume, M., Hennenfent, M., Lee, B. P., and Rajachar, R. (2020). Biomimetic hydrogels with spatial- and temporalcontrolled chemical cues for tissue engineering. *Biomater. Sci.* 8, 3248–3269. doi: 10.1039/d0bm00263a

Hernández, A., Reyes, R., Sánchez, E., Rodríguez-Évora, M., Delgado, A., and Évora, C. (2012). In vivo osteogenic response to different ratios of BMP-2 and VEGF released from a biodegradable porous system. *J. Biomed. Mater. Res. Part A* 100A, 2382–2319. doi: 10.1002/jbm.a.34183

Hipfinger, C., Subbiah, R., Tahayeri, A., Athirasala, A., Horsophonphong, S., Thrivikraman, G., et al. (2020). 3D printing of microgel-loaded modular LEGO-like cages as instructive scaffolds for tissue engineering. *bioRxiv* [Preprint]. doi: 10.1101/2020.03.02.974204

Hogan, K. J., and Mikos, A. G. (2020). Biodegradable thermoresponsive polymers: applications in drug delivery and tissue engineering. *Polymer* 211:123063. doi: 10.1016/j.polymer.2020.123063

Hutmacher, D. W., Schantz, J. T., Lam, C. X. F., Tan, K. C., and Lim, T. C. (2007). State of the art and future directions of scaffold-based bone engineering from a biomaterials perspective. *J. Tssue Eng. Regen. M* 1, 245–260. doi: 10.1002/term.24

Hwa Kim, D., Huegel, J., Taylor, B. L., Nuss, C. A., Weiss, S. N., Soslowsky, L. J., et al. (2020). Biocompatibility and bioactivity of an FGF-loaded microsphere-based bilayer delivery system. *Acta Biomater.* 111, 341–348. doi: 10.1016/j.actbio.2020.04.048

Jacob, S., Nair, A. B., Patel, V., and Shah, J. (2020). 3D printing technologies: recent development and emerging applications in various drug delivery systems. *AAPS Pharm. Sci. Tech.* 21:220. doi: 10.1208/s12249-020-01771-4

Jelonek, K., Jaworska, J., Pastusiak, M., Sobota, M., Włodarczyk, J., Karpeta-Jarzabek, P., et al. (2018). Effect of vascular scaffold composition on release of sirolimus. *Eur. J. Pharm. Biopharm.* 132, 41–49. doi: 10.1016/j.ejpb.2018.08.015

Jiang, Y., Yang, Y., Zheng, X., Yi, Y., Chen, X., Li, Y., et al. (2020). Multifunctional load-bearing hybrid hydrogel with combined drug release and photothermal conversion functions. *NPG Asia Mater.* 12:18. doi: 10.1038/s41427-020-0199-6

Kang, Y., Datta, P., Shanmughapriya, S., and Ozbolat, I. T. (2020). 3D Bioprinting of tumor models for cancer research. *ACS Appl. Bio Mater.* 3, 5552–5573. doi: 10.1021/acsabm.0c00791

Katt, M. E., Placone, A. L., Wong, A. D., Xu, Z. S., and Searson, P. C. (2016). In vitro tumor models: advantages, disadvantages, variables, and selecting the right platform. *Front. Bioeng. Biotechnol.* 4:12. doi: 10.3389/fbioe.2016.00012

Kelly, D. C., Raftery, R. M., Curtin, C. M., O'Driscoll, C. M., and O'Brien, F. J. (2019). Scaffold-based delivery of nucleic acid therapeutics for enhancedbone and cartilage repair. *J. Orthop. Res.* 37:1671. doi: 10.1002/jor.24321

Kim, H., Park, H., Lee, J. W., and Lee, K. Y. (2016). Magnetic field-responsive release of transforming growth factor beta 1 from heparin-modified alginate ferrogels. *Carbohyd. Polym.* 151:467. doi: 10.1016/j.carbpol.2016.05.090

Koons, G. L., and Mikos, A. G. (2019). Progress in three-dimensional printing with growth factors. *J. Controlled Release* 295:50. doi: 10.1016/j.jconrel.2018.12.035

Li, J., and Mooney, D. J. (2016). Designing hydrogels for controlled drug delivery. *Nat. Rev. Mater.* 1:16071. doi: 10.1038/natrevmats.2016.71

Li, X., Wang, Y., Wang, Z., Qi, Y., Li, L., Zhang, P., et al. (2018). Composite PLA/PEG/nHA/dexamethasone scaffold prepared by 3D printing for bone regeneration. *Macromol. Biosci.* 18:1800068. doi: 10.1002/mabi.201800068

Lin, C. Y. J., Kang, H., and Hollister, S. J. (2020). "Biomechanics of osteo-synthetics," in *Frontiers in Orthopaedic Biomechanics*, eds C. K. Cheng and S. Y. Woo (Singapore: Springer), 397–425. doi: 10.1007/978-981-15-3159-0_15

Linsley, C. S., and Wu, B. M. (2017). Recent advances in light-responsive ondemand drug-delivery systems. *Ther. Deliv.* 8, 89–107. doi: 10.4155/tde-2016-0060

Liu, H., Du, Y., Yang, G., Hu, X., Wang, L., Liu, B., et al. (2020). Delivering proangiogenic factors from 3D-printed polycaprolactone scaffolds for vascularized bone regeneration. *Adv. Healthc. Mater.* 9:2000727. doi: 10.1002/adhm.202000727

Liu, Y., Yu, H., Liu, Y., Liang, G., Zhang, T., and Hu, Q. (2016). Dual drug spatiotemporal release from functional gradient scaffolds prepared using 3D Bioprinting and Electrospinning. *Polym. Eng. Sci.* 56, 170–177. doi: 10.1002/pen.24239

Loebel, C., and Burdick, J. A. (2018). Engineering stem and stromal cell therapiesfor musculoskeletal tissue repair. *Cell Stem Cell* 22, 325–339. doi: 10.1016/j.stem.2018.01.014

Lu, T., and Ten Hagen, T. L. M. (2020). A novel kinetic model to describe the ultra-fast triggered release of thermosensitive liposomal drug delivery systems. *J. Controlled Release* 324, 669–678. doi: 10.1016/j.jconrel.2020.05.047

Lu, X., Jin, H., Quesada, C., Farrell, E. C., Huang, L., Aliabouzar, M., et al. (2020). Spatially-directed cell migration in acoustically-responsive scaffolds through the controlled delivery of basic fibroblast growth factor. *Acta Biomater.* 113, 217–227. doi: 10.1016/j.actbio.2020.06.015

Mao, S., Pang, Y., Liu, T., Shao, Y., He, J., Yang, H., et al. (2020). Bioprinting of in vitro tumor models for personalized cancer treatment: a review. *Biofabrication* 12:042001. doi: 10.1088/1758-5090/ab97c0

Marizza, P., Keller, S. S., Müllertz, A., and Boisen, A. (2014). Polymer-filled microcontainers for oral delivery loaded using supercritical impregnation. *J. Control. Release* 173, 1–9. doi: 10.1016/j.jconrel.2013.09.022

McHugh, K. J., Nguyen, T. D., Linehan, A. R., Yang, D., Behrens, A. M., Rose, S., et al. (2017). Fabrication of fillable microparticles and other complex 3D microstructures. *Science* 359, 1138–1142. doi: 10.1126/science.aaf7447

Mekhileri, N. V., Lim, K. S., Brown, G. C. J., Mutreja, I., Schon, B. S., Hooper, G. J., et al. (2018). Automated 3D bioassembly of micro-tissues for biofabrication of hybrid tissue engineered constructs. *Biofabrication* 10:024103. doi: 10.1088/1758-5090/aa9ef1

Mirza, I., and Saha, S. (2020). Biocompatible anisotropic polymeric particles: synthesis, characterization, and biomedical applications. *ACS Appl. Biol. Mater.* 3:8241. doi: 10.1021/acsabm.0c01075

Mohammed, A., Elshaer, A., Sareh, P., Elsayed, M., and Hassanin, H. (2020). Additive manufacturing technologies for drug delivery applications. *Int. J. Pharm.* 580:119245. doi: 10.1016/j.ijpharm.2020.119245

Moncion, A., Lin, M., O'Neill, E. G., Franceschi, R. T., Kripfgans, O. D., Putnam, A. J., et al. (2017). Controlled release of basic fibroblast growth factor for angiogenesis using acoustically-responsive scaffolds. *Biomaterials* 140, 26–36. doi: 10.1016/j.biomaterials.2017.06.012

Mondal, S., Das, S., and Nandi, A. K. (2020). A review on recent advances in polymer and peptide hydrogels. *Soft Matter.* 16, 1404–1454. doi: 10.1039/c9sm02127b

Moreira, A., Carneiro, J., Campos, J. B. L. M., and Miranda, J. M. (2021). Production of hydrogel microparticles in microfluidic devices: a review. *Microfluid. Nanofluid.* 25:10. doi: 10.1007/s10404-020-02413-8

Moreno Madrid, A. P., Mariel Vrecha, S., Sanchez, M. A., and Rodriguez, A. P. (2019). Advances in additive manufacturing for bone tissue engineering scaffolds. *Mat. Sci. Eng. C* 100:631. doi: 10.1016/j.msec.2019.03.037

Murphy, C., Kolan, K., Li, W., Semon, J., Day, D., and Leu, M. (2017). 3D bioprinting of stem cells and polymer/bioactive glass composite scaffolds for bone tissue engineering. *Int. J. Bioprinting* 3:54. doi: 10.18063/IJB.2017.01.005

Ngo, T. T., Hoffman, L., Hoople, G. D., Trevena, W., Shakya, U., and Barr, G. (2020). Surface morphology and drug loading characterization of 3D-printedmethacrylate-based polymer facilitated by supercritical carbondioxide. *J. Supercrit. Fluid* 160:104786. doi: 10.1016/j.supflu.2020.104786

Oliva, N., and Almquist, B. D. (2020). Spatiotemporal delivery of bioactive molecules for wound healing using stimuli-responsive biomaterials. *Adv. Drug Delivery Rev.* 161–162, 22–41. doi: 10.1016/j.addr.2020.07.021

Omidi, M., Almeida, L., and Tayebi, L. (2020). Microfluidic-assisted fabrication of reverse micelle/PLGA hybrid microspheres for sustained vascular endothelial growth factor delivery. *Biotechnol. Appl. Biochem.* (inpress). doi: 10.1002/bab.1971

Oztan, Y. C., Nawafleh, N., Zhou, Y., Liyanage, P. Y., Hettiarachchi, S. D., Seven, E. S., et al. (2020). Recent advances on utilization of bioprinting for tumor modelling. *Bioprinting* 18:e00079. doi: 10.1016/j.bprint.2020.e00079

Pal, A., Smith, C. I., Palade, J., Nagaraju, S., Alarcon-Benedetto, B. A., Kilbourne, J., et al. (2020). Poly(N-isopropylacrylamide)-based dual-crosslinking biohybrid injectable hydrogels for vascularization. *Acta Biomater.* 107, 138–151. doi: 10.1016/j.actbio.2020.02.041

Palmese, L. L., Fan, M., Scott, R. A., Tan, H., and Kiick, K. L. (2020). Multi-stimuli-responsive, liposome-crosslinked poly(ethylene glycol) hydrogels for drug delivery. *J. Biomat. Sci. Polym E* 32, 635–656. doi: 10.1080/09205063.2020.1855392

Parak, A., Pradeep, P., du Toit, L. C., Kumar, P., Choonara, Y. E., and Pillay, V. (2019). Functionalizing bioinks for 3D bioprinting applications. *Drug Discov. Today* 24, 198–205. doi: 10.1016/j.drudis.2018.09.012

Pedersen, S. L., Huynh, T. H., Pöschko, P., Fruergaard, A. S., Olesen, M. T. J., Chen, Y., et al. (2020). Remotely triggered liquefaction of hydrogel materials. *ACS Nano.* 14, 9145–9155. doi: 10.1021/acsnano.0c04522

Peng, Z., Sun, H., Bunpetch, V., Koh, Y., Wen, Y., Wu, D., et al. (2021). The regulation of cartilage extracellular matrix homeostasis in joint cartilage degeneration and regeneration. *Biomaterials* 268:120555. doi: 10.1016/j.biomaterials.2020.120555

Poldervaart, M. T., Gremmels, H., van Deventer, K., Fledderus, J. O., Cumur Öner, F., Verhaar, M. C., et al. (2014). Prolonged presence of VEGF promotes vascularization in 3D bioprinted scaffolds with defined architecture. *J. Control. Release* 184, 58–66. doi: 10.1016/j.jconrel.2014.04.007

Radhakrishnan, J., Varadaraji, S., Kumar Dash, S., Sharma, A., and Shanker Verma, R. (2020). Organotypic cancer tissue models for drug screening: 3D constructs, bioprinting and microfluidic chips. *Drug Discov. Today* 25, 879–890. doi: 10.1016/j.drudis.2020.03.002

Raimondo, T. M., Li, H., Kwee, B. J., Kinsley, S., Budina, E., Andersona, E. M., et al. (2019). Combined delivery of VEGF and IGF-1 promotes functional innervation in mice and improves muscle transplantation in rabbits. *Biomaterials* 216:119246. doi: 10.1016/j.biomaterials.2019.119246

Randall, C. L., Leong, T. G., Bassik, N., and Gracias, D. H. (2007). 3D lithographically fabricated nanoliter containers for drug delivery. *Adv. Drug Deliver. Rev.* 59, 1547–1561. doi: 10.1016/j.addr.2007.08.024

Richard, C., Neild, A., and Cadarso, V. J. (2020). The emerging role of microfluidics in multimaterial 3D bioprinting. *Lab. Chip.* 20, 2044–2056. doi: 10.1039/c9lc01184f

Richardson, T. P., Peters, M. C., Ennet, A. B., and Mooney, D. J. (2001). Polymeric system for dual growth factor delivery. *Nat. Biotechnol.* 19, 1029–1034. doi: 10.1038/nbt1101-1029

Ruskowitz, E. R., and DeForest, C. A. (2018). Photoresponsive biomaterials for targeted drug delivery and 4D cell culture. *Nat. Rev. Mater.* 3:17087. doi: 10.1038/natrevmats.2017.87

Salerno, A., Cesarelli, G., Pedram, P., and Netti, P. A. (2019). Modular strategies to build cell-free and cell-laden scaffolds towards bioengineered tissues and organs. *J. Clin. Med.* 8:1816. doi: 10.3390/jcm8111816

Salerno, A., Diéguez, S., Diaz-Gomez, L., Gómez-Amoza, J. L., Magariños, B., Concheiro, A., et al. (2017). Synthetic scaffolds with full pore interconnectivity for bone regeneration prepared by supercritical foaming using advanced biofunctional plasticizers. *Biofabrication* 9:035002. doi: 10.1088/1758-5090/aa78c5

Salerno, A., and Domingo, C. (2015). Bio-based polymers, supercritical fluids and tissue engineering. *Process Biochem.* 50, 826–838. doi: 10.1016/j.procbio.2015.02.009

Salerno, A., Fernández-Gutiérrez, M., San Román del Barrio, J., and Domingo Pascual, C. (2014). Macroporous and nanometre scale fibrous PLA and PLA–HA composite scaffolds fabricated by a bio safe strategy. *RSC Adv.* 4:61491. doi: 10.1039/C4RA07732F

Salerno, A., Levato, R., Mateos-Timoneda, M. A., Engel, E., Netti, P. A., and Planell, J. (2013). Modular polylactic acid microparticle-based scaffolds prepared via microfluidic emulsion/solvent displacement process: fabrication, characterization, and in vitro mesenchymal stem cells interaction study. *J. Biomed. Mater. Res. Part A* 101A, 720–732. doi: 10.1002/jbm.a.34374

Salerno, A., and Netti, P. A. (2014). "Introduction to biomedical foams," in *Biomedical Foams for Tissue Engineering Applications*, ed. P. A. Netti (Amsterdam: Woodhead Publishing), 3–39.

Salerno, A., Saurina, J., and Domingo, C. (2015). Supercritical CO2 foamed polycaprolactone scaffolds for controlled delivery of 5-fluorouracil, nicotinamide and triflusal. *Int. J. Pharm.* 496, 654–663. doi: 10.1016/j.ijpharm.2015.11.012

Salerno, A., Verdolotti, L., Raucci, M. G., Saurina, J., Domingo, C., Lamanna, R., et al. (2018). Hybrid gelatin-based porous materials with a tunable multiscale morphology for tissue engineering and drug delivery. *Eur. Polym. J.* 99, 230–239. doi: 10.1016/j.eurpolymj.2017.12.024

Santos, M. I., and Reis, R. L. (2020). Vascularization in bone tissue engineering: physiology, current strategies, major hurdles and future challenges. *Macromol. Biosci.* 10, 12–27. doi: 10.1002/mabi.200900107

Saraf, S., Jain, A., Tiwari, A., Verma, A., Kumar Panda, P., and Jain, S. K. (2020). Advances in liposomal drug delivery to cancer: an overview. *J. Drug. Deliv. Sci. Tech.* 56:101549. doi: 10.1016/j.jddst.2020.101549

Saraswat, Y. C., Ibis, F., Rossi, L., Sasso, L., Eral, H. B., and Fanzio, P. (2020). Shape anisotropic colloidal particle fabrication using 2-photon polymerization. *J. Colloid Interf. Sci.* 564, 43–51. doi: 10.1016/j.jcis.2019.12.035

Sarkar, N., and Bose, S. (2020). Controlled release of soy isoflavones from multifunctional 3D printed bone tissue engineering scaffolds. *Acta Biomater.* 114, 407–420. doi: 10.1016/j.actbio.2020.07.006

Saska, S., Pires, L. C., Cominotte, M. A., Mendes, L. S., de Oliverira, M. F., Maia, I. A., et al. (2018). Three-dimensional printing and in vitro evaluation of poly(3-hydroxybutyrate) scaffolds functionalized with osteogenic growth peptide for tissue engineering. *Mater. Sci. Eng. C* 89:265. doi: 10.1016/j.msec.2018.04.016

Shafiee, A. (2020). Design and fabrication of three-dimensional printed scaffolds for cancer precision medicine. *Tissue Eng. Part A* 26, 305–317. doi: 10.1089/ten.tea.2019.0278

Shi, X., Cheng, Y., Wang, J., Chen, H., Wang, X., Li, X., et al. (2020). 3D printed intelligent scaffold prevents recurrence and distal metastasis of breast cancer. *Theranostics* 10, 10652–10664. doi: 10.7150/thno.47933

Shrike Zhang, Y., Duchamp, M., Oklu, R., Ellisen, L. W., Langer, R., and Khademhosseini, A. (2016). Bioprinting the Cancer Microenvironment. *ACS Biomater. Sci. Eng.* 2, 1710–1721. doi: 10.1021/acsbiomaterials.6b00246

Shvartsman, D., Storrie-White, H., Lee, K., Kearney, C., Brudno, Y., Ho, N., et al. (2014). Sustained delivery of VEGF maintains innervation and promotes reperfusion in ischemic skeletal muscles via NGF/GDNF signaling. *Mol. Ther.* 22, 1243–1253. doi: 10.1038/mt.2014.76

Shultz, R. B., and Zhong, Y. (2021). Hydrogel-based local drug delivery strategies for spinal cord repair. *Neural Regen. Res.* 16, 247–253. doi: 10.4103/1673-5374.290882

Sigaux, N., Pourchet, L., Breton, P., Brosset, S., Louvrier, A., and Marquette, C. A. (2019). 3D Bioprinting:principles, fantasies and prospects. *J. Stomatol. Oral Maxillofac Surg.* 120, 128–132. doi: 10.1016/j.jormas.2018.12.014

Silva, E. D., Babo, P. S., Costa-Almeida, R., Domingues, R. M. A., Mendes, B. B., Paz, E., et al. (2018). Multifunctional magnetic-responsive hydrogels to engineer tendon-to-bone interface. *Nanomed. Nanotechnol.* 14, 2375–2385. doi: 10.1016/j.nano.2017.06.002

Skardal, A., Murphy, S. V., Crowell, K., Mack, D., Atala, A., and Soker, S. (2017). A tunable hydrogel system for long-term release of cell-secreted cytokines and bioprinted in situ wound cell delivery. *J. Biomed. Mater. Res. Part B Appl. Biomater.* 105B:1986. doi: 10.1002/jbm.b.33736

Steele, J. A. M., McCullen, S. D., Callanan, D., Autefage, H., Accardi, M. A., Dini, D., et al. (2014). Combinatorial scaffold morphologies for zonal articular cartilage engineering. *Acta Biomater.* 10, 2065–2075. doi: 10.1016/j.actbio.2013.12.030

Stewart, S. A., Domínguez-Robles, J., MvIlorum, V. J., Gonzalez, Z., Utomo, E., Mancuso, E., et al. (2020). Poly(caprolactone)-based coatings on 3D-printed biodegradable implants: a novel strategy to prolong delivery of hydrophilic drugs. *Mol. Pharm.* 17, 3487–3500. doi: 10.1021/acs.molpharmaceut.0c00515

Stubbe, B. G., De Smedt, S. C., and Demeester, J. (2004). "Programmed Polymeric Devices" for pulsed drug delivery. *Pharm. Res.* 21, 1732–1740. doi: 10.1023/B:PHAM.0000045223.45400.01

Sun, B., Lian, M., Han, Y., Mo, W., Jiang, W., Qiao, Z., et al. (2021). A 3D-Bioprinted dual growth factor-releasing intervertebral disc scaffold induces nucleus pulposus and annulus fibrosus reconstruction. *Bioact. Mater.* 6, 179–190. doi: 10.1016/j.bioactmat.2020.06.022

Sun, Q., Chen, R. R., Shen, Y., Mooney, D. J., Rajagopalan, S., and Grossman, P. M. (2005). Sustained vascular endothelial growth factor delivery enhances angiogenesis and perfusion in ischemic hind limb. *Pharm. Res.* 22, 1110–1116. doi: 10.1007/s11095-005-5644-2

Sun, Y., You, Y., Jiang, W., Wang, B., Wu, Q., and Dai, K. (2020a). 3D bioprinting dual-factor releasing and gradient-structured constructs ready to implant for anisotropic cartilage regeneration. *Sci. Adv.* 6:eaay1422. doi: 10.1126/sciadv.aay1422

Sun, Y., You, Y., Jiang, W., Wu, Q., Wang, B., and Dai, K. (2020b). Generating ready-to-implant anisotropic menisci by 3D-bioprintingprotein-releasing cell-laden hydrogel-polymer composite scaffold. *Appl. Mater. Today* 18:100469. doi: 10.1016/j.apmt.2019.100469

Tamjid, E., Bohlouli, M., Mohammadi, S., Alipour, H., and Nikkhah, M. (2020). Sustainable drug release from highly porous and architecturally engineered composite scaffolds prepared by 3D printing. *J. Biomed. Mater. Res. Part A* 108:1426. doi: 10.1002/jbm.a.36914

Tao, J., Zhang, Y., Shen, A., Diao, L., Wang, L., Cai, D., et al. (2020). Injectable chitosan-based thermosensitive hydrogel/nanoparticle-loaded system for local delivery of vancomycin in the treatment of osteomyelitis. *Int. J. Nanomed.* 15, 5855–5871. doi: 10.2147/IJN.S247088

Tarafder, S., Koch, A., Jun, Y., Chou, C., Awadallah, M. R., and Lee, C. H. (2016). Micro-precise spatiotemporal delivery system embedded in 3D printing for complex tissue regeneration. *Biofabrication* 8:025003. doi: 10.1088/1758-5090/8/2/025003

Thébault, C. J., Ramniceanu, G., Boumati, S., Michel, A., Seguin, J., Larrat, B., et al. (2020). Theranostic MRI liposomes for magnetic targeting and ultrasound triggered release of the antivascular CA4P. *J. Controlled Release* 322, 137–148. doi: 10.1016/j.jconrel.2020.03.003

Tomeh, M. A., and Zhao, X. (2020). Recent advances in microfluidics for the preparation of drug and gene delivery systems. *Mol. Pharm.* 17, 4421–4434. doi: 10.1021/acs.molpharmaceut.0c00913

Visscher, L. E., Phuc Dang, H., Knackstedt, M. A., Hutmacher, D. W., and Tran, P. A. (2018). 3D printed Polycaprolactone scaffolds with dual macro-microporosity for applications in local delivery of antibiotics. *Mat. Sci. Eng. C* 87, 78–89. doi: 10.1016/j.msec.2018.02.008

Wagner, E. R., Parry, J., Dadsetan, M., Bravo, D., Riester, S. M., Van Wijnen, A. J., et al. (2018). VEGF-mediated angiogenesis and vascularization of a fumarate-crosslinked polycaprolactone (PCLF) scaffold. *Connect. Tissue Res.* 59, 542–549. doi: 10.1080/03008207.2018.1424145

Wang, C., Ye, X., Zhao, Y., Bai, L., He, Z., Tong, Q., et al. (2020). Cryogenic 3D printing of porous scaffolds for in situ delivery of 2D black phosphorus nanosheets, doxorubicin hydrochloride and osteogenic peptide for treating tumor resection-induced bone defects. *Biofabrication* 12:035004. doi: 10.1088/1758-5090/ab6d35

Wang, H., Zhang, W., and Gao, C. (2015). Shape Transformation of light-responsive pyrene-containing micelles and their influence on cytoviability. *Biomacromolecules* 16, 2276–2281. doi: 10.1021/acs.biomac.5b00497

Wang, L., Deng, F., Wang, W., Li, A., Lu, C., Chen, H., et al. (2018). Construction of injectable self-healing macroporous hydrogels via a template-free method for tissue engineering and drug delivery. *ACS Appl. Mater. Interf.* 10, 36721–36732. doi: 10.1021/acsami.8b13077

Wang, W., Sun, L., Zhang, P., Song, J., and Liu, W. (2014). An anti-inflammatory cell-free collagen/resveratrol scaffold for repairing osteochondral defects in rabbits. *Acta Biomater.* 10:4983. doi: 10.1016/j.actbio.2014.08.022

Wang, X., Wenk, E., Zhang, X., Meinel, L., Vunjak-Novakovic, G., and Kaplan, D. L. (2009). Growth factor gradients via microsphere delivery in biopolymer scaffolds for osteochondral tissue engineering. *J. Control. Release* 134, 81–90. doi: 10.1016/j.jconrel.2008.10.021

Wen, Y., Dai, N., and Hsu, S. (2019). Biodegradable water-based polyurethane scaffolds with a sequential release function for cell-free cartilage tissue engineering. *Acta Biomater.* 88, 301–313. doi: 10.1016/j.actbio.2019.02.044

Xiong, S., Zhang, X., Lu, P., Wu, Y., Wang, Q., Sun, H., et al. (2017). A Gelatin-sulfonated Silk Composite Scaffold based on 3D printing technology enhances skin regeneration by stimulating epidermal growth and dermal neovascularization. *Sci. Rep.* 7:4288. doi: 10.1038/s41598-017-04149-y

Yang, Y., Qiao, X., Huang, R., Chen, H., Shi, X., Wang, J., et al. (2020). E-jet 3D printed drug delivery implants to inhibit growth and metastasis of orthotopic breast cancer. *Biomaterials* 230:119618. doi: 10.1016/j.biomaterials.2019.119618

Yao, Q., Nooeaid, P., Roether, J. A., Dong, Y., Zhang, Q., and Boccaccini, A. R. (2013). Bioglass® -based scaffolds incorporating polycaprolactone and chitosan coatings for controlled vancomycin delivery. *Ceram. Int.* 39, 7517–7522. doi: 10.1016/j.ceramint.2013.03.002

Ye, L., Wang, J., Liao, C., Li, S., Fang, Y., Yang, Z., et al. (2019). 3D printed composite scaffolds incorporating ruthenium complex–loaded liposomes as a delivery system to prevent the proliferation of MG-63 cells. *Macromol. Mater. Eng.* 304:1900295.

Yuba, E. (2020). Development of functional liposomes by modification of stimuli-responsive materials and their biomedical applications. *J. Mater. Chem.* 8, 1093–1107. doi: 10.1039/C9TB02470K

Zhang, H., Gong, W., Wang, Z., Yuan, S., Xie, X., Yang, Y., et al. (2014). Preparation, characterization, and pharmacodynamics of thermosensitive liposomes containing Docetaxel. *J. Pharm. Sci.* 103, 2177–2183. doi: 10.1002/jps.24019

Zhang, Y., Zhao, J., Yang, G., Zhou, Y., Gao, W., Wu, G., et al. (2019). Sustainable drug release from highly porous and architecturally engineered composite scaffolds prepared by 3D printing. *J. Biomatr. Sci. Polym. E* 30, 547–560. doi: 10.1080/09205063.2019.1586303

Zhao, W., Li, Y., Zhang, X., Zhang, R., Hu, Y., Boyer, C., et al. (2020). Photo-responsive supramolecular hyaluronic acid hydrogels for accelerated wound healing. *J. Controlled Release* 323, 24–35. doi: 10.1016/j.jconrel.2020.04.014

Zhou, C., Yang, K., Wang, K., Pei, X., Dong, Z., Hong, Y., et al. (2016). Combination of fused deposition modeling and gas foaming technique to fabricated hierarchical macro/microporous polymer scaffolds. *Mater. Design.* 109:415. doi: 10.1016/j.matdes.2016.07.094

Zhu, S., Chen, P., Chen, Y., Li, M., Chen, C., and Lu, H. (2020). 3D-Printed Extracellular Matrix/Polyethylene glycol diacrylate hydrogel incorporating the anti-inflammatory phytomolecule honokiol for regeneration of osteochondral defects. *Am. J. Sport Med.* 48, 2808–2818. doi: 10.1177/0363546520941842

Zhu, W., Cui, H., Boualam, B., Masood, F., Flynn, E., Rao, R. D., et al. (2018). 3D bioprinting mesenchymal stem cell-laden construct with core–shell nanospheres for cartilage tissue engineering. *Nanotechnology.* 29:185101. doi: 10.1088/1361-6528/aaafa1

Zhu, W., Holmes, B., Glazer, R. I., and Zhang, L. G. (2016). 3D printed nanocomposite matrix for the study of breast cancer bone metastasis. *Nanomed. Nanotechnol.* 12, 69–79. doi: 10.1016/j.nano.2015.09.010

Conflict of Interest: The authors declare that the research was conducted in the absence of any commercial or financial relationships that could be construed as a potential conflict of interest.

frontiers in Bioengineering and Biotechnology

MINI REVIEW
published: 22 July 2021
doi: 10.3389/fbioe.2021.703684

Oregano Essential Oil Micro- and Nanoencapsulation With Bioactive Properties for Biotechnological and Biomedical Applications

Gloria María Pontes-Quero[1,2,3], *Susana Esteban-Rubio*[2], *Juan Pérez Cano*[2], *María Rosa Aguilar*[1,3]* *and Blanca Vázquez-Lasa*[1,3]

[1] Group of Biomaterials, Department of Polymeric Nanomaterials and Biomaterials, Institute of Polymer Science and Technology, ICTP-CSIC, Madrid, Spain, [2] Alodia Farmacéutica SL, Santiago Grisolía 2 D130/L145, Madrid, Spain, [3] Networking Biomedical Research Centre in Bioengineering, Biomaterials and Nanomedicine, CIBER-BBN, Madrid, Spain

OPEN ACCESS

Edited by:
Aurelio Salerno,
Independent Researcher,
Barcelona, Spain

Reviewed by:
Maria Leonor Nunes,
University of Porto, Portugal
Manukumar Honnayakanahalli
Marichannegowda,
University of Maryland, United States

***Correspondence:**
María Rosa Aguilar
mraguilar@ictp.csic.es

Specialty section:
This article was submitted to
Biomaterials,
a section of the journal
Frontiers in Bioengineering and
Biotechnology

Received: 30 April 2021
Accepted: 21 June 2021
Published: 22 July 2021

Citation:
Pontes-Quero GM, Esteban-Rubio S, Pérez Cano J, Aguilar MR and Vázquez-Lasa B (2021) Oregano Essential Oil Micro- and Nanoencapsulation With Bioactive Properties for Biotechnological and Biomedical Applications. Front. Bioeng. Biotechnol. 9:703684. doi: 10.3389/fbioe.2021.703684

Due to the preservative, antioxidant, antimicrobial, and therapeutic properties of oregano essential oil (OEO), it has received an emerging interest for biotechnological and biomedical applications. However, stability and bioactivity can be compromised by its natural volatile and hydrophobic nature, and by external factors including light, heat, or oxygen. Therefore, micro- and nanoencapsulation are being employed to guarantee oregano oil protection from outside aggressions and to maximize its potential. Oregano oil encapsulation is an interesting strategy used to increase its stability, enhance its bioactivity, and decrease its volatility. At the same time, the versatility that micro- and nanocarriers offer, allows to prepare tailored systems that can provide a controlled and targeted release of the encapsulated principle, influence its bioactive activities, or even provide additional properties. Most common materials used to prepare these carriers are based on lipids and cyclodextrins, due to their hydrophobic nature, polymers due to their versatility in composition, and hybrid lipid-polymer systems. In this context, recently developed micro- and nanocarriers encapsulating oregano oil with applications in the biotechnological and biomedical fields will be discussed.

Keywords: microcarriers, nanocarriers, antimicrobial, antibacterial, antifungal, emulsion, stability

INTRODUCTION

Essential oils (EOs), derived from aromatic plants, are volatile oily liquids mainly composed of terpenoids and phenolic acids (da Silva et al., 2021). They have been used since ancient times in different cultures due to their bioactive properties. Some of the most reported properties of EOs are their antibacterial (Nazzaro et al., 2013), antifungal (D'agostino et al., 2019), antiviral (Ma and Yao, 2020), and antioxidant (Leyva-López et al., 2017) activities, mainly due to the disruption of bacterial and fungal membranes and viral envelops (Böhme et al., 2014). Nevertheless, some characteristics like immunomodulatory and anticancer activities are recently being reported, highlighting the potential use of EOs in the biomedical field (Bhalla et al., 2013; Böhme et al., 2014). For these reasons, in the last decades, it has emerged a great interest in their use in biotechnology, for example, in foods and cosmetics, and in the biomedical field, in which their excellent properties provide a great therapeutic potential (Böhme et al., 2014; Aljaafari et al., 2021). However, stability and bioactivity can be compromised by their natural volatility, low water solubility, and external

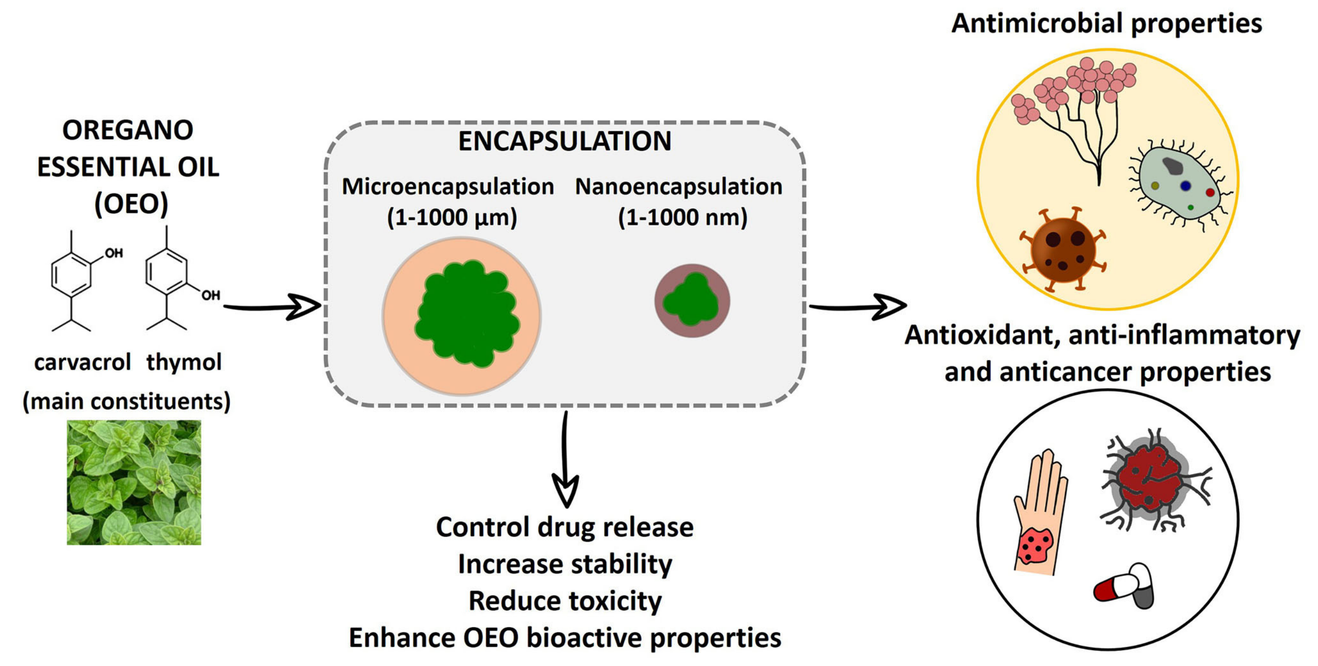

GRAPHICAL ABSTRACT |

factors, which have detrimental effects on the overall acceptability of the developed product (Turek and Stintzing, 2013).

In this context, drug delivery systems such as micro- and nanoparticles (MPs and NPs), micro- and nanocapsules (MCs and NCs), films, or nanocomposite materials have been proposed to encapsulate EOs (Zhu et al., 2021). These systems enhance EO stability in aqueous media and, as a consequence, improve their bioavailability, reduce their toxic effects, provide a controlled release of the encapsulated agent, protect them against the environment or mask their intense aroma (Cimino et al., 2021). Micro- and nanocarriers with tailored properties are of special interest due to the increased surface-to-volume ratio that their sizes offer and, consequently, an increase in their reactivity (Franklyne et al., 2016). These systems are typically based on polymers, lipid materials, or a combination of both (Kaliamurthi et al., 2019). Moreover, micro- and nanocarriers present some differences regarding their fate after its application, the ability to cross some biological barriers, entering cells, and possible tissue reactions that, depending on the application, will determine the choice of one over the other (Kohane, 2007).

Oregano essential oil (OEO) is one of the most widely used EOs worldwide. It is extracted from *Origanum vulgare* L. and formed basically by carvacrol and thymol (Teixeira et al., 2013). Both carvacrol and thymol are monoterpenes with a single phenolic ring formed from the bonding of two isoprene molecules with three functional group substituents (Memar et al., 2017). Due to this chemical structure, they provide OEO with its antibacterial and antioxidant properties, in addition to its anticancer and anti-inflammatory activities (Sakkas and Papadopoulou, 2017; Sharifi-Rad et al., 2021). Due to these activities, OEO and its components have come to the forefront and are being widely investigated to be used as a food preservative, for active packaging, and the treatment of different diseases, such as infections (Bhalla et al., 2013).

This review aims to discuss the state-of-the-art micro- and nanoencapsulation of OEO in biotechnology and biomedical applications, making emphasis on the materials used, the fabrication process, and their final bioactive properties. It is expected that the information provided here will provide the reader with a general view of the possibilities that OEO encapsulation may offer in these specific fields. In this sense, **Figure 1** collects the main types of OEO delivery systems reported, their fabrication methods, most common materials employed, and biomedical and biotechnological applications.

REVIEW METHOD

For this mini-review article, an extensive search was conducted in different web search engines using keywords such as OEO, carvacrol, thymol, microencapsulation, nanoencapsulation, microcarriers, nanocarriers, MPs, NPs, MCs, NCs, biomedical and biotechnological. The search strategy was limited to publications in English and published from 2017 to 2021. Articles were classified according to the size of the OEO delivery system and listed according to their application.

OEO MICROENCAPSULATION

Microencapsulation is a technique in which a material of interest is surrounded by a coating to form capsules or

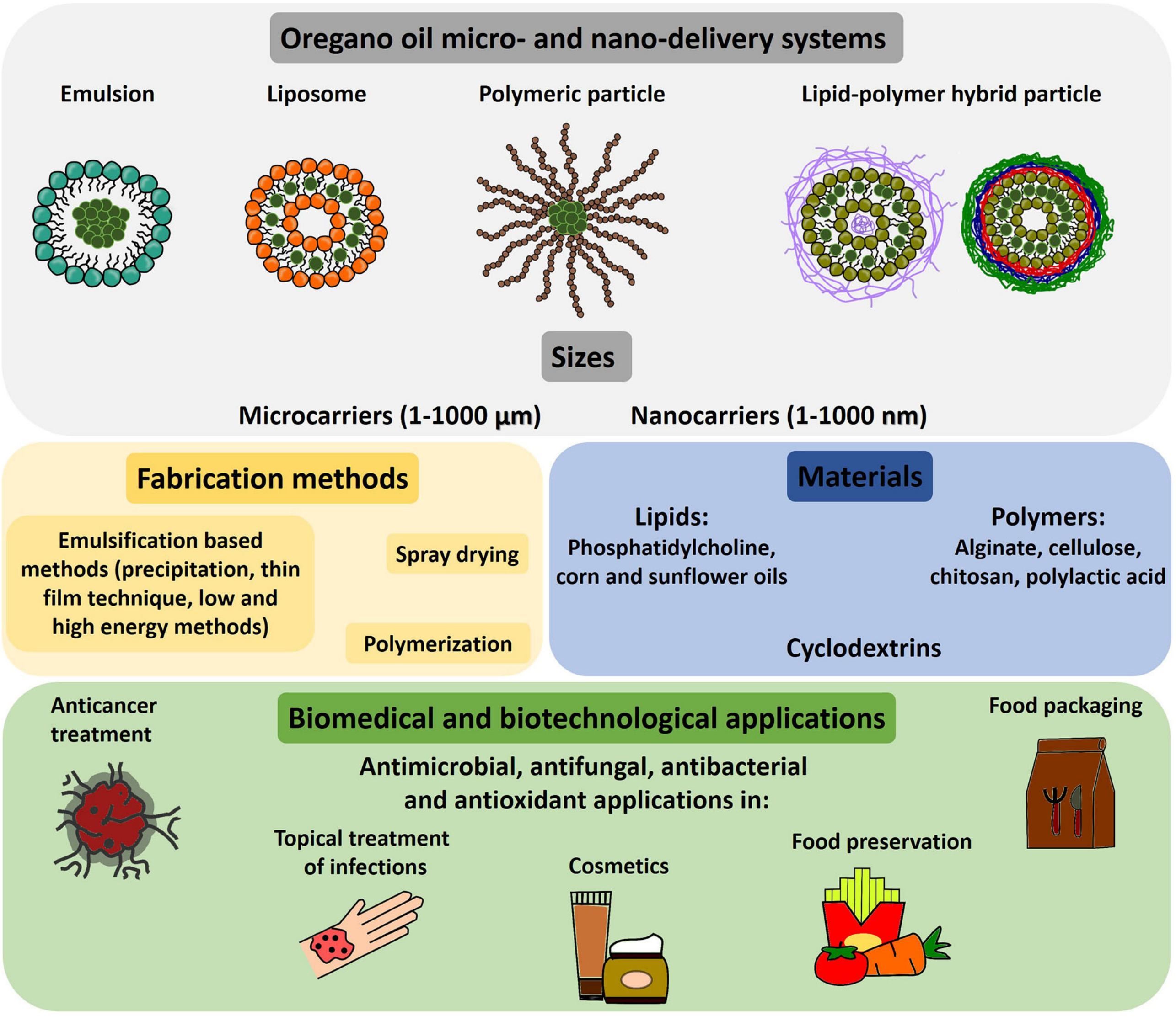

FIGURE 1 | Scheme of most common OEO delivery systems, fabrication methods, materials employed, and biomedical and biotechnological applications.

particles with sizes between 1 and 1,000 µm (Ju and Chu, 2019). Compared to macroscale particles, MPs and MCs have the advantage of having a larger surface-to-volume ratio, which is even larger for NPs, increasing the reactivity of the delivery system. Microencapsulation of OEO has been conducted through different methods such as emulsification, spray-drying, coaxial electrospray, freeze-drying, coacervation, *in situ* polymerization, or ionic gelation using mainly lipids, cyclodextrins, and polymers (Bakry et al., 2016). One of the main applications of these OEO-loaded systems is in the field of biotechnology as food preservatives, as components of active packages, and in the pharmaceutical industry (Bakry et al., 2016). Research articles published on this topic in the latest years and the main results obtained are listed in **Table 1** according to the system function or application.

The stability of microemulsions, MPs, and MCs encapsulating OEO has been widely investigated. In this sense, Cardoso-Ugarte et al. (2021) optimized OEO loaded water-in-oil-in-water (W/O/W) double emulsions in terms of primary emulsion concentrations and homogenization parameters to finally assess the antifungal activity of the best system (Cardoso-Ugarte et al., 2021). They assessed the stability of primary emulsions resulting from high-pressure and mechanical homogenization evidencing that stability, in terms of droplet size, was affected by the homogenization method of the primary emulsion. Asensio et al. (2017), for their part, studied how wall materials (hydroxypropyl methylcellulose, maltodextrin, and colloidal silicon dioxide) and storage temperatures influenced the antioxidant activity, total phenolic content, and release kinetics of OEO compounds of spray-dried microcapsules (MCs) (Asensio et al., 2017). The authors observed that the presence

TABLE 1 | Latest research reports (2017–2021) on oregano essential oil (OEO) microencapsulation with biotechnological and biomedical applications.

Function/application	Fabrication process	Composition	Results	References
Delivery system	W/O emulsion	OEO, corn oil	Emulsifier concentration affected emulsion separation, viscosity, and surface electric charge.	Cardoso-Ugarte et al., 2018
Delivery system	Emulsion	Thymol, alginate	No chemical interactions between thymol and sodium alginate. Sustained *in vitro* release.	Bhalerao and Wagh, 2019
Antifungal	W/O/W double emulsion	OEO, corn oil	Stability and droplet sizes are affected by the homogenization method of the primary emulsion. Antifungal activity against *A. niger.*	Cardoso-Ugarte et al., 2021
Antimicrobial agent	Pickering emulsion	OEO, cellulose nanocrystals	Average droplet sizes: 1.2–2.9 μm. Variations of zeta potential with pH. Antimicrobial activity by cell membrane disruption.	Zhou et al., 2018
Antimicrobial agent	O/W emulsion	OEO, high oleic sunflower oil	Nanoemulsions were not stable under acid and high salt concentration conditions. Inutec SP1 emulsions remained stable for several days.	Sedaghat Doost et al., 2017
Antimicrobial agent	Solvent evaporation	Thymol, PLGA	Improvement of thermal and storage stability sustained release of thymol and antibacterial properties against *E. coli* and *S. aureus*.	Zhu et al., 2019
Antimicrobial agent	Spray drying	Carvacrol, pectin-alginate	Encapsulation efficiency: 77%. Antimicrobial activity against *E. coli.*	Sun et al., 2019
Antioxidant additive to control food oxidation	Spray drying	OEO, hydroxypropyl methyl cellulose, maltodextrin, colloidal silicon dioxide	Release kinetics of OEO volatile compounds and the antioxidant activity of the system was controlled by wall material-lipid core ratios and temperature storage conditions.	Asensio et al., 2017
Food preservation	Co-precipitation inclusion method	OEO, β-cyclodextrin	Inclusion efficiency: 55%. Enhancement of yam shelf-life.	Huang et al., 2020
Food preservation	Ionic gelation and electrostatic interactions (coating)	OEO, alginate, whey protein concentrate	Loading and retention capacity: 64 and 57%. Freeze-drying caused an increase in size polydispersity and porosity of bead surface. Whey protein coating caused a slowdown effect on OEO release.	Gallo et al., 2020
Active packaging, personal care products, insect repellents	Co-precipitation inclusion method	OEO, β-cyclodextrin	Particle size range: 450–530 nm. Polydispersity: 0.31–0.48. Good stability in suspension. Inclusion efficiencies: 26%. *In vitro* OEO release for up to 11 days.	Kotronia et al., 2017
Topical treatment of cutaneous diseases	Double emulsion	OEO	Average particle size: 1.76 μm. Surface charge: −15 mV. Encapsulation efficiencies: 47%. Unstable with temperature.	Fraj et al., 2019
Topical cosmetics	Ultrasonication	Thymol, lignosulfonate	Average particle size range: 3.2–3.4 μm. Encapsulation efficiencies >40%.	Piombino et al., 2020
Antibiotic substitute for intestinal delivery	Melt-granulation process	Thymol, lauric acid, starch, alginate	*In vitro* slow release of thymol using simulated fluids.	Omonijo et al., 2018
Intestinal delivery	Blending of thymol with a lipid matrix	Thymol, commercial lipid matrix containing other organic acids	Stability during feed pelleting and storing processes. *In vitro* and *in vivo* prolonged release of thymol in simulated gastric and intestinal fluids and pig guts, respectively.	Choi et al., 2020

W/O, water-in-oil; W/O/W, water-in-oil-in-water; OEO, oregano essential oil; O/W, oil-in-water; PCL, polycaprolactone; PLGA, poly(lactic-co-glycolide).

of colloidal silicon dioxide in some formulations increased the release of volatile compounds, to detriment of the antioxidant activity, in terms of radical scavenging activity and Trolox equivalent antioxidant capacity, which was lost to a greater extent during storage.

Highly stable Pickering emulsions (emulsion stabilized by solid particles) loading OEO were prepared by Zhou et al. (2018) using cellulose nanocrystals as stabilizers (Zhou et al., 2018). The authors demonstrated that emulsions exhibited higher stability with increasing concentration of cellulose nanocrystals or at lower oil-water ratio and salt concentration. Furthermore, the antimicrobial efficacy of the emulsions was confirmed by efficiently inhibiting the growth of different bacteria by destroying the integrity of their cell membranes.

The influence of environmental stress conditions, such as acidification and salt addition, on the stability of OEO oil-in-water (O/W) emulsions prepared by a high energy method, has also been assessed by Sedaghat Doost et al. (2017), using two non-ionic surfactants, Tween 80 and Inutec SP1, as stabilizers (Sedaghat Doost et al., 2017). Different OEO: high oleic sunflower oil ratios were used to prepare the emulsions. Despite nanoemulsions could be formed, they were not stable under acid and high salt concentration conditions. Moreover, Tween 80 containing emulsions exhibited phase separation at all salt concentrations, while Inutec SP1 emulsions remained stable for several days. In the end, colloidal dispersions with a 50:50 OEO: high oleic sunflower oil ratio in the lipid phase stabilized by Inutec SP1 kept at 4°C showed the longest stability with no droplet size variation during 2 weeks. The effect of Tween 80 in addition to Span 20 as emulsifiers of OEO water-in-oil (W/O) emulsions was also investigated (Cardoso-Ugarte et al., 2018). In this case, the concentration of the emulsifier affected emulsion separation, led by Ostwald ripening, viscosity, and surface electric charge, showing slower separation rates in the tested emulsions with higher concentrations of Tween 80 and Span 20.

Cyclodextrins, cyclic hydrophilic oligosaccharides obtained from starch enzymatic conversion, have been employed in OEO encapsulation. For instance, Kotronia et al. (2017) encapsulated OEO into β-cyclodextrin inclusion complexes by coprecipitation methods (Kotronia et al., 2017). The systems showed suitable characteristics in terms of size, surface charge, and morphology, a controlled *in vitro* OEO release for up to 11 days, and inclusion efficiencies up to 26%. Similarly, Huang et al. (2020) prepared β-cyclodextrin systems loaded with OEO, obtaining MPs with strong interactions between β-cyclodextrin and OEO. A reduction of both gram-positive and gram-negative bacteria occurred when treated with OEO-loaded systems, especially in gram-positive bacteria. Finally, the food preservative performance of the system due to its antibacterial activity was demonstrated by reducing the browning and enhancing the shelf-life of a type of yam (Huang et al., 2020).

Alginate beads have also been used to encapsulate OEO by extrusion dripping to study the influence of its encapsulation in oil release kinetics in liquid simulating meat marinating solution (Gallo et al., 2020). Spherical particles with good encapsulation performance were obtained and subjected to electrostatic interactions with whey proteins and freeze-drying. Freeze-drying of the beads increased the particle size polydispersity and the porosity of the bead surface. Besides, beads were successfully coated with whey proteins by electrostatic interactions causing a slowdown effect on OEO *in vitro* release rates. Alginate has also been used to encapsulate thymol, one of the main components of OEO, demonstrating that no chemical interactions between thymol and sodium alginate occurred and showing sustained thymol *in vitro* release (Bhalerao and Wagh, 2019). Carvacrol, the other main component of OEO has also been microencapsulated, in a pectin-alginate matrix by Sun et al. (2019), demonstrating that the microencapsulation did not affect the radical scavenging properties of carvacrol and the antibacterial activity against *Escherichia coli* (Sun et al., 2019).

Thymol has been entrapped in other lipid and polymeric vehicles. For instance, Omonijo et al. (2018) microencapsulated thymol along with lauric acid into starch MPs with the presence or not of alginate to deliver them to pig intestinal tracts as an antibiotic substitute (Omonijo et al., 2018). Highly stable systems were obtained with an *in vitro* prolonged release of loaded compounds in the case of MPs presenting alginate, using simulated salivary, gastric, and intestinal fluids. However, the efficacy of the MPs was not demonstrated. The intestinal delivery of thymol has also been assessed when microencapsulated into commercial lipid matrices containing organic acids by Choi et al. (2020), demonstrating the stability of the systems during feed pelleting and storing processes and an *in vitro* and *in vivo* sustained release of thymol in simulated gastric and intestinal fluids and pig guts, respectively (Choi et al., 2020).

Due to the antioxidant and biocompatibility properties of lignin, lignosulfonate MPs were successfully developed by Piombino et al. (2020) to encapsulate thymol and its derivatives as topical systems with antimicrobial properties for cosmetics through environmental friendly sonication procedures. Results showed that more than 40% of each substrate was properly encapsulated, except for 2,4-dibromothymol, showing the best encapsulation efficiencies for the mono-brominated thymol derivative (76%). To test the suitability of these systems as dermal agents, the *in vitro* release of the derivatives from the MPs in solutions simulating skin pH (acetate buffer at pH 5.4) were performed, showing a slow-release, especially for O-methylated compounds, that was dependent on the inherent lipophilicity of each compound. Thymol-loaded poly(lactic-*co*-glycolide) (PLGA) MPs have also been demonstrated to be suitable microcarriers of thymol improving thermal and storage stability and controlling thymol release (Zhu et al., 2019). In addition, the antibacterial properties of the MPs against *E. coli* and *Staphylococcus aureus* were demonstrated by the disruption of their cytoplasmic membrane, since the porous structure of the MPs enhances the permeation of thymol into bacteria. The antibacterial effect was confirmed by adding the loaded MPs into naturally contaminated milk and observing that the growth of bacteria was suppressed by thymol-loaded MPs.

OEO NANOENCAPSULATION

Nanoencapsulation is another common strategy addressed to protect OEO from the environment and improve its performance (Bilia et al., 2014). In addition, the smaller size of NPs, between 1 and 1000 nm, makes them very suitable for biomedical applications, as they can be intravenously injected, can be efficiently uptaken by a variety of cell types, and can extravasate through endothelium to reach, for instance, inflammatory sites or tumors (Gelperina et al., 2005; Singh and Lillard, 2009). The latest research reports on OEO nanoencapsulation that are mainly focused on food biotechnology and biomedical applications are listed in **Table 2** according to the system function or application.

Polymeric nanocarriers have received great interest due to their versatility in composition, structure, and properties. In the study of Fraj et al. (2019), the authors compared

TABLE 2 | Latest research reports (2017–2021) on OEO nanoencapsulation with biotechnological and biomedical applications.

Function/application	Fabrication process	Composition	Results	References
Delivery system	High energy emulsion method	OEO, sunflower oil, succinic anhydride-modified starch, chitosan, sodium carboxymethylcellulose	Multilayer NPs: One layer NPs: 180 nm, −42 mV. Two layers NPs: 226 nm, 35 mV. Three layers NPs: 265 nm, −1 mV. Encapsulation efficiency: 97%.	Espinosa-Sandoval et al., 2021
Delivery system	Complex coacervation	OEO, gelatin, chia mucilage/arabic gum	Particle size range: 17–120 nm. Encapsulation efficiency: >90%.	Hernández-Nava et al., 2020
Delivery system	Ultrasonication	Neobee® 1053 medium-chain triglyceride oil	Lecithin nanoemulsions were more stable and viscoelastic than Tween 20 nanoemulsions.	Nash and Erk, 2017
Antifungal agent for food preservation	Electrospraying	OEO, PVA, chitosan	Particle size range: 337–818 nm. Encapsulation efficiency: 90%. Antifungal properties against different fungi.	Vehapi et al., 2020
Antimicrobial agent for food preservation	Emulsion	OEO, medium-chain triacylglyceride	Average droplet size range: 74–150 nm. Viscoelastic behavior of nanoemulsions. Antimicrobial activity by quorum-sensing inhibition.	Asensio et al., 2020
Antimicrobial agent for food preservation	High-frequency ultrasonication	EOs (cinnamon, rosemary, OEO)	Particle size range: 226–546 nm. Encapsulation efficiency >80%. Inhibition of *E. coli* and *L. monocytogenes.*	Dávila-Rodríguez et al., 2019
Antibacterial agent for food preservation	Nanoliposomes: lipid film hydration technique	Carvacrol, soy phosphatidylcholine	Nanoliposomes: Particle size: 271 nm. Zeta potential: 8.6 mV. Encapsulation efficiency: 98%.	Ayres Cacciatore et al., 2020
Antibacterial agent for food preservation	Nanocapsules: interfacial deposition technique	Carvacrol, Eudragit®	Particle size: 159 nm. Zeta potential: 44.8 mV. Encapsulation efficiency: 97%.	Nash and Erk, 2017
Antibacterial agent for food preservation	Standard Schlenk techniques by ring-opening polymerization	PEI, PLA	Average particle size: 115 nm. Zeta potential: 55 mV. Encapsulation efficiency: 54%. Enhanced antibacterial effect.	Niza et al., 2020
Antimicrobial agent	Single emulsion	Thymol, PLA	Average particle size range: 220–260 nm. Encapsulation efficiency: 60%. Improved antibacterial effect compared to non-encapsulated thymol.	Marcet et al., 2018
Antimicrobial agent	Novel, simple chemical synthesis	Thymol, chitosan, silver	Average particle size: 29 nm. Spherical shape, monodisperse in water, excellent blood biocompatibility.	Manukumar et al., 2017
Topical treatment of cutaneous diseases	Nanoprecipitation	OEO, PCL	Average particle size: 181 nm Polydispersity: 0.133. Surface charge: −41 mV. Encapsulation efficiencies: 85%.	Fraj et al., 2019
Anti-angiogenic system	Ultrasonication	Carvacrol, medium chain triglyceride	Hydrodynamic droplet size: 101 nm. Zeta potential: −39 mV. Decrease in the expression of several angiogenic markers in a lung adenocarcinoma model.	Khan et al., 2019
Pharmaceutical product for airway lung disease	Fusion-emulsification	Carvacrol, cocoa butter, 3,5-di-tert 4-butylhydroxytoluene, imidazolidinyl urea	Minimization of oxidative stress and histological damage generated from smoke inhalation in rodens.	Carvalho et al., 2020

OEO, oregano essential oil; PVA, polyvinyl alcohol; EO, essential oil; NP, nanoparticle; PEI, polyethylenimine; PLA, polylactic acid; PCL, polycaprolactone.

the properties of OEO-loaded NPs and MPs prepared by nanoprecipitation and double emulsion, respectively (Fraj et al., 2019). Results demonstrated that, while NPs were stable at different temperatures, MPs suffered an increase in particle size and a decrease in carvacrol component retention. In other studies, gelatin combined with chia mucilage was used as an alternative OEO delivery system to other most commonly used in complex coacervation (gelatin combined with Arabic gum)

(Hernández-Nava et al., 2020). NPs of both gelatin and chia mucilage and gelatin and Arabic gum were synthesized obtaining high encapsulation efficiencies in both cases. Moreover, the amount of Tween 80 and OEO concentration influenced the NP size, obtaining smaller particles with increasing Tween 80 due to the enhancement of the interfacial tension reduction and droplet breaking. Finally, complex coacervates with the highest encapsulation efficiencies were spray-dried obtaining the best flow properties for the gelatin-chia mucilage NPs.

Chitosan was used by Espinosa-Sandoval et al. (2021) to prepare OEO-loaded multilayer nano-emulsions by high energy methods (Espinosa-Sandoval et al., 2021). In this study, octenyl succinic anhydride-modified starch combined with partially deacetylated chitosan of medium and low molecular weight and carboxymethylcellulose was used to protect OEO in a multilayer system. Interestingly, using an *in vitro* gastric condition simulating test, the authors showed that each polymeric layer influenced OEO bioaccessibility, obtaining the highest value for the three-layer system. Spherical polymeric NPs based on polyvinyl alcohol (PVA) and chitosan loaded with OEO have also been prepared by electrospraying (Vehapi et al., 2020). Results demonstrated that the encapsulation of OEO and the presence of chitosan led to a superior antifungal effect of the nanoencapsulated system compared to free OEO.

Oregano essential oil nanoemulsions have also been reported to obtain nanocarriers with antibacterial properties. For instance, Asensio et al. (2020) prepared OEO nanoemulsions, showing that the incorporation of the oil could increase nanoemulsion stability, lower droplet size, and increase emulsion viscosity (Asensio et al., 2020). Furthermore, nanoemulsions exhibited good antimicrobial activity by the inhibition of cell-to-cell communication of gram-negative bacteria, also known as *quorum-sensing* (ability to detect and respond to cell population density by gene regulation). Dávila-Rodríguez et al. (2019) prepared O/W nanoemulsions encapsulating three different EOs, cinnamon, rosemary, and OEO, using a high-frequency ultrasound technique. Results proved that nanoencapsulated EOs were more effective than free EOs since a lower amount of EO was required to provide the antibacterial effect. Moreover, OEO nanoemulsions proved to be the most effective antimicrobial systems against *E. coli* and *Listeria monocytogenes* (Dávila-Rodríguez et al., 2019).

Another advantage that encapsulation can offer is masking the intense aroma of OEO components. Carvacrol encapsulation into nanostructures, nanoliposomes, and polymeric Eudragit® NCs were developed by Ayres Cacciatore et al. (2020), establishing that its encapsulation could be interesting to reduce its aroma due to its controlled release (Ayres Cacciatore et al., 2020). The effect of lecithin or Tween 20 on O/W nanoemulsions encapsulating carvacrol was studied by Nash and Erk (2017), concluding that, while lecithin nanoemulsions were highly viscoelastic and gave stability to the nanoemulsion, Tween 20 did not (Nash and Erk, 2017).

Oregano essential oil encapsulation using polycationic polymers can improve its antibacterial effect due to the enhanced bacterial uptake that positive charges cause. Polyethylenimine (PEI)-coated polylactic acid (PLA) NPs encapsulating carvacrol have also been developed as antimicrobial agents (Niza et al., 2020). In this study, NPs coated with PEI possessed a positively charged surface that facilitated their uptake by bacteria compared to negatively charged ones, enhancing the antibacterial effect of the encapsulated carvacrol. Moreover, NPs displayed higher antibacterial activity than free carvacrol, a sustained release, and stability during storage.

Other biomedical applications of carvacrol-loaded nanocarriers have been reported. Khan et al. (2019) demonstrated the potent anti-angiogenic effect both, *in vitro* and *in vivo,* of carvacrol-loaded O/W nanoemulsions, by reducing the expression of several angiogenic markers such as COX-2, VEGF, and CD31 in a lung adenocarcinoma model (Khan et al., 2019). Furthermore, solid lipid NPs incorporating carvacrol were prepared to treat lung damage of airway smoke inhalation and tested in an *in vivo* rat model by Carvalho et al. (2020). Results showed that carvacrol-loaded solid lipid NPs could minimize oxidative stress and inhalation injury and histological damage generated from smoke inhalation in rodents compared to the negative control.

To improve the antibacterial effect of thymol, different nanocarriers have been developed. An example is that of biodegradable PLA NPs developed by Marcet et al. (2018). PLA was found to be the key variable in optimizing NP preparation in terms of size and encapsulation efficiency, producing NPs with high storage stability at several pHs and improved antimicrobial properties compared to non-encapsulated thymol. In other studies, thymol was loaded into intrinsic antibacterial chitosan silver NPs showing interesting antioxidant properties through radical scavenging and antibacterial activity due to the three components against different gram-positive bacterial strains (Manukumar et al., 2017).

CONCLUSIONS

Although oregano oil has been used in different cultures since ancient times, it has received special attention in the last decades due to its preservative, antimicrobial, and therapeutic characteristics. However, its bioactivity is compromised by its highly volatile and hydrophobic nature and by external environmental factors. Hence, different drug delivery systems are being explored as a strategy to increase its stability and bioavailability, protect it from the environment, control its release, and even enhance its properties. In this review, the latest research on micro- and nanocarriers encapsulating OEO focusing on biomedical and biotechnological applications revealed that carriers such as emulsions and polymeric-based systems seem to be the most appropriate ones for encapsulation of this compound. Stability has been demonstrated to be particularly important in this type of delivery system since it determines the final performance of the loaded system, and it is dependent on multiple parameters such as the composition, the fabrication method, and the storing conditions. On the contrary, the mechanism of action by which OEO exerts its activities is not deeply investigated in most of the reviewed articles, but instead, they focused on the properties and final performance of the loaded delivery system. Overall, the process of OEO encapsulation stands out as a possible alternative for the preservation of this oil against environmental conditions, increasing its stability and maintaining its bioactive properties, mainly its antioxidant and antimicrobial ones. Furthermore, design and formulation on the carrier employed to encapsulate this oil, can influence and enhance its bioactive properties and even can provide the final delivery system with additional and beneficial properties.

AUTHOR CONTRIBUTIONS

GP-Q: conceptualization and writing—original draft. SE-R: conceptualization, project administration, and funding acquisition. JP: conceptualization, resources, and funding acquisition. MA and BV-L: conceptualization, resources, writing—review and editing, supervision, project administration, and funding acquisition. All authors contributed to the article and approved the submitted version.

FUNDING

The authors appreciatively acknowledge financial support from the project IND2017/IND7614, supported by the Comunidad de Madrid (Spain) and Alodia Farmacéutica SL.

REFERENCES

Aljaafari, M. N., AlAli, A. O., Baqais, L., Alqubaisy, M., AlAli, M., Molouki, A., et al. (2021). An overview of the potential therapeutic applications of essential oils. *Molecules* 26:628. doi: 10.3390/molecules26030628

Asensio, C. M., Paredes, A. J., Martin, M. P., Allemandi, D. A., Nepote, V., and Grosso, N. R. (2017). Antioxidant stability study of oregano essential oil microcapsules prepared by spray-drying. *J. Food Sci.* 82, 2864–2872. doi: 10.1111/1750-3841.13951

Asensio, C. M., Quiroga, P. R., Al-Gburi, A., Huang, Q., and Grosso, N. R. (2020). Rheological behavior, antimicrobial and quorum sensig inhibition study of an argentinean oregano essential oil nanoemulsion. *Front. Nutr.* 7:193. doi: 10.3389/fnut.2020.569913

Ayres Cacciatore, F., Dalmás, M., Maders, C., Ataíde Isaía, H., Brandelli, A., and da Silva Malheiros, P. (2020). Carvacrol encapsulation into nanostructures: characterization and antimicrobial activity against foodborne pathogens adhered to stainless steel. *Food Res. Int.* 133:109143. doi: 10.1016/j.foodres.2020.109143

Bakry, A. M., Abbas, S., Ali, B., Majeed, H., Abouelwafa, M. Y., Mousa, A., et al. (2016). Microencapsulation of oils: a comprehensive review of benefits, techniques, and applications. *Compr. Rev. Food Sci. Food Saf.* 15, 143–182. doi: 10.1111/1541-4337.12179

Bhalerao, Y. P., and Wagh, S. J. (2019). *In vitro* sustained release study of Thymol from Sodium Alginate Beads synthesized by Emulsion Microencapsulation, Int. *J. Pharm. Res.* 11, 397–403. doi: 10.31838/ijpr/2019.11.02.064

Bhalla, Y., Gupta, V. K., and Jaitak, V. (2013). Anticancer activity of essential oils: a review. *J. Sci. Food Agric.* 93, 3643–3653. doi: 10.1002/jsfa.6267

Bilia, A. R., Guccione, C., Isacchi, B., Righeschi, C., Firenzuoli, F., and Bergonzi, M. C. (2014). Essential oils loaded in nanosystems: a developing strategy for a successful therapeutic approach, evidence-based complement. *Altern. Med.* 2014:651593. doi: 10.1155/2014/651593

Böhme, K., Barros-Velázquez, J., Calo-Mata, P., and Aubourg, S. P. (2014). "Antibacterial, antiviral, and antifungal activity of essential oils: mechanisms and applications," in *Antimicrob. Compd. Curr. Strateg. New Altern.*, eds T. G. Villa and P. Veiga-Crespo (Berlin, Heidelberg: Springer Berlin Heidelberg), 51–81.

Cardoso-Ugarte, G. A., López-Malo, A., Palou, E., Ramírez-Corona, N., Jiménez-Fernández, M., and Jiménez-Munguía, M. T. (2021). Stability of oregano essential oil encapsulated in double (w/o/w) emulsions prepared with mechanical or high-pressure homogenization and its effect in Aspergillus niger inhibition. *J. Food Process. Preserv.* 45:e15104. doi: 10.1111/jfp p.15104

Cardoso-Ugarte, G. A., Ramírez-Corona, N., López-Malo, A., Palou, E., San Martín-González, M. F., and Jiménez-Munguía, M. T. (2018). Modeling phase separation and droplet size of W/O emulsions with oregano essential oil as a function of its formulation and homogenization conditions. *J. Dispers. Sci. Technol.* 39, 1065–1073. doi: 10.1080/01932691.2017.1382370

Carvalho, F. O., Silva, É. R., Nunes, P. S., Felipe, F. A., K., Ramos, P. P., et al. (2020). Effects of the solid lipid nanoparticle of carvacrol on rodents with lung injury from smoke inhalation, Naunyn. Schmiedebergs. *Arch. Pharmacol.* 393, 445–455. doi: 10.1007/s00210-019-01731-1

Choi, J., Wang, L., Ammeter, E., Lahaye, L., Liu, S., Nyachoti, M., et al. (2020). Evaluation of lipid matrix microencapsulation for intestinal delivery of thymol in weaned pigs. *Transl. Anim. Sci.* 4, 411–422. doi: 10.1093/tas/txz176

Cimino, C., Maurel, O. M., Musumeci, T., Bonaccorso, A., Drago, F., Souto, E. M. B. et al. (2021). Essential oils: pharmaceutical applications and encapsulation strategies into lipid-based delivery systems. *Pharmaceutics* 13:327. doi: 10.3390/pharmaceutics13030327

da Silva, B. D., Bernardes, P. C., Pinheiro, P. F., Fantuzzi, E., and Roberto, C. D. (2021). Chemical composition, extraction sources, and action mechanisms of essential oils: natural preservative and limitations of use in meat products. *Meat Sci.* 176:108463. doi: 10.1016/j.meatsci.2021.108463

D'agostino, M., Tesse, N., Frippiat, J. P., Machouart, M., and Debourgogne, A. (2019). Essential oils and their natural active compounds presenting antifungal properties. *Molecules* 24:3713. doi: 10.3390/molecules24203713

Dávila-Rodríguez, M., López-Malo, A., Palou, E., Ramírez-Corona, N., and Jiménez-Munguía, M. T. (2019). Antimicrobial activity of nanoemulsions of cinnamon, rosemary, and oregano essential oils on fresh celery. *LWT* 112:108247. doi: 10.1016/j.lwt.2019.06.014

Espinosa-Sandoval, L., Ochoa-Martínez, C., Ayala-Aponte, A., Pastrana, L., Gonçalves, C., and Cerqueira, M. A. (2021). Polysaccharide-based multilayer nano-emulsions loaded with oregano oil: production, characterization, and *in vitro* digestion assessment. *Nanomaterials* 11:878. doi: 10.3390/nano11040878

Fraj, A., Jaâfar, F., Marti, M., Coderch, L., and Ladhari, N. (2019). A comparative study of oregano (*Origanum vulgare* L.) essential oil-based polycaprolactone nanocapsules/microspheres: preparation, physicochemical characterization, and storage stability. *Ind. Crops Prod.* 140:111669. doi: 10.1016/j.indcrop.2019.111669

Franklyne, J. S., Mukherjee, A., and Chandrasekaran, N. (2016). Essential oil micro- and nanoemulsions: promising roles in antimicrobial therapy targeting human pathogens. *Lett. Appl. Microbiol.* 63, 322–334. doi: 10.1111/lam.12631

Gallo, T. C. B, Cattelan, M. G., Alvim, I. D., and Nicoletti, V. R. (2020). Oregano essential oil encapsulated in alginate beads: release kinetics as affected by electrostatic interaction with whey proteins and freeze-drying. *J. Food Process. Preserv.* 44:e14947. doi: 10.1111/jfpp.14947

Gelperina, S., Kisich, K., Iseman, M. D., and Heifets, L. (2005). The potential advantages of nanoparticle drug delivery systems in chemotherapy of tuberculosis. *Am. J. Respir. Crit. Care Med.* 172, 1487–1490. doi: 10.1164/rccm.200504-613PP

Hernández-Nava, R., López-Malo, A., Palou, E., Ramírez-Corona, N., and Jiménez-Munguía, M. T. (2020). Encapsulation of oregano essential oil (*Origanum vulgare*) by complex coacervation between gelatin and chia mucilage and its properties after spray drying. *Food Hydrocoll.* 109:106077. doi: 10.1016/j.foodhyd.2020.106077

Huang, H., Huang, C., Yin, C. M., Khan, R. U., Zhao, H., et al. (2020). Preparation and characterization of β-cyclodextrin–oregano essential oil microcapsule and its effect on storage behavior of purple yam. *J. Sci. Food Agric.* 100, 4849–4857. doi: 10.1002/jsfa.10545

Ju, X.-J., and Chu, L.-Y. (2019). "Chapter 9–Lab-on-a-chip fabrication of polymeric microparticles for drug encapsulation and controlled release," in *Micro Nano Technol.*, eds H. A. Santos, D. Liu, and P. A. Zhang (New York, NY: William Andrew Publishing), 217–280.

Kaliamurthi, S., Selvaraj, G., Hou, L., Li, Z., Wei, Y., Gu, K., et al. (2019). Synergism of essential oils with lipid based nanocarriers: emerging trends in preservation of grains and related food products. *Grain Oil Sci. Technol.* 2, 21–26. doi: 10.1016/j.gaost.2019.04.003

Khan, I., Bhardwaj, M., Shukla, S., Lee, H., Oh, M.-H., Bajpai, V. K., et al. (2019). Carvacrol encapsulated nanocarrier/nanoemulsion abrogates angiogenesis by downregulating COX-2, VEGF and CD31 *in vitro* and *in vivo* in a lung adenocarcinoma model. *Colloids Surf. B Biointerfaces* 181, 612–622. doi: 10.1016/j.colsurfb.2019.06.016

Kohane, D. S. (2007). Microparticles and nanoparticles for drug delivery. *Biotechnol. Bioeng.* 96, 203–209. doi: 10.1002/bit.21301

Kotronia, M., Kavetsou, E., Loupassaki, S., Kikionis, S., Vouyiouka, S., and Detsi, A. (2017). Encapsulation of oregano (*Origanum onites* L.) essential oil in β-cyclodextrin (β-CD): synthesis and characterization of the inclusion complexes. *Bioengineering* 4:74. doi: 10.3390/bioengineering4030074

Leyva-López, N., Gutiérrez-Grijalva, E. P., Vazquez-Olivo, G., and Heredia, J. B. (2017). Essential oils of oregano: biological activity beyond their antimicrobial properties. *Molecules* 22:989. doi: 10.3390/molecules22060989

Ma, L., and Yao, L. (2020). Antiviral effects of plant-derived essential oils and their components: an updated review. *Molecules* 25:2627. doi: 10.3390/molecules25112627

Manukumar, H. M., Umesha, S., and Kumar, H. N. N. (2017). Promising biocidal activity of thymol loaded chitosan silver nanoparticles (T-C@AgNPs) as anti-infective agents against perilous pathogens. *Int. J. Biol. Macromol.* 102, 1257–1265. doi: 10.1016/j.ijbiomac.2017.05.030

Marcet, I., Weng, S., Sáez-Orviz, S., Rendueles, M., and Díaz, M. (2018). Production and characterisation of biodegradable PLA nanoparticles loaded with thymol to improve its antimicrobial effect. *J. Food Eng.* 239, 26–32. doi: 10.1016/j.jfoodeng.2018.06.030

Memar, M. Y., Mohammad, Raei, P., Alizadeh, N., Akbari Aghdam, M., and Kafil, H. S. (2017). Carvacrol and thymol: strong antimicrobial agents against resistant isolates. *Rev. Med. Microbiol.* 28, 63–68. doi: 10.1097/MRM.0000000000000100

Nash, J. J., and Erk, K. A. (2017). Stability and interfacial viscoelasticity of oil-water nanoemulsions stabilized by soy lecithin and Tween 20 for the encapsulation of bioactive carvacrol. *Colloids Surf. A Physicochem. Eng. Asp.* 517, 1–11. doi: 10.1016/j.colsurfa.2016.12.056

Nazzaro, F., Fratianni, F., De Martino, L., Coppola, R., and De Feo, V. (2013). Effect of essential oils on pathogenic bacteria. *Pharmaceuticals (Basel)* 6, 1451–1474. doi: 10.3390/ph6121451

Niza, E. M., BoŽik, Bravo, I., Clemente-Casares, P., Lara-Sanchez, A., Juan, A., et al. (2020). PEI-coated PLA nanoparticles to enhance the antimicrobial activity of carvacrol. *Food Chem.* 328:127131. doi: 10.1016/j.foodchem.2020.127131

Omonijo, F. A., Kim, S., Guo, T., Wang, Q., Gong, J., Lahaye, L., et al. (2018). Development of novel microparticles for effective delivery of thymol and lauric acid to pig intestinal tract. *J. Agric. Food Chem.* 66, 9608–9615. doi: 10.1021/acs.jafc.8b02808

Piombino, C., Lange, H., Sabuzi, F., Galloni, P., Conte, V., and Crestini, C. (2020). Lignosulfonate microcapsules for delivery and controlled release of thymol and derivatives. *Molecules* 25:866. doi: 10.3390/molecules25040866

Sakkas, H., and Papadopoulou, C. (2017). Antimicrobial activity of basil, oregano, and thyme essential oils. *J. Microbiol. Biotechnol.* 27, 429–438. doi: 10.4014/jmb.1608.08024

Sedaghat Doost, A., Sinnaeve, D., De Neve, L., and Van der Meeren, P. (2017). Influence of non-ionic surfactant type on the salt sensitivity of oregano oil-in-water emulsions. *Colloids Surf. A Physicochem. Eng. Asp.* 525, 38–48. doi: 10.1016/j.colsurfa.2017.04.066

Sharifi-Rad, M., Berkay Yilmaz, Y., Antika, G., Salehi, B., Tumer, T. B., Kulandaisamy Venil, C., et al. (2021). Phytochemical constituents, biological activities, and health-promoting effects of the genus Origanum. *Phyther. Res.* 35, 95–121. doi: 10.1002/ptr.6785

Singh, R., and Lillard, Jr, J. W. (2009). Nanoparticle-based targeted drug delivery. *Exp. Mol. Pathol.* 86, 215–223. doi: 10.1016/j.yexmp.2008.12.004

Sun, X., Cameron, R. G., and Bai, J. (2019). Microencapsulation and antimicrobial activity of carvacrol in a pectin-alginate matrix. *Food Hydrocoll.* 92, 69–73. doi: 10.1016/j.foodhyd.2019.01.006

Teixeira, B., Marques, A., Ramos, C., Serrano, C., Matos, O., Neng, N. R., et al. (2013). Chemical composition and bioactivity of different oregano (*Origanum vulgare*) extracts and essential oil. *J. Sci. Food Agric.* 93, 2707–2714. doi: 10.1002/jsfa.6089

Turek, C., and Stintzing, F. C. (2013). Stability of essential oils: a review. *Compr. Rev. Food Sci. Food Saf.* 12, 40–53. doi: 10.1111/1541-4337.12006

Vehapi, M., Yilmaz, A., and Özçimen, D. (2020). Fabrication of oregano-olive oil loaded PVA/chitosan nanoparticles via electrospraying method. *J. Nat. Fibers.* doi: 10.1080/15440478.2020.1774463. [Epub ahead of print].

Zhou, Y., Sun, S., Bei, W., Zahi, M. R., Yuan, Q., and Liang, H. (2018). Preparation and antimicrobial activity of oregano essential oil Pickering emulsion stabilized by cellulose nanocrystals. *Int. J. Biol. Macromol.* 112, 7–13. doi: 10.1016/j.ijbiomac.2018.01.102

Zhu, Y., Li, C., Cui, H., and Lin, L. (2021). Encapsulation strategies to enhance the antibacterial properties of essential oils in food system. *Food Control.* 123:107856. doi: 10.1016/j.foodcont.2020.107856

Zhu, Z., Min, T., Zhang, X., and Wen, Y. (2019). Microencapsulation of thymol in poly(lactide-co-glycolide) (PLGA): physical and antibacterial properties. *Materials* 12:1133. doi: 10.3390/ma12071133

Conflict of Interest: JP is the CEO and founder of Alodia Farmacéutica SL and SE-R is an employee of the same company.

The remaining authors declare that the research was conducted in the absence of any commercial or financial relationships that could be construed as a potential conflict of interest.

REVIEW
published: 18 October 2021
doi: 10.3389/fbioe.2021.735090

Polysaccharide-Based Hydrogels for Microencapsulation of Stem Cells in Regenerative Medicine

Si-Yuen Lee[1]*, Jingyi Ma[2], Tze Sean Khoo[3], Norfadhilatuladha Abdullah[4], Nik Nur Farisha Nik Md Noordin Kahar[5], Zuratul Ain Abdul Hamid[5] and Muzaimi Mustapha[6]

[1]Department of Medicine, School of Medical Sciences, Universiti Sains Malaysia, Kota Bharu, Malaysia, [2]Duke-NUS Medical School, Singapore, Singapore, [3]UKM Medical Molecular Biology Institute, National University of Malaysia, Bangi, Malaysia, [4]Advanced Membrane Technology Research Centre, Faculty of Chemical and Energy Engineering, Universiti Teknologi Malaysia, Skudai, Malaysia, [5]School of Materials and Mineral Resources Engineering, Universiti Sains Malaysia, Nibong Tebal, Malaysia, [6]Department of Neurosciences, School of Medical Sciences, Universiti Sains Malaysia, Kota Bharu, Malaysia

OPEN ACCESS

Edited by:
Filippo Causa, University of Naples Federico II, Italy

Reviewed by:
Rami Mhanna, American University of Beirut, Lebanon
Zaozao Chen, Southeast University, China

***Correspondence:**
Si-Yuen Lee
siyuenlee@usm.my

Specialty section:
This article was submitted to Biomaterials, a section of the journal Frontiers in Bioengineering and Biotechnology

Received: *02 July 2021*
Accepted: *27 September 2021*
Published: *18 October 2021*

Citation:
Lee S-Y, Ma J, Khoo TS, Abdullah N, Nik Md Noordin Kahar NNF, Abdul Hamid ZA and Mustapha M (2021) Polysaccharide-Based Hydrogels for Microencapsulation of Stem Cells in Regenerative Medicine. Front. Bioeng. Biotechnol. 9:735090. doi: 10.3389/fbioe.2021.735090

Stem cell-based therapy appears as a promising strategy to induce regeneration of damaged and diseased tissues. However, low survival, poor engraftment and a lack of site-specificity are major drawbacks. Polysaccharide hydrogels can address these issues and offer several advantages as cell delivery vehicles. They have become very popular due to their unique properties such as high-water content, biocompatibility, biodegradability and flexibility. Polysaccharide polymers can be physically or chemically crosslinked to construct biomimetic hydrogels. Their resemblance to living tissues mimics the native three-dimensional extracellular matrix and supports stem cell survival, proliferation and differentiation. Given the intricate nature of communication between hydrogels and stem cells, understanding their interaction is crucial. Cells are incorporated with polysaccharide hydrogels using various microencapsulation techniques, allowing generation of more relevant models and further enhancement of stem cell therapies. This paper provides a comprehensive review of human stem cells and polysaccharide hydrogels most used in regenerative medicine. The recent and advanced stem cell microencapsulation techniques, which include extrusion, emulsion, lithography, microfluidics, superhydrophobic surfaces and bioprinting, are described. This review also discusses current progress in clinical translation of stem-cell encapsulated polysaccharide hydrogels for cell delivery and disease modeling (drug testing and discovery) with focuses on musculoskeletal, nervous, cardiac and cancerous tissues.

Keywords: polysaccharide hydrogels, stem cells, microencapsulation, regenerative medicine, cell delivery, disease modeling

INTRODUCTION

Regenerative medicine offers great potential for restoring individual tissues or organs using patient's stem cells incorporated with scaffolds (Mason and Dunnill, 2008). A number of stem cell-biomaterial related studies have been performed with the aim of treating various diseases and injuries, such as neurodegenerative disorders, diabetes, cardiovascular diseases, liver diseases, musculoskeletal defects, osteoarthritis and wound injuries (Crevensten et al., 2004; Kuo et al., 2008; Segers and Lee, 2008; Mazhari et al., 2020). Stem cells possess self-renewal capability and the potential to

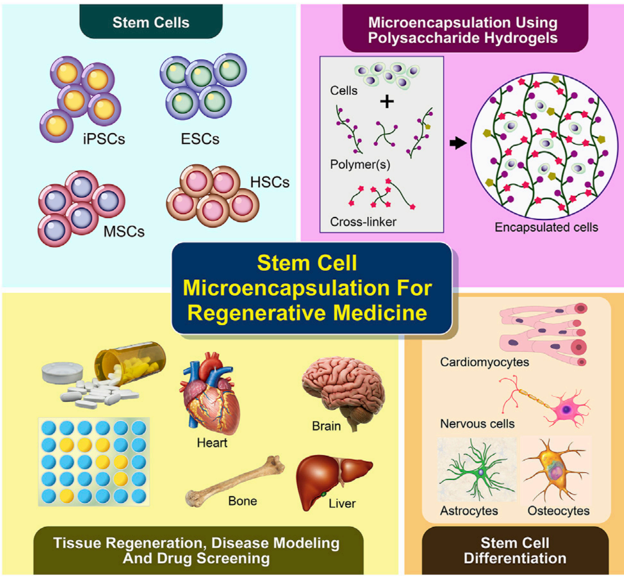

FIGURE 1 | Microencapsulation of stem cells using polysaccharide-based hydrogels supports cell differentiation and viability in 3D, which has been recently applied in tissue regeneration or cell therapy and disease modeling for future drug screening.

differentiate into multiple lineages, which include pluripotent stem cells (embryonic stem cells, ESCs and induced pluripotent stem cells, iPSCs) and multipotent stem cells (hemopoietic stem cells, HSC; mesenchymal stem cells, MSCs and adult stem cells, ASCs) (Leeper et al., 2010). Owing to their distinctive abilities and characteristics, stem cells have been identified as an unprecedented and important source of clinically relevant differentiated cells for application in regenerative medicine, particularly as cell delivery components for stem cell therapy and *in-vitro* (disease) models for drug discovery (**Figure 1**).

The use of biomaterial scaffolds, which can resemble intrinsic extracellular matrix (ECM) and direct stem cells, is crucial in the regeneration of functional tissues. It is challenging to design and develop scaffolds that can support cell survival, promote bioactivity and improve cell retention at the administered sites for cell delivery, cell transplantation as well as disease modeling (Parisi-Amon et al., 2013; Mayfield et al., 2014). In this respect, hydrogels are among the most promising biomaterials for recreating the native ECM properties due to their high-water content, biological compatibility and moldability (Slaughter et al., 2009). Various types of hydrogels made of natural polymers, synthetic polymers and co-polymers with optimized physical and chemical properties have been developed for regenerative medicine (Engler et al., 2006; Huebsch et al., 2010). Biophysical cues including porosity, degradation and mechanical strength or stiffness, have been incorporated into hydrogels in a spatiotemporally controlled manner to systematically modulate the behavior of stem cells such as cell proliferation, differentiation and migration (Yang et al., 2016). In addition, advanced chemical strategies and conjugation of functional materials or molecules were found to improve the cell-matrix interaction and functionality of hydrogels (Phelps et al., 2012). In the selection of hydrogel materials, natural polymers (e.g., polysaccharides and proteins) have gained much interest in the construction of ECM for stem cells and their derivatives owing to their hydrophilicity, biocompatibility, low cytotoxicity, biodegradability, softness, similarity to physiological environment and tunability into an injectable gel (Gomez-Florit et al., 2020).

This review focuses on the natural hydrogels derived from polysaccharides, including agarose, alginate, carrageenan, chitosan, gellan gum and hyaluronic acid. Despite major advantages of polysaccharide hydrogels, these materials are not without limitations. For example, they do not have strong mechanical properties, and some may not easily be controlled due to their batch-to-batch variation. For these reasons, polysaccharide hydrogels are often combined with protein-based or synthetic polymers, creating composite or co-polymer hydrogels, and are still widely experimented (Jabbari et al., 2016). In addition to aiding the retention of microencapsulated stem cells by providing biological and physical supports, polysaccharide hydrogels also serve as semi-permeable membranes with interconnected pores, which allows nutrient supply, mass transfer and waste removal from the microencapsulated cells. Hydrogels further protect the microencapsulated cells from immune attacks of host immune biosystems. They can be easily modified to incorporate various cell-interactive moieties to facilitate stem cell-based therapy by enhancing cell viability and specifically directing stem cell differentiation to target tissues. (Burdick and Vunjak-Novakovic, 2009; Guilak et al., 2009). Accordingly, this gives rise to the emergence of many methods for stem cell microencapsulation and application in regenerative medicine.

In the first part of this review, we discuss the type and characteristics of stem cells which have been widely used for microencapsulation and tissue regeneration. We also highlight selected polysaccharide polymers that can be processed under mild conditions to produce biomimetic hydrogels suitable for stem cell microencapsulation. The advanced microencapsulation techniques that allow the production of polysaccharide hydrogels with controlled size, in the form of beads, particles or capsules within the range of micrometers will be introduced. Finally, we further discuss the application of microencapsulated stem cells using biomimetic polysaccharide hydrogels in stem cell therapy or cell delivery and disease modeling.

STEM CELLS

Stem cells are unspecialized cells with the ability to self-renew and differentiate into at least one type of mature cells. Based on the potential of differentiation, stem cells can be classified into totipotent stem cells (able to generate all types of cells including germ cells), pluripotent stem cells (able to generate all types of cells except for cells of the embryonic membrane), and multipotent stem cells (able to generate more than one type of mature cells). In this section, we will discuss pluripotent stem cells

(PSCs) e.g., ESCs and iPSCs, and two types of multipotent stem cells e.g., HSCs and MSCs.

Embryonic Stem Cells

ESCs are derived from the inner cell mass (ICM) of the blastocyst, a pre-implanted embryo developed 4 days after fertilization. Isolation of the ICM can be achieved by immunosurgery or mechanical dissection. ESCs are cultivated by culturing with either feeder cells of various sources or cell-free media conditioned by fibroblasts and supplemented with appropriate growth factors. Notably, the three-dimensional (3D) culture system is preferred over the traditional two-dimensional (2D) culture system as it provides a niche that closely resembles the physiological environment. Multiple 3D cultures have been developed, with the most physiologically relevant matrix being hyaluronic acid (HA)-based hydrogel. Functions of human ESCs can be confirmed by their potential to differentiate into cells of all three germ layers *in vitro* as well as *in vivo* (teratoma formation assay in severe combined immunodeficiency mice). So far, many cell types have been successfully obtained from ESCs, including endoderm-derived hepatocytes, pancreatic beta cells, lung epithelium, mesoderm-derived bone, cartilage, cardiomyocytes, hematopoietic cells, endothelial cells, and ectoderm-derived keratinocytes, retinal pigment epithelium and neurons. The basic paradigm of PSC-based cell therapy is that PSCs are first differentiated into the desired cell type, followed by transplantation of the differentiated cells into patients (Vazin and Freed, 2010). While ESCs possess immense therapeutic potential, their use is limited by 1) ethical issues as human embryos are destroyed to isolate ESCs, and 2) transplanted cells derived from allogenic ESCs as they are subjective to host immune rejection. To this end, ESCs can be replaced by iPSCs (Moradi et al., 2019).

Induced Pluripotent Stem Cells

The iPSCs are derived from somatic cells that are dedifferentiated *in vitro* to a pluripotent stage using either an integrative or non-integrative approach. In the former, retroviral or lentiviral vectors are used to deliver four reprograming factors (Oct4, Sox2, Klf4, and c-Myc). The latter approach involves episomal DNA plasmids, Sendai virus, adenovirus, synthesized modified mRNA, microRNAs, proteins and small molecules. Compared to the integrative approach, the non-integrative approach has a lower reprograming efficiency but a minimal risk of inducing mutagenesis, and is therefore considered more suitable for stem cell-based therapies (Moradi et al., 2019). Like ECSs, the growth of iPSCs *in vitro* also requires appropriate extracellular matrices and environmental cues, which can be achieved with the introduction of animal cells, hydrogels, individual matrix proteins, synthetic surfaces, and some commercially well-defined and xenogeneic-free components (Chen et al., 2014). However, directing iPSCs to a specific cell lineage remains a challenge and each differentiation progress likely requires unique features in the culture system. While a 3D culture system is favorable to the generation of many other cell types, a recent study has shown that it may impair the differentiation of iPSCs towards mesenchymal stem cells-like phenotype as compared to a 2D culture system (Goetzke et al., 2019). iPSCs are equally suitable for all the biomedical applications of ESCs, such as drug screening, toxicological studies, disease modeling and cell therapies. Several iPSC-based clinical trials to treat macular degeneration, Parkinson's disease and heart diseases are ongoing. In recent cases where iPSCs are derived from a patient with certain disease-causing genetic mutations, cell therapy can potentially revert the mutations by applying CRISPR/Cas9 technology (Moradi et al., 2019).

Mesenchymal Stem Cells

MSCs are commonly derived from adult human bone marrow and adipose tissue stromal vascular fraction. MSCs can be genetically distinguished from non-MSCs with an "MSC classifier" based on their gene expression profile. The number of MSCs in bone marrow is low but a large number of cells can be acquired by *in vitro* expansion. MSCs can be differentiated into various types of mesodermal tissues, including cartilage, bone, adipose tissue, stroma, muscle and tendon. This process requires treatment of MSCs with specific stimuli introduced in specific chronological order (temporal stochasticity). Differentiation of MSCs *in vitro* is also affected by the cellular environment (e.g., hypoxia, inflammatory cues) and the properties of the substrate. For example, rigid culture surfaces have been shown to favor osteogenesis whereas soft gels are conducive to adipogenesis. Due to the ease of isolation and expansion, MSCs have been widely applied in regenerative medicine. Over the past decade, however, the focus of MSC application has shifted from cell replacement to the paracrine function of MSCs. MSCs have been found to secrete multiple growth factors, cytokines, and immunomodulatory molecules, which is a unique feature of MSCs among the other stem cell types (Pittenger et al., 2019). In order to scale up the production of MSCs for clinical applications, 3D culture systems such as microcarriers and stirred-tank bioreactors, are the most common to achieve a higher surface-to-volume ratio than monolayer cultures (Koh et al., 2020; Tsai et al., 2020).

Hemopoietic Stem Cells

HSCs are traditionally harvested from bone marrow but now predominantly from cytokine-mobilized peripheral blood stem cells. $CD34^{+}$ peripheral blood stem cells are enriched using immunomagnetic separation and characterized by flow cytometry based on the expression of specific cell markers ($CD34^{+}$, $CD38^{-}$, $CD45RA^{-}$, $CD90^{+}$, CD49f) (Morgan et al., 2017). HSCs are able to produce all types of mature blood cells through differentiation of increasingly lineage-specific progenitors, which is regulated by both intrinsic factors (transcription factor, epigenetic regulators, and metabolic pathways) and extrinsic factors (humeral and neural signals, and local microenvironmental cues) (Pinho and Frenette, 2019). Bone marrow transplantation has been a curative therapy for a variety of hematological diseases over the last 4 decades and its implication has been advanced with gene editing techniques. However, bone marrow transplantation is still hindered by the immunological complications of allogenic transplantation as well as the suboptimal *ex vivo* expansion of HSCs in monolayer culture to provide sufficient amount of stem cells for marrow

TABLE 1 | Polysaccharides derived natural hydrogels microencapsulated with different type of stem cells and their response.

Polysaccharide material	Gelation mechanism	Stem cell type[1]	Significant biological responses	References
Agarose	Thermal	ESCs	Agarose hydrogel functionalized with VEGFA and successfully induced blood progenitor cells	Rahman et al. (2010)
		ASCs	Bio-fabricated ASCs spheroids into 'lockyballs' enabled spheroid aggregation, delivery and engraftment	Silva et al. (2016)
		MSCs	3D bioprinting agarose hydrogel supported MSCs survival in a tissue-like structure composed of a range of mechanically discrete microdomains	Forget et al. (2017)
Alginate	Ionic/chemical crosslinking	ESCs	Co-encapsulated functional β-like cells from human ESCs and CXCL12 enhanced insulin secretion in diabetic mice whilst evaded the pericapsular fibrotic response	Alagpulinsa et al. (2019)
		iPSCs	Alginate hydrogel functionalized with RGD peptide supported survival of functional neurons and allowed optogenetic stimulation	Lee et al. (2019)
		MSCs	Microfluidics encapsulated single-cell MSCs in alginate microgels enhanced osteogenesis and accelerated mineralization	An et al. (2020)
Carrageenan (CRG)	Thermal Ionic crosslinking	ASCs	Injectable k-CRG and non-injectable CRG co-encapsulated with TGF-β1 increased cell viability, induced chondrogenic differentiation and expression, and synthesized proteoglycans	Popa et al. (2015)
		MSCs	Excellent structural strength and optimal concentrations obtained by 3D bioprinted CRG-alginate composite without significant negative effects on the cell viability	Kim et al. (2019)
		iPSCs and MSCs	Micropatterned κ-CRG hydrogel systems of defined shapes supported the growth of stem cells and enabled the spatial control of stem cell niche	Vignesh et al. (2018)
Chitosan	Ionic/chemical crosslinking	ESCs	Chitosan incorporated with VEGF and endothelial cells to induce neovascularization	Lee et al. (2015)
		MSCs	Injectable thermo-responsive chitosan promoted wound healing, supported MSC's secretion of growth factor and inhibited inflammation factors	Xu et al. (2019b)
		ASCs	N-methacrylate glycol chitosan (MGC) hydrogels incorporated with RGD peptide sustained cell viability, increased cell spreading and metabolic activity. Encapsulated ASCs promoted murine $CD31^+$ endothelial cell recruitment to the peri-implant region	Dhillon et al. (2019)
Gellan Gum (GG)	Thermal Ionic/chemical crosslinking	ESCs and iPSCs	Bioamine-crosslinked and laminin-functionalized GG hydrogel further induced neural cell viability, maturity and supported neurite migration	Koivisto et al. (2017)
		ASCs	GG composited with collagen type-1 and bioactive glass was found to support osteogenic differentiation of ASCs	Vuornos et al. (2020)
		iPSCs	The covalent hydrazone crosslinking GG blended with gelatin supported a prolonged culture of cardiomyocytes in 3D, allowed the cardiac model to maintain its elasticity and closely mimicked the native heart for at least 7 days	Koivisto et al. (2019)
Hyaluronic acid (HA)	Thermal Ionic/chemical crosslinking	iPSCs	The soft 3D methacrylated hyaluronic acid (Me-HA) hydrogel-encapsulated hiPSC-NPCs displayed robust neurite outgrowth and showed high level of spontaneous neural differentiation	Wu et al. (2017)
		MSCs	Encapsulation of human vascular endothelial-cadherin (hVE-cad-Fc) fusion protein functionalized MSC aggregates (FMA) using HA-based hydrogel demonstrated better recovery of cardiac function and improved revascularization of infarcted myocardium in comparison to the conventional hydrogel-MSC delivery system	Lyu et al. (2020)
		ESCs	HA backbone was chemically modified with gelatin to encapsulate and deliver hESC-neural stem cells, successfully improved locomotor function in a rat spinal cord injury model	Zarei-Kheirabadi et al. (2020)

[1]*ESCs: Embryonic Stem Cells; iPSCs: induced Pluripotent Stem Cells; MSCs: Mesenchymal Stem Cells; ASCs: Adipose-derived Adult Stem Cells.*

reconstitution (Ng and Alexander, 2017; Pinho and Frenette, 2019). 3D cultures may improve HSC yields by providing space as well as a more faithful simulation of tissue microenvironment than 2D. Recently, a 3D scaffold made of polydimethylsiloxane to mimic the natural hematopoietic niche has been demonstrated to support the viability, multipotency and self-renewal of human HSCs *in vitro* (Marx-Blümel et al., 2020).

POLYSACCHARIDE HYDROGELS

Agarose

Agarose is extracted from red algae and seaweed and consists of a galactose-based backbone 1,4-linked 3,6-anhydro-α-1-galactose and 1,3-linked β-D-galactose derivatives (Zarrintaj et al., 2018). It has a thermoresponsive property, i.e., in a gel state at room

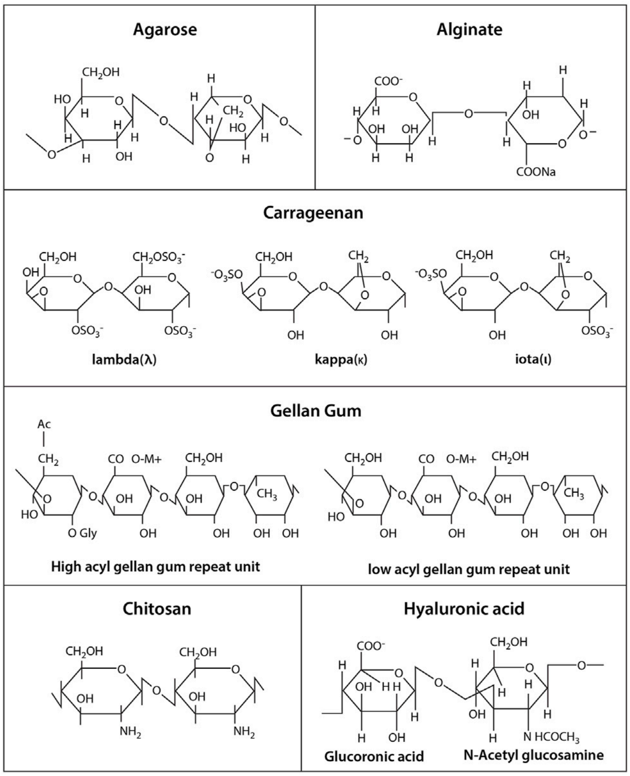

FIGURE 2 | Chemical structures of polysaccharide hydrogels.

temperature but in a solution state at an increased temperature. This makes agarose a favorable biomaterial for its easy tunable mechanical properties during synthesis. Agarose solutions containing cells can be prepared and emulsified at 37°C, then gelated to microgels in an ice bath. As shown in **Table 1**, previous and current studies of stem cell encapsulation in agarose have been reported. An earlier research activity showed that agarose was used as a scaffold for vascular endothelial growth factor (VEGF) immobilization to encapsulate and differentiate ESCs during early stages of development toward blood progenitor cells (Rahman et al., 2010). Stem cells were encapsulated into agarose microwells to form structures known as 'lockyballs'. The 'lockyball' interior structure consisted of an aggregate of human adipose stem cells that is surrounded by a synthetic coating, which contained multiple binding sites for other 'lockyballs' (Silva et al., 2016). In addition, agarose has been used as a printable bioink for generating specific tissues from human stem cells where recent work illustrated how MSCs are printed using an agarose-based bioink at different formulations, which can provide a versatile platform for stem cell therapy (Forget et al., 2017).

Alginate

Alginate is a polysaccharide derived from brown algae containing guluronic acid (G units) and mannuronic acid (M units) (**Figure 2**). Alginate-based biomaterials have been widely used for biomedical and pharmaceutical applications because of their biocompatibility and ionic crosslinking. It has been the most popular natural polymer matrix for cell microencapsulation due to quick gelation without using toxic chemicals or organic solvent (Andersen et al., 2015; Ching et al., 2017). Divalent cations such as calcium, barium or magnesium are used as ionic crosslinkers to form ionic bridges between alginate G units. The most frequent used crosslinker, calcium chloride ($CaCl_2$), is highly soluble in aqueous medium which can trigger rapid or poorly controlled gelation. To decrease the gelation rate, calcium carbonate ($CaCO_3$) or calcium sulfate ($CaSO_4$) is added. For example, calcium ions (Ca^{2+}) will be released from $CaCO_3$ when glucono-δ-lactone is applied in alginate/$CaCO_3$ mixture, subsequently initiating alginate gelation in a gradual manner (Crow and Nelson, 2006). Furthermore, the Ca^{2+} release from alginate hydrogel may induce hemostasis, which leads to interest in covalently crosslinking.

In stem cell encapsulation, alginate hydrogel was combined with ESCs to generate functional human beta-like cells (SC-β cells) (Maguire et al., 2006). The capacity of these cells to co-microencapsulate with immunomodulatory chemokine (CXCL12) in alginate can evade the fibrotic foreign body reaction and induce long-term glycemic correction in an immunocompetent murine model of type-1 diabetes without systemic immunosuppression (Maguire et al., 2006; Alagpulinsa et al., 2019). Bone and cartilage have also been regenerated using microfluidics or bioprinting methods where MSCs or iPSCs were not only encapsulated in suspension. However, single-cell encapsulation has been achieved lately to prevent non-homogeneous differentiation (Nguyen et al., 2017; An et al., 2020).

Although alginate has been fundamentally easy to utilize for stem cell microencapsulation, it lacks biological active moieties. In order to improve cell-cell and cell-matrix interaction for efficient stem cell-based therapy, alginate has been modified, coated or composited with other biologically active molecules or polymers (e.g., gelatin, hyaluronic acid, chitosan, poly-L-lysine, various growth factors, peptides and proteins). For instance, when a combination of alginate and HA hydrogel was formulated for MSC microencapsulation, an optimal composition of 1% alginate and 0.25% HA was found to greatly enhance cell growth and support release of therapeutic proteins (Cañibano-Hernández et al., 2017). Lee and co-workers covalently conjugated alginate with ECM-derived peptide (e.g., arginine-glycine-aspartic acid, RGD),successfully stimulated iPSCs and neural derivatives, promoted cell viability and differentiation as well as allowed optogenetics application in the 3D culture system (Lee et al., 2019). Hence, alginate-based hydrogels can be further tailored to better resemble the natural ECM microenvironments by providing multiple specific signals to stem cells and their derivatives.

Carrageenan

Carrageenan is a sulphated polysaccharide extracted from red seaweeds (Rhodophyceae), which contains repeating disaccharide units of 4-linked b-D-galactopyranose (G-unit) and 4-linked a-D-galactopyranose (D-unit) or 4-linked 3,6-anhydrogalactose (DA-unit), with a variable portion of sulphate group (Campo et al., 2009). It can be categorized into three main families - kappa (κ), iota (ι) and lambda (λ), based on the number and position of the sulphate group in the repeating galactose units. Among them, κ-carrageenan (k-CRG) has primarily and recently been exploited in cell therapy due to its distinguishing properties, including thermoresponsive nature, facile gelation, moldability, close resemblance to glycosaminoglycans (GAGs) and good injectability under physiological conditions (Campo et al., 2009; Mohite and Patil, 2014). Stem cells are encapsulated within κ-CRG hydrogels in a mild condition with ionic gelation mechanism (Mohite and Patil, 2014).

Several recent studies show a promising performance of κ-CRG hydrogels. For example, injectable κ-CRG hydrogels encapsulated with human ASCs and TGF-β1 for cartilage regeneration were reported to enhance cell viability and proliferation, increase chondrogenic differentiation and expression level, and stimulate production of proteoglycans and other ECM components of cartilage (Popa et al., 2015). Carrageenan has also been compositely incorporated with other polymers such as alginate and chitosan for preparing hydrogel beads and fibers. It has demonstrated good processability at different formulations for application in tissue regeneration and cell delivery (Kim et al., 2019). Recently, a bioprinted co-polymer hydrogel consisting of carrageenan and alginate encapsulated with MSCs, has demonstrated excellent structural strength and biological activity (Kim et al., 2019).

Chitosan

Another commonly used polysaccharide polymer, chitosan, is derived by the deacetylation of chitin. It consists of glucosamine units such as β-(1→4)-linked D-glucosamine and N-acetyl-D-glucosamine (Wan and Tai, 2013). Chitosan has been extensively used in tissue regeneration because of its excellent biocompatibility, biodegradability, hydrophilicity and structural similarity to glycosaminoglycans (GAGs) (Kim et al., 2008). The gelation of chitosan hydrogels can be controlled using pH (Chang et al., 2015) and the hydrogel properties can be modified for stem cell encapsulation through chemical crosslinking (Muzzarelli et al., 2016). Numerous works showed that 3D chitosan hydrogels at different concentrations promoted osteogenic and chondrogenic differentiation of human stem cells (Muzzarelli et al., 2015). Other researchers have combined chitosan hydrogels with stem cells and growth factors to treat spinal cord injury (Li et al., 2016). Chitosan-based hydrogels have been further modified or functionalized to increase the biological activities of encapsulated cells (Dhillon et al., 2019). Since it can also provide analgesic effect and hemostatic activity, much current research focuses on its application in wound healing (Xu H. et al., 2019; Soriano-Ruiz et al., 2019). For example, injectable thermo-sensitive hydrogel loaded MSCs from umbilical cord blood was found to successfully accelerate wound closure and support tissue remodeling and regeneration of skin appendages for cutaneous wound healing. (Xu Y. et al., 2019; Soriano-Ruiz et al., 2019). Furthermore, chitosan-based hydrogel encapsulating ESC-derived endothelial cells and VEGF induced robust cell retention and promoted neovascularization through vasculogenesis and angiogenesis (Lee et al., 2015). Recently, studies show chitosan bioink is suitable for printing stem cell-derived constructs (Roehm and Madihally, 2018). However, optimization and more studies are required to ensure stem cell survival and differentiation.

Gellan Gum

Gellan gum (GG), an anionic polysaccharide polymer, is obtained from *Sphingomonas Elodea*. It contains repeating units of β-D-glucose, β-D-glucuronic acid and α-L-rhamnose in a molar ratio of 2:1:1 (Prajapati et al., 2013). It has been immensely used for the encapsulation of drugs, enzymes, cells and microorganism attributed to its hydrophilicity and excellent gelling property in the presence of cations (Wang et al., 2008; Chakraborty et al., 2014).

Like many other polysaccharide polymers, GG is a relatively inert biomaterial that requires further modification and improvement to support cell adherence. GG-based hydrogels are functionalized with various type of peptides by covalently conjugating them into the molecular backbone itself (Chakraborty et al., 2014). GG has been studied for the regeneration of bone (Vuornos et al., 2020), cartilage (Park et al., 2020) and spinal cord (Gomes et al., 2016). In neural regeneration, Koivisto and co-workers have demonstrated that bioamine-crosslinked GG hydrogels supported viability of both ESCs and iPSCs derived neuronal cells, and further confirmed that functionalized GG hydrogels with laminin resulted in cell type-specific behavior, neuronal cell maturity and neurite migration (Koivisto et al., 2017). Other studies reported that the development of composite GG, incorporated with collagen type-1 and bioactive glass, can support the osteogenic induction of human ASCs (Vuornos et al., 2020). This suggested that a specific type of peptide/protein, growth factor and composite material plays a key role in triggering specific stem cell differentiation, hence these factors need to be considered in hydrogel synthesis and modification.

Hyaluronic Acid

Hyaluronic acid (HA), also known as hyaluronan, is one of the major components of ECM and consists of multiple sites for cell adhesion (Knopf-Marques et al., 2016). It is a non-sulphated glycosaminoglycan with repeating disaccharide units of glucoronate and N-acetylglucosamine (Khademhosseini et al., 2006). Many studies have demonstrated that HA regulates stem cell niches, thus making it suitable for stem cell microencapsulation and culture (López-Ruiz et al., 2019). HA has been developed as a hydrogel scaffold for promoting self-renewal and vascular differentiation of human ESCs (Gerecht et al., 2007). Other research groups detailed the incorporation of bone marrow derived MSCs with injectable HA hydrogel to engineer cartilage tissue (Jooybar et al., 2019), and MSCs encapsulated with a photocrosslinkable HA-collagen hydrogel to generate bone tissue (Zhang et al., 2019). Tissue regeneration using encapsulated stem cells in HA appears as a promising strategy to promote wound healing as well as to repair damaged nerve tissues (da Silva et al., 2017; Wu et al., 2017). In addition, HA microcarriers and HA bioinks provide a conducive environment for stem cell growth (Shendi et al., 2017; Law

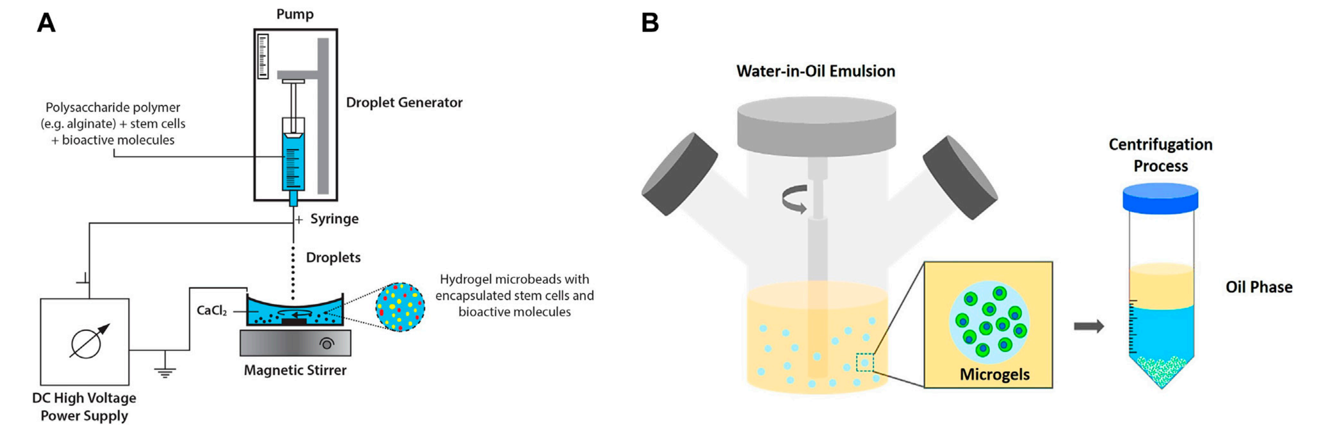

FIGURE 3 | Extrusion and emulsion methods. **(A)** Electrostatic/electrospray droplet extrusion technique for microencapsulation of stem cells and bioactive molecules. Figure adapted with permission from **Figure 1** of (Verica et al., 2008). **(B)** Emulsification technique (water-in-oil emulsion) produces hydrogels for cell encapsulation. Figure adapted with permission from **Figure 6** of (Choe et al., 2018).

et al., 2018; Sakai et al., 2018). For instance, HA blended with methylcellulose supported MSCs viability at above 75% in the bioprinted structures, and the cells retained viability for at least 1 week after 3D bioprinting (Law et al., 2018).

MICROENCAPSULATION TECHNIQUES

Extrusion

Extrusion method, which includes air jet extrusion, syringe droplet extrusion, centrifugational extrusion, electrostatic extrusion and vibrational extrusion, is among the most common methods applied to microencapsulate cells for regenerative medicine. Among the extrusion methods, electrostatic/electrospray droplet extrusion has been widely applied for stem cell microencapsulation study (Kim et al., 2019) Hydrogel beads of approximately 50 µm are produced and the reduction of cell viability can be avoided by the use of organic solvent. The process involves gravitational dripping where a suspension of hydrogel precursor and cells are extruded via a needle into a hardening solution (**Figure 3A**) (Hashemi and Kalalinia, 2015).

There are several factors that influence the diameter of the cell encapsulated microspheres such as density of solution, diameter of the extrusion needle/nozzle and surface tension of the droplets. Peng and co-workers reported the optimization of electrospray technique to encapsulate human bone marrow stromal cell (hBMCs) in alginate-gelatin microspheres (Xu H. et al., 2019). In the study, non-aggregated, polydispersity and defined spherical microspheres were produced with alginate (1.5%, w/v) and gelatin (0.5%, w/v) using a 30 G needle and 8 kV voltage. When compared to alginate microsphere alone, alginate-gelatin improved cell proliferation and viability by up to 21 days. A method to control cell-release tunable microbead hydrogels containing adipose stem cells (ASCs) had also been developed (Leslie et al., 2017). In this study, electrostatic extrusion dripping was employed to produce enzymatically modulated hydrogels. Nevertheless, a major limitation of this technique is the presence of cells which often leads to the clogging of nozzle. In certain cases, nozzle inner diameter and applied pressure are two factors that cause cell damage (Cidonio et al., 2019). The clogging issue can be reduced by ensuring cell suspension is homogenous as well as flushing the nozzle with sodium citrate. Meanwhile, employing right parameters and a blunt nozzle may prevent cell damage.

Emulsion

Cell encapsulation by emulsion method is typically carried out by dispersing hydrogel precursor in non-miscible solution, namely water-in-oil emulsion. At equilibrium, internal gelation occurs in which the emulsified hydrogels are later collected by a centrifugation process (Choe et al., 2018; **Figure 3B**). Despite advantages of this technique e.g., low production cost and high scalability, broad size distribution and cell disruptions at oil interface have raised some concerns (Daly et al., 2020). Prolonged exposure towards oil and surfactants resulted in cytotoxic environment that disrupted cells and subsequently reduced cell viability (Chan et al., 2013). Water-in-water emulsion drop, which involved a one-phase system, has been reported as a template to produce microgels. However, a specific combination of two immiscible aqueous solutes is required, which would limit the potential use of this modified approach. To obtain uniform micro encapsules, a few studies have investigated the application of double emulsion technique (Chan et al., 2013; Liu E. Y. et al., 2018). Choi and co-workers adopted double emulsion drop technique with ultrathin oil shell being as a sacrificial template (Choi et al., 2016) The monodisperse emulsion drops were formed via coaxial flow aqueous pre-polymer solution surrounded by oil phase and directly emulsified into a continuous aqueous phase. Upon UV

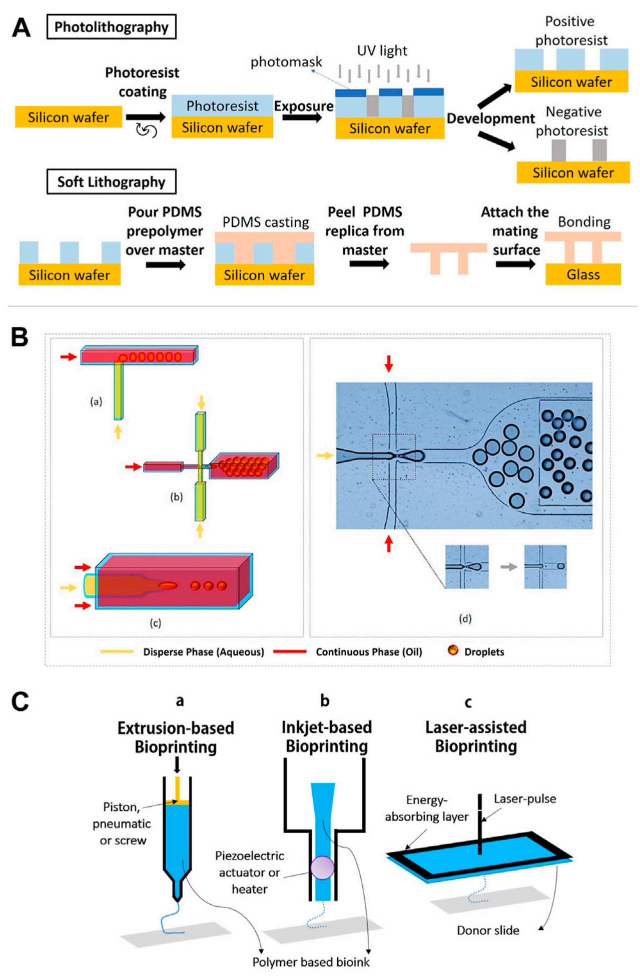

FIGURE 4 | Lithography, microfluidics and bioprinting methods for stem cell microencapsulation. **(A)** Schematic diagram shows the process of photolithography and soft lithography. **(B)** Geometric illustrations of three microfluidic devices: (a) T-junction, the perpendicular flow of the continuous phase is sheared by dispersed phase and thereby generates droplets. (b) Flow-focusing, droplets are produced by shearing the dispersed phase from two directions. (c) Co-flow, the dispersed phase is forced through a capillary inside a bigger capillary where continuous phase is pumped. (d) Droplet generation by flow-focusing device (use of fluorinated oil with stabilizing agent and dispersed phase as water solution of dye). Figure adapted with permission from **Figure 1** of (Hayat et al., 2018; Alkayyali et al., 2019). **(C)** Schematic diagram of (a) piston extrusion-based bioprinting, (b) piezoelectric actuator inkjet-based bioprinting, and (c) laser-assisted bioprinting.

exposure, dewetting occurred and the hydrogels solidified. The researchers demonstrated that this approach can support large-scale hydrogel production and increase cell viability attributed to the shorter exposure of cells to oil phase (Choi et al., 2016).

Lithography

There are two common methods of lithography for the fabrication of microfluidic cell culture devices, namely photolithography and soft lithography. This technique is used to pattern hydrogels at the micro and nanoscale with bioactive features to improve cell differentiation, spreading and migration (Guan et al., 2017) In photolithography, a silicon wafer is spin-coated with a viscous photoresist, which will start to crosslink when exposed to high energy of UV light. The designed pattern of hydrogel is formed (**Figure 4A**). Soft lithography has been introduced to replicate a mold of the microstructure, allowing nanofabrication by pouring a polymer solution or spin-coated onto a master for crosslink until a rubbery replica is formed (Gasperini et al., 2014) The channels in the replica can be filled or loaded with a suspension of a hydrogel precursor and cells. Master is a photoresist patterned silicon wafer with polydimethylsiloxane (PDMS) chosen as an elastomer to cover the surface of the master because of its transparency, gas permeability and biocompatibility (Tang et al., 2021). In addition, soft lithography possesses unique advantages as it could provide a good resolution (~35 nm), which is more competitive when compared to electron beam lithography (~15 nm) (Lin et al., 2018). By using soft lithography, the fabrication of polymer materials allows procedures to pattern non-planar substrates with a wide range of materials (Rose et al., 2019).

Currently, several advanced lithography techniques have been established such as microcontact printing, replica molding, micro-transfer molding and solvent assisted micro-molding/micropatterning. Previous research by Suh and co-workers demonstrated that a soft lithographic technique using HA is compatible with microcontact printing and molding approaches (Suh et al., 2004). During microcontact printing, PDMS stamps were used with oxygen plasma in order to enhance the adhesion of HA to the stamps. Results showed that the pattern transfer by this method had a good edge definition where the height of the printed HA was higher (~90 nm) than typically obtained by self-assembled monolayers. However, microcontact printing and photolithography are restricted to many other polymers which require ionic or thermal crosslinking. Series of fabrication steps are laborious and often damage encapsulated cells during curing and demolding. Recent work to overcome these issues by using simple paraffin wax molds was reported to successfully generate defined shapes on alginate-gelatin and κ-carrageenan hydrogel surface. This supports the viability of both MSCs and iPSCs (Vignesh et al., 2018).

Moreover, an advanced lithography based 3D bio-printing has also been introduced where both UV and visible light can be applied to cure photocrosslinkable bioinks as well as to improve the resolution and to achieve multi-material printing ability (Liang et al., 2020). Factors such as temperature change, curing or drying during processing, UV initiators in UV crosslinking and light intensity could have detrimental effects on the viability of encapsulated stem cells. Thus, further improvement and optimization are required.

Microfluidics

Microfluidics is a method which deals with the handling of fluids in microenvironments that allows the formation of micro gels. In stem cell culture, microfluidics involves a small-scale system, which focuses on the flow volume and channel size, and is increasingly being explored (McKee and Chaudhry, 2017). The microfluidics is also used to simulate the *in vivo* microenvironment via perfusion media exchange and creating chemical gradients of soluble factors for low amount of cells or single cells (Halldorsson et al., 2015). Droplet-based microfluidics appears as a powerful method and versatile technique to reconstruct microenvironments with remarkably high throughput and tight control over cells, biomolecules and extracellular matrix. There are active and passive methods of droplet-based microfluidics. The most common devices in cell microencapsulation are derived from passive methods, including flow-focusing, co-flow and T-junction design (**Figure 4B**) (Rossow et al., 2017). Details on the active and passive droplet-based microfluidics methods can refer to the recent review article (Zhu and Wang, 2017). Generally, flow-focusing and co-flow microfluidic devices form droplets as a reaction to shear stress of a continuous phase on a dispersed phase. Both phases are normally immiscible liquids. Meanwhile for the T-junction devices, a droplet is created when the two channels collide with each other at the right angle and leave through a perpendicular stem (Alkayyali et al., 2019). The size and shape of the droplets in microfluidics-based synthesis is influenced by the sizes of the microchannel and flow rates of the two phases. T-junction is a common technique in microfluidics for cell microencapsulation owing to ease of droplets and uniform size distribution of microbeads (Alkayyali et al., 2019). Stem cells such as ESCs, have been embedded in agarose hydrogel using T-junction technique (Kumachev et al., 2011).

Bioprinting

Bioprinting is an emerging technology for tissue regeneration because of its ability to produce bio-artificial organs and to mimic the cell-matrix native microenvironments (Lei and Wang, 2016). In general, 3D bioprinting is utilized to deposit biomaterials layer by layer with the assistance of digital 3D computer aided design (CAD). There are three common techniques employed in advanced tissue regeneration and organ manufacturing areas. They are inkjet bioprinting, laser-assisted bioprinting and extrusion-based bioprinting (**Figure 4C**). The working principle in the inkjet bioprinting technology is simple and similar to home printing techniques where the hydrogel is printed separately layer by layer using thermal and acoustic methods. The heat from the printer head forces the cells and biomaterials out of the nozzle through pressure pulses. In addition, extrusion-based bioprinting uses the same extrusion principle where the fluids are released by a pressure assisted system. In laser-assisted bioprinting, a vapor pressure (laser pulse) forms bubbles between the solution and a piece of glass (donor slide) where the pressure will shoot a small droplet of solution towards the collector substrate drop by drop. Subsequently, the repeated processes produce a tissue-like structure. During the process, the polymer solution is transformed into a 3D structure by crosslinking, which involves ionic crosslink or UV photo polymerization (Markstedt et al., 2015). The printing temperature is set between 1°C and 37°C to avoid causing overheating damage to the encapsulated cells (Lei and Wang, 2016).

The important feature of 3D bio-printers is to print living cells together with polymeric hydrogels and other bioactive compounds, either alone or in combination with other polymers as the main composition of bioinks. This will impact the mechanical and cellular behaviors of the generated biological structures. Previous studies showed that the use of polysaccharide polymers and copolymers as bioinks can produce a stable microenvironment for stem cells to grow, proliferate, differentiate and migrate (Liu F. et al., 2018). There are four types of hydrogel bioinks that are classified based on the crosslinking methods such as ionic-crosslinked bioink, thermo-sensitive bioink, photosensitive bioink and shear-thinning bioink (Xu et al., 2020). Each bioprinting technique has limitations and different requirements for the bioinks which can affect the encapsulated stem cells. Although inkjet bioprinting and laser-assisted bioprinting are able to position multiple cell types accurately with high cell survivability, inkjet bioprinting has the limitations of vertical printing and restricted material viscosities to produce a 3D architecture, whereas laser bioprinting only positions the bioink onto a prefabricated matrix and suffers from less stability, low scalability and high cost. In contrast, extrusion bioprinting has quick fabrication times for any 3D microstructures but poor cell viability. Thus, combining different bioprinting techniques could solve the existing limitations and adopt advantages from each other (Željka et al., 2018). Current research demonstrates the feasibility and efficiency of using more than one cell microencapsulation technique. Integrating 3D bioprinting (digital micromirror device (DMD)-based projection printing) and microfluidics improved bioprinting time and speed with less than 20 s for two to three bioinks and allowed more than one type of cell (Amir et al., 2018).

Superhydrophobic Surfaces

Hydrophilicity of most pristine hydrogels can cause inert characteristics and affect the functionality of the hydrogels. In an encapsulated hydrogel system, small molecules and solutes can freely diffuse across the hydrogel layer. Nevertheless, in certain cases where larger molecules or components present in the system, this may block the interaction of the cells and the hydrogel matrix (Pérez-Luna and González-Reynoso, 2018). It has been shown that surface-coating hydrogels with a super hydrophobic surface can prevent contamination within hydrogel beads and control the entrance of solvents for molecular exchange with the surrounding environment (Lima et al., 2011). This technique was adopted to produce alginate hydrogels coated with polystyrene surfaces and crosslinked with $CaCl_2$ to encapsulate MSCs and fibronectin (Lima et al., 2013). It is practically important to entrap water soluble molecules such as fibronectin, which can easily diffuse to the media. In the study, MSCs isolated from Wistar rat's bone marrow were immobilized into alginate beads through a process of gelification of liquid precursor droplets onto biomimetic superhydrophobic surfaces. In the microencapsulation and gelification process, no additional process of precipitation and aggressive mechanical strength were used, the hydrogel was rapidly formed without aggregations in 5 min. The results demonstrated that alginate beads at 2% of

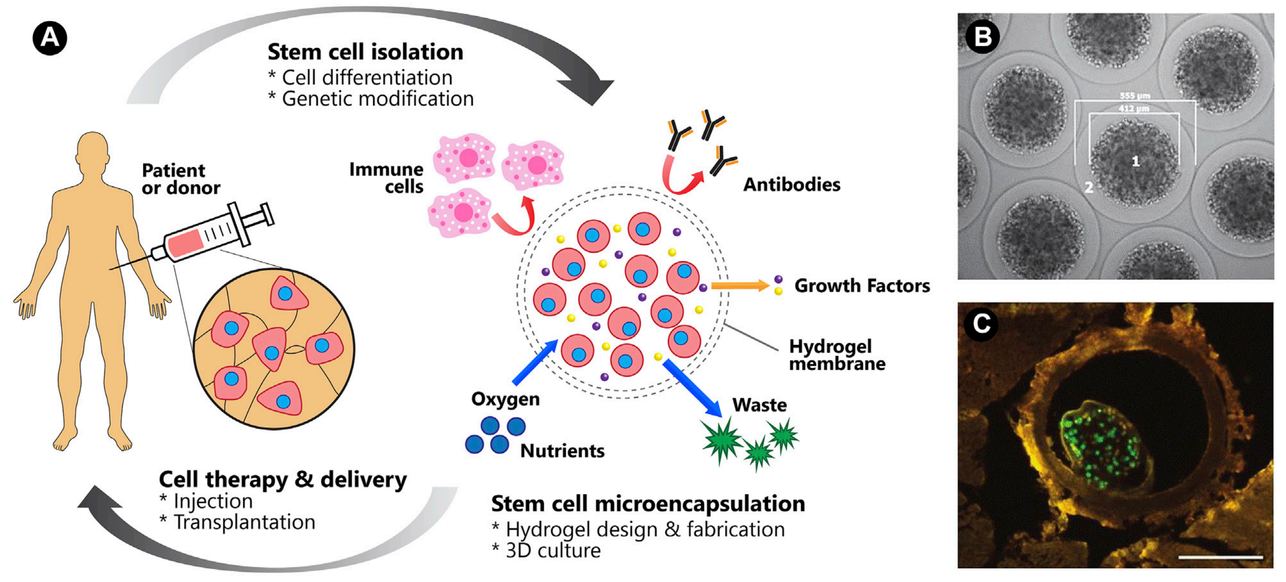

FIGURE 5 | Cell therapy and delivery. **(A)** A schematic of the microencapsulation of human stem cells and its benefits for clinical translation. Figure adapted with permission from **Figure 1** of (Choe et al., 2018). **(B)** GLP-1 CellBeads illustrating the central core bead containing GLP-1-secreting MSCs (1) and the surrounding alginate shell (2). **(C)** A green fluorescence protein-tagged CellBead within a coronary vessel. Scale bar: 250 μm. **Figures 5B,C** adapted with permission from **Figures 1A,B** of (Wright et al., 2012).

concentration were found to remain stable for 21 days whilst hybrid bone regeneration was accelerated. Major advantages of this technique, including mild processing conditions, controllable hydrogel size, high encapsulation loading, and mechanical forces are not required during formation of the particles. However, it is difficult to bind and incorporate with other superhydrophobic nanoparticles without sacrificing or degrading its superhydrophobic nature. Several in-depth reviews are available, which focus on the materials and methods used to produce superhydrophobic surfaces (Eric et al., 2016; Karim et al., 2019).

MOVING TOWARDS CLINICAL TRANSLATION

Stem Cell Therapy

While stem cell therapies have made significant progress preclinically, clinical translation remains challenging due to the massive cell death during transplantation and the failure of the graft to integrate into the host tissue. Hydrogel-based delivery systems emerge as a promising platform to tackle these challenges by preventing mechanical cell damage during cell delivery and creating a favorable microenvironment post-transplantation. Hydrogels derived from natural, synthetic materials or a hybrid of both have been engineered with desirable features. The design of injectable hydrogels allows for localized cell delivery in a minimally invasive manner. Moreover, the ability of hydrogel systems to co-deliver bioactive molecules and to be modified further, enhanced the therapeutic effects (Youngblood et al., 2018) (**Figure 5**). In this section, the recent progress of polysaccharide-based hydrogels for cell delivery in the musculoskeletal, cardiac, neural and cancerous tissues towards clinical translation is reviewed.

Musculoskeletal Tissues

Cell therapies for musculoskeletal tissue restoration are at different levels of evidence in clinical trials. Various sources of stem cells (bone marrow-derived MSCs, umbilical cord-derived MSCs, synovial MSCs, induced PSC, muscle satellite cells) and multiple delivery methods (implantation, arthroscopy, injection) are being explored to optimize the therapeutic effects (Loebel and Burdick, 2018). Modification of hydrogel biophysical properties such as incorporation of integrin-binding motifs has been proven to augment the muscle regeneration. RGD-coupled alginate hydrogel encapsulated gingival mesenchymal stem cells (GMSCs) delivered with multiple myogenic growth factors (containing 6-Bromo-1-methylindirubin-3′-oxime, forskolin, and basic-fibroblast growth factor) was reported to stimulate the expression of myogenetic-related genes and support myogenic differentiation. In animal trial, muscle-like structures were formed in small islands 8 weeks after ubcutaneous transplantation of GMSCs in microbeads into immunocompromised mice (Ansari et al., 2016).

In cartilage repair, the advanced design of a hydrogel system transforms stem cell therapy to the next level with promising clinical application. An alginate (Alg)/polyacrylamide (PAAm) double network (DN) hydrogel system functionalized with transforming growth factor beta-3 (TGF-b3)-encapsulated nanoparticles has been shown to improve the regeneration of

TABLE 2 | Clinical trials using polysaccharide hydrogels with/without stem cells as of January 2021 (ClinicalTrials.gov).

Polysaccharide hydrogels	Disease/Condition	Intervention/Treatment	Clinical trial	Id number
Hyaluronic acid	Musculoskeletal: Cartilage Defect	Device: ChonDux (combination of HA and PEG encapsulated with MSCs	Terminated (Enrolment suspended; follow up continue)	NCT01110070
Hyaluronic acid	Musculoskeletal: Degeneration Articular Cartilage Knee	Biological: Cartistem (HA hydrogel encapsulated with MSCs derived from allogenic human umbilical cord blood)	Completed phase 2	NCT01733186
Alginate	Neural: Intracerebral Hemorrhage	Drug: GLP-1 CellBeads (alginate microcapsules containing allogenic MSCs, transfected to secrete Glucagon like peptide-1)	Phase 2 (Terminated for improvement of study medication)	NCT01298830
Alginate	Cardiac: Vesicoureteral reflux	Drug: Chondrocyte-alginate gel suspension	Phase 3	NCT00004487
Alginate	Cardiac: Acute Myocardial Infarction; congestive heart failure	Device: IK-5001 (Alginate + calcium gluconate + saline solution	Completed	NCT01226563
Alginate	Cardiac: Dilated cardiomyopathy	Device: Algisyl-LVR	Completed phase 2	NCT00847964
Alginate	Cardiac: Dilated cardiomyopathy; heart failure with reduced ejection fraction	Device: Algisyl-LVR	Completed phase 3	NCT01311791
Alginate	Cardiac: Dilated cardiomyopathy; heart failure	Device: Algisyl	Not yet recruiting	NCT03082508

cartilage in rats, which is attributed to its physical stability and controlled release of TGF-b3 (Saygili et al., 2021). HA appears as an important component in the hydrogel system. It has been studied in combination with 1) polyethylene glycol and MSCs, namely ChonDux hydrogel, and 2) allogenic human umbilical cord blood derived MSCs, namely Cartistem® for clinical trials (Park et al., 2017; Wolf et al., 2020). Results from the clinical trials suggest that these hydrogel systems are safe and effective for cartilage regeneration to treat cartilage defect in osteoarthritis (**Table 2**). Despite being highly effective and biodegradable, adverse events such as joint pain, joint effusion and inflammation limit the clinical translation of HA hydrogel systems (Abhirup et al., 2020).

While hydrogel has exhibited great potential in regenerating many types of musculoskeletal tissues, its application in craniofacial bone tissue repair has been restricted due to its weak adherence to the host tissue. This has been resolved with encapsulating gingival MSCs with an alginate-based, adhesive, photocrosslinkable hydrogel with modifiable mechanical properties. This approach has exhibited satisfying biocompatibility, biodegradability and osteoconductivity in a rat peri-implantitis model (Hasani-Sadrabadi et al., 2020).

Cardiac Tissues

Heart failure is among the major causes of death worldwide. Massive cell death in cardiovascular diseases means substantial amount of stem cells are required to reconstitute the cardiac tissue. Co-transplantation of stem cells with hydrogels appeared as one of the appealing strategies to improve both cell delivery and cell survival. A recent study screened the efficacy of matrigel, alginate and hyaluronate as carriers to deliver hESC-derived cardiomyocytes (hESC-CM) using a rat acute myocardial infarction (AMI) model. Although all three delivery systems give rise to improved cardiac function compared with the saline control group, hyaluronate hydrogel is superior in improving cardiac functional recovery, delaying left ventricular remodeling, and preventing arrhythmias (Tan et al., 2020).

Innovative hydrogel designs have emerged to improve the therapeutic efficacies of stem cell therapies via targeted delivery, improved cell retention and increased cell viability (Peña et al., 2018). A bioglass/g-polyglutamic acid/chitosan (BG/g-PGA/CS) injectable composite hydrogel loaded with MSCs has resulted in enhanced cardiac tissue repair in a rat AMI model (Gao et al., 2020). Incorporation of bioactive molecules including cytokines and/or growth factors may increase the efficacy of stem cell therapy by stimulating stem cell proliferation *in vivo* after transplantation. Increase in graft size compared to controls in a rat AMI model has been observed when insulin-like growth factor-1 (IGF-1) was delivered in chitosan hydrogel with human placenta-derived MSCs (Yao et al., 2020). In addition, encapsulation of human vascular endothelial-cadherin (hVE-cad-Fc) fusion protein functionalized MSC aggregates (FMA) using HA-based hydrogel has exhibited better recovery of cardiac function and improved revascularization of infarcted myocardium in comparison to the conventional hydrogel-MSC delivery system (Lyu et al., 2020). In clinical trials, until now, only alginate hydrogels were applied as a device (without cells and bioactive molecules) in treating heart failure, namely IK-5001, Algisyl-LVR and Algisyl (Frey et al., 2014; Lee et al., 2015). Details on promising alginate-based systems in cardiac regeneration and clinical trials can be referred to the current review paper (Giada et al., 2020).

Neural Tissues

Delivery of stem cells that can either produce therapeutic molecules to support neural regeneration, or simply substitute the injured or dead cells, is a major paradigm of cell therapy in the management of neural tissue damage (Hlavac et al., 2020). The clinical application potential of various types of hydrogels have been reported. A commercially available HA hydrogel (the

HyStem-C Cell Culture Scaffold Kit, BioTime Inc. Alameda, CA, GS313), of which the HA backbone was chemically modified with gelatin to encapsulate and deliver human ESC derived neural stem cells, successfully improved locomotor function in a rat spinal cord injury model (Zarei-Kheirabadi et al., 2020).

Hydrogels provide a 3D microarchitecture that is conducive for neural regeneration in many ways. For example, they provide the physical cues to guide stem cell differentiation, allow the release of bioactive molecules (e.g., brain-derived neurotrophic factor, BDNF) in a controlled manner and shield stem cells from host immune surveillance (Madhusudanan et al., 2020). HA hydrogels functionalized with RGD adhesive peptide and heparin have been demonstrated to promote post-transplantation survival of the highly fragile human ESC-derived midbrain dopaminergic neurons (Vazin and Freed, 2010). In the setting of neurosensory hearing loss, encapsulating BDNF-producing MSCs with ultra-high viscous-alginate has been shown to prevent spiral ganglion neurons from degeneration when applied to the cochlear implant surface in deafened guinea pigs (Scheper et al., 2019). Interestingly, MSCs encapsulated in agarose-carbomer based hydrogel secreted CCL2 chemokine to preserve cytoarchitecture and promote functional recovery in spinal cord injury (Papa et al., 2018). In addition, hydrogel microbeads made of alginate–Ca^{2+}were used to differentiate and scale up dopaminergic neurons from encapsulated human iPSC-derived precursor cells. Sufficient cell number was obtained when retrieved for transplantation and the cells were found well integrated with the host brain in pre-clinical study (Komatsu et al., 2015). In clinical trials, allogenic MSCs, transfected to secrete glucagon like peptide-1, were encapsulated in alginate microcapsules (GLP-1 CellBeads). Phase-II results showed no safety issues or adverse events after implantation in the stroke patients with space-occupying intracerebral hemorrhage or traumatic brain injury (Heile and Brinker, 2011).

Cancerous Tissues

The role of stem cell therapy in the management of cancer patients is not restricted to replace damaged tissue after cancer treatment (e.g., transplantation of HSCs to facilitate hematological recovery, iPSCs-derived hepatocytes to repair liver tissues), but also involves localized delivery of anti-cancer therapies. Stem cells have been engineered to exhibit tumor-killing properties through the expression of cytotoxic enzymes that process prodrugs (e.g., cytosine deaminase, herpes simplex virus-thymidine kinase), secretory factors (e.g., TNF-alpha-related apoptosis-inducing ligand/TRAIL, IFN-beta) and oncolytic viruses (e.g., herpes simplex virus, HSV). A recent role of stem cells is to carry chemotherapy-containing nanoparticles and protect them from host immune clearance. In cancer immunotherapy, transplantation of HSCs expressing chimeric antigen receptors (CARs) or T-cell receptors (TCR) that are specific for tumor-associated antigen, is a promising strategy to treat hematological malignancies (Zhang et al., 2017). However, this approach is less feasible for solid tumors due to poor infiltration, which could be solved with a localized implantation system. Tumor-targeting CAR T cells and stimulator of IFN genes (STING) agonist delivered by alginate scaffolds has been demonstrated to eradicate solid tumors, which systemic T cell injection alone failed to achieve (Smith et al., 2017). In addition to the implantable form, an injectable hydrogel has shown impressive therapeutic effects as a carrier for cancer vaccine and anti-PD-1 monoclonal antibodies (Li et al., 2020). A recent review covers this area in depth from the hydrogel materials, therapeutic strategies as well as clinical perspectives (Correa et al., 2021).

Disease Modeling

Apart from its application in cell therapy, biomimetic polysaccharide hydrogels also harbor great potential in disease modeling. However, unlike hydrogels for cell therapy, which emphasize on the homing and engraftment ability, the preferred choice of hydrogels for disease modeling are disease-specific, with emphasis on candidates which carry characteristics that could facilitate the replication of disease phenotypes. Polysaccharide hydrogels have distinct advantages with the ease of modification in mechanical property, permeability, accessibility to nutrients and the ability to imitate the pathophysiological states of various diseases including musculoskeletal, cardiac, neural diseases and cancers.

Musculoskeletal Disease

One of the most prevalent musculoskeletal diseases is osteoarthritis (OA), attributed to the degeneration of articular cartilage which involved the loss of chondrocytes. Traditional 2D culture of chondrocytes was found to be suboptimal as chondrocytes dedifferentiated within two passages in such a condition (Aurich et al., 2018). Nevertheless, when chondrocytes were encapsulated in alginate hydrogel in 3D culture condition, chondrocytes maintained their differentiated form (Aurich et al., 2018). It was later discovered that the maintenance of the chondrogenic phenotype was attributed to physical entrapment instead of the chemical interaction with the alginate molecules (Cooke et al., 2017). In addition, chondrocytes encapsulated in alginate methacrylate (ALMA) also exhibited frictional properties, which were similar to stage-3 to stage-4 OA (Meinert et al., 2017). When Meinert and co-workers applied a sliding shear motion on the encapsulated chondrocytes to replicate the mechanical environment of the native cartilage, the chondrocytes responded to the excessive strain by increasing the expression of matrix metalloproteinase-3, which facilitated the degradation of surrounding ECM proteins, resulting in the reduction of stiffness. In the effort to investigate the role of stiffness in the pathogenesis of OA, models of chondrocytes encapsulated in 2% (low stiffness) or 4.5% (high stiffness) agarose to imitate the stiffness of the osteoarthritic or healthy cartilage were created respectively (Jutila et al., 2015). Metabolites were found to be differentially regulated when the low and high stiffness models were subjected to a minimum of 15 min of dynamic compression. Moreover, chondrocytes encapsulated in alginate also responded to various anabolic cues such as connective tissue growth factor (CTGF), bone morphogenetic protein 4 (BMP-4), fibroblast growth factor-

2 (FGF-2), insulin growth factor-I (IGF-I), epidermal growth factor (EGF), and Cadherin11 or Matrix Gla Protein (MGP) by increasing the synthesis of glycosaminoglycan (GAG), one of the main proteoglycans that plays a role in maintaining a healthy cartilage structure (Neidlin et al., 2018).

Neural Disease

One of the early 3D *in vitro* models of neural tissues was developed by encapsulating neural stem cells (NSCs) in alginate, agarose and carboxy-methyl chitosan via 3D bioprinting, which had allowed *in situ* differentiation of NSCs into functional GABAergic neurons, astrocytes and oligodendrocytes (Gu and Mooney, 2016). The efficient *in situ* differentiation was attributed to the stiffness of the hydrogel, which was maintained at 0.8 kPa, which closely mimicked the stiffness of the human's brain (Handorf et al., 2015). The stiffness was further reduced to 0.51 kPa by encapsulating iPSC-derived neural progenitors (iPSC-NPC) in the softer methacrylated hyaluronic acid (Me-HA) hydrogel. The soft stiffness had facilitated spontaneous neural differentiation and neurite outgrowth of iPSC-NPC. In addition, it induced expression of neuron-specific proteins in iPSC-NPC derived from Down's syndrome patients, which otherwise have impaired neurogenesis (Wu et al., 2017). It is important to note that despite many studies having demonstrated the success of 2D cultures in recapitulating the phenotypic hallmarks of various neurodegenerative diseases including amyotrophic lateral sclerosis, Alzheimer's, Parkinson's and Huntington's disease, the majority of studies belong to the familial cases (Centeno et al., 2018). *In vitro* modeling of the more prevalent, sporadic version of such diseases are often more challenging as the replication of disease phenotypes are highly dependent on the physical, chemical and mechanical cues in the microenvironment. A recent study had demonstrated that the amyloid-β plaques formed in an Alzheimer's disease model may exhibit varying cytotoxicity depending on whether they were confined in 2D or 3D space (Simpson et al., 2020). Agarose, collagen, hyaluronic acid and polyethylene glycol hydrogel cultures were shown to enhance the amyloid-β aggregation towards the larger species which confer lower cytotoxicity as compared to when amyloid-β plaques were found in monolayer cultures. This implies that any future development of Alzheimer's disease model requires careful consideration concerning the pore size of the hydrogels to recapitulate the physiological condition in the brain.

Cardiac Disease

To date, the majority of 3D *in vitro* cardiac disease models were mainly based on cells that were microencapsulated in ECM proteins such as fibrin, gelatin, collagen and Matrigel (Sacchetto et al., 2020). However, ECM protein-based hydrogels suffer from limitations due to batch-to-batch variation, poor mechanical properties and rapid degradation. Integration of polysaccharide hydrogels with ECM proteins could improve the versatility of the resulting hydrogels by offering flexible control over their mechanical properties. For example, gelatin, which has gelation temperature below physiological condition, suffers from poor mechanical properties. When combined with gellan gum, it supported a prolonged culture of cardiomyocytes in 3D. The covalent hydrazone crosslinking of gelatin and gellan gum had allowed the cardiac model to maintain its elasticity, which closely mimicked the native heart for at least 7 days (Koivisto et al., 2019). The state of maturation of the microencapsulated cardiomyocytes, however, was not determined in this study. Maturation of cardiomyocytes is crucial for the accurate modeling of heart diseases and in particular diseases which have late-onset such as heart failures and atrial fibrillation. Composite hydrogels made of hyaluronic acid and collagen had been shown to improve the magnitude of cardiac contraction force (Dahlmann et al., 2013). Moreover, the resulting cardiomyocytes exhibited a well-developed and organized sarcomeric structure that collectively indicated improved cardiac maturation. When microencapsulated cardiomyocytes differentiated from iPSC were co-cultured with endothelial cells and stromal cells in Gly-Arg-Gly-Asp-Ser-Pro (GRGDSP) peptide-coupled alginate hydrogel, they achieved structural maturation after 15 days of culture, as evidenced by the presence of matured myofibril alignment accompanied by elongated and well-organized sarcomeres, which were absent in the control cardiomyocytes aggregates (Abecasis et al., 2020). The resulting model also demonstrated dose-dependent response towards known cardiotoxins such as doxorubicin. Similar dose-dependent toxicity response was also observed in the endothelialized heart-on-a-chip model established by adopting bioprinted alginate-gelatin methacryloyl (GelMA) composite hydrogels, making them useful for drug screening (Zhang et al., 2016).

Cancers

Tumor microenvironments with their complexity, diversity and dynamic nature, play critical roles in cancer development and metastasis (Hanahan and Weinberg, 2011). A current research trend involved the creation of 3D tumor microenvironments recapitulating native tumors by using various engineered polymeric hydrogels (Gu and Mooney, 2016) and stem cells, which enabled the studies of basic cancer biology and screening of the efficacy of anticancer drugs (Roudsari and West, 2016) (**Figure 6**). At present, 67% of drugs failed phase two clinical trials whilst only 12% completed all stages (Hay et al., 2014). Disease modeling in cancer utilizing natural polymeric hydrogels encapsulated with stem cells has not been widely investigated as compared to other non-communication diseases. *Cancer* stem cells and cancer cell lines are commonly used for encapsulation to mimic the heterogeneity of tumor microenvironment. Recently, 3D bioprinted tumor constructs using modified alginate-gelatin-fibrinogen biomaterials and glioma stem cells were reported to support cell survival, glioma stem cell proliferation, inheritance of cancer stem cell characteristics as well as to exhibit differentiation and vascularization potential (Xingliang et al., 2016; Zhu et al., 2016). When this model tested with temozolomide, higher resistance against temozolomide were found as compared to those in the 2D cell culture model. Another 3D bioprinted hydrogel infused with hydroxyapatite nanoparticles was

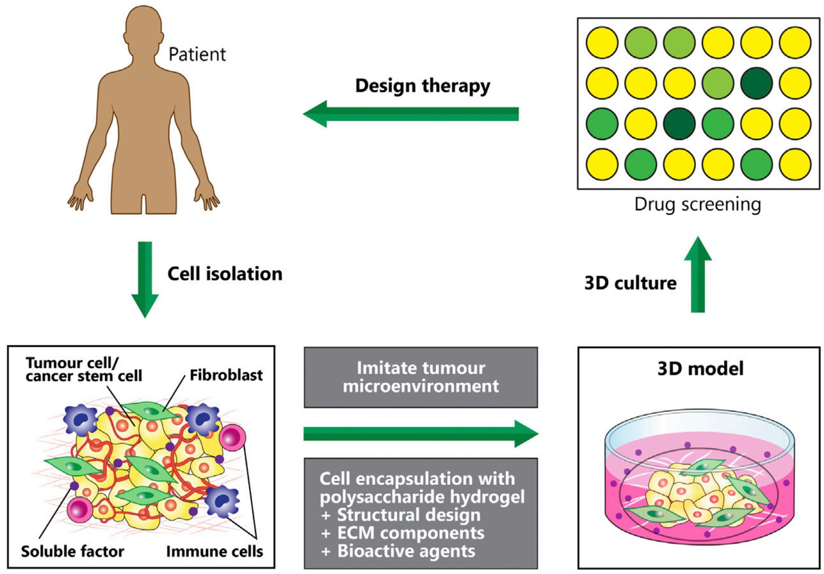

FIGURE 6 | Disease modeling: Creating 3D *in vitro* human tumour models to mimic various microenvironmental cues of human tumours, which can be used to screen anticancer therapeutics. Hydrogel fabrication and cell microencapsulation are involved in engineering the microenvironmental conditions. Impact of each condition on the efficacy of the therapeutic approaches is determined by efficient manipulation and regulation of the microenvironment conditions.

developed to mimic tumor and bone microenvironments (Zhu et al., 2016). This model served as a tool for exploring cancer metastasis (invasive of breast cancer to bone) and assessing anticancer drug sensitivity. The breast cancer cell spheroids exhibited high migratory ability when co-cultured with bone marrow derived MSCs and demonstrated higher anticancer drug resistance when compared to the 2D culture model.

FUTURE PERSPECTIVE AND CONCLUSION

We reviewed studies on stem cell microencapsulation in hydrogels, highlighting the polysaccharide polymers, recent microencapsulation techniques and clinical translation in cell-based therapy (cell delivery) and disease modeling (drug testing and discovery). Despite current promising results and potentials, there are still several challenges and issues remaining. The relatively low viability of encapsulated cells is among the issues. For example, microencapsulation techniques that involve photopolymerization with radial initiators during encapsulation may cause cell damage whilst oil emulsion can destroy the lipid membrane of cells. Thus, current techniques need to be enhanced to reduce the use of radicals, decrease light intensity as well as to limit contact time with the oil phase.

Moreover, most of the techniques are established and tested for stem cells encapsulation at a small scale. Further optimization for large-scale production in the future studies are required to meet the criteria of good manufacturing production (GMP) guidelines. In clinical trials, large quantity of stem cells with approximately 10^7–10^{10} cells per patient is administered. It is tricky to uniformly encapsulate and expand a large number of cells whilst high cell viability and functionality still remained during and after the 3D culture processes. It is believed that advances in micro-technology and smart material synthesis will help to solve the issues and offer new options for stem cell microencapsulation. The use of a bioreactor in 3D culture and large-scale production may improve cell expansion and cell quality. Importantly, hydrogel materials and processes for stem cell microencapsulation should further modify and customize according to their specific applications in clinical translation as well as display the desired structural, biological, and physicochemical properties. The hydrogel materials must also obtain an approval from regulatory authority such as Food and Drug Administration (FDA) and the equivalent.

To increase the ability of hydrogels and cells to respond to physical, chemical and biological stimuli, diversity in material design is a prospect. Novel synthetic ECM mimetics are suggested to formulate into natural polymers to enable dynamic changes in their properties and reaction to their external environment. Future interest has been drawn to produce ‘smart hydrogels.’ Several types of ‘smart hydrogels’ suitable for stem cell encapsulation and delivery are light responsive hydrogels, electro responsive hydrogels, magnetic responsive hydrogels, pH-responsive hydrogels, glucose responsive hydrogels and biochemical responsive hydrogels (Mantha et al., 2019). Stimuli-responsive hydrogels or cell vehicles could direct migration and cell homing *in vivo* (Wan et al., 2020). Hydrogel materials with programed shape and size are expected to transform post-implantation to fit the defect or transplant site with precise geometry.

Nowadays, advanced hydrogel designs are progressing toward multicomponent and multicellular approaches to increase complexities and heterogeneities in the hydrogel constructs for better tissue integration, sustainable function and effective therapeutic strategy. Multicellular constructs such as stem cell-derived organoids incorporated with polysaccharide hydrogels present the opportunity to create compositionally tailored *in-vitro* tissue models in a high-throughput manner. The models can be utilized in future drug testing and discovery, including toxicological screening and the possibility for drug stratification at a personalized level (when combined with patient-derived iPSCs). It is also foreseen that the reviewed and suggested strategies may potentially apply in precision medicine and personalized tissue regeneration.

The microencapsulation methods discussed in this review are the approaches currently available. Latest and upcoming development such as next-generation 3D bioprinting, namely 4D bioprinting, is believed to provide enormous application in regenerative medicine when moving towards clinical translation. 4D bioprinting could be used for 'smart hydrogels' fabrication and advanced stem cell microencapsulation. It offers capability to synthesis shape-programed and functional structured hydrogels in a regulated manner, leading to construction of active multilayered, functional tissues and disease models with dynamic and hierarchical structures (Liaw et al., 2018). Under multiple stimuli, the complex shape transformation processes and functional transitions can facilitate tissue remodeling and maturation.

In conclusion, we detailed various commonly used polysaccharide hydrogels and their unique properties, types of stem cells and current microencapsulation methods with recent studies demonstrating the potential of stem cell-encapsulated hydrogels in cell delivery and disease modeling for treating diseases. While the choice of hydrogel material and design impact the viability and differentiation of encapsulated stem cells, the different microencapsulation techniques have also shown variable cell activities post-encapsulation. There are still many problems to solve when moving towards clinical translation. Future developments are now focusing on the combining of different materials, multiple cell types and more than one microencapsulation technique to work in a complementary mode. The challenges and limitations discussed herein need to be further addressed in future studies to promote the therapeutic activity and applicability of microencapsulated stem cells in regenerative medicine.

AUTHOR CONTRIBUTIONS

S-YL, JM, TSK, NA, NK, and ZH wrote the manuscript. S-YL defined the scope and supervised the work. MM edited the final manuscript. All the authors contributed to the article and approved the submitted version.

FUNDING

Fundamental Research Grant Scheme (FRGS/1/2020/TK0/USM/02/32–6171275) from the Ministry of Higher Education and Short-Term Grant (304/PPSP/6315153) from the Universiti Sains Malaysia supported this work and related research.

ACKNOWLEDGMENTS

The authors thank Sarah Kinnersly for proofreading the article.

REFERENCES

Abecasis, B., Canhão, P. G. M., Almeida, H. V., Calmeiro, T., Fortunato, E., Gomes-Alves, P., et al. (2020). Toward a Microencapsulated 3D hiPSC-Derived *In Vitro* Cardiac Microtissue for Recapitulation of Human Heart Microenvironment Features. *Front. Bioeng. Biotechnol.* 8, 540744. doi:10.3389/fbioe.2020.580744

Abhirup, M., John, R. C., Aaron, C., and Samir, M. (2020). Hydrogels in the Clinic. *Bioeng. Transl. Med.* 5, e10158. doi:10.1002/btm2.v5.2

Alagpulinsa, D. A., Cao, J. J. L., Driscoll, R. K., Sîrbulescu, R. F., Penson, M. F. E., Sremac, M., et al. (2019). Alginate-microencapsulation of Human Stem Cell-Derived β Cells with CXCL 12 Prolongs Their Survival and Function in Immunocompetent Mice without Systemic Immunosuppression. *Am. J. Transpl.* 19 (7), 1930–1940. doi:10.1111/ajt.15308

Alison, B., Amogha, T., Yuan, N., Nanjing, H., John, Z., and Zhang, J. (2020). Advances in Diagnostic Microfluidics: Advances in Clinical Chemistry. *Clin. Adv. Periodontics* 10, 1–72. doi:10.1002/cap.v10.1

Alkayyali, T., Cameron, T., Haltli, B., Kerr, R. G., and Ahmadi, A. (2019). Microfluidic and Cross-Linking Methods for Encapsulation of Living Cells and Bacteria - A Review. *Analytica Chim. Acta* 1053, 1–21. doi:10.1016/j.aca.2018.12.056

Amir, K., Daniel, N., Luis, I., Hossein, G., Sushila, M., Guillermo, U., et al. (2018). Microfluidics-Enabled Multimaterial Maskless Stereolithographic Bioprinting. *Adv. Mater.* 30, 1800242. doi:10.1002/adma.201800242

An, C., Liu, W., Zhang, Y., Pang, B., Liu, H., Zhang, Y., et al. (2020). Continuous Microfluidic Encapsulation of Single Mesenchymal Stem Cells Using Alginate Microgels as Injectable Fillers for Bone Regeneration. *Acta Biomater.* 111, 181–196. doi:10.1016/j.actbio.2020.05.024

Andersen, T., Auk-Emblem, P., and Dornish, M. (2015). 3D Cell Culture in Alginate Hydrogels. *Microarrays* 4 (2), 133–161. doi:10.3390/microarrays4020133

Ansari, S., Chen, C., Xu, X., Annabi, N., Zadeh, H. H., Wu, B. M., et al. (2016). Muscle Tissue Engineering Using Gingival Mesenchymal Stem Cells Encapsulated in Alginate Hydrogels Containing Multiple Growth Factors. *Ann. Biomed. Eng.* 44, 1908–1920. doi:10.1007/s10439-016-1594-6

Aurich, M., Hofmann, G. O., Gras, F., and Rolauffs, B. (2018). Human Osteochondritis Dissecans Fragment-Derived Chondrocyte Characteristics *Ex Vivo*, after Monolayer Expansion-Induced De-differentiation, and after Re-differentiation in Alginate Bead Culture. *BMC Musculoskelet. Disord.* 19 (1), 168. doi:10.1186/s12891-018-2079-6

Burdick, J. A., and Vunjak-Novakovic, G. (2009). Engineered Microenvironments for Controlled Stem Cell Differentiation. *Tissue Eng. A* 15 (2), 205–219. doi:10.1089/ten.tea.2008.0131

Campo, V. L., Kawano, D. F., Silva, D. B. d., and Carvalho, I. (2009). Carrageenans: Biological Properties, Chemical Modifications and Structural Analysis - A Review. *Carbohydr. Polym.* 77 (2), 167–180. doi:10.1016/j.carbpol.2009.01.020

Cañibano-Hernández, A., Saenz Del Burgo, L., Espona-Noguera, A., Orive, G., Hernández, R. M., Ciriza, J., et al. (2017). Alginate Microcapsules Incorporating Hyaluronic Acid Recreate Closer *In Vivo* Environment for Mesenchymal Stem Cells. *Mol. Pharm.* 14 (7), 2390–2399. doi:10.1021/acs.molpharmaceut.7b00295

Centeno, E. G. Z., Cimarosti, H., and Bithell, A. (2018). 2D versus 3D Human Induced Pluripotent Stem Cell-Derived Cultures for Neurodegenerative

Disease Modelling. *Mol. Neurodegener.* 13 (27), 1–12. doi:10.1186/s13024-018-0258-4

Chakraborty, S., Jana, S., Gandhi, A., Sen, K. K., Zhiang, W., and Kokare, C. (2014). Gellan Gum Microspheres Containing a Novel α-amylase from marine Nocardiopsis Sp. Strain B2 for Immobilization. *Int. J. Biol. Macromol.* 70, 292–299. doi:10.1016/j.ijbiomac.2014.06.046

Chan, H. F., Zhang, Y., Ho, Y.-P., Chiu, Y.-L., Jung, Y., and Leong, K. W. (2013). Rapid Formation of Multicellular Spheroids in Double-Emulsion Droplets with Controllable Microenvironment. *Sci. Rep.* 3, 3462. doi:10.1038/srep03462

Chang, S.-H., Lin, H.-T. V., Wu, G.-J., and Tsai, G. J. (2015). pH Effects on Solubility, Zeta Potential, and Correlation between Antibacterial Activity and Molecular Weight of Chitosan. *Carbohydr. Polym.* 134, 74–81. doi:10.1016/j.carbpol.2015.07.072

Chen, K. G., Mallon, B. S., McKay, R. D. G., and Robey, P. G. (2014). Human Pluripotent Stem Cell Culture: Considerations for Maintenance, Expansion, and Therapeutics. *Cell Stem Cell* 14 (1), 13–26. doi:10.1016/j.stem.2013.12.005

Ching, S. H., Bansal, N., and Bhandari, B. (2017). Alginate Gel Particles-A Review of Production Techniques and Physical Properties. *Crit. Rev. Food Sci. Nutr.* 57 (6), 1133–1152. doi:10.1080/10408398.2014.965773

Choe, G., Park, J., Park, H., and Lee, J. (2018). Hydrogel Biomaterials for Stem Cell Microencapsulation. *Polymers* 10 (9), 997. doi:10.3390/polym10090997

Choi, C.-H., Wang, H., Lee, H., Kim, J. H., Zhang, L., Mao, A., et al. (2016). One-step Generation of Cell-Laden Microgels Using Double Emulsion Drops with a Sacrificial Ultra-thin Oil Shell. *Lab. Chip* 16, 1549–1555. doi:10.1039/C6LC00261G

Cidonio, G., Glinka, M., Dawson, J. I., and Oreffo, R. O. C. (2019). The Cell in the Ink: Improving Biofabrication by Printing Stem Cells for Skeletal Regenerative Medicine. *Biomaterials* 209, 10–24. doi:10.1016/j.biomaterials.2019.04.009

Cooke, M. E., Pearson, M. J., Moakes, R. J. A., Weston, C. J., Davis, E. T., Jones, S. W., et al. (2017). Geometric Confinement Is Required for Recovery and Maintenance of Chondrocyte Phenotype in Alginate. *APL Bioeng.* 1, 016104. doi:10.1063/1.5006752

Correa, S., Grosskopf, A. ., Hernandez, H. ., Chan, D., Yu, A. ., Staplethon, L., et al. (2021). Translational Applications of Hydrogels. *Chem. Soc. Rev.* 121, 11385. doi:10.1021/acs.chemrev.0c01177

Crevensten, G., Walsh, A. J. L., Ananthakrishnan, D., Page, P., Wahba, G. M., Lotz, J. C., et al. (2004). Intervertebral Disc Cell Therapy for Regeneration: Mesenchymal Stem Cell Implantation in Rat Intervertebral Discs. *Ann. Biomed. Eng.* 32 (3), 430–434. doi:10.1023/B:ABME.0000017545.84833.7c

Crow, B. B., and Nelson, K. D. (2006). Release of Bovine Serum Albumin from a Hydrogel-Cored Biodegradable Polymer Fiber. *Biopolymers* 81, 419–427. doi:10.1002/bip.20442

da Silva, L. P., Santos, T. C., Rodrigues, D. B., Pirraco, R. P., Cerqueira, M. T., Reis, R. L., et al. (2017). Stem Cell-Containing Hyaluronic Acid-Based Spongy Hydrogels for Integrated Diabetic Wound Healing. *J. Invest. Dermatol.* 137, 1541–1551. doi:10.1016/j.jid.2017.02.976

Dahlmann, J., Krause, A., Möller, L., Kensah, G., Möwes, M., Diekmann, A., et al. (2013). Fully Defined *In Situ* Cross-Linkable Alginate and Hyaluronic Acid Hydrogels for Myocardial Tissue Engineering. *Biomaterials* 34 (4), 940–951. doi:10.1016/j.biomaterials.2012.10.008

Daly, A. C., Riley, L., Segura, T., and Burdick, J. A. (2020). Hydrogel Microparticles for Biomedical Applications. *Nat. Rev. Mater.* 5, 20–43. doi:10.1038/s41578-019-0148-6

Dhillon, J., Young, S. A., Sherman, S. E., Bell, G. I., Amsden, B. G., Hess, D. A., et al. (2019). Peptide-modified Methacrylated Glycol Chitosan Hydrogels as a Cell-Viability Supporting Pro-angiogenic Cell Delivery Platform for Human Adipose-Derived Stem/stromal Cells. *J. Biomed. Mater. Res.* 107 (3), 571–585. doi:10.1002/jbm.a.36573

Engler, A. J., Sen, S., Sweeney, H. L., and Discher, D. E. (2006). Matrix Elasticity Directs Stem Cell Lineage Specification. *Cell* 126 (4), 677–689. doi:10.1016/j.cell.2006.06.044

Eric, J., Stefan, T., Yolonda, L., and Mark, W. (2016). Superhydrophobic Materials for Biomedical Applications. *Biomaterials* 104, 87–103. doi:10.1016/j.biomaterials.2016.06.050

Forget, A., Blaeser, A., Miessmer, F., Köpf, M., Campos, D. F. D., Voelcker, N. H., et al. (2017). Mechanically Tunable Bioink for 3D Bioprinting of Human Cells. *Adv. Healthc. Mater.* 6 (20), 1700255. doi:10.1002/adhm.201700255

Frey, N., Linke, A., Süselbeck, T., Müller-Ehmsen, J., Vermeersch, P., Schoors, D., et al. (2014). Intracoronary Delivery of Injectable Bioabsorbable Scaffold (IK-5001) to Treat Left Ventricular Remodeling after ST-Elevation Myocardial Infarctionffold (IK-5001) to Treat Left Ventricular Remodeling after ST-Elevation Myocardial Infarction: a FIrst-In-Man Study. *Circ. Cardiovasc. Interv.* 7, 806–812. doi:10.1161/circinterventions.114.001478

Gao, L., Yi, M., Xing, M., Li, H., Zhou, Y., Xu, Q., et al. (2020). *In Situ* activated Mesenchymal Stem Cells (MSCs) by Bioactive Hydrogels for Myocardial Infarction Treatment. *J. Mater. Chem. B* 8, 7713–7722. doi:10.1039/d0tb01320j

Gasperini, L., Mano, J. F., and Reis, R. L. (2014). Natural Polymers for the Microencapsulation of Cells. *J. R. Soc. Interf.* 11 (100), 20140817. doi:10.1098/rsif.2014.0817

Gerecht, S., Burdick, J. A., Ferreira, L. S., Townsend, S. A., Langer, R., and Vunjak-Novakovic, G. (2007). Hyaluronic Acid Hydrogel for Controlled Self-Renewal and Differentiation of Human Embryonic Stem Cells. *Proc. Natl. Acad. Sci.* 104 (27), 11298–11303. doi:10.1073/pnas.0703723104

Giada, C., Amparo, G. ., Ruben, F., Peter, P., Alessandra, R., Micheal, M., et al. (2020). Alginate Formulations: Current Developments in the Race for Hydrogel-Based Cardiac Regeneration. *Front. Bioeng. Biotechnol.* 8, 414. doi:10.3389/fbioe.2020.00414

Goetzke, R., Keijdener, H., Franzen, J., Ostrowska, A., Nüchtern, S., Mela, P., et al. (2019). Differentiation of Induced Pluripotent Stem Cells towards Mesenchymal Stromal Cells Is Hampered by Culture in 3D Hydrogels. *Sci. Rep.* 9, 15578. doi:10.1038/s41598-019-51911-5

Gomes, E. D., Mendes, S. S., Leite-Almeida, H., Gimble, J. M., Tam, R. Y., Shoichet, M. S., et al. (2016). Combination of a Peptide-Modified Gellan Gum Hydrogel with Cell Therapy in a Lumbar Spinal Cord Injury Animal Model. *Biomaterials* 105, 38–51. doi:10.1016/j.biomaterials.2016.07.019

Gomez-Florit, M., Pardo, A., Domingues, R. M. A., Graça, A. L., Babo, P. S., Reis, R. L., et al. (2020). Natural-Based Hydrogels for Tissue Engineering Applications. *Molecules* 25, 5858. doi:10.3390/molecules25245858

Gu, L., and Mooney, D. J. (2016). Biomaterials and Emerging Anticancer Therapeutics: Engineering the Microenvironment. *Nat. Rev. Cancer* 16, 56–66. doi:10.1038/nrc.2015.3

Guan, X., Avci-Adali, M., Alarçin, E., Cheng, H., Kashaf, S. S., Li, Y., et al. (2017). Development of Hydrogels for Regenerative Engineering. *Biotechnol. J.* 12 (5), 1600394. doi:10.1002/biot.201600394

Guilak, F., Cohen, D. M., Estes, B. T., Gimble, J. M., Liedtke, W., and Chen, C. S. (2009). Control of Stem Cell Fate by Physical Interactions with the Extracellular Matrix. *Cell Stem Cell* 5 (1), 17–26. doi:10.1016/j.stem.2009.06.016

Halldorsson, S., Lucumi, E., Gómez-Sjöberg, R., and Fleming, R. M. T. (2015). Advantages and Challenges of Microfluidic Cell Culture in Polydimethylsiloxane Devices. *Biosens. Bioelectron.* 63 (63), 218–231. doi:10.1016/j.bios.2014.07.029

Hanahan, D., and Weinberg, R. A. (2011). Hallmarks of Cancer: The Next Generation. *Cell* 144, 646–674. doi:10.1016/j.cell.2011.02.013

Handorf, A. M., Zhou, Y., Halanski, M. A., and Li, W.-J. (2015). Tissue Stiffness Dictates Development, Homeostasis, and Disease Progression. *Organogenesis* 11 (1), 1–15. doi:10.1080/15476278.2015.1019687

Hasani-Sadrabadi, M. M., Sarrion, P., Pouraghaei, S., Chau, Y., Ansari, S., Li, S., et al. (2020). An Engineered Cell-Laden Adhesive Hydrogel Promotes Craniofacial Bone Tissue Regeneration in Rats. *Sci. Transl. Med.* 12 (534), eaay6853. doi:10.1126/scitranslmed.aay6853

Hashemi, M., and Kalalinia, F. (2015). Application of Encapsulation Technology in Stem Cell Therapy. *Life Sci.* 143, 139–146. doi:10.1016/j.lfs.2015.11.007

Hay, M., Thomas, D. W., Craighead, J. L., Economides, C., and Rosenthal, J. (2014). Clinical Development success Rates for Investigational Drugs. *Nat. Biotechnol.* 32, 40–51. doi:10.1038/nbt.2786

Hayat, Z., and El Abed, A. I. (2018). High-Throughput Optofluidic Acquisition of Microdroplets in Microfluidic Systems. *Micromachines* 9 (4), 183. doi:10.3390/mi9040183

Heile, A., and Brinker, T. (2011). Clinical Translation of Stem Cell Therapy in Traumatic Brain Injury: the Potential of Encapsulated Mesenchymal Cell Biodelivery of Glucagon-like Peptide-1. *Dialogues Clin. Neurosci.* 13, 279–286. doi:10.31887/dcns.2011.13.2/aheile

Hlavac, N., Kasper, M., and Schmidt, C. E. (2020). Progress toward Finding the Perfect Match: Hydrogels for Treatment of central Nervous System Injury. *Mater. Today Adv.* 6, 100039. doi:10.1016/j.mtadv.2019.100039

Huebsch, N., Arany, P. R., Mao, A. S., Shvartsman, D., Ali, O. A., Bencherif, S. A., et al. (2010). Harnessing Traction-Mediated Manipulation of the Cell/matrix Interface to Control Stem-Cell Fate. *Nat. Mater* 9 (6), 518–526. doi:10.1038/nmat2732

Jabbari, E., Leijten, J., Xu, Q., and Khademhosseini, A. (2016). The Matrix Reloaded: The Evolution of Regenerative Hydrogels. *Mater. Today* 19 (4), 190–196. doi:10.1016/j.mattod.2015.10.005

Jooybar, E., Abdekhodaie, M. J., Alvi, M., Mousavi, A., Karperien, M., and Dijkstra, P. J. (2019). An Injectable Platelet Lysate-Hyaluronic Acid Hydrogel Supports Cellular Activities and Induces Chondrogenesis of Encapsulated Mesenchymal Stem Cells. *Acta Biomater.* 83, 233–244. doi:10.1016/j.actbio.2018.10.031

Jutila, A. A., Zignego, D. L., Schell, W. J., and June, R. K. (2015). Encapsulation of Chondrocytes in High-Stiffness Agarose Microenvironments for *In Vitro* Modeling of Osteoarthritis Mechanotransduction. *Ann. Biomed. Eng.* 43 (5), 1132–1144. doi:10.1007/s10439-014-1183-5

Karim, K., Sohrabi, B., and Atyeh, R. (2019). Superhydrophobicity: Advanced Biological and Biomedical Applications. *Biomaterials* 7, 3110–3137. doi:10.1039/c9bm00558g

Khademhosseini, A., Eng, G., Yeh, J., Fukuda, J., Blumling, J., Langer, R., et al. (2006). Micromolding of Photocrosslinkable Hyaluronic Acid for Cell Encapsulation and Entrapment. *J. Biomed. Mater. Res.* 79A (3), 522–532. doi:10.1002/jbm.a.30821

Kim, I.-Y., Seo, S.-J., Moon, H.-S., Yoo, M.-K., Park, I.-Y., Kim, B.-C., et al. (2008). Chitosan and its Derivatives for Tissue Engineering Applications. *Biotechnol. Adv.* 26, 1–21. doi:10.1016/j.biotechadv.2007.07.009

Kim, H., Bae, C., Kook, Y.-M., Koh, W.-G., Lee, K., and Park, M. H. (2019). Mesenchymal Stem Cell 3D Encapsulation Technologies for Biomimetic Microenvironment in Tissue Regeneration. *Stem Cel Res. Ther.* 10 (1), 51. doi:10.1186/s13287-018-1130-8

Knopf-Marques, H., Pravda, M., Wolfova, L., Velebny, V., Schaaf, P., Vrana, N. E., et al. (2016). Hyaluronic Acid and its Derivatives in Coating and Delivery Systems: Applications in Tissue Engineering, Regenerative Medicine and Immunomodulation. *Adv. Healthc. Mater.* 5 (22), 2841–2855. doi:10.1002/adhm.201600316

Koh, B., Sulaiman, N., Fauzi, M. B., Law, J. X., Ng, M. H., Idrus, R. B. H., et al. (2020). Three Dimensional Microcarrier System in Mesenchymal Stem Cell Culture: A Systematic Review. *Cell Biosci.* 10, 75. doi:10.1186/s13578-020-00438-8

Koivisto, J. T., Joki, T., Parraga, J. E., Pääkkönen, R., Ylä-Outinen, L., Salonen, L., et al. (2017). Bioamine-crosslinked Gellan Gum Hydrogel for Neural Tissue Engineering. *Biomed. Mater.* 12 (23), 025014–120602. doi:10.1088/1748-605X/aa62b0

Koivisto, J. T., Gering, C., Karvinen, J., Maria Cherian, R., Belay, B., Hyttinen, J., et al. (2019). Mechanically Biomimetic Gelatin-Gellan Gum Hydrogels for 3D Culture of Beating Human Cardiomyocytes. *ACS Appl. Mater. Inter.* 11 (2), 20589–20602. doi:10.1021/acsami.8b22343

Komatsu, M., Konagaya, S., Egawa, E. Y., and Iwata, H. (2015). Maturation of Human iPS Cell-Derived Dopamine Neuron Precursors in Alginate-Ca2+ Hydrogel. *Biochim. Biophys. Acta Gen. Subjects* 1850 (9), 1669–1675. doi:10.1016/j.bbagen.2015.04.011

Kumachev, A., Greener, J., Tumarkin, E., Eiser, E., Zandstra, P. W., and Kumacheva, E. (2011). High-throughput Generation of Hydrogel Microbeads with Varying Elasticity for Cell Encapsulation. *Biomaterials* 32 (16), 1477–1483. doi:10.1016/j.biomaterials.2010.10.033

Kuo, T. K., Hung, S. P., Chuang, C. H., Chen, C. T., Shih, Y. R. V., Fang, S. C. Y., et al. (2008). Stem Cell Therapy for Liver Disease: Parameters Governing the Success of Using Bone Marrow Mesenchymal Stem Cells. *Gastroenterology* 134 (7), 2111–2121. doi:10.1053/j.gastro.2008.03.015

Law, N., Doney, B., Glover, H., Qin, Y., Aman, Z. M., Sercombe, T. B., et al. (2018). Characterisation of Hyaluronic Acid Methylcellulose Hydrogels for 3D Bioprinting. *J. Mech. Behav. Biomed. Mater.* 77, 389–399. doi:10.1016/j.jmbbm.2017.09.031

Lee, R. J., Hinson, A., Bauernschmitt, R., Matschke, K., Fang, Q., Mann, D. L., et al. (2015). The Feasibility and Safety of Algisyl-LVR as a Method of Left Ventricular Augmentation in Patients with Dilated Cardiomyopathy: Initial First in Man Clinical Resultsfirst in Man Clinical Result. *Int. J. Cardiol.* 199, 18–24. doi:10.1016/j.ijcard.2015.06.111

Lee, S. Y., George, J. H., Nagel, D. A., Ye, H., Kueberuwa, G., and Seymour, L. W. (2019). Optogenetic Control of iPS Cell-derived Neurons in 2D and 3D Culture Systems Using Channelrhodopsin-2 Expression Driven by the Synapsin-1 and Calcium-calmodulin Kinase II Promoters. *J. Tissue Eng. Regen. Med.* 13, 369–384. doi:10.1002/term.2786

Leeper, N. J., Hunter, A. L., and Cooke, J. P. (2010). Stem Cell Therapy for Vascular Regeneration. *Circulation* 122, 517–526. doi:10.1161/CIRCULATIONAHA.109.881441

Lei, M., and Wang, X. (2016). Biodegradable Polymers and Stem Cells for Bioprinting. *Molecules* 21 (5), 539. doi:10.3390/molecules21050539

Leslie, S. K., Kinney, R. C., Schwartz, Z., and Boyan, B. D. (2017). Microencapsulation of Stem Cells for Therapy. *Methods Mol. Biol.* 1479, 251–259. doi:10.1007/978-1-4939-6364-5_20

Li, H., Ham, T. R., Neill, N., Farrag, M., Mohrman, A. E., Koenig, A. M., et al. (2016). A Hydrogel Bridge Incorporating Immobilized Growth Factors and Neural Stem/Progenitor Cells to Treat Spinal Cord Injury. *Adv. Healthc. Mater.* 5 (7), 802–812. doi:10.1002/adhm.201500810

Li, J., Luo, Y., Li, B., Xia, Y., Wang, H., and Fu, C. (2020). Implantable and Injectable Biomaterial Scaffolds for Cancer Immunotherapy. *Front. Bioeng. Biotechnol.* 8, 612950. doi:10.3389/fbioe.2020.612950

Liang, R., Gu, Y., Wu, Y., Bunpetch, V., and Zhang, S. (2020). Lithography-Based 3D Bioprinting and Bioinks for Bone Repair and Regeneration. *ACS Biomater. Sci. Eng.* 7 (3), 806–816. doi:10.1021/acsbiomaterials.9b01818

Liaw, C.-Y., Ji, S., and Guvendiren, M. (2018). Human Tissue Models: Engineering 3D Hydrogels for Personalized *In Vitro* Human Tissue Models (Adv. Healthcare Mater. 4/2018). *Adv. Healthc. Mater.* 7, 1870021. doi:10.1002/adhm.201870021

Lima, A. C., Song, W., Blanco-Fernandez, B., Alvarez-Lorenzo, C., and Mano, J. F. (2011). Synthesis of Temperature-Responsive dextran-MA/PNIPAAm Particles for Controlled Drug Delivery Using Superhydrophobic Surfaces. *Pharm. Res.* 28, 1294–1305. doi:10.1007/s11095-011-0380-2

Lima, A. C., Batista, P., Valente, T. A. M., Silva, A. S., Correia, I. J., and Mano, J. F. (2013). Novel Methodology Based on Biomimetic Superhydrophobic Substrates to Immobilize Cells and Proteins in Hydrogel Spheres for Applications in Bone Regeneration. *Tissue Eng. Part A* 19, 1175–1187. doi:10.1089/ten.tea.2012.0249

Lin, Y., Gao, C., Gritsenko, D., Zhou, R., and Xu, J. (2018). Soft Lithography Based on Photolithography and Two-Photon Polymerization. *Microfluid Nanofluid* 22, 1. doi:10.1007/s10404-018-2118-5

Liu, E. Y., Jung, S., Weitz, D. A., Yi, H., and Choi, C.-H. (2018a). High-throughput Double Emulsion-Based Microfluidic Production of Hydrogel Microspheres with Tunable Chemical Functionalities toward Biomolecular Conjugation. *Lab. Chip* 18, 323–334. doi:10.1039/C7LC01088E

Liu, F., Chen, Q., Liu, C., Ao, Q., Tian, X., Fan, J., et al. (2018b). Natural Polymers for Organ 3D Bioprinting. *Polymers* 10 (11), 1278. doi:10.3390/polym10111278

López-Ruiz, E., Jiménez, G., Jiménez, G., Álvarez de Cienfuegos, L., Antich, C., Sabata, R., et al. (2019). Dvances of Hyaluronic Acid in Stem Cell Therapy and Tissue Engineering, Including Current Clinical Trials. *eCM* 37, 186–213. doi:10.22203/eCM.v037a12

Loebel, C., and Burdick, J. A. (2018). Engineering Stem and Stromal Cell Therapies for Musculoskeletal Tissue Repair. *Cell Stem Cell* 22 (3), 325–339. doi:10.1016/j.stem.2018.01.014

Lyu, Y., Xie, J., Liu, Y., Xiao, M., Li, Y., Yang, J., et al. (2020). Injectable Hyaluronic Acid Hydrogel Loaded with Functionalized Human Mesenchymal Stem Cell Aggregates for Repairing Infarcted Myocardium. *ACS Biomater. Sci. Eng.* 6 (12), 6926–6937. doi:10.1021/acsbiomaterials.0c01344

Madhusudanan, P., Raju, G., and Shankarappa, S. (2020). Hydrogel Systems and Their Role in Neural Tissue Engineering. *J. R. Soc. Interf.* 17 (162), 20190505. doi:10.1098/rsif.2019.0505

Maguire, T., Novik, E., Schloss, R., and Yarmush, M. (2006). Alginate-PLL Microencapsulation: Effect on the Differentiation of Embryonic Stem Cells into Hepatocytes. *Biotechnol. Bioeng.* 93 (3), 581–591. doi:10.1002/bit.20748

Mantha, S., Pillai, S., Khayambashi, P., Upadhyay, A., Zhang, Y., Tao, O., et al. (2019). Smart Hydrogels in Tissue Engineering and Regenerative Medicine. *Materials (Basel)* 12, 332. doi:10.3390/ma12203323

Markstedt, K., Mantas, A., Tournier, I., Martínez Ávila, H., Hägg, D., and Gatenholm, P. (2015). 3D Bioprinting Human Chondrocytes with Nanocellulose-Alginate Bioink for Cartilage Tissue Engineering Applications. *Biomacromolecules* 16 (5), 1489–1496. doi:10.1021/acs.biomac.5b00188

Marx-Blümel, L., Marx, C., Weise, F., Frey, J., Perner, B., Schlingloff, G., et al. (2020). Biomimetic Reconstruction of the Hematopoietic Stem Cell Niche for *In Vitro* Amplification of Human Hematopoietic Stem Cells. *PLoS One* 15 (6), e0234638. doi:10.1371/journal.pone.0234638

Mason, C., and Dunnill, P. (2008). A Brief Definition of Regenerative Medicine. *Regen. Med.* 3 (1), 1–5. doi:10.2217/17460751.3.1.1

Mayfield, A. E., Tilokee, E. L., Latham, N., McNeill, B., Lam, B.-K., Ruel, M., et al. (2014). The Effect of Encapsulation of Cardiac Stem Cells within Matrix-Enriched Hydrogel Capsules on Cell Survival, post-ischemic Cell Retention and Cardiac Function. *Biomaterials* 35 (1), 133–142. doi:10.1016/j.biomaterials.2013.09.085

Mazhari, S., Gitiara, A., Baghaei, K., Hatami, B., Rad, R. E., Asadirad, A., et al. (2020). Therapeutic Potential of Bone Marrow-Derived Mesenchymal Stem Cells and Imatinib in a Rat Model of Liver Fibrosis. *Eur. J. Pharmacol.* 882, 173263. doi:10.1016/j.ejphar.2020.173263

McKee, C., and Chaudhry, G. R. (2017). Advances and Challenges in Stem Cell Culture. *Colloids Surf. B: Biointerfaces* 159, 62–77. doi:10.1016/j.colsurfb.2017.07.051

Meinert, C., Schrobback, K., Levett, P. A., Lutton, C., Sah, R. L., and Klein, T. J. (2017). Tailoring Hydrogel Surface Properties to Modulate Cellular Response to Shear Loading. *Acta Biomater.* 52, 105–117. doi:10.1016/j.actbio.2016.10.011

Mohite, B. V., and Patil, S. V. (2014). A Novel Biomaterial: Bacterial Cellulose and its new era Applications. *Biotechnol. Appl. Biochem.* 61 (2), 101–110. doi:10.1002/bab.1148

Moradi, S., Mahdizadeh, H., Šarić, T., Kim, J., Harati, J., Shahsavarani, H., et al. (2019). Research and Therapy with Induced Pluripotent Stem Cells (iPSCs): Social, Legal, and Ethical Considerations. *Stem Cel Res. Ther* 10 (1), 341. doi:10.1186/s13287-019-1455-y

Morgan, R. A., Gray, D., Lomova, A., and Kohn, D. B. (2017). Hematopoietic Stem Cell Gene Therapy: Progress and Lessons Learned. *Cell Stem Cell* 21, 574–590. doi:10.1016/j.stem.2017.10.010

Muzzarelli, R., El Mehtedi, M., Bottegoni, C., Aquili, A., and Gigante, A. (2015). Genipin-crosslinked Chitosan Gels and Scaffolds for Tissue Engineering and Regeneration of Cartilage and Bone. *Mar. Drugs* 13, 7314–7338. doi:10.3390/md13127068

Muzzarelli, R. A. A., El Mehtedi, M., Bottegoni, C., and Gigante, A. (2016). Physical Properties Imparted by Genipin to Chitosan for Tissue Regeneration with Human Stem Cells: A Review. *Int. J. Biol. Macromol.* 93 (12), 1366–1381. doi:10.1016/j.ijbiomac.2016.03.075

Neidlin, M., Korcari, A., Macheras, G., and Alexopoulos, L. G. (2018). Cue-Signal-Response Analysis in 3D Chondrocyte Scaffolds with Anabolic Stimuli. *Ann. Biomed. Eng.* 46, 345–353. doi:10.1007/s10439-017-1964-8

Ng, A. P., and Alexander, W. S. (2017). Haematopoietic Stem Cells: Past, Present and Future. *Cell Death Discov.* 3, 17002. doi:10.1038/cddiscovery.2017.2

Nguyen, D., Hägg, D. A., Forsman, A., Ekholm, J., Nimkingratana, P., Brantsing, C., et al. (2017). Cartilage Tissue Engineering by the 3D Bioprinting of iPS Cells in a Nanocellulose/Alginate Bioink. *Sci. Rep.* 7, 658. doi:10.1038/s41598-017-00690-y

Papa, S., Vismara, I., Mariani, A., Barilani, M., Rimondo, S., De Paola, M., et al. (2018). Mesenchymal Stem Cells Encapsulated into Biomimetic Hydrogel Scaffold Gradually Release CCL2 Chemokine *In Situ* Preserving Cytoarchitecture and Promoting Functional Recovery in Spinal Cord Injury. *J. Control. Release* 278, 49–56. doi:10.1016/j.jconrel.2018.03.034

Parisi-Amon, A., Mulyasasmita, W., Chung, C., and Heilshorn, S. C. (2013). Protein-Engineered Injectable Hydrogel to Improve Retention of Transplanted Adipose-Derived Stem Cells. *Adv. Healthc. Mater.* 2 (3), 428–432. doi:10.1002/adhm.201200293

Park, Y.-B., Ha, C.-W., Lee, C.-H., Yoon, Y. C., and Park, Y.-G. (2017). Cartilage Regeneration in Osteoarthritic Patients by a Composite of Allogeneic Umbilical Cord Blood-Derived Mesenchymal Stem Cells and Hyaluronate Hydrogel: Results from a Clinical Trial for Safety and Proof-Of-Concept with 7 Years of Extended Follow-Up. *Stem Cells Transl. Med.* 6 (2), 613–621. doi:10.5966/sctm.2016-0157

Park, A., Choi, J. H., Lee, S., Been, S., Song, J. E., and Khang, G. (2020). Application of Double Network of Gellan Gum and Pullulan for Bone Marrow Stem Cells Differentiation towards Chondrogenesis by Controlling Viscous Substrates. *J. Tissue Eng. Regen. Med.* 14 (2), 1592–1603. doi:10.1002/term.3116

Pérez-Luna, V., and González-Reynoso, O. (2018). Encapsulation of Biological Agents in Hydrogels for Therapeutic Applications. *Gels* 4, 61. doi:10.3390/gels4030061

Peña, B., Laughter, M., Jett, S., Rowland, T. J., Taylor, M. R. G., Mestroni, L., et al. (2018). Injectable Hydrogels for Cardiac Tissue Engineering. *Macromol. Biosci.* 18 (6), 1800079. doi:10.1002/mabi.201800079

Phelps, E. A., Enemchukwu, N. O., Fiore, V. F., Sy, J. C., Murthy, N., Sulchek, T. A., et al. (2012). Maleimide Cross-Linked Bioactive PEG Hydrogel Exhibits Improved Reaction Kinetics and Cross-Linking for Cell Encapsulation and *In Situ* Delivery. *Adv. Mater.* 24 (1), 64–70. doi:10.1002/adma.201103574

Pinho, S., and Frenette, P. S. (2019). Haematopoietic Stem Cell Activity and Interactions with the Niche. *Nat. Rev. Mol. Cel Biol.* 20, 303–320. doi:10.1038/s41580-019-0103-9

Pittenger, M. F., Discher, D. E., Péault, B. M., Phinney, D. G., Hare, J. M., and Caplan, A. I. (2019). Mesenchymal Stem Cell Perspective: Cell Biology to Clinical Progress. *Npj Regen. Med.* 4 (4), 22. doi:10.1038/s41536-019-0083-6

Popa, E. G., Caridade, S. G., Mano, J. F., Reis, R. L., and Gomes, M. E. (2015). Chondrogenic Potential of Injectable κ -carrageenan Hydrogel with Encapsulated Adipose Stem Cells for Cartilage Tissue-Engineering Applications. *J. Tissue Eng. Regen. Med.* 9 (5), 550–563. doi:10.1002/term.1683

Prajapati, V. D., Jani, G. K., Zala, B. S., and Khutliwala, T. A. (2013). An Insight into the Emerging Exopolysaccharide Gellan Gum as a Novel Polymer. *Carbohydr. Polym.* 93 (2), 670–678. doi:10.1016/j.carbpol.2013.01.030

Rahman, N., Purpura, K. A., Wylie, R. G., Zandstra, P. W., and Shoichet, M. S. (2010). The Use of Vascular Endothelial Growth Factor Functionalized Agarose to Guide Pluripotent Stem Cell Aggregates toward Blood Progenitor Cells. *Biomaterials* 31 (32), 8262–8270. doi:10.1016/j.biomaterials.2010.07.040

Roehm, K. D., and Madihally, S. V. (2018). Bioprinted Chitosan-Gelatin Thermosensitive Hydrogels Using an Inexpensive 3D Printer. *Biofabrication* 10 (1), 015002. doi:10.1088/1758-5090/aa96dd

Rose, M. A., Bowen, J. J., and Morin, S. A. (2019). Emergent Soft Lithographic Tools for the Fabrication of Functional Polymeric Microstructures. *ChemPhysChem* 20, 909–925. doi:10.1002/cphc.201801140

Rossow, T., Lienemann, P. S., and Mooney, D. J. (2017). Cell Microencapsulation by Droplet Microfluidic Templating. *Macromol. Chem. Phys.* 218 (2), 1600380. doi:10.1002/macp.201600380

Roudsari, L. C., and West, J. L. (2016). Studying the Influence of Angiogenesis in *In Vitro* Cancer Model Systems. *Adv. Drug Deliv. Rev.* 97, 250–259. doi:10.1016/j.addr.2015.11.004

Sacchetto, C., Vitiello, L., de Windt, L. J., Rampazzo, A., and Calore, M. (2020). Modeling Cardiovascular Diseases with Hipsc-Derived Cardiomyocytes in 2d and 3d Cultures. *Int. J. Mol. Sci.* 21 (9), 3404. doi:10.3390/ijms21093404

Sakai, S., Ohi, H., Hotta, T., Kamei, H., and Taya, M. (2018). Differentiation Potential of Human Adipose Stem Cells Bioprinted with Hyaluronic Acid/gelatin-Based Bioink through Microextrusion and Visible Light-Initiated Crosslinking. *Biopolymers* 109 (2), e23080. doi:10.1002/bip.23080

Saygili, E., Kaya, E., Ilhan-Ayisigi, E., Saglam-Metiner, P., Alarcin, E., Kazan, A., et al. (2021). An Alginate-Poly(acrylamide) Hydrogel with TGF-β3 Loaded Nanoparticles for Cartilage Repair: Biodegradability, Biocompatibility and Protein Adsorption. *Int. J. Biol. Macromol.* 172, 381–393. doi:10.1016/j.ijbiomac.2021.01.069

Scheper, V., Hoffmann, A., Gepp, M. M., Schulz, A., Hamm, A., Pannier, C., et al. (2019). Stem Cell Based Drug Delivery for protection of Auditory Neurons in a guinea Pig Model of Cochlear Implantation. *Front. Cel. Neurosci.* 13 (117), 1–16. doi:10.3389/fncel.2019.00177

Segers, V. F. M., and Lee, R. T. (2008). Stem-cell Therapy for Cardiac Disease. *Nature* 451 (7181), 937–942. doi:10.1038/nature06800

Shendi, D., Albrecht, D. R., and Jain, A. (2017). Anti-Fas Conjugated Hyaluronic Acid Microsphere Gels for Neural Stem Cell Delivery. *J. Biomed. Mater. Res.* 105 (2), 608–618. doi:10.1002/jbm.a.35930

Silva, K. R., Rezende, R. A., Pereira, F. D. A. S., Gruber, P., Stuart, M. P., Ovsianikov, A., et al. (2016). Delivery of Human Adipose Stem Cells Spheroids into Lockyballs. *PLoS One* 11 (11), e0166073. doi:10.1371/journal.pone.0166073

Simpson, L. W., Szeto, G. L., Boukari, H., Good, T. A., and Leach, J. B. (2020). Impact of Four Common Hydrogels on Amyloid-β (Aβ) Aggregation and Cytotoxicity: Implications for 3D Models of Alzheimer's Disease. *ACS Omega* 5 (32), 20250–20260. doi:10.1021/acsomega.0c02046

Slaughter, B. V., Khurshid, S. S., Fisher, O. Z., Khademhosseini, A., and Peppas, N. A. (2009). Hydrogels in Regenerative Medicine. *Adv. Mater.* 21 (32-33), 3307–3329. doi:10.1002/adma.200802106

Smith, T. T., Moffett, H. F., Stephan, S. B., Opel, C. F., Dumigan, A. G., Jiang, X., et al. (2017). Biopolymers Codelivering Engineered T Cells and STING Agonists Can Eliminate Heterogeneous Tumors. *J. Clin. Invest.* 127 (6), 2176–2191. doi:10.1172/JCI87624

Soriano-Ruiz, J. L., Gálvez-Martín, P., López-Ruiz, E., Suñer-Carbó, J., Calpena-Campmany, A. C., Marchal, J. A., et al. (2019). Design and Evaluation of Mesenchymal Stem Cells Seeded Chitosan/glycosaminoglycans Quaternary Hydrogel Scaffolds for Wound Healing Applications. *Int. J. Pharm.* 570, 118632. doi:10.1016/j.ijpharm.2019.118632

Suh, K. Y., Khademhosseini, A., Yang, J. M., Eng, G., and Langer, R. (2004). Soft Lithographic Patterning of Hyaluronic Acid on Hydrophilic Substrates Using Molding and Printing. *Adv. Mater.* 16, 584–588. doi:10.1002/adma.200306180

Tan, Y., Wang, L., Chen, G., Liu, W., Li, Z., Wang, Y., et al. (2020). Hyaluronate Supports hESC-cardiomyocyte Cell Therapy for Cardiac Regeneration after Acute Myocardial Infarction. *Cell Prolif* 53, 1–10. doi:10.1111/cpr.12942

Tang, Q., Li, X., Lai, C., Li, L., Wu, H., Wang, Y., et al. (2021). Fabrication of a Hydroxyapatite-PDMS Microfluidic Chip for Bone-Related Cell Culture and Drug Screening. *Bioactive Mater.* 6 (1), 169–178. doi:10.1016/j.bioactmat.2020.07.016

Tsai, A.-C., Jeske, R., Chen, X., Yuan, X., and Li, Y. (2020). Influence of Microenvironment on Mesenchymal Stem Cell Therapeutic Potency: From Planar Culture to Microcarriers. *Front. Bioeng. Biotechnol.* 8, 640. doi:10.3389/fbioe.2020.00640

Vazin, T., and Freed, W. J. (2010). Human Embryonic Stem Cells: Derivation, Culture, and Differentiation: A Review. *Restor. Neurol. Neurosci.* 28 (4), 589–603. doi:10.3233/RNN-2010-0543

Verica, M., Nevenka, R., Jasna, D., Bojana, O., Viktor, N., and Branko, B. (2008). Application of Electrostatic Extrusion – Flavour Encapsulation and Controlled Release. *Sensors* 8, 1488–1496. doi:10.3390/s8031488

Vignesh, S., Gopalakrishnan, A., M.R., P., Nair, S. V., Jayakumar, R., and Mony, U. (2018). Fabrication of Micropatterned Alginate-Gelatin and K-Carrageenan Hydrogels of Defined Shapes Using Simple Wax Mould Method as a Platform for Stem Cell/induced Pluripotent Stem Cells (iPSC) Culture. *Int. J. Biol. Macromol.* 112, 737–744. doi:10.1016/j.ijbiomac.2018.02.031

Vuornos, K., Huhtala, H., Kääriäinen, M., Kuismanen, K., Hupa, L., Kellomäki, M., et al. (2020). Bioactive Glass Ions for *In Vitro* Osteogenesis and Microvascularization in Gellan Gum-collagen Hydrogels. *J. Biomed. Mater. Res.* 108 (4), 1332–1342. doi:10.1002/jbm.b.34482

Wan, A. C. A., and Tai, B. C. U. (2013). CHITIN - A Promising Biomaterial for Tissue Engineering and Stem Cell Technologies. *Biotechnol. Adv.* 31, 1776–1785. doi:10.1016/j.biotechadv.2013.09.007

Wan, Z., Zhang, P., Liu, Y., Lv, L., and Zhou, Y. (2020). Four-dimensional Bioprinting: Current Developments and Applications in Bone Tissue Engineering. *Acta Biomater.* 101, 26–42. doi:10.1016/j.actbio.2019.10.038

Wang, C., Gong, Y., Lin, Y., Shen, J., and Wang, D.-A. (2008). A Novel Gellan Gel-Based Microcarrier for anchorage-dependent Cell Delivery. *Acta Biomater.* 4 (5), 1226–1234. doi:10.1016/j.actbio.2008.03.008

Wolf, M. T., Zhang, H., Sharma, B., Marcus, N. A., Pietzner, U., Fickert, S., et al. (2020). Two-Year Follow-Up and Remodeling Kinetics of ChonDux Hydrogel for Full-Thickness Cartilage Defect Repair in the Knee. *Cartilage* 11 (4), 447–457. doi:10.1177/1947603518800547

Wright, E. J., Farrell, K. A., Malik, N., Kassem, M., Lewis, A. L., Wallrapp, C., et al. (2012). Encapsulated Glucagon-like Peptide-1-Producing Mesenchymal Stem Cells Have a Beneficial Effect on Failing Pig Hearts. *Stem Cell Transl. Med.* 1 (10), 759–769. doi:10.5966/sctm.2012-0064

Wu, S., Xu, R., Duan, B., and Jiang, P. (2017). Three-dimensional Hyaluronic Acid Hydrogel-Based Models for *In Vitro* Human iPSC-Derived NPC Culture and Differentiation. *J. Mater. Chem. B* 5, 3870–3878. doi:10.1039/c7tb00721c

Xingliang, D., Cheng, M., Qing, L., and Tao, X. (2016). 3D Bioprinted Glioma Stem Cells for Brain Tumor Model and Applications of Drug Susceptibility. *Biofabrication* 8 (4), 045005. doi:10.1088/1758-5090/8/4/045005

Xu, H., Huang, S., Wang, J., Lan, Y., Feng, L., Zhu, M., et al. (2019a). Enhanced Cutaneous Wound Healing by Functional Injectable Thermo-Sensitive Chitosan-Based Hydrogel Encapsulated Human Umbilical Cord-Mesenchymal Stem Cells. *Int. J. Biol. Macromol.* 137, 433–441. doi:10.1016/j.ijbiomac.2019.06.246

Xu, Y., Peng, J., Richards, G., Lu, S., and Eglin, D. (2019b). Optimization of Electrospray Fabrication of Stem Cell-Embedded Alginate-Gelatin Microspheres and Their Assembly in 3D-Printed Poly(ε-Caprolactone) Scaffold for Cartilage Tissue Engineering. *J. Orthop. Transl.* 18, 128–141. doi:10.1016/j.jot.2019.05.003

Xu, J., Zheng, S., Hu, X., Li, L., Li, W., Parungao, R., et al. (2020). Advances in the Research of Bioinks Based on Natural Collagen, Polysaccharide and Their Derivatives for Skin 3D Bioprinting. *Polymers* 12, 1237. doi:10.3390/polym12061237

Yang, C., DelRio, F. W., Ma, H., Killaars, A. R., Basta, L. P., Kyburz, K. A., et al. (2016). Spatially Patterned Matrix Elasticity Directs Stem Cell Fate. *Proc. Natl. Acad. Sci. USA* 113 (31), E4439–E4445. doi:10.1073/pnas.1609731113

Yao, Y., Yang, L., Feng, L.-f., Yue, Z.-w., Zhao, N.-h., Li, Z., et al. (2020). IGF-1C Domain-Modified Hydrogel Enhanced the Efficacy of Stem Cells in the Treatment of AMI. *Stem Cel Res. Ther.* 11, 136. doi:10.1186/s13287-020-01637-3

Youngblood, R. L., Truong, N. F., Segura, T., and Shea, L. D. (2018). It's All in the Delivery: Designing Hydrogels for Cell and Non-viral Gene Therapies. *Mol. Ther.* 26 (9), 2087–2106. doi:10.1016/j.ymthe.2018.07.022

Zarei-Kheirabadi, M., Sadrosadat, H., Mohammadshirazi, A., Jaberi, R., Sorouri, F., Khayyatan, F., et al. (2020). Human Embryonic Stem Cell-Derived Neural Stem Cells Encapsulated in Hyaluronic Acid Promotes Regeneration in a Contusion Spinal Cord Injured Rat. *Int. J. Biol. Macromol.* 148, 1118–1129. doi:10.1016/j.ijbiomac.2020.01.219

Zarrintaj, P., Manouchehri, S., Ahmadi, Z., Saeb, M. R., Urbanska, A. M., Kaplan, D. L., et al. (2018). Agarose-based Biomaterials for Tissue Engineering. *Carbohydr. Polym.* 187, 66–84. doi:10.1016/j.carbpol.2018.01.060

Željka, P., Patrick, M. R., Said, A., Sujith, R., Ralf, S., Ole, J., et al. (2018). An Introduction to 3D Bioprinting: Possibilities, Challenges and Future Aspects. *Materials (Basel)* 11, 219. doi:10.3390/ma11112199

Zhang, Y. S., Arneri, A., Bersini, S., Shin, S.-R., Zhu, K., Goli-Malekabadi, Z., et al. (2016). Bioprinting 3D Microfibrous Scaffolds for Engineering Endothelialized Myocardium and Heart-On-A-Chip. *Biomaterials* 110, 45–59. doi:10.1016/j.biomaterials.2016.09.003

Zhang, C.-L., Huang, T., Wu, B.-L., He, W.-X., and Liu, D. (2017). Stem Cells in Cancer Therapy: Opportunities and Challenges. *Oncotarget* 8, 75756–75766. doi:10.18632/oncotarget.20798

Zhang, T., Chen, H., Zhang, Y., Zan, Y., Ni, T., Liu, M., et al. (2019). Photo-crosslinkable, Bone Marrow-Derived Mesenchymal Stem Cells-Encapsulating Hydrogel Based on Collagen for Osteogenic Differentiation. *Colloids Surf. B: Biointerfaces* 174, 528–535. doi:10.1016/j.colsurfb.2018.11.050

Zhu, P., and Wang, L. (2017). Passive and Active Droplet Generation with Microfluidics: a Reviewfluidics: A Review. *Lab. Chip* 17, 34–75. doi:10.1039/c6lc01018k

Zhu, W., Holmes, B., Glazer, R. I., and Zhang, L. G. (2016). 3D Printed Nanocomposite Matrix for the Study of Breast Cancer Bone Metastasis. *Nanomed. Nanotechn. Biol. Med.* 12 (1), 69–79. doi:10.1016/j.nano.2015.09.010

Conflict of Interest: The authors declare that the research was conducted in the absence of any commercial or financial relationships that could be construed as a potential conflict of interest.

Publisher's Note: All claims expressed in this article are solely those of the authors and do not necessarily represent those of their affiliated organizations, or those of the publisher, the editors and the reviewers. Any product that may be evaluated in this article, or claim that may be made by its manufacturer, is not guaranteed or endorsed by the publisher.

frontiers in Bioengineering and Biotechnology

BRIEF RESEARCH REPORT
published: 28 January 2022
doi: 10.3389/fbioe.2021.816089

One-Step Generation and Purification of Cell-Encapsulated Hydrogel Microsphere With an Easily Assembled Microfluidic Device

Tao Zhang[1,2]*, *Hong Zhang*[3,4], *Wuping Zhou*[1,2], *Keming Jiang*[1,2], *Cong Liu*[2], *Ru Wang*[5], *Yuanshuai Zhou*[3], *Zhiqiang Zhang*[2], *Qian Mei*[2], *Wen-Fei Dong*[1,2]*, *Minxuan Sun*[1,3]* and *Haiwen Li*[2]*

[1]School of Biomedical Engineering (Suzhou), Division of Life Sciences and Sciences and Medicine, University of Science and Technology of China, Hefei, China, [2]CAS Key Lab of Bio-Medical Diagnostics, Suzhou Institute of Biomedical Engineering and Technology, Chinese Academy of Science, Suzhou, China, [3]Jiangsu Key Laboratory of Medical Optics, Suzhou Institute of Biomedical Engineering and Technology, Chinese Academy of Sciences, Suzhou, China, [4]School of Life Sciences, Shanghai University, Shanghai, China, [5]School of Life Science and Technology, Changchun University of Science and Technology, Changchun, China

OPEN ACCESS

Edited by:
Raffaele Vecchione,
Italian Institute of Technology (IIT), Italy

Reviewed by:
Brunella Corrado,
University of Naples Federico II, Italy
Edmondo Battista,
Università degli Studi di Napoli Federico II, Italy

***Correspondence:**
Wen-Fei Dong
wenfeidong@sibet.ac.cn
Minxuan Sun
minxun.sun@sibet.ac.cn
Haiwen Li
lihw@sibet.ac.cn
Tao Zhang
zhangtao@sibet.ac.cn

Specialty section:
This article was submitted to Biomaterials, a section of the journal Frontiers in Bioengineering and Biotechnology

Received: 16 November 2021
Accepted: 29 December 2021
Published: 28 January 2022

Citation:
Zhang T, Zhang H, Zhou W, Jiang K, Liu C, Wang R, Zhou Y, Zhang Z, Mei Q, Dong W-F, Sun M and Li H (2022) One-Step Generation and Purification of Cell-Encapsulated Hydrogel Microsphere With an Easily Assembled Microfluidic Device. Front. Bioeng. Biotechnol. 9:816089. doi: 10.3389/fbioe.2021.816089

Cell-laden hydrogel microspheres with uniform size show great potential for tissue repair and drug screening applications. Droplet microfluidic systems have been widely used for the generation of cell-laden hydrogel microspheres. However, existing droplet microfluidic systems are mostly based on complex chips and are not compatible with well culture plates. Moreover, microspheres produced by droplet microfluidics need demulsification and purification from oil, which requires time and effort and may compromise cell viability. Herein, we present a simple one-step approach for producing and purifying hydrogel microspheres with an easily assembled microfluidic device. Droplets were generated and solidified in the device tubing. The obtained hydrogel microspheres were then transferred to a tissue culture plate filled with cell culture media and demulsified through evaporation of the oil at 37°C. The removal of oil caused the gelled microspheres to be released into the cell culture media. The encapsulated cells demonstrated good viability and grew into tumor spheroids in 12–14 days. Single cell-laden hydrogel microspheres were also obtained and grown into spheroid in 14 days. This one-step microsphere generation method shows good potential for applications in automated spheroid and organoid cultures as well as drug screening, and could potentially offer benefits for translation of cell/microgel technologies.

Keywords: one-step purification, cell-encapsulated, hydrogel microsphere, microfluidic, spheroid

INTRODUCTION

Spheroids are three-dimensional (3D) spherical cellular aggregates that allow cells to interact with neighboring cells and their extracellular matrix. Spheroids can recapitulate cell morphology as well as reproduce gene expression, cell connectivity, and tissue morphology. Compared with two-dimensional models, spheroids are more physiologically relevant and predictive (Du et al., 2008; Dyson, 2019). Spheroids have therefore become the most common and versatile three-dimensional model since they were first used in cell cultures in the 1950s (Dyson, 2019; Boucherit et al., 2020; Sivakumar et al., 2020; Decarli et al., 2021; Roper et al., 2021).

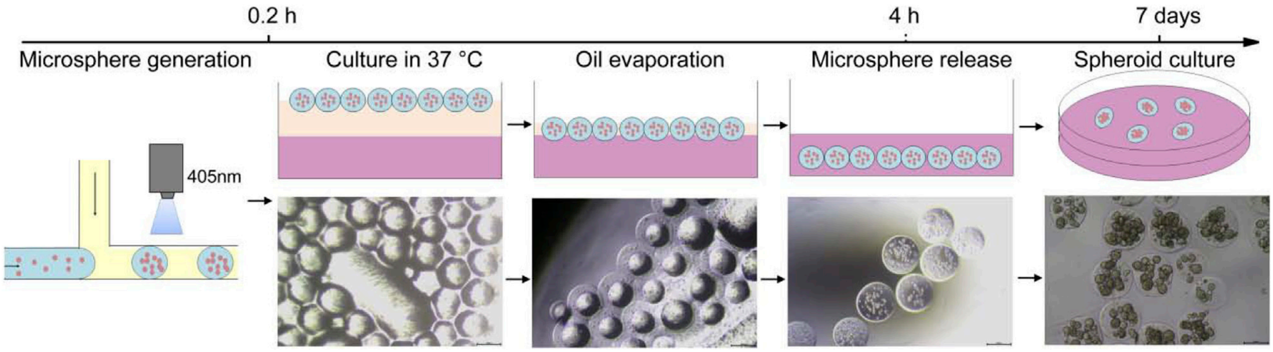

GRAPHICAL ABSTRACT |

Various scaffold-free and scaffold-based approaches have been developed to generate three-dimensional spheroids. Scaffold-free approaches include using hanging drop plates (Kelm et al., 2003; Guo et al., 2014), low cell attachment plates (Ivanov et al., 2015), and emerging techniques such as magnetic levitation (Türker et al., 2018), ultrasound waves, and acoustic waves. Scaffold-free approaches are easy to perform and can be applied to various cell types (Franchi-Mendes et al., 2021). Microfabrication techniques such as photolithography (Du et al., 2008; Brandenberg et al., 2020) and micromolding (Tekin et al., 2011; Tao et al., 2019) have also been used to create spheroids, allowing the volume and shape of spheroids to be precisely controlled. However, most spheroid fabrication approaches require an excessive amount of time and effort, and producing uniform spheroids with a high throughput and in a reproducible manner is particularly challenging.

Droplet microfluidics is a versatile technology that allows for the manipulation of small volumes of liquids on a microfluidic chip (Zhu et al., 2019; Mohamed et al., 2020; Balasubramanian et al., 2021). Previous studies have applied droplet microfluidics in the fields of molecular and cellular biology and analytical chemistry for applications such as clonal development (Dolega et al., 2015), drug screening (Courtney et al., 2017), single-molecule/single-cell analysis (Najah et al., 2012; Shembekar et al., 2018; Shao et al., 2020), tissue engineering (Liu et al., 2018), organoid modeling (Vadivelu et al., 2017; Zhang et al., 2021), and spheroid fabrication (Lopa et al., 2020; Mohamed et al., 2020). Droplet microfluidic technology is especially suitable for 3D cell cultures (Eqbal et al., 2021). Three-dimensional cell culture technology based on microfluidic droplets has many advantages. For instance, droplet size distributions from tens to hundreds of microns allow nutrients and oxygen to effectively diffuse into cells. In addition, droplet microfluidic systems provide high throughput and high controllability, and they can produce uniform cell-encapsulated microspheres with tunable microenvironments in a high throughput manner. Currently, various materials and microfluidic chips have been used to generate hydrogel microspheres for cell culture and spheroid fabrication.

The preparation of microdroplets by microfluidic methods typically uses two incompatible liquids as a continuous phase and a discrete phase, and the generation of droplets is controlled by the microtubule structure and two-phase flow rate ratio of the microfluidic chip. Through precise pressure control, uniform and high-throughput droplet generation can be achieved. The obtained droplets can then be solidified into microspheres by a photosensitive or thermal reaction. After gelation, demulsification and centrifugation are carried out to obtain the encapsulated hydrogel microspheres (Caballero Aguilar et al., 2021). However, this method is complex and time-consuming, and exposing the cells to demulsifiers affects their viability. Alternatively, other studies have used an aqueous two-phase system as a template for hydrogel microspheres generation in water to avoid extra washing steps (Moon et al., 2015; Mao et al., 2017; Liu et al., 2018). However, aqueous two-phase systems require two water phase reagents that are immiscible with each other. Only a limited number of reagent combinations, such as polyethylene glycol and dextran, meet this requirement. Therefore, the limited number of solution combinations hinders the wide application of this technology in cell encapsulation.

To avoid this problem, Choi et al. developed a method for the one-step generation of monodisperse cell-laden hydrogel microspheres. They first generated double emulsion droplets with an ultrathin oil shell, then used UV light to solidify the droplets. After polymerization of the inner droplets, the thin oil shells of the double emulsion droplets gradually wet and subsequently transfer into the aqueous solution. This results in hydrogel microspheres dispersed in the aqueous phase without extra washing steps (Choi et al., 2016). However, this method requires complex microfluidic control and is not compatible with conventional cell culture plate systems. Recently, on-chip methods for the generation and purification of hydrogel microspheres in an integrated microfluidic chip have been developed (Deng et al., 2011; Hong et al., 2012; Choi et al., 2016; Mohamed et al., 2019). Deng et al. designed filter blocks in a microfluidic chip for on-chip hydrogel microsphere filtration. The filter blocks separated hydrogel microspheres from an oil phase by infusing the oil phase and the aqueous phase. After filtration, the hydrogel microspheres were sequentially maintained by the filter blocks (Deng et al., 2011). In another study, Hong et al. extracted collagen microspheres from a mineral oil phase into a cell culture with an aqueous extraction chamber.

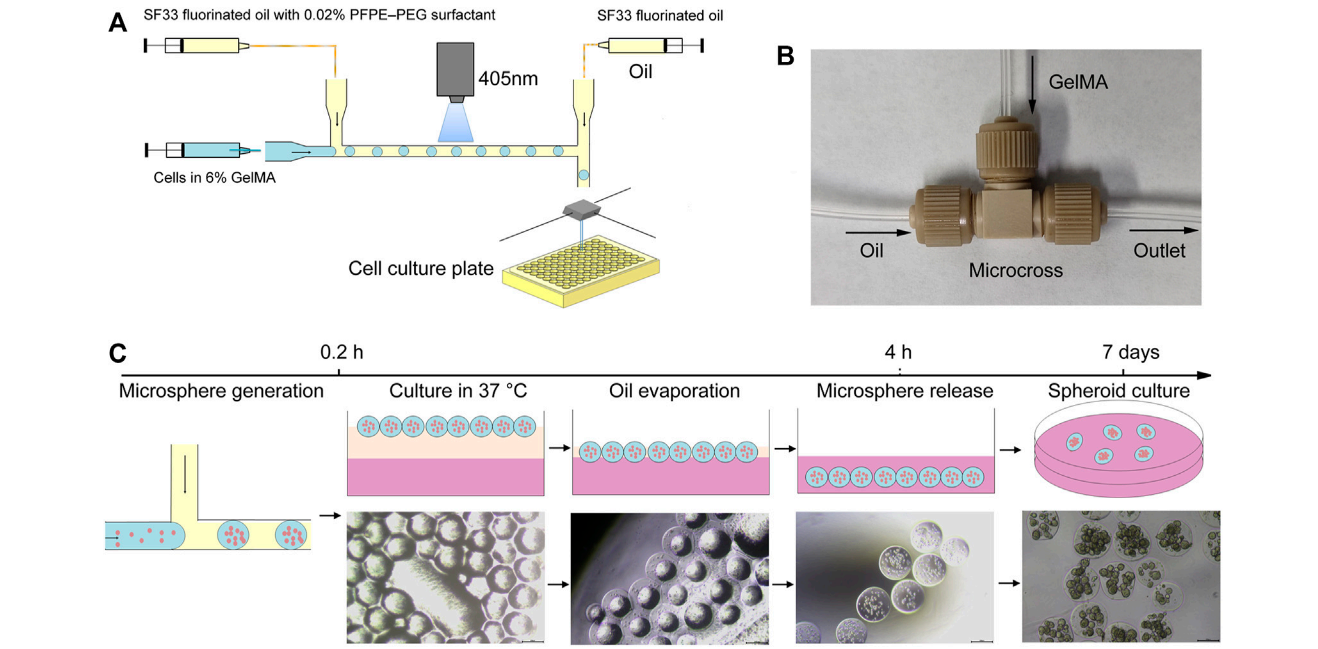

FIGURE 1 | Schematic illustration of the developed microfluidic system for one-step hydrogel microsphere generation. **(A)** Schematic diagram of the microfluidic platform. **(B)** Configuration of the microfluidic chip. **(C)** Generation and separation procedures for obtaining hydrogel microspheres.

The fluid exchange and filter gates on the chip aided the separation and release of the microspheres into the aqueous solution (Hong et al., 2012). Other microfluidic chip-integrated on-chip fabrication and purification methods and off-microfluidic approaches have also been used for hydrogel microsphere purification (Lee et al., 2014). For instance, hydrogel microspheres have filtered by a micropost array to achieve their removal from an oil phase to an aqueous phase (Mohamed et al., 2019). However, these methods require complex chip design and processing steps.

In this study, a simple one-step approach for generating and purifying encapsulated hydrogel microspheres was designed. Droplets were generated with a commercial adapter and solidified in the system's tubing. The hydrogel microspheres were then transferred to a tissue culture plate filled with cell culture media. The gelled microspheres were demulsified through oil evaporation, causing them to be released into the cell culture media. The obtained encapsulated cells maintained good viability and grew into tumor spheroids in 14 days. The one-step microsphere generation method presented herein may have potential application in biomedical fields.

METHODS

Materials

Gelatin methacryloyl (GelMA) and Lithium phenyl(2,4,6-trimethylbenzoyl) phosphinate (LAP) were obtained from Stemeasy Biotech Co., Ltd. (Wuxi, China). HFE7500 fluorinated oil were purchased from 3M Company (Shanghai, China), and SF33 fluorinated oil were purchased from Chemours Co., Ltd. (Shanghai, China). Perfluoropolyether–polyethylene glycol (PFPE–PEG) block-copolymer fluorosurfactants (PEG-based fluorosurfactants) were synthesized as described previously (Holtze et al., 2008). Calcein-AM/PI Double Stain Kit was purchased from Yeasen Biotech Co., Ltd. (Shanghai, China). 0.22 μm filters were purchased from Millipore (Bedford, MA, United States). All other chemicals were analytical grade, and double-distilled water was used throughout the experiments. MicroCross were obtained from IDEX Health & Science LLC (Oak Harbor, WA, United States).

MicroCross Construction and Droplet Generation

A microfluidic T-junction platform was designed and constructed for droplet generation, as shown in **Figure 1**. An IDEX MicroCross T-junction and a fluorinated ethylene-polypropylene (FEP) tube were used for device fabrication. The inner diameter of the MicroCross was 250 μm. HFE7500 fluorinated oil containing 1% PFPE–PEG fluorinated surfactant was selected as the continuous phase and 6% photocrosslinkable gelatin, GelMA in PBS, containing 0.4% photoinitiator LAP was selected as the disperse phase. To generate droplets, the continuous phase and disperse phase were loaded into two syringes (20 and 1 ml, respectively),

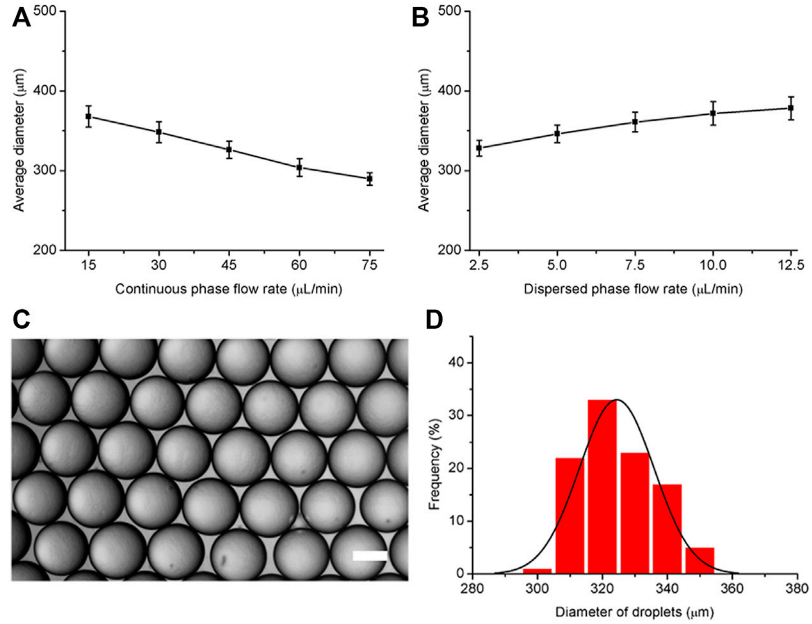

FIGURE 2 | Effects of the disperse phase and continuous phase flow rates on the diameter of generated droplets. **(A)** Variation in droplet diameter with increasing continuous phase flow rate from 15 to 75 μl/min (disperse phase flow rate: 5 μl/min). **(B)** Variation in droplet diameter with increasing disperse phase flow rate from 2.5 to 12.5 μl/min (continuous phase flow rate: 30 μl/min). **(C)** Representative microscopy image of droplets generated by the microfluidic system. **(D)** Size distribution of the droplets. The scale bar represents 200 μm.

which were propelled by peristaltic pumps (Baoding Longer Precision Pump Co., Ltd.). At the junction section, the disperse phase was broken into small droplets under the shear force caused by the continuous phase.

Generation of Cell-Laden Hydrogel Microspheres

HCT116 and U87 cells were digested by trypsin-EDTA and resuspended in DMEM supplemented with 10% FBS at a density of 8×10^6 cells/ml. Photocrosslinkable GelMA and photoinitiator LAP were dissolved in PBS and filtered with a 0.22 μm filter. The disperse phase was prepared by mixing 100 μl cell suspension with 200 μL 12% GelMA and 100 μL 1.6% LAP. A volatile fluorinated oil SF33 with low boiling point (33°C) containing 0.02% PFPE–PEG fluorosurfactant was chosen as the continuous phase. The continuous phase and disperse phase were loaded into two syringes (20 and 1 ml, respectively), which were propelled by peristaltic pumps. Droplets generated at the T-junction were cured using 405 nm light for 15 s. The obtained hydrogel microspheres were transferred to a tissue culture plate filled with cell culture media by an second oil syringe with SF33 fluorinated oil downstream of emulsification. Cells were cultured at 37°C in a humidified 5% CO_2 and 95% air atmosphere.

Cell Viability Assessment

Cell viability was assessed using a commercial Calcein-AM/PI Double Stain Kit (Shanghai Yeasen Biotech. Co., Ltd.) according to the manufacturer's instructions. Live/dead staining solution was prepared by adding 1 μl calcein AM and 3 μL ethidium homodimer into 1 ml assay buffer. The cell-laden hydrogel microspheres were harvested and centrifuged at 1,000 rpm for 5 min. Then, the cell-laden hydrogel microspheres were suspended in assay buffer and stained by live/dead staining solution at room temperature for 20 min. After staining, the hydrogel microspheres were imaged using a fluorescence microscope. The live and dead cell numbers were identified and the ratio of live cells to the total number of cells was determined using ImageJ software (Ma et al., 2017).

Statistical Analysis

Each experiment was performed at least three times. Data were presented as mean± standard deviation. Image analysis, data treatments, and statistical analysis were performed using ImageJ and Origin. Statistical analysis was performed using one-way ANOVA, and statistical significance was established at $p < 0.05$.

RESULTS

Design and Fabrication of the Assembled Microfluidic Platform

To generate and purify cell-encapsulated hydrogel microspheres in one step, we developed an easily assembled microfluidic platform. The microfluidic platform consisted of three major modules: a T-junction microfluidic module for droplets generation, a blue light curing module for on-line hydrogel microsphere gelation, and a microsphere injection module for

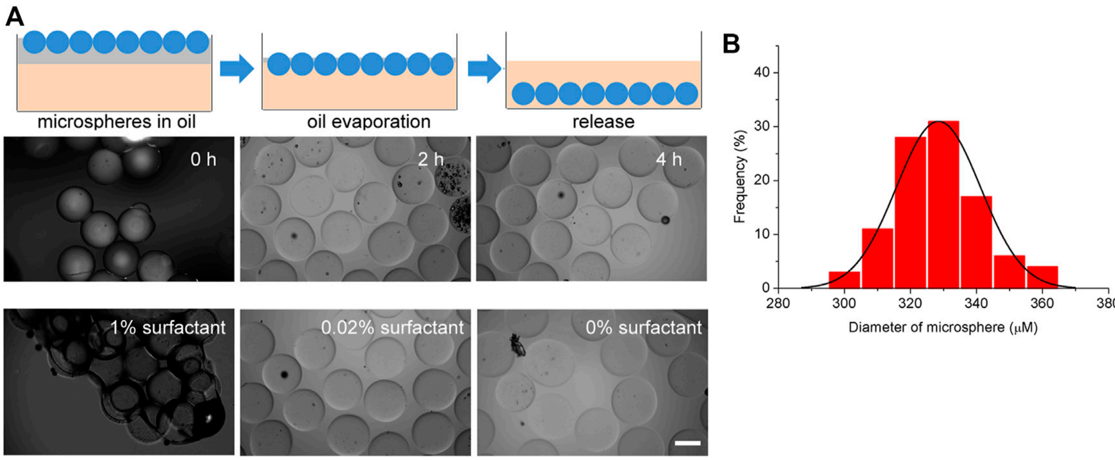

FIGURE 3 | Generation and extraction of hydrogel microspheres. **(A)** Schematic diagram of the microsphere extraction process by oil evaporation. **(B)** Size distribution of the hydrogel microspheres. **(C)** Representative microscopy image of extraction process. The scale bar represents 200 μm.

microsphere distribution and purification (**Figure 1A**). The T-junction microfluidic module was designed and fabricated using commercial IDEX adapters. To generate droplets of an appropriate volume, several adapters were assessed, and micro static mixing T-junction with 250 μm and 150 internal diameter were chosen for droplet generation (**Figure 1B**). After droplet generation, the droplets were immediately solidified using a blue light (wavelength of 405 nm, power density of 2000 mW/cm^2) in the FEP tube (**Supplementary Video S1**). An second oil syringe downstream of emulsification was used to increase the spacing between droplet and distribute the hydrogel microspheres into cell culture plates containing cell culture media. When the microsphere reaches the outlet, the second oil syringe extruded the microsphere into the 96 well plate, and then the tube outlet moved to the next position through the two-dimensional mobile platform, and extruded the next drop of microsphere into the 96 well plate. The cell culture plates were then transferred to a CO_2 incubator. In the 37°C environment, the oil phase gradually evaporated within 4 h, leading to the direct transfer of the gel microspheres into the cell culture media without an additional washing step (**Figure 1C**).

Formation of Emulsion Droplets With the Assembled Microfluidic System

To assess the efficiency of the assembled microfluidic system for droplet generation, HFE7500 fluorinated oil and SF33 fluorinated oil were tested. HFE7500 oil is less volatile and the droplets generated are stable at room temperature. In contrast, SF33 oil is volatile and the droplets are not as stable as droplets generated with HFE7500 oil and some droplets fuse when the droplets gather together. So we chose HFE7500 oil for the initial optimization of fabrication conditions. HFE7500 with 1 wt% PFPE–PEG fluorosurfactant and 6% GelMA in PBS were loaded into two syringes and propelled by peristaltic pumps. At the T-junction, the disperse phase was broken into small droplets under the shear force generated by the continuous phase.

To evaluate the effect of the continuous phase on droplet generation, the flow rate of the continuous phase was increased from 15 to 75 μl/min while the flow rate of the disperse phase was held constant at 5 μl/min. The results show that the droplet size gradually decreased from 368 to 290 μm as the continuous phase flow rate increased to 75 μl/min (**Figure 2A**). To test the effect of the disperse phase on droplet generation, the flow rate of the disperse phase was increased from 2.5 to 12.5 μl/min while the flow rate of the continuous phase was held constant at 30 μl/min. The results in **Figure 2B** show that the droplet size increased when the flow rate of the disperse phase was increased. These results reveal that the droplet size can be adjusted by the flow rates of the continuous phase and the disperse phase. It was also determined that droplets are less likely to collide and coalescence and the droplet size becomes more uniform with increasing flow rate ratio of the continuous phase to the disperse phase. And the results also indicated that the assembled microfluidic system could generate monodispersed emulsion droplets and the average diameter was 326 ± 11 μm (**Figures 2C,D**).

Production of Monodisperse Hydrogel Microspheres Through Oil Evaporation

To produce monodisperse hydrogel microspheres, a volatile fluorinated oil SF33 with low boiling point (33°C) was used. HFE7500 oil was not used because HFE7500 oil is less volatile and the use of HFE7500 is not compatible with the oil evaportation method. Different from the demulsification and purification methods used before, we report a hydrogel microsphere production method without demulsification and washing steps. After the droplets were generated and solidified by 405 nm light for 15 s in the microfluidic system tubing, the resulting hydrogel microspheres were transferred to a cell culture plate filled with cell culture media. Although the density of fluorinated oil SF33 (1.36 g/ml) was higher than that of culture medium, the microspheres in the fluorinated oil remained on top of the cell

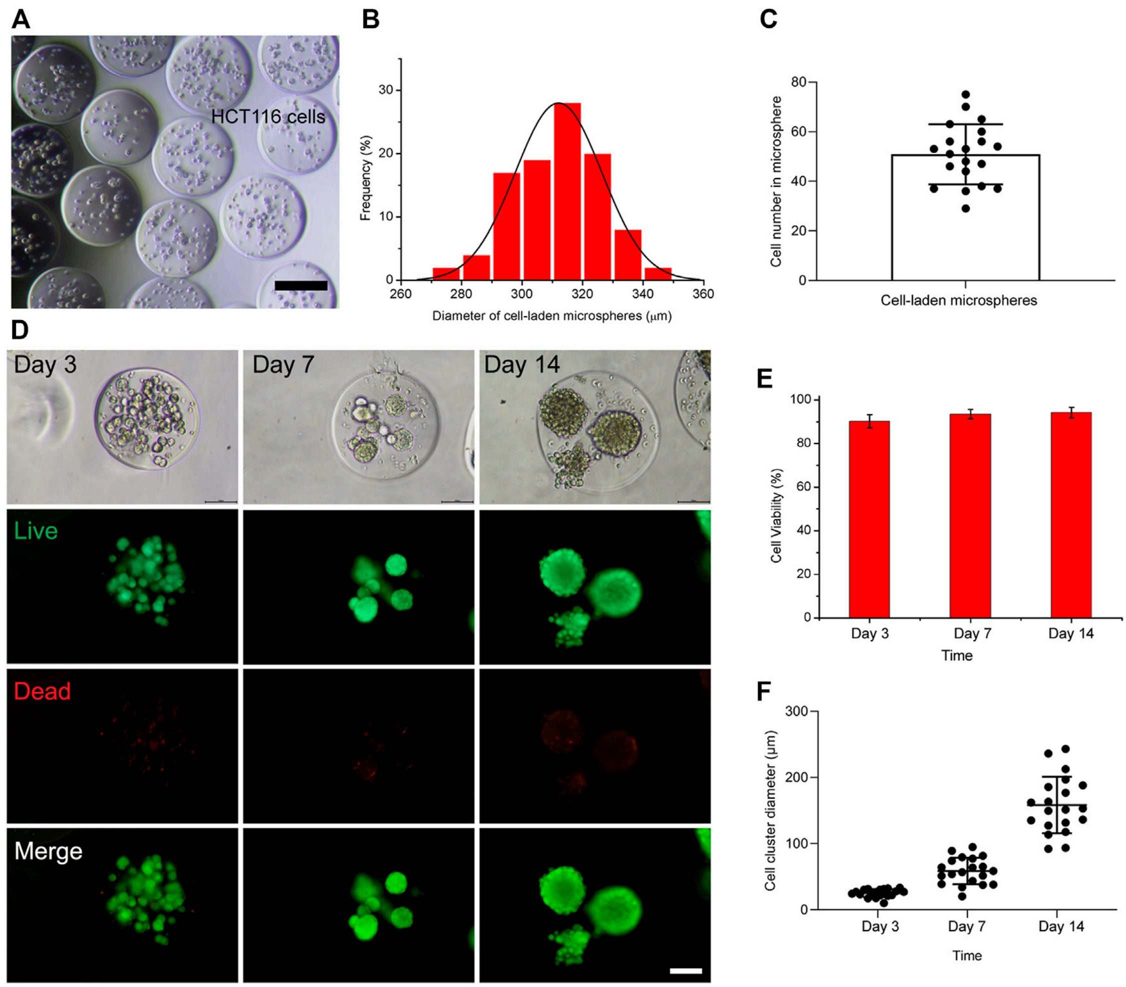

FIGURE 4 | Generation of cell-laden hydrogel microspheres in the microfluidic system. **(A)** Representative image of cell-laden hydrogel microspheres. The scale bar represents 200 μm. **(B)** Size distribution of cell-laden hydrogel microspheres. **(C)** The number of cell-encapsulated in the hydrogel microspheres. **(D)** Fluorescence microscopy image of HCT116-laden hydrogel microspheres after culturing for 3, 7, and 14 days. The scale bar represents 100 μm. **(E)** Percentage viability of encapsulated cells in the hydrogel microspheres of 3, 7, and 14 days. **(F)** The diameter of the cell spheroids formed within the hydrogel microspheres after culturing for 3, 7, and 14 days.

culture media due to interfacial tension. The tissue culture plate was then placed in a 37°C incubator. Because the incubator temperature was higher than the boiling point of the fluorinated oil (33°C), the oil phase evaporated in 4 h, destroying the stability of the surfactant layer on the droplet surfaces. As a result, the hydrogel microspheres were gradually released from the oil phase into the cell culture medium over 4 h (**Figure 3A**). The size distribution of the hydrogel microsphere indicated microspheres were monodisperse and the average diameter was 328 ± 13 μm (**Figure 3B**). It should be noted that the surfactant concentration in the continuous phase should be within an appropriate range. When the surfactant concentration is lower than 0.02%, droplet coalescence occurs before photocuring takes place. When the surfactant concentration is too high, such as 1%, the microspheres aggregate together after oil partially evaporation. Microspheres hang on the surface of the aqueous phase due to the hydrophobic effect of surfactants and are unable to be released into the aqueous phase (**Figure 3C**).

Generation of Tumor Spheroid Using the Microfluidic Platform

The utility of the hydrogel microsphere production method for the generation of tumor spheroid was studied. HCT116 cells were suspended in 6% GelMA and encapsulated into droplets (**Figure 4A**). The size distribution of these hydrogel microspheres was then measured. As shown in **Figure 4B**, the average diameter of the cell-laden hydrogel microspheres was 313 μm within a 5% coefficient of variation, indicating that they were homogeneous. The number of cell-encapsulated in the microspheres was 50 ± 12 μm (**Figure 4C**). Cell viability was evaluated after encapsulation, and the results show that the HCT116 cells maintained good viability and formed cell clusters in the hydrogel microspheres after 7–14 days of culturing (**Figures 4D–F**).This microfluidic system was further verified with the U87 tumor cell line. In contrast to the densely packed cellular organization formed by HCT116 cells (**Supplementary Figure S1**), the U87 cells behaved completely differently after being encapsulated into hydrogel microspheres. The U87 cells spread out from the hydrogel microspheres after culturing for 12 days (**Supplementary Figure S2**). The cell viability of the encapsulated U87 cells was assessed with a live cell staining kit. The results show that the encapsulated cell viability was comparable to that of non-encapsulated cells, indicating that this microfluidic system is highly biocompatible with 3D cell cultures.

Single cell-laden hydrogel microspheres have been shown to have great potential in the fields of stem cells and tissue engineering. Herein, we generated single U87 tumor cell-laden hydrogel microspheres by adjusting the diameter of the microcross (**Supplementary Figure S3A**). 100 μm microspheres which is the favorable size for single cell applications were generated. Single cell tumor spheroid formed after 14 days culture, and the live cell staining revealed the U87 cells maintained good viability (**Supplementary Figure S3B**).

DISCUSSION

Prior work has documented the potential of droplet microfluidic in spheroid and organoid generation. For example, uniform patient-derived tumor spheroids and engineering human islet organoids have been fabricated using droplet microfluidic based platform (Siltanen et al., 2016; Tao et al., 2019). Droplet microfluidic ensures high-throughput formation of cell-encapsulated hydrogel microspheres of controlled size and cell seeding density by adjusting flow velocity and cell suspension concentration. Morever, droplet microfluidic based platform requires only 30–50% percentage of 3D culture medium compared with traditional 3D culture. Besides, hydrogel microspheres generated by droplet microfluidic can be used combing with other microfluidic device for more complex interdisciplinary studies. However, current technologies for cell-laden microsphere generation need either demulsification and centrifugation or complex microfluidic device to transfer the encapsulated hydrogel microspheres into the culture medium (Caballero Aguilar et al., 2021). These methods are complex and time-consuming, and exposing the cells to demulsifiers affects their viability (Mohamed et al., 2020).

In this study, we developed an easily assembled microfluidic platform for one-step and high-throughput monodisperse hydrogel microsphere preparation and cell encapsulation. Compared with traditional hydrogen microsphere fabrication methods, this method does not require the addition of a demulsifier or other chemicals, reducing the toxic effect on cells and improving the cell survival rate. Evaporation-based microfluidic strategy has been used to produce cell encapsulated hydrogel microsphere. However, evaporation of oil phase resulted in an aggregation of cell encapsulated hydrogel microspheres, and only 40% percentage of cells survive after 6 days culture (Fan et al., 2015). We found that the realization of hydrogel microsphere fabrication without a separate washing step relies on the concentration of surfactant in the oil phase. The surfactant concentration should not be too high, so as to ensure that hydrogel microspheres don't aggregate and can be released into the culture medium. The surfactant concentration also should not be too low, so as to ensure that the droplets do not fuse before gelation. By adjusting the concentration of surfactant, monodisperse hydrogel microspheres were prepared by real-time solidification in the microfluidic system tube, and over 90% percentage of cells keep alive after 14 days culture. It should be noted that the surfactant in the oil phase should be biocompatible, otherwise the residual surfactant after oil volatilization may affect cell survival (Clausell-Tormos et al., 2008).

Several studies have indicated that spheroids above 200 μm undergo core necrosis (Vadivelu et al., 2017; Corrado et al., 2019). Due to the limitation of mass transport, cells encapsulated in the hydrogel microspheres suffer from different levels of waste products, low nutrients and even hypoxia. Hypoxia may induce cell death in the hydrogel microspheres of a few hundred micrometers (Ling et al., 2007). Previous study indicated that the microsphere diffusivity depends on the microsphere size relative to the network pore size and also on the stress relaxation dynamics of the network. The diffusion of nutrients, growth factors and other molecules in hydrogel can change depending the degree of crosslinking (Burla et al., 2020). Studies also indicated that the concentration of GelMA and its degree of crosslinking are inversely proportional to the degree of porosity and the network pore size, and the decrease of gel concentration is correlated with decreased stiffness of the gel, which promotes cell proliferation and survival (Cuvellier et al., 2021); [45]. Compared with 7.5–10% GelMA used in previous study, low-concentration (6%) GelMA is chosen for cell-encapsulated microsphere generation in our study. By reducing the LAP concentration and the UV exposure time, the viability of the cells are improved while keeping the stability of the microsphere. Moreover, we found that low-concentration gelma microspheres were more likely to aggregate when separated by demulsification and centrifugation, while the microspheres were more likely to disperse rather than aggregate through the oil-phase evaporation and hydrophilic adsorption separation.

Besides, the assembled microfluidic platform is compatible with existing 96 well plates and other cell culture systems, which is conducive to the realization of high-throughput three-dimensional culturing and screening. This method is expected to have important application value in the fields of tumor high-throughput drug screening and organoid preparation.

However, some limitations are worth noting. Cells such as HCT116 generated more than one cluster in one microsphere. Similar results has also been reported in prevrious study (Choi et al., 2016). This may affects the uniform of spheroid generated. Recently, cell aggregation in low-concentration matrigel has been used for uniform spheroids generation. Cells sediment by gravity and aggregate into tumor spheroids (Brandenberg et al., 2020). Cell aggregation for uniform spheroids generation in droplet microfluidic should be further evaluated. It also should be noted that many of the encapsulated cells in the system were located in a non-central position in the hydrogel microspheres, resulting in the partial encapsulation of the cells and allowing some cells to escape into the cell culture. Non-central encapsulation can lead to asymmetric biomechanical stimuli and biochemical culture conditions, which may affect the uniformity of the generated spheroids or organoids. Hence, a strategy for centering the encapsulated cells in the hydrogel microspheres for long-term 3D culturing needs to be developed in the future.

DATA AVAILABILITY STATEMENT

The original contributions presented in the study are included in the article/**Supplementary Material**, further inquiries can be directed to the corresponding authors.

AUTHOR CONTRIBUTIONS

TZ: Conceptualization, Methodology, Investigation, Formal analysis, Writing—original draft. HZ: Investigation, Formal analysis. WZ: Visualization. KJ: Validation. CL: Software. RW: Investigation. YZ: Resources. ZZ: Resources. QM: Validation. W-FD: Supervision. MS: Conceptualization, Funding acquisition, Writing—review and editing. HL: Funding acquisition, Writing—review and editing.

FUNDING

This work was supported by grants from the Major Science and Technology Innovation Program of Shandong Province (2019JZZY020910), the Primary Research & Development Plan of Jiangsu Province (BE2019051), the National key research development program of China (2017YFF0108604) and the Medical engineering combined program of Sibet (Y851411105).

SUPPLEMENTARY MATERIAL

The Supplementary Material for this article can be found online at: https://www.frontiersin.org/articles/10.3389/fbioe.2021.816089/full#supplementary-material

REFERENCES

Balasubramanian, S., Chen, J., Wigneswaran, V., Bang-Berthelsen, C. H., and Jensen, P. R. (2021). Droplet-Based Microfluidic High Throughput Screening of Corynebacterium Glutamicum for Efficient Heterologous Protein Production and Secretion. *Front. Bioeng. Biotech.* 9. doi:10.3389/fbioe.2021.668513

Boucherit, N., Gorvel, L., and Olive, D. (2020). 3D Tumor Models and Their Use for the Testing of Immunotherapies. *Front. Immunol.* 11. doi:10.3389/fimmu.2020.603640

Brandenberg, N., Hoehnel, S., Kuttler, F., Homicsko, K., Ceroni, C., Ringel, T., et al. (2020). High-throughput Automated Organoid Culture via Stem-Cell Aggregation in Microcavity Arrays. *Nat. Biomed. Eng.* 4 (9), 863–874. doi:10.1038/s41551-020-0565-2

Burla, F., Sentjabrskaja, T., Pletikapic, G., van Beugen, J., and Koenderink, G. H. (2020). Particle Diffusion in Extracellular Hydrogels. *Soft Matter* 16 (5), 1366–1376. doi:10.1039/c9sm01837a

Caballero Aguilar, L. M., Duchi, S., Onofrillo, C., O'Connell, C. D., Di Bella, C., and Moulton, S. E. (2021). Formation of Alginate Microspheres Prepared by Optimized Microfluidics Parameters for High Encapsulation of Bioactive Molecules. *J. Colloid Interf. Sci.* 587, 240–251. doi:10.1016/j.jcis.2020.12.026

Choi, C.-H., Wang, H., Lee, H., Kim, J. H., Zhang, L., Mao, A., et al. (2016). One-step Generation of Cell-Laden Microgels Using Double Emulsion Drops with a Sacrificial Ultra-thin Oil Shell. *Lab. Chip* 16 (9), 1549–1555. doi:10.1039/c6lc00261g

Clausell-Tormos, J., Lieber, D., Baret, J.-C., El-Harrak, A., Miller, O. J., Frenz, L., et al. (2008). Droplet-based Microfluidic Platforms for the Encapsulation and Screening of Mammalian Cells and Multicellular Organisms. *Chem. Biol.* 15 (5), 427–437. doi:10.1016/j.chembiol.2008.04.004

Corrado, B., Gregorio, V., Imparato, G., Attanasio, C., Urciuolo, F., and Netti, P. A. (2019). A Three-dimensional Microfluidized Liver System to Assess Hepatic Drug Metabolism and Hepatotoxicity. *Biotechnol. Bioeng.* 116 (5), 1152–1163. doi:10.1002/bit.26902

Courtney, M., Chen, X., Chan, S., Mohamed, T., Rao, P. P. N., and Ren, C. L. (2017). Droplet Microfluidic System with On-Demand Trapping and Releasing of Droplet for Drug Screening Applications. *Anal. Chem.* 89 (1), 910–915. doi:10.1021/acs.analchem.6b04039

Cuvellier, M., Ezan, F., Oliveira, H., Rose, S., Fricain, J.-C., Langouët, S., et al. (2021). 3D Culture of HepaRG Cells in GelMa and its Application to Bioprinting of a Multicellular Hepatic Model. *Biomaterials* 269. doi:10.1016/j.biomaterials.2020.120611

Decarli, M. C., Amaral, R., Dos Santos, D. P., Tofani, L. B., Katayama, E., Rezende, R. A., et al. (2021). Cell Spheroids as a Versatile Research Platform: Formation Mechanisms, High Throughput Production, Characterization and Applications. *Biofabrication* 13 (3). doi:10.1088/1758-5090/abe6f2

Deng, Y., Zhang, N., Zhao, L., Yu, X., Ji, X., Liu, W., et al. (2011). Rapid Purification of Cell Encapsulated Hydrogel Beads from Oil Phase to Aqueous Phase in a Microfluidic Device. *Lab. Chip* 11 (23), 4117–4121. doi:10.1039/c1lc20494g

Dolega, M. E., Abeille, F., Picollet-D'hahan, N., and Gidrol, X. (2015). Controlled 3D Culture in Matrigel Microbeads to Analyze Clonal Acinar Development. *Biomaterials* 52, 347–357. doi:10.1016/j.biomaterials.2015.02.042

Du, Y., Lo, E., Ali, S., and Khademhosseini, A. (2008). Directed Assembly of Cell-Laden Microgels for Fabrication of 3D Tissue Constructs. *Proc. Natl. Acad. Sci.* 105 (28), 9522–9527. doi:10.1073/pnas.0801866105

Dyson, P. J. (2019). The Rise of 3D Cellular Spheroids: Efficient Culture via Upward Growth from a Superamphiphobic Surface. *Natl. Sci. Rev.* 6 (6), 1068–1069. doi:10.1093/nsr/nwz158

Eqbal, M. D., Naaz, F., Sharma, K., and Gundabala, V. (2021). Microfluidics-based Generation of Cell Encapsulated Microbeads in the Presence of Electric fields and Spatio-Temporal Viability Studies. *Colloid Surf. B* 208, 112065. doi:10.1016/j.colsurfb.2021.112065

Fan, R., Naqvi, K., Patel, K., Sun, J., and Wan, J. (2015). Evaporation-based Microfluidic Production of Oil-free Cell-Containing Hydrogel Particles. *Biomicrofluidics* 9 (5), 052602. doi:10.1063/1.4916508

Franchi-Mendes, T., Lopes, N., and Brito, C. (2021). Heterotypic Tumor Spheroids in Agitation-Based Cultures: A Scaffold-free Cell Model that Sustains Long-Term Survival of Endothelial Cells. *Front. Bioeng. Biotech.* 9. doi:10.3389/fbioe.2021.649949

Guo, W. M., Loh, X. J., Tan, E. Y., Loo, J. S. C., and Ho, V. H. B. (2014). Development of a Magnetic 3D Spheroid Platform with Potential Application for High-Throughput Drug Screening. *Mol. Pharmaceutics* 11 (7), 2182–2189. doi:10.1021/mp5000604

Holtze, C., Rowat, A. C., Agresti, J. J., Hutchison, J. B., Angilè, F. E., Schmitz, C. H. J., et al. (2008). Biocompatible Surfactants for Water-In-Fluorocarbon Emulsions. *Lab. Chip* 8 (10), 1632–1639. doi:10.1039/b806706f

Hong, S., Hsu, H.-J., Kaunas, R., and Kameoka, J. (2012). Collagen Microsphere Production on a Chip. *Lab. Chip* 12 (18), 3277–3280. doi:10.1039/c2lc40558j

Ivanov, D. P., Parker, T. L., Walker, D. A., Alexander, C., Ashford, M. B., Gellert, P. R., et al. (2015). *In Vitro* co-culture Model of Medulloblastoma and Human Neural Stem Cells for Drug Delivery Assessment. *J. Biotechnol.* 205, 3–13. doi:10.1016/j.jbiotec.2015.01.002

Kelm, J. M., Timmins, N. E., Brown, C. J., Fussenegger, M., and Nielsen, L. K. (2003). Method for Generation of Homogeneous Multicellular Tumor Spheroids Applicable to a Wide Variety of Cell Types. *Biotechnol. Bioeng.* 83 (2), 173–180. doi:10.1002/bit.10655

Lee, D.-H., Jang, M., and Park, J.-K. (2014). Rapid One-step Purification of Single-Cells Encapsulated in Alginate Microcapsules from Oil to Aqueous Phase Using a Hydrophobic Filter Paper: Implications for Single-Cell Experiments. *Biotechnol. J.* 9 (10), 1233–1240. doi:10.1002/biot.201400319

Ling, Y., Rubin, J., Deng, Y., Huang, C., Demirci, U., Karp, J. M., et al. (2007). A Cell-Laden Microfluidic Hydrogel. *Lab. Chip* 7 (6), 756–762. doi:10.1039/b615486g

Liu, H. T., Wang, H., Wei, W. B., Liu, H., Jiang, L., and Qin, J. H. (2018). A Microfluidic Strategy for Controllable Generation of Water-In-Water Droplets as Biocompatible Microcarriers. *Small* 14 (36), e1801095. doi:10.1002/smll.201801095

Lopa, S., Piraino, F., Talò, G., Mainardi, V. L., Bersini, S., Pierro, M., et al. (2020). Microfluidic Biofabrication of 3D Multicellular Spheroids by Modulation of Non-geometrical Parameters. *Front. Bioeng. Biotechnol.* 8, 366. doi:10.3389/fbioe.2020.00366

Ma, T., Gao, X., Dong, H., He, H., and Cao, X. (2017). High-throughput Generation of Hyaluronic Acid Microgels via Microfluidics-Assisted Enzymatic Crosslinking And/or Diels-Alder Click Chemistry for Cell Encapsulation and Delivery. *Appl. Mater. Today* 9, 49–59. doi:10.1016/j.apmt.2017.01.007

Mao, A. S., Shin, J.-W., Utech, S., Wang, H., Uzun, O., Li, W., et al. (2017). Deterministic Encapsulation of Single Cells in Thin Tunable Microgels for Niche Modelling and Therapeutic Delivery. *Nat. Mater* 16 (2), 236–243. doi:10.1038/nmat4781

Mohamed, M. G. A., Ambhorkar, P., Samanipour, R., Yang, A., Ghafoor, A., and Kim, K. (2020). Microfluidics-based Fabrication of Cell-Laden Microgels. *Biomicrofluidics* 14 (2), 021501. doi:10.1063/1.5134060

Mohamed, M. G. A., Kheiri, S., Islam, S., Kumar, H., Yang, A., and Kim, K. (2019). An Integrated Microfluidic Flow-Focusing Platform for On-Chip Fabrication and Filtration of Cell-Laden Microgels. *Lab. Chip* 19 (9), 1621–1632. doi:10.1039/c9lc00073a

Moon, B.-U., Jones, S. G., Hwang, D. K., and Tsai, S. S. H. (2015). Microfluidic Generation of Aqueous Two-phase System (ATPS) Droplets by Controlled Pulsating Inlet Pressures. *Lab. Chip* 15 (11), 2437–2444. doi:10.1039/c5lc00217f

Najah, M., Griffiths, A. D., and Ryckelynck, M. (2012). Teaching Single-Cell Digital Analysis Using Droplet-Based Microfluidics. *Anal. Chem.* 84 (3), 1202–1209. doi:10.1021/ac202645m

Roper, S. J., Linke, F., Scotting, P. J., and Coyle, B. (2021). 3D Spheroid Models of Paediatric SHH Medulloblastoma Mimic Tumour Biology, Drug Response and Metastatic Dissemination. *Sci. Rep-uk* 11 (1). doi:10.1038/s41598-021-83809-6

Shao, F., Yu, L., Zhang, Y., An, C., Zhang, H., Zhang, Y., et al. (2020). Microfluidic Encapsulation of Single Cells by Alginate Microgels Using a Trigger-Gellified Strategy. *Front. Bioeng. Biotechnol.* 8, 583065. doi:10.3389/fbioe.2020.583065

Shembekar, N., Hu, H., Eustace, D., and Merten, C. A. (2018). Single-Cell Droplet Microfluidic Screening for Antibodies Specifically Binding to Target Cells. *Cel Rep.* 22 (8), 2206–2215. doi:10.1016/j.celrep.2018.01.071

Siltanen, C., Yaghoobi, M., Haque, A., You, J., Lowen, J., Soleimani, M., et al. (2016). Microfluidic Fabrication of Bioactive Microgels for Rapid Formation and Enhanced Differentiation of Stem Cell Spheroids. *Acta Biomater.* 34, 125–132. doi:10.1016/j.actbio.2016.01.012

Sivakumar, H., Devarasetty, M., Kram, D. E., Strowd, R. E., and Skardal, A. (2020). Multi-Cell Type Glioblastoma Tumor Spheroids for Evaluating Sub-population-specific Drug Response. *Front. Bioeng. Biotechnol.* 8, 538663. doi:10.3389/fbioe.2020.538663

Tao, T., Wang, Y., Chen, W., Li, Z., Su, W., Guo, Y., et al. (2019). Engineering Human Islet Organoids from iPSCs Using an Organ-On-Chip Platform. *Lab. Chip* 19 (6), 948–958. doi:10.1039/c8lc01298a

Tekin, H., Tsinman, T., Sanchez, J. G., Jones, B. J., Camci-Unal, G., Nichol, J. W., et al. (2011). Responsive Micromolds for Sequential Patterning of Hydrogel Microstructures. *J. Am. Chem. Soc.* 133 (33), 12944–12947. doi:10.1021/ja204266a

Türker, E., Demirçak, N., and Arslan-Yildiz, A. (2018). Scaffold-free Three-Dimensional Cell Culturing Using Magnetic Levitation. *Biomater. Sci.* 6 (7), 1745–1753. doi:10.1039/c8bm00122g

Vadivelu, R. K., Kamble, H., Shiddiky, M. J. A., and Nguyen, N.-T. (2017). Microfluidic Technology for the Generation of Cell Spheroids and Their Applications. *Micromachines-Basel* 8 (4). doi:10.3390/mi8040094

Zhang, W. J., Li, D. H., Jiang, S. W., Galan, E. A., and Jiang, S. W., (2021). Microfluidic Droplets as Structural Templates for Matrigel to Enable 1-week Large Organoid Modeling. *Chem. Eng. Sci.* 238. doi:10.1016/j.ces.2021.116632

Zhu, K., Yu, Y., Cheng, Y., Tian, C., Zhao, G., and Zhao, Y. (2019). All-Aqueous-Phase Microfluidics for Cell Encapsulation. *ACS Appl. Mater. Inter.* 11 (5), 4826–4832. doi:10.1021/acsami.8b19234

Conflict of Interest: The authors declare that the research was conducted in the absence of any commercial or financial relationships that could be construed as a potential conflict of interest.

Publisher's Note: All claims expressed in this article are solely those of the authors and do not necessarily represent those of their affiliated organizations, or those of the publisher, the editors, and the reviewers. Any product that may be evaluated in this article, or claim that may be made by its manufacturer, is not guaranteed or endorsed by the publisher.

frontiers in Bioengineering and Biotechnology

ORIGINAL RESEARCH
published: 09 March 2022
doi: 10.3389/fbioe.2022.851893

Engineered Bacterial Cellulose Nanostructured Matrix for Incubation and Release of Drug-Loaded Oil in Water Nanoemulsion

Concetta Di Natale[1,2,3], Vincenza De Gregorio[1,2], Elena Lagreca[2,3], Francesca Mauro[2,3], Brunella Corrado[1,2], Raffaele Vecchione[2] and Paolo Antonio Netti[1,2,3]*

[1]Interdisciplinary Research Centre on Biomaterials, University of Naples Federico II, Naples, Italy, [2]Istituto Italiano di Tecnologia, Naples, Italy, [3]Department of Chemical Materials, Industrial Production Engineering, University of Naples Federico II, Naples, Italy

Bacterial cellulose (BC) is a highly pure form of cellulose produced by bacteria, which possesses numerous advantages such as good mechanical properties, high chemical flexibility, and the ability to assemble in nanostructures. Thanks to these features, it achieved a key role in the biomedical field and in drug delivery applications. BC showed its ability to modulate the release of several drugs and biomolecules to the skin, thus improving their clinical outcomes. This work displays the loading of a 3D BC nanonetwork with an innovative drug delivery nanoemulsion system. BC was optimized by static culture of SCOBY (symbiotic colony of bacteria and yeast) and characterized by morphological and ultrastructural analyses, which indicate a cellulose fiber diameter range of 30–50 nm. BC layers were then incubated at different time points with a nanocarrier based on a secondary nanoemulsion (SNE) previously loaded with a well-known antioxidant and anti-inflammatory agent, namely, coenzyme-Q10 (Co-Q10). Incubation of Co-Q10–SNE in the BC nanonetwork and its release were analyzed by fluorescence spectroscopy.

Keywords: bacterial cellulose, drug delivery, nanocellulose network, nanoemulsion, antioxidant

Edited by:
*Xiubo Zhao,
The University of Sheffield,
United Kingdom*

Reviewed by:
*Qing Qing,
Changzhou University, China
Angelina Angelova,
UMR8612 Institut Galien Paris Sud
(IGPS), France*

****Correspondence:***
*Raffaele Vecchione
Raffaele.vecchione@iit.it*

Specialty section:
*This article was submitted to
Biomaterials,
a section of the journal
Frontiers in Bioengineering and
Biotechnology*

Received: *10 January 2022*
Accepted: *03 February 2022*
Published: *09 March 2022*

Citation:
Di Natale C, De Gregorio V, Lagreca E, Mauro F, Corrado B, Vecchione R and Netti PA (2022) Engineered Bacterial Cellulose Nanostructured Matrix for Incubation and Release of Drug-Loaded Oil in Water Nanoemulsion. Front. Bioeng. Biotechnol. 10:851893. doi: 10.3389/fbioe.2022.851893

1 INTRODUCTION

In the last few years, the choice of appropriate drug delivery systems has achieved great attention in the pharmaceutical field. A successful drug delivery is influenced by several factors (La Manna et al., 2021b; Di Natale et al., 2021d) including the identification of a suitable biomaterial (Lagreca et al., 2020) to be used as a building block for the assembly of the final system (Del Valle et al., 2009). For example, very recently, nanostructure plasmalogen-loaded cubosomes or hexosomes were reported as innovative delivery systems for the lipophilic antioxidant compound, opening new opportunities for bioinspired nanoassemblies (Angelova et al., 2021; Mathews et al., 2021). In this context, another interesting material, which is synthesized from bacteria and presents a nanostructured matrix useful for drug encapsulation and release, is the bacterial cellulose (BC); it possesses a great versatility in terms of *in situ* modulation, post-synthesis chemical modifications, biocompatibility, or ease of sterilization (Barud et al., 2016; Carvalho et al., 2019). In addition, it also shows high purity and water absorption capacity, as well as single mechanical properties, good permeability, or resistance to degradation (Badshah et al., 2020; Parte et al., 2020; Gregory et al., 2021). Thanks to these properties, BC is achieving great interest in biomedical research concerning, for example, the wound dressing for skin burns or the microsurgery for the restoration of artificial blood vessels (Klemm et al., 2001; Carvalho et al., 2019). From the chemical point of view, BC is organized in a tridimensional (3D) nanofibrillar network, and this singular property makes it a suitable macromolecular support for drug encapsulation and, therefore, for the development of specific controlled release systems (Tan et al., 2019). Several studies displayed the ability of BC networks to modulate the release and bioavailability of drugs in percutaneous administration, and hence, they were suggested as supports for topical or transdermal drug delivery (Almeida et al., 2014). For example, BC fibers loaded with silver nanoparticles, in topic formulations, demonstrated an antibacterial activity up to 99.99% against *Escherichia coli* and *Staphylococcus aureus* (Fortunati et al., 2014; Volova et al., 2018). Other studies instead showed the ability of nanofibrils as aerogels to encapsulate drugs such as anti-inflammatories, anticancer, steroids or biomolecules as peptides, and proteins or antibodies (Gopi et al., 2018). Apart from drug loading, the possibility of regulating their release is also remarkable, and BC nanofibers revealed the ability to modulate the release of both hydrophobic and hydrophilic compounds, thus providing versatile materials with respect to drug delivery (Picheth et al., 2017). Several studies, indeed, revealed as BC nanofibers can allow a sustained and controlled release of antioxidant molecules such as quercetin and vanillic or cinammic acid for food or cosmetic applications (Trombino et al., 2008; Li et al., 2019; Morais et al., 2019).

The present work proposes a method to load the BC nanonetwork with stabilized lipophilic compounds and allow its release in a time frame of hours which is compliant with skin applications. To the best of our knowledge, no Co-Q10 nanocarrier has ever been encapsulated within cellulose fibers. In detail, we used an ultra-stable oil-in-water (O/W) SNE coated by a thin layer of chitosan (CT) (Vecchione et al., 2016a; Vecchione et al., 2016b; Vecchione et al., 2014), a positively charged polyelectrolyte, able to encapsulate lipophilic molecules such as curcumin (Fotticchia et al., 2017; Vecchione et al., 2017; Langella et al., 2018; Vecchioneet al. 2016), lycopene (Quagliariello et al., 2018), and Co-Q10 (Quagliariello et al., 2020). In the latter stage of work, the nanocarriers were loaded with Co-Q10 acting as antioxidant and anti-inflammatory agents meant for oral delivery, proving high loading capability and molecular stability preservation. However, Co-Q10 is also very well-known as an antioxidant for skin applications (El-Leithy et al., 2017). Starting from these considerations, here, we propose the development of a BC-Co-Q10-SNE nanonetwork for a double release approach where the cellulose network releases the Co-Q10–loaded SNE which, upon degradation, can finally release active Co-Q10 to the skin. Our BC was produced by the SCOBY using optimized conditions in terms of humidity (98%) and temperature (30°C), as well as the culture media volume that assured the correct moist status, avoiding the production of a thick layer with BC exfoliation (Alkhalifawi and Hassan, 2014; Lahiri et al., 2021). Several spectroscopic techniques such as scanning electron microscopy (SEM) and infrared ray (IR) were used for BC morphological and chemical characterizations, while Co-Q10-SNE loading and release were studied by confocal microscopy and fluorescence, respectively, by following Co-Q10 autofluorescence.

This study aims to be a proof of concept for a new use of BC as a drug delivery system; future analysis will indeed focus on the production of inflamed micro-tissues which will subsequently be treated with the BC-Co-Q10-SNE described in this study.

2 MATERIAL AND METHODS

2.1 Materials

Both soybean oil (density at 20°C of $0.922\,g\,ml^{-1}$) and the surfactant Lipoid E80 (egg lecithin powder 80–85% enriched with phosphatidyl choline (PC) and 7–9.5% content in phosphatidyl ethanolamine (PE)) were purchased from Lipoid GmbH and used without further purification. Millipore Milli-Q water was used for the preparation of all nanoemulsions and solutions. Chitosan (CT, LMW 90–150 kDa, and DDA 84% determined *via* 1H-NMR) was purchased from Sigma-Aldrich (Milan, Italy). Ubidecarenone, coenzyme-Q10 (Co-Q10), was kindly offered by the Faravelli Group. Kombucha SCOBY was purchased from KEFIRA, and glucose and agar were purchased from Sigma-Aldrich.

2.2 Methods

2.2.1 Media Preparation and SCOBY Culture

For Kombucha SCOBY (KEFIRA) culture, a tea broth and an agar plate were prepared with the following protocol: 860 ml of deionized water (dH_2O) was boiled before adding 140 g/L of glucose; 10 sachets (20 g) of black tea were added and steeped for 10 min. Consequently, the tea bags were removed, and the sweetened tea was cooled at room temperature; then, apple vinegar (140 ml/L) was added. The medium was autoclaved at 121°C for 15 min. For solid medium, the agar was autoclaved separately. To improve the fermentation process of the SCOBY, one piece (1 × 1 cm) of the SCOBY was aseptically added into the liquid broth and cultured for 3 days. Then, an aliquot of 1 ml of the previously fermented SCOBY, which acts as a starter, was inoculated into the culture broth at a concentration of 0.05% (1 ml/20 ml). For BC production, starters of the SCOBY were cultured in 50 ml tubes, and two different experimental phases were performed: uncontrolled fermentation conditions (UCC) and controlled fermentation conditions (CC). For the CC, the static fermentation process took place in a dark CO_2 incubator in a controlled humidified atmosphere (≥80%) with constant temperature at 30°C for 3 days, in order to guarantee an optimal environment for symbiont growth. The cap of the tube was removed and perforated parafilm, previously sterilized, and was used to cover the lid and increase the exchange of O_2 with the external surface. This process was repeated in triplicates. Tests were performed in triplicates as well. Viable count assay was performed, as reported earlier.

2.2.2 Live/Dead Assay

In order to select the SCOBY pieces to use for the experimental phase, the viability percentage was assessed by using the Live/

Dead BacLight Bacterial Viability Stain Kit (Molecular Probes, Eugene, and OR). First, the best concentration of the viability kit stain mixture (SYTO9 and propidium iodide (PI)) was selected, which allowed us to distinguish live cells from dead cells (SYTO9: PI, 1:2 v/v). Briefly, freshly grown SCOBY pieces were opportunely cut, harvested, and washed three times with 0.85% sodium chloride (NaCl) solution. Then, 30 µl of a mixture of SYTO9 and PI (1:2) was diluted in a final volume of 5 ml, and each SCOBY piece was incubated with 1 ml in darkness for 15 min at room temperature, according to the manufacturer's instructions. The non-viable SCOBY were prepared by 95% ethanol treatment of bacteria for 30 min (positive control). The SCOBY pieces were washed twice with 0.85% NaCl after the treatments and examined under a confocal microscope (Confocal Leica TCS SP5 II femtosecond laser scanning system, Leica). Filters were set to 493–522 nm for SYTO9 and 618–676 nm for PI. Confocal images were obtained with 40x objective (optical zoom 1.5). Each sample was scanned at randomly selected areas as a series of vertical optical sections, each one 0.50 µm thick. Quantitative analyses of each SCOBY piece were carried out by analyzing the digital images of live (green) and dead (red) bacteria by ImageJ software. Each image was divided in regions of interest (ROIs) with comparable areas, and thresholding was performed. The fluorescence intensity per unit area was measured and calculated as the percentage of viable cells. Thereafter, the culture parameter was set, maintaining the temperature at 30°C and the humidity (>98%) for controlled experimental cultures (CCs). To obtain the CC condition, the samples were placed in an incubator at 30°C by inserting a 10-cm high tank with an evaporating surface of 20 cm to obtain constant humidity >80% without water refill during the entire experimental phase. Conversely, for uncontrolled experimental cultures (UCCs), SCOBY pieces were cultured at room temperature (~23°C) and environmental humidity (~50%).

2.2.3 Ultrastructural Characterization of the BC Layer

For ultrastructural analysis of the fibrillar structure of BC, the BC layers obtained by UCC and CC were primarily fixed with 4% paraformaldehyde. Then, it was fixed with 2.5% of glutaraldehyde in 0.1 M of sodium cacodylate and was left for 1–4 h at the room temperature. In due course of time, it was washed thrice for 10 min in 0.1 M sodium cacodylate and sucrose and buffered at the normal temperature. It was then buffered with 1% osmium tetroxide ($OsO_{4)}$ in 0.1 M sodium cacodylate for 1 h at 4°C and afterward again, washed thrice with 0.1 M sucrose buffer solution. Dehydration was performed on the sample using ethanol at 30, 50, 70, and 95% for 15–60 min at 4°C. Finally, 100% of ethanol was applied for 15–60 min at the room temperature thrice. Image analyses were performed by ImageJ software by using the DiameterJ plugin (Hotaling et al., 2015). First of all, the scale bar of the image was measured by using the scale option after using the zoom option from the toolbar. SEM images (1024 × 768 pixels) were obtained, as already described (Di Natale et al., 2019; Bagheri et al., 2021; Di Natale et al., 2021a; Di Natale et al., 2021b; Di Natale et al., 2021c; Di Natale et al., 2021d; Florio et al., 2021; Di Natale et al., 2020a; Di Natale et al., 2020b; La Manna et al., 2021a; La Manna et al., 2021b), and then segmented using the algorithms provided by "DiameterJ Segment" to convert the image into binary forms. Then, segmented images were processed by DiameterJ to measure the diameter of the cellulose bundles and fibers. In addition, DiameterJ was also used to measure the BC network parameters as the mean pore area, porosity percent, and numbers of pores:

$$Mean\ pore\ area = \frac{\text{TOTAL NUMBER OF BLACK PIXEL COUNTED IN PORES}}{\text{TOTAL NUMBER OF PORES IN IMAGE}}, \tag{1}$$

$$\%\ porosity = \frac{\text{TOTAL NUMBER OF BLACK PIXELS}}{\text{TOTAL NUMBER OF PIXELS IN IMAGE}}. \tag{2}$$

2.2.4 Infrared Spectroscopy

The BC chemical structure was confirmed by IR. BC sheet of 1 cm. The measurements were carried out in the range of 500–4,000 cm^{-1} in absorption or transmission modes (64 scans, 4 cm^{-1} resolution) (Thermo Fisher Scientific Instruments, Nicolet 6,700, Waltham, MA, United States). The spectra were subject to ATR correction, smoothing, and baseline correction to be normalized (Di Natale et al., 2021a).

2.2.5 Co-Q10-SNE Production and Characterization

At first, a primary Co-Q10 negatively charged oil-in-water (O/W) nanoemulsion (NE) at 20 wt% of oil concentration was prepared, as previously reported (Vecchione et al., 2014; Quagliariello et al., 2020; Profeta et al., 2021). Briefly, first the oil phase was obtained by adding the surfactant to the soybean oil. For the analysis, 5.8 g of Lipoid E80 was dissolved in 24 ml of soybean oil at 60°C and mixed using the immersion sonicator (Ultrasonic Processor VCX500 Sonic and Materials). An amount of 4.08 g of Co-Q10 was dissolved in the oil phase at 60°C for 1 h, then added dropwise to the aqueous phase (Milli-Q water), and mixed again using the immersion sonicator. The pre-emulsion was passed at 2000 bar through the high-pressure valve homogenizer (Microfluidics M110PS) for three individual cycles to greatly reduce the initial size; then, the reservoir was continuously refilled for 200 steps.

Co-Q10-NE was then functionalized with CT to have a positively charged SNE. In detail, to achieve the secondary emulsion, a first layer of CT was deposited above the primary one by following an already developed procedure (Vecchione et al., 2014; Vecchione et al., 2016). Briefly, a 0.1 M acetic acid solution of CT pH 4 (0.2 wt %) was prepared, and the 20 wt% oil-O/W NE was then added to the CT solution under vigorous stirring for 15 min to allow uniform CT deposition. Final concentrations of oil and CT were 10 and 0.1 wt%, respectively, while the pH of the final NE (SNE) was 4. O/W NE and SNE were characterized by measuring the size, polydispersity index (PDI), and ζ-potential values through a dynamic light scattering (DLS) instrument (Zetasizer ZS, Nanoseries ZEN 3600, Malvern Instruments Ltd., Malvern, United Kingdom, λ = 632.8 nm). All the samples were diluted up to a droplet concentration of approximately 0.025 wt% by using Milli-Q water. A detecting angle of 173 was used. A default refractive index ratio (1.5900) and three runs for each measurement (1 run lasting 100 s) were used in the calculations of the particle size distribution. ζ-potential analysis was carried out by setting 30 runs for each measurement. The morphology of Co-Q10-

SNE was observed by Cryo-TEM analysis. For the preparation of the frozen-hydrated sample, the plunge freezing method was performed. Briefly, a drop of 3 μl of the sample was deposited on 200-mesh holey carbon grids (Ted Pella, United States); then, it was inserted in the chamber of a FEI Vitrobot Mark IV (FEI Company, the Netherland) at 4°C and 90% of humidity. The droplet of the sample was blotted with a filter paper for 1 s (blot force 1, drain time 0.5 s) and then, the grid was plunged into liquid propane. Then, the grid was stored in liquid nitrogen in a grid box until it was finally transferred to a cryo-specimen 626 holder (Gatan, Inc., United States) and loaded into the Cryo-transmission electron microscope for imaging. To obtain the image of the nanocarriers, we used a Tecnai G2 20, a Cryo-TEM transmission electron microscope (FEI Company, the Netherlands) equipped with a LaB6 emitter (acceleration voltage of 200 kV), and recorded with a 2 × 2 k CCD-Eagle 2HS camera. The frozen-hydrated sample is a radiation-sensitive material, so to avoid damaging it, the observation was carried out in a low-dose mode.

2.2.6 Co-Q10-SNE Encapsulation and Release: Confocal Microscopy and Fluorescence

For the experiment, 5 mg of cellulose layers (5 mm diameter) were suspended in 1.5 ml of Co-Q10-SNE and incubated at room temperature at different time points (15 min and 30 min) with a gentle agitation. All the tests were executed in triplicates. All samples were stored at 4°C, and SNE adsorption on cellulose layers was evaluated by confocal microscopy. Samples were imaged using a Leica TCS SP5 STED-CW gated microscope (Leica-Microsystems, Mannheim, Germany) with HCX IRAPO L 25.0 × 0.95 water objective (Di Natale et al., 2020a; Jamaledin et al., 2020; Di Natale et al., 2021a; Battisti et al., 2019; La Manna et al., 2021a). A laser source of 488 nm was used to excite the Co-Q10 in the oil core. Moreover, a semi-quantitative analysis was performed on at least five images for each z-plane to obtain the mean fluorescence intensity of the loaded Co-Q10-SNE. Using ImageJ software, the mean gray value (MGV) of the green channel was measured for each image (Celetti et al., 2016; Di Natale et al., 2018). Co-Q10-SNE release studies were carried out by suspending 5 mg of BC-Co-Q10-SNE in 1.5 ml of water. Samples were incubated at 37°C and shaken under gentle conditions. At fixed time points (15, 30 min, 1, 2, 3, and 24 h), 1 ml of the sample was withdrawn after cellulose layer sedimentation using centrifugation for 5 min at 10,000 rpm (MicroCL21R, Centrifuge, Thermoscientific, United States). The pellet was resuspended in the same volume of fresh buffer. The collected supernatants were analyzed by fluorescence (Microplate Readers Perkin Elmer); the excitation wavelength was 450 nm, and the maximum emission was recorded between 470 and 600 nm. The fluorescence intensity peak was determined at 551 nm. All the tests were executed in triplicates.

3 RESULTS AND DISCUSSION

3.1 Cellulose Production: Morphological and Chemical Characterization

In order to validate the SCOBY (**Figure 1A**) for BC production in static culture, preliminary viability assay was performed by using Live/Dead assay. SCOBY portions (1cmx1cm) were observed under a confocal microscope in the central and peripheral areas, obtaining a reliable measurement of the entire sample. SCOBY pieces on which symbiont viability reaches at least 50% were used for the experimental phase, as reported in representative images and 3D reconstruction (**Figure 1B**). Quantitative analysis of the SCOBY portion showed a viability of 79 ± 3.5% by measuring the intensity of green (for viable bacteria) and red (for non-viable bacteria) fluorescence measured by the area. SCOBY pieces with a strong reduction in the cell viability were not used for the experimental phase (data not showed). Once the SCOBY pieces to use for BC production are selected, two different culture conditions were set: a temperature of 30°C and the humidity >98% for the controlled experimental culture (CC) and room temperature (~23°C) and environmental humidity (~50%) for the uncontrolled experimental culture (UCC). To carry out the morphological characterization of the BC produced in UCC at different stages of maturation, BC layers were produced in static conditions without refreshing the medium. Each layer (about 1 mm thick) was separated from the layer below due to a variation of the medium/air interface and a reduction in the volume of the medium over time with a reduced humidity. The BC layers obtained with this procedure showed different ripeness degrees, starting from the bottom (in direct contact with the liquid suspension) with the lowest ripeness up to the more superficial ones (in direct contact with air), which appear to be, from a macroscopic analysis, more consistent and thicker >1 mm. These tests made it possible to observe a variation in the cellulose consistency based on the degree of maturation whose chemistry was studied by IR spectroscopy. In detail, three layers (internal, intermediate, and external) were obtained at 72 h, and they showed the typical BC peaks (Keshk et al., 2009; Castro et al., 2011; Tabarsa et al., 2017) with the bands at 3,353 cm^{-1} and 2924 cm^{-1} relative to the stretching of the OH and CH groups, respectively; a peak observed at 1738 cm^{-1} and 1,640 cm^{-1} associated with the stretching of the C = O groups, and the bending of the OH groups referred to absorbed water molecules into cellulose fibers, a peak at 1,046 cm^{-1} corresponding to the vibration of the pyranose ring–C–O–C, and the peak at 889 cm^{-1} related to the presence of β-glycosidic bonds (**Figure 2**). The three layers also revealed a similar degree of polymerization with the presence of the peak at 1738 cm^{-1}, even if, its intensity grows as the superficiality of the layer increases (**Figure 2**). To avoid the development of this crosslinked BC, which could hinder the correct SNE incubation, BC was grown under CC conditions, as explained earlier, and the correct maturation level was analyzed by IR. From the morphological analysis, the samples grown under CC conditions appear to have an adequate hydration status, highlighted by the lower degree of compactness, as well as greater transparency. In contrast, the unique layer produced under UCC conditions is thicker and not transparent at all, indicating a greater degree of compactness and less hydration, which is reflected in a greater degree of crosslinking in the IR spectrum (**Figure 3** red spectrum). Spectra of UCC and CC BC obtained at 72 h, corroborated our hypothesis; indeed, BC obtained in CC conditions showed only the maturation peak at 1,640 cm^{-1} (**Figure 3**, violet

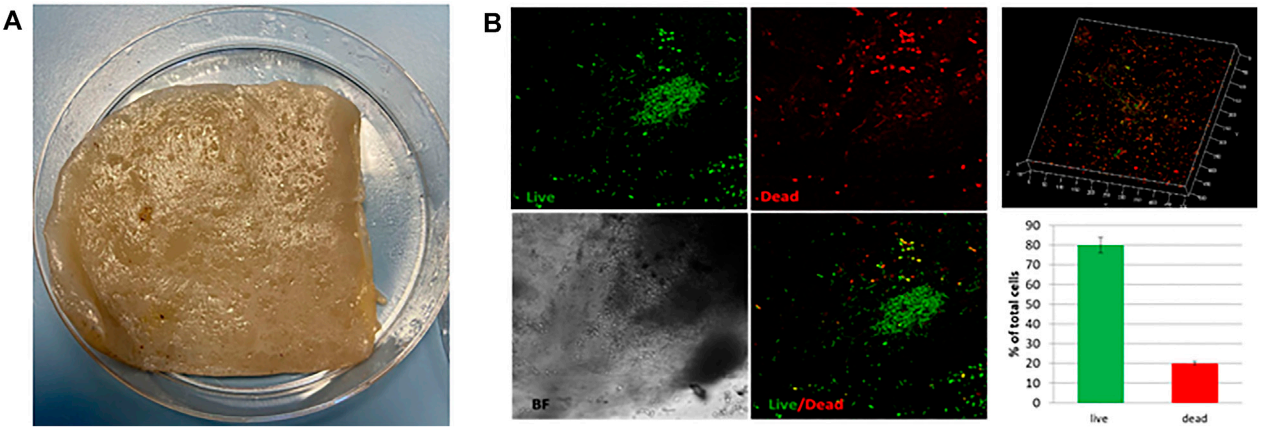

FIGURE 1 | (A) Representative image of the SCOBY portion for BC production. **(B)** Live/Dead fluorescence images of the SCOBY. 3D reconstruction of the observed portion and the percentage of live (green) and dead (red) bacteria.

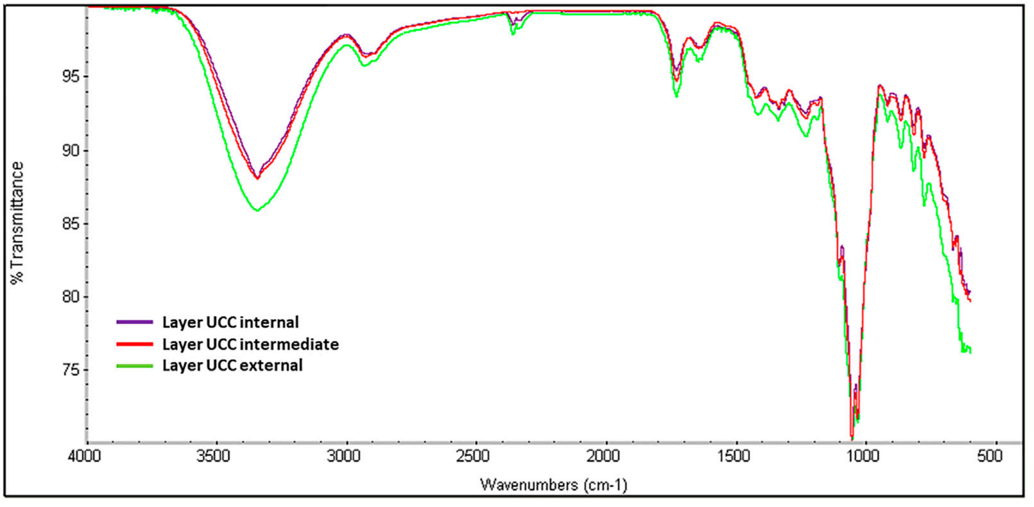

FIGURE 2 | IR analysis of UCC internal, intermediate, and external layers obtained at 72 h.

spectrum) in contrast with the UCC BC which revealed the crosslinked band at 1738 cm^{-1} (**Figure 3** red spectrum). IR spectra strongly confirmed that the moisture content seemed to be directly related to the degree of compactness (revealed by the crosslinking) of BC, demonstrating that the adjusted humidity environment allows reaching a loosening of the cellulose structure useful for nanocarriers' penetration upon incubation.

3.2 Ultrastructural Characterization of BC

To achieve the ultrastructural characterization of the BC produced in UCC or in CC, BC layers were produced in static conditions without refreshing the medium (**Figure 4A**). Representative SEM images showed a different degree of compactness of the cellulose fiber network. In particular, the external layer in UCC highlighted a greater degree of compactness, as shown in **Figure 4B**. Quantitative data of the SEM images showed for the single layer obtained in CC a significantly greater mean pore area and porosity percentage with a smaller number of pores ($p < 0.05$) than the layers obtained in UCC, especially the superficial layer (External). In detail, the porosity values are 39.0, 41.7, and 35.9, while the mean pore area values are 0.0107, 0.0151, and 0.0129 μm^2 for the external, intermediate, and internal layers, respectively, indicating a slight difference between the superficial layer and the most internal layers obtained in UCC although not statistically significant (**Figure 4C**).

At last, all samples showed the fiber diameters in a range of 30–50 nm, and a comparable fiber frequency was also reported (**Figure 4D**), indicating that the main difference among BC produced by the SCOBY is in assembly of the fiber rather than in the single fibers.

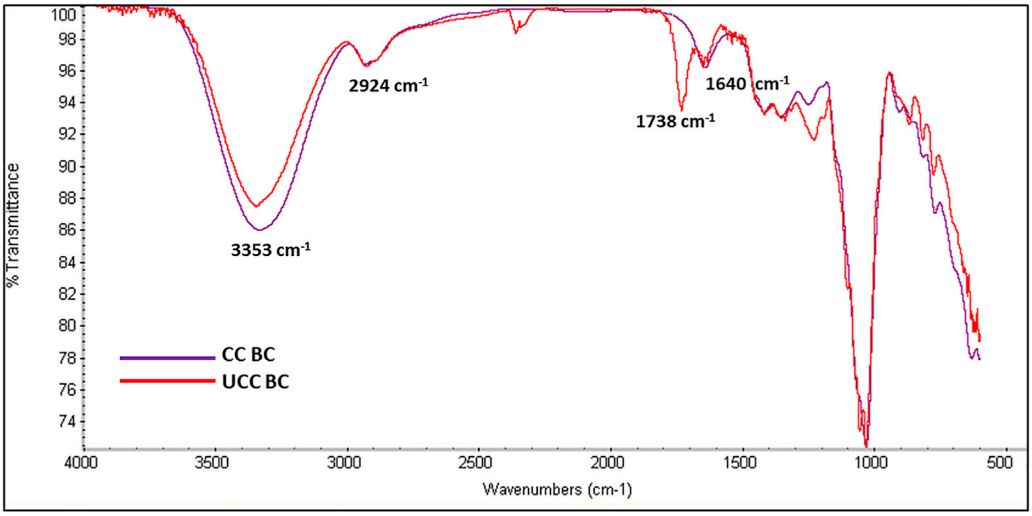

FIGURE 3 | IR spectra of CC (violet spectrum) and UCC BC (red spectrum) at 72 h.

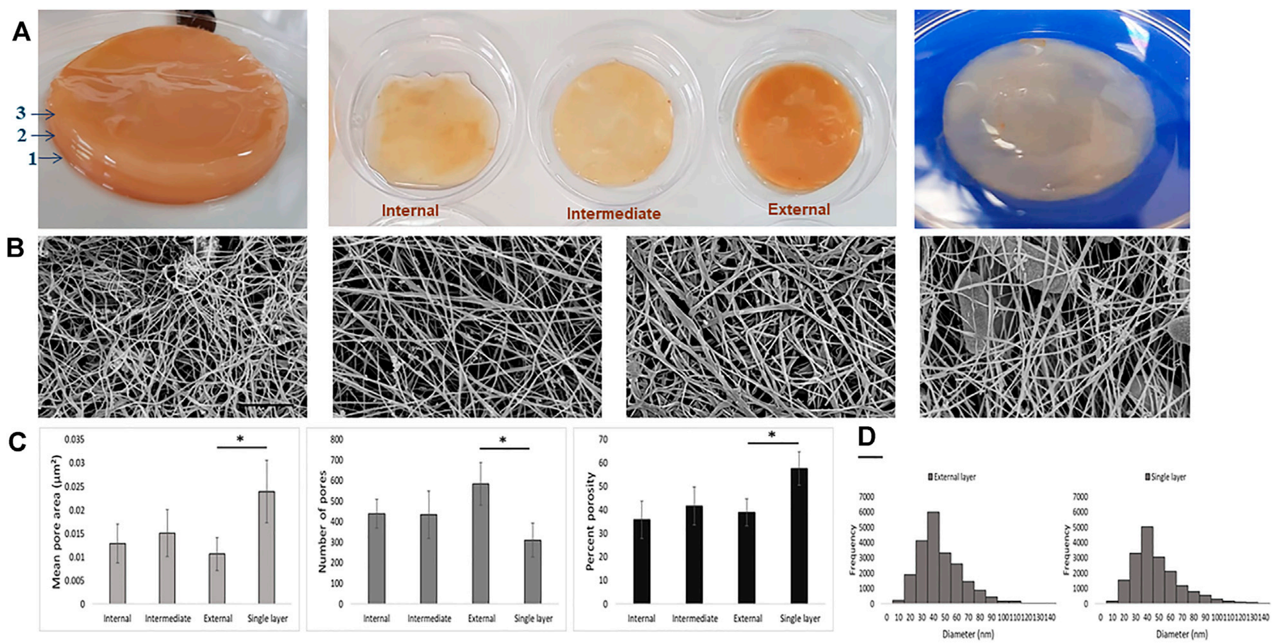

FIGURE 4 | (A) Qualitative images of BC layers produced under UCC (left and middle) and CC (right). **(B)** Representative SEM images of the different BC layers (internal, intermediate, external, and single layer, from left); scale bar 1 µm. **(C)** Mean pore area, number of pores, and porosity percentage of BC networks of the different BC layers. **(D)** Fiber diameter histogram of external and single BC layers produced in UCC and CC, respectively.

3.3 Co-Q10-SNE Encapsulation and Release by BC

As stated in the Materials and Method section, primary and secondary Co-Q10-NEs were produced by a method developed in our laboratory (Quagliariello et al., 2020). Co-Q10-NE and Co-Q10-SNE size distribution and uniformity were evaluated by DLS measurements, as reported in **Supplementary Figures S1A, B**. In detail, Co-Q10-NE displayed an average size of 112.4 ± 0.65 nm with a PDI of 0.12 ± 0.04 and a surface charge of −46.8 ± 0.40 mV (**Supplementary Figure S1C**), while Co-Q10-SNE reported an average size of 103.0 ± 1.0 nm with a PDI of 0.090 ± 0.025 and a charge of -+39.9 ± 0.07 mV (**Supplementary Figure S1C**), in agreement with those reported in the literature (Vecchione et al., 2016; Quagliariello et al., 2018; Vecchione et al., 2014; Profeta et al., 2021). Before starting incubation experiments, we also evaluated the chemical stability of our SNEs over time, and as

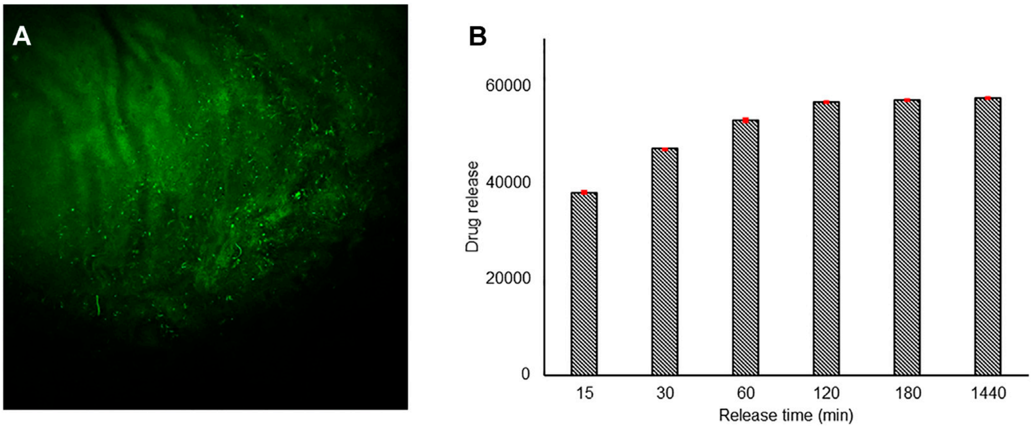

FIGURE 5 | Confocal images of the BC-Co-Q10 SNE, **(A)** 15 min incubation time λ_{exc} 450 nm, λ_{emiss} 470–600 nm. **(B)** Release kinetic studies of the Co-Q10 SNE from BC incubated for 15 min.

shown in **Supplementary Figure S1D**, they remained stable for up to 30 days, without any variation in size or PDI. Nanocarriers' uniformity and stability were also confirmed by Cryo-TEM analysis (**Supplementary Figure S2**), where Co-Q10-SNE showed monodispersed spherical nanostructures of ~100 nm.

As to incubation experiments, 1cm x 1cm layers of BC were used and incubated at two different time points (15 and 30 min) with 1 ml of Co-Q10-SNE. The correct incubation was then evaluated by confocal microscopy, following the autofluorescence of Co-Q10 at 551 nm, as shown in **Figures 5A,B** and **Supplementary Figure S3**. Confocal analysis revealed no difference in the fluorescence intensity of both samples **(Figure 5A**, **Supplementary Figure S3A)** underlying as the ultrastructure of BC allows a complete loading of SNEs already at 15 min. This result was corroborated by Co-Q10-SNE release studies where similar quantities of the Co-Q10-SNE were released from both BC samples. These analyses were carried out by fluorescence, following the maximum of Co-Q10-SNE emission at 551 nm. In detail, 5 mg of BC-Co-Q10-SNEs were suspended in 1.5 ml of water and incubated at 37°C for different time periods from 15 to 1,440 min and after 1 ml of the supernatant was removed at each time and analyzed. The quantification of release kinetics showed that for both samples (BC incubated at 15 and 30 min), the Co-Q10-SNE fluorescence signal increased during the time reaching the saturation point from 120 to 1.440 min (**Figure 5B**, **Supplementary Figure S3B**). These results were reached optimizing the BC preparation process to obtain a single not a crosslinked layer of nanofibers. Indeed, by conducting preliminary experiments on UCC BC layers, we noted that more external layers were not able to incubate the Co-Q10-SNE, and encapsulation is mostly superficial in all the samples analyzed, both at 15 and 30 min **(Supplementary Figures S4A–F**).

The reported results show that the BC networks produced with our conditions can carry out a sustained release of drugs. Our double release approach based on the use of a drug-encapsulated nanocarrier within BC could help obtain a prolonged antioxidant drug release, enhancing their therapeutic effects; it is, indeed, reported that encapsulated antioxidants show a better stability, and their gradual and sustained release leads to a superior antioxidant profile (Khalil et al., 2019). However, simple drug encapsulation in BC is not able to completely achieve the described effects, for example, curcumin loaded in cellulose acetate electrospun nanofibers showed a great initial burst that gradually increased over time in an uncontrolled manner (Khoshnevisan et al., 2018). Conversely, we proposed a delivery system which can guaranty a controlled and time-sustained release highly wished for antioxidants. In addition, by tuning the SNE size (Vecchione et al., 2014), in principle, we may easily tune the release kinetics according to the required needs.

4 CONCLUSION

The current research work was carried out to evaluate the potential application of BC as a drug delivery system (an explicative final system was reported in **Supplementary Figure S5**). The BC layers were prepared starting from the SCOBY culture using UCC and CC conditions. Preliminary incubation studies showed that under UCC conditions, only the innermost layer, the least crosslinked layer, started to incubate the nanocarrier (**Supplementary Figure S4**), and therefore, to reproduce the best loading conditions, we optimized the BC preparation process, to assure the production of a mature not crosslinked BC nanonetworks. Characterization data showed that CC-BC layers were mature, and IR data corroborate these results, demonstrating the presence of chemical bands related to BC nanofibers that are not crosslinked. The Co-Q10-SNE loading and *in vitro* release studies revealed that BC matrices can encapsulate the drug already in 15 min; indeed, confocal images and fluorescence kinetic studies highlighted no differences with the BC incubated for 30 min. In detail, the quantification of release kinetics demonstrated that for both samples, the Co-Q10-SNE fluorescence signal increases in intensity during the time reaching the saturation point from 120 to 1.440 min. The obtained results concluded that our BC produced in CC conditions could represent a novel matrix for the delivery of drug-encapsulated nanocarriers. Indeed, thanks to the optimization of BC synthesis, it could guaranty enough hydration to demonstrate for the first time the ability to incubate O/W nanoemulsions, which are ideal nanocarriers for the encapsulation and stabilization of lipophilic and water-labile molecules, such as Co-Q10. Additionally, by playing with the SNE size and with BC synthesis conditions, we may modulate nanocarriers and therefore biomolecule release to the skin. However, further research works are required to explore this potential application. Future analysis will indeed focus on the production of inflamed micro-tissues that will be then healed with the BC-Co-Q10-SNE and appropriately analyzed to evaluate the therapeutic power of the proposed system.

DATA AVAILABILITY STATEMENT

The raw data supporting the conclusion of this article will be made available by the authors, without undue reservation.

AUTHOR CONTRIBUTIONS

CD and EL performed Co-Q10-SNE encapsulation and release (confocal microscopy and fluorescence confocal analysis) and IR BC analysis; EL prepared and characterized Co-Q10-SNE; VD, BC, and FM produced and characterized BC by SEM. CD, VD, EL, and RV wrote the original draft, and all authors revised the original manuscript. RV and PN contributed to conceptualization.

FUNDING

This work was supported by "PON—Mise Imprese e Competitività 2014/2020—Bando Fabbrica Intelligente, Agrifood e Scienze della Vita-Biomatrix".

ACKNOWLEDGMENTS

The author thanks Dr. Fabio Formiggini for his help to acquire confocal images and Dr. Valentina Mollo for her support in the acquisition of Cryo-TEM images.

SUPPLEMENTARY MATERIAL

The Supplementary Material for this article can be found online at: https://www.frontiersin.org/articles/10.3389/fbioe.2022.851893/full#supplementary-material

REFERENCES

Alkhalifawi, I., and Hassan, I. A. (2014). Factors Influence on the Yield of Bacterial Cellulose of Kombucha (Khubdat Humza). *Baghdad Sci.J* 11 (3), 1420–1428. doi:10.21123/bsj.11.3.1420-1428

Almeida, I. F., Pereira, T., Silva, N. H. C. S., Gomes, F. P., Silvestre, A. J. D., Freire, C. S. R., et al. (2014). Bacterial Cellulose Membranes as Drug Delivery Systems: An *In Vivo* Skin Compatibility Study. *Eur. J. Pharmaceutics Biopharmaceutics* 86 (3), 332–336. doi:10.1016/J.EJPB.2013.08.008

Angelova, A., Angelov, B., Drechsler, M., Bizien, T., Gorshkova, Y. E., and Deng, Y. (2021). Plasmalogen-Based Liquid Crystalline Multiphase Structures Involving Docosapentaenoyl Derivatives Inspired by Biological Cubic Membranes. *Front. Cel Develop. Biol.* 9 (February), 16. doi:10.3389/FCELL.2021.617984/BIBTEX

Badshah, M., Ullah, H., Wahid, F., and Khan, T. (2021). Properties and Applications of Modified Bacterial Cellulose-Based Materials. *Cnano* 17 (3), 351–364. doi:10.2174/1573413716999201106145528

Bagheri, N., Mazzaracchio, V., Cinti, S., Colozza, N., Di Natale, C., Netti, P. A., et al. (2021). Electroanalytical Sensor Based on Gold-Nanoparticle-Decorated Paper for Sensitive Detection of Copper Ions in Sweat and Serum. *Anal. Chem.* 93 (12), 5225–5233. doi:10.1021/ACS.ANALCHEM.0C05469/SUPPL_FILE/AC0C05469_SI_001.PDF

Barud, H. G. D. O., da Silva, R. R., da Silva Barud, H., Tercjak, A. B., Gutierrez, J., Lustri, W. R., et al. (2016). A Multipurpose Natural and Renewable Polymer in Medical Applications: Bacterial Cellulose. *Carbohydr. Polym.* 153 (November), 406–420. doi:10.1016/J.CARBPOL.2016.07.059

Battisti, M., Vecchione, R., Casale, C., Pennacchio, F. A., Lettera, V., Jamaledin, R., et al. (2019). Non-Invasive Production of Multi-Compartmental Biodegradable Polymer Microneedles for Controlled Intradermal Drug Release of Labile Molecules. *Front. Bioeng. Biotechnol.* 7 (November), 296. doi:10.3389/FBIOE.2019.00296/BIBTEX

Carvalho, T., Guedes, G., Sousa, F. L., FreireFreire, C. S. R., and Santos, H. A. (2019). Latest Advances on Bacterial Cellulose-Based Materials for Wound Healing, Delivery Systems, and Tissue Engineering. *Biotechnol. J.* 14 (12), 1900059. doi:10.1002/biot.201900059

Castro, C., Zuluaga, R., Putaux, J.-L., Caro, G., Mondragon, I., and Gañán, P. (2011). Structural Characterization of Bacterial Cellulose Produced by Gluconacetobacter Swingsii Sp. From Colombian Agroindustrial Wastes. *Carbohydr. Polym.* 84 (1), 96–102. doi:10.1016/J.CARBPOL.2010.10.072

Celetti, G., Di Natale, C., Causa, F., Battista, E., and Netti, P. A. (2016). Functionalized Poly(Ethylene Glycol) Diacrylate Microgels by Microfluidics: *In Situ* Peptide Encapsulation for in Serum Selective Protein Detection. *Colloids Surf. B: Biointerfaces* 145 (September), 21–29. doi:10.1016/J.COLSURFB.2016.04.036

Del Valle, Martín., Galán, M. A., and Carbonell, R. G. (2009). Drug Delivery Technologies: The Way Forward in the New Decade. *Ind. Eng. Chem. Res.* 48 (5), 2475–2486. doi:10.1021/IE800886M

El-Leithy, E. S., Makky, A. M., Khattab, A. M., Hussein, D. G., and Hussein, Doaa. G. (2017). Optimization of Nutraceutical Coenzyme Q10 Nanoemulsion with Improved Skin Permeability and Anti-wrinkle Efficiency. *Drug Develop. Ind. Pharm.* 44 (2), 316–328. doi:10.1080/03639045.2017.1391836

Florio, D., Di Natale, C., Scognamiglio, P. L., Leone, M., La Manna, S., Di Somma, S., et al. (2021). Self-Assembly of Bio-Inspired Heterochiral Peptides. *Bioorg. Chem.* 114 (September), 105047. doi:10.1016/J.BIOORG.2021.105047

Fortunati, E., Rinaldi, S., Peltzer, M., Bloise, N., Visai, L., Armentano, I., et al. (2014). Nano-Biocomposite Films with Modified Cellulose Nanocrystals and Synthesized Silver Nanoparticles. *Carbohydr. Polym.* 101 (1), 1122–1133. doi:10.1016/J.CARBPOL.2013.10.055

Fotticchia, T., Vecchione, R., Scognamiglio, P. L., Guarnieri, D., Calcagno, V., Di Natale, C., et al. (2017). Enhanced Drug Delivery into Cell Cytosol via Glycoprotein H-Derived Peptide Conjugated Nanoemulsions. *ACS Nano* 11, 9802–9813. doi:10.1021/acsnano.7b03058

Gopi, S., Balakrishnan, P., Geethamma, V. G., Pius, A., and Thomas, S. (2018). Applications of Cellulose Nanofibrils in Drug Delivery. *Appl. Nanocomposite Mater. Drug Deliv.* 21, 692–702. doi:10.1016/B978-0-12-813741-3.00004-2

Gregory, D. A., Tripathi, L., Fricker, A. T. R., Asare, E., Orlando, I., Raghavendran, V., et al. (2021). Bacterial Cellulose: A Smart Biomaterial with Diverse Applications. *Mater. Sci. Eng. R: Rep.* 145 (July), 100623. doi:10.1016/J.MSER.2021.100623

Hotaling, N. A., Bharti, K., Kriel, H., and Simon, C. G. (2015). DiameterJ: A Validated Open Source Nanofiber Diameter Measurement Tool. *Biomaterials* 61 (August), 327–338. doi:10.1016/J.BIOMATERIALS.2015.05.015

Jamaledin, R., Sartorius, R., Di Natale, C., Vecchione, R., De Berardinis, P., and Netti, P. A. (2020). Recombinant Filamentous Bacteriophages Encapsulated in Biodegradable Polymeric Microparticles for Stimulation of Innate and Adaptive Immune Responses. *Microorganisms* 8 (5), 650. doi:10.3390/microorganisms8050650

Keshk, S. M. A. S., Razek, T. M. A., and Sameshima, K. (2009). Bacterial Cellulose Production from Beet Molasses. *Afr. J. Biotechnol.* 5 (17), 1519–1523. doi:10.4314/ajb.v5i17.43149

Khalil, I., Yehye, W. A., Etxeberria, A. E., Alhadi, A. A., Dezfooli, S. M., Julkapli, N. B. M., et al. (20192020). Nanoantioxidants: Recent Trends in Antioxidant Delivery Applications. *Antioxidants* 9 (1), 24. doi:10.3390/ANTIOX9010024

Khoshnevisan, K., Maleki, H., Samadian, H., Shahsavari, S., Sarrafzadeh, M. H., Larijani, B., et al. (2018). Cellulose Acetate Electrospun Nanofibers for Drug Delivery Systems: Applications and Recent Advances. *Carbohydr. Polym.* 198 (October), 131–141. doi:10.1016/J.CARBPOL.2018.06.072

Klemm, D., Schumann, D., Udhardt, U., and Marsch, S. (2001). Bacterial Synthesized Cellulose - Artificial Blood Vessels for Microsurgery. *Prog. Polym. Sci.* 26 (9), 1561–1603. doi:10.1016/S0079-6700(01)00021-1

La Manna, S., Florio, D., Di Natale, C., Napolitano, F., Malfitano, A. M., Netti, P. A., et al. (2021a). Conformational Consequences of NPM1 Rare Mutations: An Aggregation Perspective in Acute Myeloid Leukemia. *Bioorg. Chem.* 113 (August), 104997. doi:10.1016/J.BIOORG.2021.104997

La Manna, S., Di Natale, C., Onesto, V., and Marasco, D. (2021b). Self-Assembling Peptides: From Design to Biomedical Applications. *Ijms* 22 (23), 12662. doi:10.3390/IJMS222312662

Lagreca, E., Onesto, V., Di Natale, C., La Manna, S., Netti, P. A., and Vecchione, R. (2020). Recent Advances in the Formulation of PLGA Microparticles for Controlled Drug Delivery. *Prog. Biomater.* 9 (4), 153–174. doi:10.1007/S40204-020-00139-Y

Lahiri, D., Nag, M., Dutta, B., Dey, A., Sarkar, T., Pati, S., et al. (2021). Bacterial Cellulose: Production, Characterization, and Application as Antimicrobial Agent. *Ijms* 202122 (23), 12984. doi:10.3390/IJMS222312984

Langella, A., Calcagno, V., De Gregorio, V., Urciuolo, F., Imparato, G., Vecchione, R., et al. (2018). *In Vitro* Study of Intestinal Epithelial Interaction with Engineered Oil in Water Nanoemulsions Conveying Curcumin. *Colloids Surf. B: Biointerfaces* 164 (April), 232–239. doi:10.1016/J.COLSURFB.2018.01.028

Li, X., Liu, Y., Yu, Y., Chen, W., Liu, Y., and Yu, H. (2019). Nanoformulations of Quercetin and Cellulose Nanofibers as Healthcare Supplements with Sustained Antioxidant Activity. *Carbohydr. Polym.* 207 (March), 160–168. doi:10.1016/J.CARBPOL.2018.11.084

Mathews, P. D., Mertins, O., Angelov, B., and Angelova, A. (2022). Cubosomal Lipid Nanoassemblies with PH-Sensitive Shells Created by Biopolymer Complexes: A Synchrotron SAXS Study. *J. Colloid Interf. Sci.* 607, 440–450. doi:10.1016/j.jcis.2021.08.187

Morais, E. S., Silva, N. H. C. S., Sintra, T. E., Santos, S. A. O., Neves, B. M., Almeida, I. F., et al. (2019). Anti-Inflammatory and Antioxidant Nanostructured Cellulose Membranes Loaded with Phenolic-Based Ionic Liquids for Cutaneous Application. *Carbohydr. Polym.* 206 (February), 187–197. doi:10.1016/J.CARBPOL.2018.10.051

Di Natale, C., Celetti, G., Scognamiglio, P. L., Cosenza, C., Battista, E., Causa, F., et al. (2018). Molecularly Endowed Hydrogel with an In Silico-Assisted Screened Peptide for Highly Sensitive Small Molecule Harvesting. *Chem. Commun.* 54 (72), 10088–10091. doi:10.1039/C8CC04943B

Di Natale, C., La Manna, S., Malfitano, A. M., Di Somma, S., Florio, D., Scognamiglio, P. L., et al. (2019). Structural Insights into Amyloid Structures of the C-Terminal Region of Nucleophosmin 1 in Type A Mutation of Acute Myeloid Leukemia. *Biochim. Biophys. Acta (Bba) - Proteins Proteomics* 1867 (6), 637–644. doi:10.1016/J.BBAPAP.2019.01.010

Di Natale, C., Florio, D., Di Somma, S., Di Matteo, A., Federici, L., Netti, P. A., et al. (2020a). Proteostasis Unbalance of Nucleophosmin 1 in Acute Myeloid Leukemia: An Aggregomic Perspective. *Int. J. Biol. Macromolecules* 164 (December), 3501–3507. doi:10.1016/J.IJBIOMAC.2020.08.248

Di Natale, C., Onesto, V., Lagreca, E., Vecchione, R., and Netti, P. A. (2020b). Tunable Release of Curcumin with an In Silico-Supported Approach from Mixtures of Highly Porous PLGA Microparticles. *Materials* 13 (8), 1807. doi:10.3390/MA13081807

Di Natale, C., Battista, E., Lettera, V., Reddy, N., Pitingolo, G., Vecchione, R., et al. (2021a). Easy Surface Functionalization and Bioconjugation of Peptides as Capture Agents of a Microfluidic Biosensing Platform for Multiplex Assay in Serum. *Bioconjug. Chem.* 32 (8), 1593–1601. doi:10.1021/ACS.BIOCONJCHEM.1C00146

Di Natale, C., Lagreca, E., Panzetta, V., Gallo, M., Passannanti, F., Vitale, M., et al. (2021b). Morphological and Rheological Guided Design for the Microencapsulation Process of Lactobacillus Paracasei CBA L74 in Calcium Alginate Microspheres. *Front. Bioeng. Biotechnol.* 9 (May), 380. doi:10.3389/FBIOE.2021.660691/BIBTEX

Di Natale, C., Natale, C. F., Florio, D., Netti, P. A., Morelli, G., Ventre, M., et al. (2021c). Effects of Surface Nanopatterning on Internalization and Amyloid Aggregation of the Fragment 264-277 of Nucleophosmin 1. *Colloids Surf. B: Biointerfaces* 197 (January), 111439. doi:10.1016/J.COLSURFB.2020.111439

Di Natale, C., De Rosa, D., Profeta, M., Jamaledin, R., Attanasio, A., Lagreca, E., et al. (2021d). Design of Biodegradable Bi-compartmental Microneedles for the Stabilization and the Controlled Release of the Labile Molecule Collagenase for Skin Healthcare. *J. Mater. Chem. B* 9 (2), 392–403. doi:10.1039/D0TB02279A

Parte, F. G. B., Santoso, S. P., Chou, C.-C., Verma, V., Wang, H.-T., Ismadji, S., et al. (2020). Current Progress on the Production, Modification, and Applications of Bacterial Cellulose. *Crit. Rev. Biotechnol.* 40 (3), 397–414. doi:10.1080/07388551.2020.1713721

Picheth, G. F., Pirich, C. L., Sierakowski, M. R., Woehl, M. A., Sakakibara, C. N., de Souza, C. F., et al. (2017). Bacterial Cellulose in Biomedical Applications: A Review. *Int. J. Biol. Macromolecules* 104 (November), 97–106. doi:10.1016/J.IJBIOMAC.2017.05.171

Profeta, M., Di Natale, C., Lagreca, E., Mollo, V., Netti, P. A., and Vecchione, R. (2021). Cell Membrane-Coated Oil in Water Nano-Emulsions as Biomimetic Nanocarriers for Lipophilic Compounds Conveyance. *Pharmaceutics* 13 (7), 1069. doi:10.3390/pharmaceutics13071069

Quagliariello, V., Vecchione, R., Coppola, C., Di Cicco, C., De Capua, A., Piscopo, G., et al. (2018). Cardioprotective Effects of Nanoemulsions Loaded with Anti-inflammatory Nutraceuticals against Doxorubicin-Induced Cardiotoxicity. *Nutrients* 10 (9), 1304. doi:10.3390/nu10091304

Quagliariello, V., Vecchione, R., De Capua, A., Lagreca, E., Iaffaioli, R. V., Botti, G., et al. (2020). Nano-Encapsulation of Coenzyme Q10 in Secondary and Tertiary Nano-Emulsions for Enhanced Cardioprotection and Hepatoprotection in Human Cardiomyocytes and Hepatocytes during Exposure to Anthracyclines and Trastuzumab. *Ijn* Vol. 15 (July), 4859–4876. doi:10.2147/IJN.S245170

Tabarsa, T., Sheykhnazari, S., Ashori, A., Mashkour, M., and Khazaeian, A. (2017). Preparation and Characterization of Reinforced Papers Using Nano Bacterial Cellulose. *Int. J. Biol. Macromolecules* 101 (August), 334–340. doi:10.1016/J.IJBIOMAC.2017.03.108

Tan, T. H., Lee, H. V., Yehya Dabdawb, W. A., and Hamid, S. B. B. O. A. A. (2019). A Review of Nanocellulose in the Drug-Delivery System. *Mater. Biomed. Eng. Nanomaterials-Based Drug Deliv.*, 131–164. doi:10.1016/B978-0-12-816913-1.00005-2

Trombino, S., Cassano, R., Bloise, E., Muzzalupo, R., Leta, S., Puoci, F., et al. (2008). Design and Synthesis of Cellulose Derivatives with Antioxidant Activity. *Macromol. Biosci.* 8 (1), 86–95. doi:10.1002/MABI.200700110

Vecchione, R., Ciotola, U., Sagliano, A., Bianchini, P., Diaspro, A., and Netti, P. A. (2014). Tunable Stability of Monodisperse Secondary O/W Nano-Emulsions. *Nanoscale* 6 (15), 9300–9307. doi:10.1039/c4nr02273d

Vecchione, R., Iaccarino, G., Bianchini, P., Marotta, R., D'autilia, F., Quagliariello, V., et al. (2016a). Ultrastable Liquid-Liquid Interface as Viable Route for Controlled Deposition of Biodegradable Polymer Nanocapsules. *Small* 12 (22), 3005–3013. doi:10.1002/smll.201600347

Vecchione, R., Quagliariello, V., Calabria, D., Calcagno, V., De Luca, E., Iaffaioli, R. V., et al. (2016b). Curcumin Bioavailability from Oil in Water Nano-Emulsions: *In Vitro* and *In Vivo* Study on the Dimensional, Compositional and Interactional Dependence. *J. Controlled Release* 233 (July), 88–100. doi:10.1016/j.jconrel.2016.05.004

Vecchione, R., Quagliariello, V., Giustetto, P., Calabria, D., Sathya, A., Marotta, R., et al. (2017). Oil/Water Nano-Emulsion Loaded with Cobalt Ferrite Oxide Nanocubes for Photo-Acoustic and Magnetic Resonance Dual Imaging in Cancer: *In Vitro* and Preclinical Studies. *Nanomedicine: Nanotechnology, Biol. Med.* 13 (1), 275–286. doi:10.1016/J.NANO.2016.08.022

Volova, T. G., Shumilova, A. A., Shidlovskiy, I. P., Nikolaeva, E. D., Sukovatiy, A. G., Vasiliev, A. D., et al. (2018). Antibacterial Properties of Films of Cellulose Composites with Silver Nanoparticles and Antibiotics. *Polym. Test.* 65 (February), 54–68. doi:10.1016/J.POLYMERTESTING.2017.10.023

Conflict of Interest: The authors declare that the research was conducted in the absence of any commercial or financial relationships that could be construed as a potential conflict of interest.

Publisher's Note: All claims expressed in this article are solely those of the authors and do not necessarily represent those of their affiliated organizations, or those of the publisher, the editors, and the reviewers. Any product that may be evaluated in this article, or claim that may be made by its manufacturer, is not guaranteed or endorsed by the publisher.

Advantages of publishing in Frontiers

OPEN ACCESS
Articles are free to read for greatest visibility and readership

FAST PUBLICATION
Around 90 days from submission to decision

HIGH QUALITY PEER-REVIEW
Rigorous, collaborative, and constructive peer-review

TRANSPARENT PEER-REVIEW
Editors and reviewers acknowledged by name on published articles

Frontiers
Avenue du Tribunal-Fédéral 34
1005 Lausanne | Switzerland

Visit us: www.frontiersin.org
Contact us: frontiersin.org/about/contact

REPRODUCIBILITY OF RESEARCH
Support open data and methods to enhance research reproducibility

DIGITAL PUBLISHING
Articles designed for optimal readership across devices

FOLLOW US
@frontiersin

IMPACT METRICS
Advanced article metrics track visibility across digital media

EXTENSIVE PROMOTION
Marketing and promotion of impactful research

LOOP RESEARCH NETWORK
Our network increases your article's readership